Exploring Bacteria-Surface Interactions

Alessandro M. Carabelli MSc

Thesis submitted to the University of Nottingham
for the degree of Doctor of Philosophy

September 2019

Abstract

Bacteria adhere to almost any surface. Medical-device biofilm-centred infections pose an enormous threat, particularly from multi-antibiotic resistant pathogens. Biofilm formation is largely understood and encompasses an initial, reversible bacterial cell surface-attachment phase followed by irreversible surface-attachment, leading to the formation of biofilms that can be up to 1,000 times more resistant to antibiotics and refractory to host immune defences. A better understanding of bacterial-surface interactions should aid human intervention into this process to reduce biofilm formation on implanted medical devices.

Previously, Hook *et al.* screened an (meth)acrylate polymer microarray in high-throughput for polymers that prevent biofilm formation by a selection of bacterial pathogens including *Pseudomonas aeruginosa*. This resulted in the discovery of poly(ethylene glycol dicyclopentenyl ether acrylate) (pEGdPEA) which has recently been approved for human use as a coating (BACTIGON®) for urinary tract catheters. However, the mechanism(s) by which pEGdPEA prevents biofilm formation is not known beyond the observation that it does not inhibit bacterial growth. This thesis describes the response of bacteria to pEGdPEA in comparison with that of a biofilm-promoting polymer, poly(neopentyl glycol propoxylate diacrylate polymer) (pNGPDA). Fluorescence and electron microscopy after 24 h of incubation with *P. aeruginosa* showed that little extracellular matrix formed on pEGdPEA in contrast with pNGPDA where a robust biofilm was observed.

A method for spatio-temporal characterisation of bacterial motility at and above surfaces was developed using a custom designed microscope that allowed the interaction of *Pseudomonas* on different materials to be followed over time. This multimode 2D-3D microscope utilised several optical techniques simultaneously with the ability to record stable video data of individual bacterial cells: namely digital holography, differential interference contrast (DIC), TIRM (total internal reflection microscopy), TIRF (total internal reflection fluorescent microscopy)

and widefield epifluorescence microscopy. The behaviour of large numbers of bacterial cells was characterised simultaneously from videos using high-throughput motion analysis algorithms. To study bacteria surface adhesion strength on different chemistries a method was developed using microfluidics and xurography or *razor writing* to form channels. *P. aeruginosa* cells showed weaker surface adhesion strength, moved faster and with shorter residence times on pEGdPEA compared with pNGPDA. *P. aeruginosa* cells were also observed, post cell-division, to leave the pEGdPEA surface with a higher frequency than from the pNGPDA surface. By using a *cdrA::gfp* fusion as a cyclic diguanylate (c-di-GMP) biosensor, the inability of *P. aeruginosa* cells interacting with pEGdPEA to increase c-di-GMP levels was observed and contrasted markedly with the rapid induction of high levels of fluorescence in cells on pNGPDA.

Biofilm-forming bacterial cells are phenotypically distinct from their free-swimming, planktonic counterparts. Much work has focused on the extracellular polymeric substance (EPS) which is known to affect surface adhesion. Here, by combining EPS staining and bacterial tracking, *P. aeruginosa* was shown not to deposit exopolysaccharides on pEGdPEA, in contrast to that observed on pro-biofilm pNGPDA. These data, together with weaker adhesion strength, higher frequency of detachment events and lower c-di-GMP intracellular levels, suggest that on pEGdPEA, *P. aeruginosa* is unable to switch from the reversible to irreversible attachment stage. The key signalling and sensing pathways used by *P. aeruginosa* to respond to surfaces were investigated and the data obtained suggest that bacteria actively "decide" whether to attach to a particular surface and that the decision not to form a biofilm on pEGdPEA is likely to involve the *sadB* pathway. SadB is a cytoplasmic protein with an, as yet, unknown function but its upstream regulatory pathway involves c-di-GMP signalling. How this protein is involved in the ability of bacteria to maintain a surface-associated state which leads to an irreversible attachment is described.

Bacteria have been shown to clump as multicellular aggregates during the process of biofilm formation either in bulk (as planktonic aggregates) or at the surface. Here differential planktonic aggregation with respect to pEGdPEA and pNGPDA is described where greater aggregation was observed on the latter. The

formation of aggregates in the bulk liquid phase above these polymers was characterised using bright-field microscopy and laser diffraction analysis. The differential aggregation observed was also examined for ‘aggregation inducing’ signals by analysis of the cell-free spent media using liquid chromatography-tandem mass spectrometry (LC-MS/MS). Comparative metabolomics enabled the identification of the aggregation-inducing signal *N*-(3-oxododecanoyl)-L-homoserine lactone, which was at a significantly lower concentration in spent medium from cells previously exposed to pEGdPEA compared with the pro-biofilm pNGPDA. These data provide new insights into the understanding of how bacteria, after being in contact with different surface chemistries, are able to alter their bulk liquid phase behaviour. Additionally, this highlights the potential of novel use of these polymer surfaces to investigate bacterial biofilm development and to develop new solutions for the prevention of bacterial biofilm-centred infections.

Acknowledgements

A work of this size would not have been possible and should not have been undertaken without collaborating. Collaboration is necessary and essential to the very nature of serious research and curious inquiry.

All my gratitude goes to my supervisors to have given me this great opportunity to be part of a team which is scientifically world-leading. Dr Andrew Hook, Prof. Morgan Alexander, Dr Noah Russell and Prof. Paul Williams' support has been invaluable, and I feel privileged to have been moulded by their guidance, questions, ideas and corrections. My work was generously funded by the University of Nottingham and the Schools of Pharmacy and Life Sciences.

The technical assistance from Dr Alvin C. K. Teo, Nicola Weston, Salah Abdelrazig, Prof. Xinyong Chen and Francesco Pappalardo has made my progression through this project quicker and helped me to developed multiple skills with several instruments.

I have been proud to be part of the Advanced Materials and Healthcare Technologies Division, the *Stick or not to stick* group and the School of Life Sciences CBS Microbiology group helping me to raise new questions and inspiring me to come up with new ideas. I would particularly like to thank Dr Jean Dubern and Dr Matthew Fletcher for their contribution making mutated bacteria and their advanced skills as microbiologists, and to Dr Laurence Burroughs who has more than anyone given me a new way of working with great passion and attention to details.

I send my love to my parents, my extended family as a whole and my second family (Nassifs) for giving me support, friendship and love. Aline for having boosted my desire for knowledge and my aspirations. I am also so grateful to Benedetta and Giovanni, Laura and all my friends here in Nottingham and in London (Stefano, Gianluca and Ettore) whose encouragement has been

unwavering, and who have been beside me throughout my project reminding me what really matters in life.

Finally, a thank you to all past and present in C30 who remind me every day that it is more than an office. In particular my friends, colleagues and students, Andrew Blok, Marco Isgro', Andrew Woodward, Thais, Paula, Ania and my dearest friend Olutoba Sanni.

“Dans les champs de l'observation
le hasard ne favorise que les esprits préparés.”
(“In the fields of observation
chance favours only the prepared mind.")
Louis Pasteur (1822-1895)

Contributions

List of experiments	Contributors
Mutant construction	Dr Jean Dubern
Atomic Force Measurements	Francesco Pappalardo
ToF-SIMS	Dr Alvin Teo
ESEM	Nichola Weston
Holography Data	Dr Nicola Farthing
MATLAB scripts used where stated	Dr Andrew Hook
LC-MS/MS	Dr Salah Abdelrazig Nigel Halliday

Table of Contents

Contents 9

Figures 14

List of Tables 26

List of Abbreviations 27

Chapter 1 *30*

Introduction *30*

1.1 The Problem: Healthcare-Associated Infections 30

1.2 What is a biofilm? 33

1.3 Bacterial Biofilm Life Cycle 35

1.4 Bacterial Surface Appendages 37

1.4.1 Pili 37

1.4.2 Flagellum Structure 40

1.5 From Swimming to Biofilm Formation: Key Stages in Biofilm Formation 42

1.5.1 Bacterial Motility 42

1.5.2 Surface Sensing Systems 50

1.5.3 Bacterial Surface Interactions 54

1.5.4 Bacterial Cell Aggregation, Micro-colony Formation and Surface Exploration 61

1.5.5 Cell-to-cell Communication 62

1.6 Anti-biofilm Strategies 66

1.6.1 Prevention of Protein Adsorption 66

1.6.2 Prevention of Bacterial Adhesion 71

1.6.3 Bacterial Killing Strategies 76

1.7 Aims and Objectives 79

Chapter 2 *81*

Review of techniques *81*

2.1 Chemicals and Free Radical Chain Reactions 81

2.2 Surface Analysis 82

2.2.1 Time of Flight Secondary Ion Mass Spectrometry 82

2.2.2 Water Contact Angle 85
2.2.3 Atomic Force Microscopy 86
2.3 Bacterial Strains 90
2.4 Microscopy 90
2.4.1 Multimode Microscope Description 90
2.4.1 Image Processing and Segmentation 96
2.4.2 Fluorescence Confocal Laser Scanning Microscopy 98
2.4.3 Environment Scanning Electron Microscopy 99
2.5 Quantification and Statistical analysis 100
Chapter 3 *101*
How Single Cell Behaviour and Biofilm Formation is Influenced by the Nature of the Polymer Substrate *101*
3.1 Introduction 101
3.1.1 Aims 102
3.2 Experimental 103
3.2.1 Polymer Preparation 103
3.2.2 Time-of-Flight Mass Spectrometry 104
3.2.3 Bacterial Growth Conditions and Biofilm Assay 105
3.2.4 Microscope and Bacterial Tracking 106
3.2.5 Bacterial Matrix Visualisation 108
3.2.6 Investigation of Bacterial Footprints and Trails 108
3.3 Results 109
3.3.1 Time-of-Flight Mass Spectrometry 109
3.3.2 *P. aeruginosa* Fails to Form Mature Biofilms on pEGdPEA 111
3.3.3 Biofilm Characterisation 113
3.3.4 *P. aeruginosa* Behaviour During Early Stage Surface Interactions 115
3.3.5 The Role of the Bacterial Appendages on the Ability of Bacteria to Leave the Polymer Surfaces 119
3.3.6 *P. aeruginosa* Motility Across Different Surfaces 120
3.3.7 pNGPDA but not pEGdPEA Stimulates an Increase in c-di-GMP 123
3.3.8 pEGdPEA Affects ExoPolysaccharide Production of *P. aeruginosa* 126
3.4 Discussion 128

3.5 Conclusions 131

Chapter 4 *133*

Development of a P. aeruginosa Surface Detachment Assay on Different Polymers under Flow Stress *133*

4.1 Introduction 133

4.1.1 Microfluidics: Flow Rate in a Channel 134

4.1.2 Poiseuille Flow and Shear Stress 135

4.1.3 Microchannel and Laminar Flow 136

4.1.4 Materials Used for the Preparation of the Microfluidic System 137

4.1.5 Aims 138

4.2 Experimental 138

4.2.1 Polymer Preparation 138

4.2.2 Microfluidics Device 139

4.2.3 Microscope 143

4.2.4 Bacterial Growth Conditions 143

4.2.5 Bacterial Biofilm Assay 143

4.2.6 Water Contact Angle 144

4.2.7 Atomic Force Microscopy 144

4.3 Results 145

4.3.1 How Strongly Do *P. aeruginosa* Cells Attach to pNGPDA and pEGdPEA Surfaces? 145

4.3.2 Bacterial Surface Appendages Involvement in Adhesion 146

4.3.3 Do T4P and Functional Flagella Contribute to Biofilm Development on pNGPDA and pEGdPEA? 149

4.3.4 Water Contact Angle 150

4.3.5 Atomic Force Microscopy 151

4.4 Discussion 154

4.5 Conclusions 158

Chapter 5 *160*

The Role of the SadB in Bacterial Surface Sensing *160*

5.1 Introduction 160

5.1.1 Aims 162

5.2 Experimental 163
5.2.1 Polymer Preparation 163
5.2.2 Bacteria Growth Conditions and Biofilm Assay 163
5.2.3 Environmental Scanning Electron Microscopy (ESEM) 163
5.2.4 c-di-GMP Production 163
5.2.5 Microfluidic Bacterial Detachment Assay 164
5.2.6 Microscopy 164
5.3 Results 164
5.3.1 Overexpression of *sadB* Enables *P. aeruginosa* to Form Biofilms on pEGdPEA 164
5.3.2 Can *sadB* Restore Biofilm Formation by *motAB* and *motCD* Mutants? 168
5.3.3 The *sadB* Gene and Daughter Cell Fate 169
5.3.4 SadB and Adhesion Strength 171
5.3.5 Impact of *sadB* on c-di-GMP Levels 172
5.4 Discussion 176
5.5 Conclusions 178
Chapter 6 *180*
Investigating the Effect of Chemically Distinct Polymer Surfaces on P. aeruginosa Aggregation *180*
6.1 Introduction 180
6.1.1 Aims 181
6.2 Experimental 181
6.2.1 Polymer Preparation 181
6.2.2 Bacterial Culture 182
6.2.3 Quorum Sensing Signal Molecule (QSSM) Extraction 182
6.2.4 Analytical Methodologies 182
6.2.5 Microscopy 183
6.2.6 Liquid Chromatography-Tandem Mass Spectrometry (LC-MS/MS) 183
6.3 Results 184
6.3.1 Exposure to a pNGPDA Influences *P. aeruginosa* Aggregation 184
6.3.2 *P. aeruginosa* Aggregates are Rich in eDNA and EPS 187
6.3.3 Aggregate Formation by Different *P. aeruginosa* PAO1 Sublines 189

6.3.4 Does *P. aeruginosa* Produce Aggregation-Inducing Factors on pNGPDA but not on pEGdPEA? 190

6.3.5 3-oxo-C12-HSL is a Key Factor Promoting Bacterial Planktonic Cell Aggregation 191

6.3.6 Exogenous 3-oxo-C12-HSL Increases Aggregation and Biofilm Formation on pEGdPEA 192

6.4 Discussion 197

6.5 Conclusions 199

Chapter 7 *201*

Conclusion and Future Work *201*

7.1 Conclusions 201

7.2 Future work 204

Chapter 8 *209*

Appendixes *209*

8.1 Appendix 1 209

8.2 Appendix 2 213

8.3 Appendix 3 223

8.4 Appendix 4 226

8.5 Appendix 5 226

8.6 Appendix 6 228

8.7 Appendix 7 232

8.8 Appendix 8 232

8.9 Appendix 9 233

Bibliography *237*

Table of Figures

Figure 1.1 Examples of indwelling medical devices. Image adapted from [10]. 30

Figure 1.2 Expected mortality caused by AMR. Number of deaths worldwide per year for different causes (blue bars). Expected mortality in 2050 caused by AMR is highlighted in violet. Figure taken from ref. [1]. 32

Figure 1.3 Example of a biofilm. EPS matrix is highlighted in yellow. Image adapted from ref. [26]. 33

Figure 1.4 Schematic life cycle of *P. aeruginosa* from planktonic to surface sensing, biofilm formation and dispersal. Image adapted from ref. [56]. 36

Figure 1.5 Representative electron micrograph of *P. aeruginosa*. Pili (black arrows) and flagellum (white arrow) are highlighted. Image taken from ref. [60]. 37

Figure 1.6 A) The type 1 pili and the P pili from uropathogenic *Escherichia coli* (UPEC) obtained from the combination of different subunits (Fim and Pap). Figure from ref. [59]. B) Schematic of the T4P machinery in *Thermus thermophilus*. Figure from ref.[68]. 39

Figure 1.7 Schematic diagram of A) a bacterial flagellum and B) the flagellar motor. Figure adapted from ref. [82]. 41

Figure 1.8 Different bacterial species display differences in the position and number of flagella. Electron micrographs and the insets describe the structure of polar-flagellated *P. aeruginosa*, *Caulobacter crescentus* (*C. crescentus*), the lophotrichous *Helicobacter pylori*, the amphitrichous *Campylobacter jejuni* and the peritrichously flagellated *B. subtilis* and *E. coli*. The insets schematically indicate the respective patterns. Figure taken from ref. [96]. 43

Figure 1.9 Circular trajectories are determined by a wall-induced torque acting on the cell head and flagellar bundle. The inset presents trajectories of a non-tumbling mutant of *E. coli* (HCB437). Figure adapted from [102]. 44

Figure 1.10 3D motility patterns made by *P. aeruginosa*. A) 3D schematic of trajectories obtained; B) xy-projection of trajectories; C) representation of 5 motility patterns; D) frequency of each motility mode. Values obtained over 35 trajectories. Figure taken from [97]. 46

Figure 1.11 Flagella and T4P-mediated motility in *P. aeruginosa*: A) spinning; B) swimming. T4P mediated motility: C) crawling; D) walking; E) slingshot. Figure adapted from ref. [103]. 47

Figure 1.12 Mechanism for *P. aeruginosa* of crawling motility by pili-mediated pulling or by a slingshot obtained by the release of a T4P. Figure taken from ref. [106]. 48

Figure 1.13 Representative micrographs of *P. aeruginosa* strain ATCC 15692 T4P deficient mutant Δ*pilA*, WT, and flagella deficient mutant Δ*fliM* biofilms on glass coverslips. Large cluster are observed with twitching deficient bacteria, indicating that bacteria are not able to cover wider areas. The flagella deficient mutant is not able to create biofilm and cell clusters. Image taken from ref. [103]. 50

Figure 1.14 The structure of c-di-GMP is shown (center). Enzymes known as DGCs that carry a conserved GGDEF domain, synthesised c-di-GMP from two molecules of GTP. This second messenger can be degraded by two families of PDE: those with an EAL domain which linearise the molecule to pGpG, and other proteins with HD-GYP domain which generate two molecules of GMP. Figure taken from [133]. 53

Figure 1.15 Crosstalk regulation between c-di-GMP and TCS / DGC systems during *P. aeruginosa* biofilm formation. The activation and inhibition pathways are marked with solid and dashed lines, respectively. Figure taken from [139]. 54

Figure 1.16 Schematic mechanism of upstream motility in *E. coli* under different flow rates. Figure taken from [102]. 55

Figure 1.17 Schematic interaction energy versus distance profiles of DLVO interaction. The attractive van der Waals and the repulsive electrostatic potentials form the total interaction energy. Image adapted from ref. [147]. 56

Figure 1.18 Total interaction energy between a bacterial cell and a surface depending on ionic strength. Image taken from ref [149]. 57

Figure 1.19 Depiction of Gram-positive and Gram-negative cell envelopes: CAP = covalently attached protein; IMP= integral membrane protein; LP= lipoprotein; LPS= lipopolysaccharide; LTA= lipoteichoic acid; OMP= outer membrane protein; WTA= wall teichoic acid. Image taken from [162]. 59

Figure 1.20 Psl trail left behind by bacteria, brightfield microscopy image of the *P. aeruginosa* (left) on glass borosilicate; Psl trail stained by fluorescently conjugated HHA lectin (center); merged image with trail pseudo-coloured in red (right). Scale bar is 10 μm. Figure taken from [154]. 62

Figure 1.21 Some examples of AHLs and oligopeptide autoinducers in gram negative and gram-positive bacteria respectively. Figure taken from [186]. 63

Figure 1.22 PolySB modification of a peripherally inserted central catheter surface (PICC). PolySB is bound to the surface of the PICC to form a conformal polymer surface. The zwitterionic polySB modification coordinates both free and bound water molecules to create a hydrophilic surface. PolySB-modified PICC has reduced thrombus accumulation. Image taken from ref. [223]. 70

Figure 1.23 Ethylene glycol containing monomers used by Hook *et al*. to create thermally switchable polymers with controlled anti-microbial activity. Figure taken from ref. [5].. 72

Figure 1.24 Five hit polymers that Hook *et al.* identified. Figure taken from ref. [7]. 73

Figure 1.25 Hypothesis of model of how motile bacteria such as *P. aeruginosa* respond to a novel class of polymeric bacteria. 75

Figure 2.1 Radical chain reactions have three distinct phases: initiation, propagation, and termination. 82

Figure 2.2 A) Schematic of primary ions hitting a surface and releasing secondary ions. B) ©IONTOF schematic of a SIMS instrument. 83

Figure 2.3 500 x 500 µm ToF-SIMS image of $C_5H_7^+$ (*m/z* 67.06) of a copolymeric surface obtained using an IONTOF IV instrument and SurfaceLab6 software. 84

Figure 2.4 A) Example of droplet deposited onto a polymeric surface. B) WCA has been plotted against time (dots). Linear regression was fitted with $R^2 = 0.80$. $y_0 = 62.7$. 86

Figure 2.5 A) Schematic of the basic set-up of an atomic force microscope. The movement of the tip across the surface is detected by a laser deflected onto the top of the cantilever. B) Photograph of the MFP 3D (Asylum Research) used in this project. 87

Figure 2.6 Diagram of a standard force *vs* distance curve showing the regions from which stiffness and adhesion of the surface are derived. 89

Figure 2.7 Schematic of the multimode 2/3D microscope used in this study including the optical ensemble for the remote-image relay. The remote image relay allows scanning of the focal plane to acquire and reconstruct z-stacks without disturbing the sample. The microscope is also equipped with lasers to enable DHM. Image taken from [268]. 91

Figure 2.8 DIC principle. A) Beam path. B) Birefringent prisms. C) Condenser prism which performs a vectorial decomposition of the linearly polarised light into two vibration directions that are perpendicularly polarised to each other. Image taken from [269]. 92

Figure 2.9 A) Schematic of the principle behind the holographic microscope. B) Example of recorded image at the focal plane showing the interference patterns of PAO1 in LB medium. 94

Figure 2.10 Remote image relay system.[267] 95

Figure 2.11 A) Identified objects before drift corrections (dots). Lines connect the same object found in multiple z planes due to drift. B) Objects in 3D volume after drift correction. .. 95

Figure 2.12 A-B) Schematic of bespoke holder to use coverslips coated with different polymers. The 22 × 22 mm coverslip was sealed at the bottom using a silicone and halogen free high-vacuum grease (Apiezon M). 98

Figure 2.13 Schematic of the basic components of a confocal microscope.[216] 99

Figure 3.1 Chemical structure of A) pNGPDA and B) pEGdPEA. 104

Figure 3.2 Schematic of glass coverslip (22 x 22 mm) with polymer spotted onto it. A cross with two and one dot in two corners were drawn with a marker pen in order to have reference of areas visualised through microscopy..... 109

Figure 3.3 Surface characterisation. ToF-SIMS characterisation of polymer-coated coverslips. Positive ion ToF-SIMS spectra of pEGdPEA (pink), NGPDA-co-EGdPEA (1:1) (orange), pNGPDA (blue). $C_5H_7^+$ (*m/z* 67.06) and $C_3H_7O^+$ (*m/z* 59.05) are characteristic ions for pEGdPEA and pNGPDA respectively (A). Comparison of normalised ion intensities for $C_5H_7^+$ (B) and $C_3H_7O^+$ (C) for the 3 polymers. D) An example corresponding secondary ion image (500 x 500 µm) for both $C_5H_7^+$ (m/z 67.06) and $C_3H_7O^+$ (m/z 59.05) ions using pNGPDA-co-EGdPEA. The two monomers polymerised homogeneously. 111

Figure 3.4 A) Confocal images (10×, 0.3) of *P. aeruginosa m-cherry* tagged after 24 h (top) and 72 h (bottom) on pNGPDA (left), pNGPDA-co-EGDPEA (middle), and pEGdPEA (right). Samples were washed 2× in PBS and 1× in H2O. Scale bar is 50 µm. B) Quantification of bacterial biomass for the 3 polymer surfaces. Error bars show ± 1 standard deviation (N=3). Significance was determined by analysis of variance One-way ANOVA and Tukey's post-test comparison for differences between the indicated samples. **** $p<0.001$, *** $p<0.001$. 112

Figure 3.5 ESEM representative images of *P. aeruginosa* grown for 24 h on pNGPDA (left) and pEGdPEA (right). Images captured at 10,000× (A) and 1,000× (B) magnification. Bacteria were found embedded in the biofilm matrix on pNGPDA, whereas no matrix could be observed when grown on pEGdPEA. Scale bar is 2-10 µm respectively..... 113

Figure 3.6 A) Confocal images (40×,1.2) of *P. aeruginosa gfp* tagged after 24 h on pNGPDA (left), pNGPDA-co-EGDPEA (middle), and pEGdPEA (right). eDNA was stained through propidium iodide (red) after samples were washed 2× in PBS and 2× in H_2O. Top-square shows higher magnification of biofilm on pNGPDA. Single cells are resolved but dead cells are not indicating it might be eDNA. Scale bar is 10 µm. B) Quantification of eDNA coverage on pNGPDA (blue), pEGdPEA (pink) and NGPDA-co-EGdPEA (orange). Error bars show ± 1 standard deviation (N=3). **** p<0.0001, *** p<0.001, * p<0.05. 114

Figure 3.7 ESEM representative images of PAO1-W wild-type grown for 24 h on 3 hit polymers: BnMA and iBMA (monomer E in [8] and monomer 7 in [6]) and TMCHMA (monomer 12 in [6]). Images captured at 5,000× magnification. No matrix could be observed when grown on anti-biofilm surfaces as shown in the schematic (right). Scale bars are 2 µm. 115

Figure 3.8 Examples of 3D swimming motility tracks obtained using DHM microscopy with PAO1-W on pNGPDA. Colourmap shows average speed of tracks. 116

Figure 3.9 Histogram of average speed (A) and K_{MSD} (B) of tracks at the presence of pNGPDA (blue) and pEGdPEA (pink) (N=9) considering more than n>200 tracks for each sample. Bin is 5 and 0.5. 116

Figure 3.10 Quantification of *P. aeruginosa* coverage of the polymers. A) DIC brightfield (40×,1.3) images of PAO1-W on pNGPDA, pNGPDA-co-EGdPEA and pEGdPEA after 1 h from inoculation. B) Categorical scatter plot of bacterial coverage. Error bars show ± 1 standard deviation (N=3). Scale bar is 3 µm. 117

Figure 3.11 Number of bacteria per frame *vs* time increases much faster for pNGPDA (blue) than pEGdPEA (pink). Dots represent mean ± 1 standard deviation (N=3). 117

Figure 3.12 DIC brightfield (40×,1.3) images of PAO1-W on pNGPDA (left) and pEGdPEA (right) after 3 h from inoculation. Scale bar is 3 µm. 118

Figure 3.13 Histogram of residence time of PAO1-W on pNGPDA (blue bar) and pEGdPEA (pink bar) between t = 1 h to t = 2 h after inoculation. Solid bars represent fraction of bacteria at different residence times (bin = 2 min). Dashed lines represent data fit to Gaussian functions for pNGPDA (blue) and pEGdPEA (pink). Shaded areas represent 95% CI of the fit deviation. R^2=0.86 for pNGPDA and R^2=0.91 for pEGdPEA (N=3 considering more than 700 bacteria). Welch's t test was applied to compare distribution assuming different variance. *** p<0.001. 118

Figure 3.14 A) Schematic of the branching division events. B) Bar graph shows proportion of the population for PAO1-W in different branching divisions where pNGPDA (blue) and pEGdPEA (pink). Values obtained considering n>100 doubling events (N=3) between t = 1 h to t = 2 h from inoculation. PAO1-W branching distribution for the two polymers were

found to be different (p<0.001) through two-way ANOVA and Sidak's multiple comparison. 119

Figure 3.15 Bar graph shows proportion of population for each bacterial strain in different branching division considering pNGPDA (blue) and pEGdPEA (pink). Values obtained considering n>100 doubling events for 3 independent replicates (N=3) between t = 1 h to t = 2 h from inoculation. Sidak's multiple comparison has been used to find statistical differences (Appendix 6)..... 120

Figure 3.16 Representative colour maps of tracks of *P. aeruginosa* Δ*pilA* (top-left) Δ*fliC* (top-right) and Δ*pilA*Δ*fliC* (bottom) on pNGPDA measured over 1 h of exposure to surfaces. No motility was observed for *P. aeruginosa* Δ*pilA* or Δ*pilA*Δ*fliC mutants*. On the contrary, motility was observed using *P. aeruginosa* Δ*fliC*. Thus, the surface motility observed was T4P driven. Scale bar is 10 µm. 121

Figure 3.17 A) Representative colour maps of PAO1-W twitching tracks on pNGPDA and pEGdPEA measured over 1 h of exposure to surfaces. Colours show different speeds as indicated by the intensity scale. Scale bar is 10 µm. B) Histogram of radius of curvature for all tracks on different polymers. n>12,000 (N=3). Higher radius of curvature corresponds to more directional motility.[288] Bin is 2. C) Histogram of PAO1-W speeds on pNGPDA and pEGdPEA (N=3). Bin = 2. Dashed lines represent data fit to Gaussian functions. Shaded areas represent 95% CI of the fits. **** p<0.0001 using Welch's t test assuming different variance. 122

Figure 3.18 Scatter plot showing the mean speed of cells during an entire trajectory as a function of the fraction of the cell's tracked lifetime that was spent tilting (vertical position). Linear fits (y = m*x + b) to each dataset yield: for pEGdPEA, m = 0.5 ± 1.3, b = 13.0 ± 0.8; for pNGPDA, m = -0.9 ± 3.0, b = 9.8 ± 1.2. As a proxy readout for tilting, the projected aspect ratio in each frame has been examined as described in section 1.5.1.2..... 123

Figure 3.19 Representative colour maps of tracks of *P. aeruginosa cdrA*::*gfp* on pNGPDA (left) and pEGdPEA (right). Colours show instantaneous fluorescence intensity measured (F) according to the intensity scale shown. Tracks were obtained from images acquired using widefield epifluorescence microscopy (40×, 1.3) every 30 s for 60 min and then processed through a custom single-cell tracking algorithm. Scale bar is 10 µm. 124

Figure 3.20 A) Histogram of F for all tracks on different polymers. n> 1,000 for three independent experiments (N=3). Dashed lines represent data fit to Gaussian functions. Shaded areas represent 95% CI of the fits. B) Evaluation of single-cell mean (F values) *cdrA* expression by stationary (speed < 1 nm s^{-1}) and (C) motile cells (speed > 1 nm s^{-1}) on each polymer. Error bars show ± 1 standard deviation (N=3). Unpaired t-test with Welch's correction was used to compared curves (****p<0.0001). 125

Figure 3.21 Histogram of speeds for all the tracks on pNGPDA (blue) and pEGdPEA (pink) respectively. Bin=1. 125

Figure 3.22 DIC images of tracked *P. aeruginosa* at t = 0 h and t = 2.5 h (highlighted with a star; fluorescent lectin stained EPS trails after 2.5 h and a merged image of the 2 channels. Scale bar is 1 µm. 127

Figure 3.23 CLSM images captured at t = 2.5 h on pEGdPEA (right) and pNGPDA (left). Colourmap shows fluorescence level of ConA bound to EPS at surfaces. Scale bars are 10 µm. 127

Figure 3.24 Mean fluorescence intensity measured on pNGPDA and pEGdPEA after 2.5 h from inoculation and after background subtraction. Unpaired t-test (**p<0.01). Error bars show ± 1 standard deviation (N=3). 128

Figure 4.1 Different ways to describe the flow rate Q as either a volume per unit or the product of area and velocity. Figure adapted from [294]. 135

Figure 4.2 Schematic of the velocity profile of a liquid in a microfluidics channel showing a different velocity u depending on the distance from the centre (r). Velocity increases away from the wall and reaches its maximum at the centre of the channel where $r = 0$ and its minimum at the wall where $r = R$ in which R is the half dimension of the channel (either width or height). Image adapted from [294]. 135

Figure 4.3 A-B-C) Schematic of the "cutting edge" technology for cell biology provided by tape-based devices. A computer device is associated to a razor printer to cut a biocompatible double-side adhesive tape. D) Representative microfluidic channel geometry is cut into the primary liner and silicon tape but not into the secondary liner. The microchannel obtained is 14 mm × 1 mm × 50 µm. E) The secondary liner is removed and the silicone tape flipped over to adhere to the PDMS. Once adhered, access ports are cut with a biopsy punch F), before the primary liner is removed and the device attached to a surface of interest G). 140

Figure 4.4 A) To hold the tubing in place, steel tubes were preferred for connections. B) Tygon tubing was used to bridge the sleeved tubing with the steel tube for connection with the PDMS layer/microfluidics channels..... 142

Figure 4.5 Microfluidics detachment experiment. A) Enlarged view of the microfluidics channel system. B) Microscope set-up with pump, microfluidics, injector and medium. C) Schematic of the removal process of adhered cells. Figure readapted from [341]..... 142

Figure 4.6 Measurement of bacterial adhesion strength to pNGPDA and pEGdPEA. surfaces. The number of PAO1-W surface associated cells on pNGPDA (blue-circles), pEGdPEA (pink-circles) and NGPDA-co-EGdPEA (orange-triangles) surfaces with increasing shear

stress τ (Pa) applied through an increase in flow rate. Error bars represent ± 1 SEM (N=3). 145

Figure 4.7 Number of *P. aeruginosa* Δ*pilA* cells (green), Δ*fliC* (purple) and PAO1-W WT (blue) on pNGPDA with increasing shear stress τ_{50} (Pa) applied through an increase in flow rate; shear stress τ_{50} indicates the shear stress necessary to detach 50% of cells. 146

Figure 4.8 Number of *P. aeruginosa* Δ*pilA* (left) and Δ*fliC* (right) cells on pEGdPEA (pink) and pNGPDA (blue) surfaces with increasing shear stress τ_{50} (Pa) applied through an increase in flow rate; shear stress τ_{50} indicates the shear stress necessary to detach 50% of cells. 147

Figure 4.9 Involvement of the flagellar stators in adhesion onto pNGPDA and pEGdPEA. Number of *P. aeruginosa* Δ*motAB* (A), Δ*motCD* (B) and Δ*motABCD* (C) cells on pEGdPEA (pink) and pNGPDA (blue) surfaces with increasing shear stress τ; shear stress τ_{50} indicates the shear stress necessary to detach 50% of adhered cells. The *mot* mutants differently from wild-type and and *pilA* mutant, presented also cells at the surfaces which were not surface adhered and washed off at low shear stress $\tau < 0.6$ Pa as evidenced with violet dots. Error bars show ± 1 SEM (N=3). 148

Figure 4.10 Shear stress τ_{50} of PAO1-W, Δ*pilA*, Δ*motAB*, Δ*motCD* and Δ*motABCD* cells on pEGdPEA (pink) and pNGPDA (blue). Error bars represent ± 1 standard deviation (N=3). ****p<0.0001, *p<0.05. Significance was determined by 2-way Anova analysis using Sidak's method for multiple comparisons of differences between the indicated samples. 149

Figure 4.11 A) Confocal images (10×, 0.3) of *P. aeruginosa m-cherry* tagged PAO1-W, Δ*pilA*, Δ*motAB*, Δ*motCD and* Δ*motABCD* after 24 h on pNGPDA (top) and pEGdPEA (bottom). Samples were washed 2× in PBS and 1× in H_2O. Scale bar is 50 µm. B) Quantification of bacterial biomass for surfaces. Error bars show ± 1 standard deviation (N=3). Significance was determined by 2-way ANOVA multiple comparison with Sidak's correction for differences between the indicated samples. ****p<0.0001 and ***p<0.001. Data provided by Dr Jean Dubern. 150

Figure 4.12 WCA measurements on pNGPDA (blue), pEGdPEA (pink) and pNGPDA-co-EGdPEA (orange). Error bars show ± 1 standard deviation (N=9). ***p<0.001, **p< 0.01 and *p<0.05. Statistics assessed using One-way ANOVA with Tukey's multiple correction. 151

Figure 4.13 AFM height images of pNGPDA (blue) and pEGdPEA (pink) for areas of 1×1, 10×10 and 20×20 µm^2. Images were previously line flattened to remove surface curvature and slope. 152

Figure 4.14 Determination of the root mean square roughness (nm) of the at 1 μm^2, 100 μm^2 and 400 μm^2 from the surfaces in dry conditions. Values are the mean of four images taken over 4 different samples. The error bars equal ± 1 standard deviation (N=4). Significance was determined by analysis of variance 2-way ANOVA and Sidak's post-test comparison for differences between the samples. 152

Figure 4.15 F-D curves of representative experimental runs showing the different degrees of deformation for pNGPDA (blue) and pEGdPEA (pink) in dry conditions (n=169). 153

Figure 4.16 Biofilm biomass *vs* shear stress τ_{50} of PAO1-W wild-type (blue), pili (green) and flagella stators mutants (violet, orange and black, for *ΔmotAB*, *ΔmotCD* and *ΔmotABCD* respectively) on pNGPDA. The error bars equal ± 1 standard deviation (N=3). Linear fit (y = m*x + b) yields m = 0.5 and b = 2.4. R^2 = 0.98. 158

Figure 5.1 Possible SadB involvement in flagellar regulation upon environmental signal in *P. fluorescens*. Image taken from [377]..... 161

Figure 5.2 Confocal images (10×, 0.3) of *m-cherry* tagged *P. aeruginosa* PAO1-W pME6032 (empty vector), PAO1-W pME6032::*sadB*, Δ*sadB* pME6032 (empty vector) and Δ*sadB* pME6032::*sadB* after 24 h on pNGPDA (top) and pEGdPEA (bottom). Samples were washed 2× in PBS and 1× in H_2O. Scale bar is 50 μm. Data provided by Dr Jean Dubern. 165

Figure 5.3 Quantification of bacterial biomass for surfaces of *P. aeruginosa* m-cherry tagged PAO1-W pME6032 (empty vector), PAO1-W pME6032::*sadB*::, Δ*sadB* pME6032 (empty vector) and Δ*sadB* pME6032::*sadB*: after 24 h on pNGPDA (top) and pEGdPEA (bottom). Error bars show ± 1 standard deviation (N=3). ****p<0.0001. Significance was determined by Two-way Anova analysis using Sidak's multiple comparison for differences between the indicated samples. 166

Figure 5.4 The impact of *sadB* overexpression on biofilm formation on resistant polymers BnMA, iBMA and TMCHMA respectively. ESEM representative images of PAO1-W pME6032 (empty vector) and PAO1-W pME6032::*sadB*, grown for 24 h on the 3 polymers. Images captured at 5,000× magnification. Overexpression of *sadB* results in the production of biofilm matrix on biofilm resistant surfaces (lower panel) whereas no matrix could be observed when grown on anti-biofilm surfaces as shown in the upper panel. Scale bars are 2 μm. 167

Figure 5.5 Confocal images (10×, 0.3) (A) and quantification (B) of *m-cherry* tagged *P. aeruginosa* PAO1-W pME6032 (empty vector- blue square) (top), PAO1-W pME6032::*sadB* (bottom- violet triangle), after 24 h on BnMA, iBMA and TMCHMA. Samples were washed 2× in PBS and 1× in H_2O. Scale bar is 50 μm. Data provided by Dr Jean Dubern. 167

Figure 5.6 Comparison of *P. aeruginosa* biofilm formation on polymer surfaces by using *mot* mutants overexpressing or not *sadB*. Confocal images (10×, 0.3) of m-cherry tagged *P. aeruginosa* PAO1 Δ*motAB* and Δ*motCD* transformed with pME6032 (empty vector) or pME6032::*sadB* after 24 h on pNGPDA (top) and pEGdPEA (bottom). Samples were washed 2× in PBS and 1× in H_2O. Scale bar is 50 µm..... 168

Figure 5.7 Quantification of bacterial biomass for surfaces of *m-cherry* tagged *P. aeruginosa* PAO1-W Δ*motAB* and Δ*motCD* pME6032 (empty vector) or pME6032:: *sadB* after 24 h on pNGPDA (top) and pEGdPEA (bottom). Samples were washed 2× in PBS and 1× in H_2O. Error bars show ± 1 standard deviation (N=3). Significance was determined by Two-way Anova analysis using Sidak's multiple comparison for differences between the indicated samples. ****p<0.0001. 169

Figure 5.8 Bar graph shows proportion of population for each bacterial strain in different branching division considering pNGPDA (blue) and pEGdPEA (pink). Values obtained considering n>100 doubling events for each of 3 independent replicates (N=3) between t = 1 h to t = 2 h after inoculation. Tukey's multiple comparison test for the different strains on pNGPDA and pEGdPEA considering the three branching divisions is reported in Appendix 6. 171

Figure 5.9 Number of *P. aeruginosa* Δ*sadB* (A), *pME6032::sadB* (B), Δ*motAB pME6032::sadB* (C) cells on pEGdPEA (pink) and pNGPDA (blue) surfaces with increasing shear stress applied through an increase in flow rate. D) Shear stress τ_{50} necessary to detach 50% of PAO1-W wild-type, PAO1-W pME6032::*sadB*, Δ*sadB* pME6032 (empty vector) cells on pEGdPEA. Error bars represent ± 1 standard deviation unit (N=3). Significance was determined by Anova analysis using Tuckey's multiple comparison for differences between samples..... 172

Figure 5.10 Combined DIC and widefield epifluorescence image of *P. aeruginosa* PAO1-W p*cdrA::gfp* after 1 h of exposure to pNGPDA. Scale bar is 2 µm. 173

Figure 5.11 Representative epifluorescence microscopy time series images of *P. aeruginosa* PAO1-W wild-type, *sadB* and *mot* mutants transformed with *cdrA*::*gfp* with or without pME6032*::sadB* over the first 3 h of incubation. Image size is 150 x 150 µm. 175

Figure 5.12 Fraction of *P. aeruginosa* wild-type, stator and *sadB* mutant/overproducing cells expressing *cdrA::gfp* 3 h after inoculation. Images were processed using ImageJ (NIH). A threshold was used to identified bacteria which were expressing c-di-GMP (section 5.2.4). Data are obtained from DIC and epifluorescence microscopy images of bacteria grown on pNGPDA (blue) and pEGdPEA (pink) respectively. Two-way ANOVA with Sidak's multiple comparison has been used to find statistical differences (Appendix 9). 176

Figure 6.1 Sequence of DIC images (10×, 0.3) after 27, 28, 82, 83 min of *P. aeruginosa* exposure to pNGPDA. The aggregates observed derived from planktonic cells and deposited onto the polymer surface. 185

Figure 6.2 Quantification of *P. aeruginosa* aggregate arrival rate using brightfield DIC microscopy (10×, 0.3) on pNGPDA (blue) and pEGdPEA (pink). Aggregates rates were quantified using ImageJ software (version 1.44) (NIH, USA) and an automatic threshold was set to ascertain the pixel that contain aggregates (> 10 µm). Note that the cells were grown under static conditions. Error bars show ± 1 standard deviation (N=3). 186

Figure 6.3 LDA characterisation of *P. aeruginosa* cells and aggregates after 24 h incubation and exposure to pNGPDA, pNGPDA-co-EGdPEA or pEGdPEA (N = 3). Aggregates (>10 µm) were observed for cells cultured in contact with pNGPDA (blue), whereas the cells were predominantly in the planktonic state upon contact with pEGdPEA (pink). An intermediate cell size distribution of planktonic cells and aggregates (up to 10 µm) was observed for the pNGPDA-co-EGdPEA copolymer (orange). 187

Figure 6.4 Confocal (top) and brightfield (bottom) images (63x, 1.4) of *P. aeruginosa* after 4 h on pNGPDA (left), and pEGdPEA (right). Samples were imaged directly in a custom designed holder with YOYO-1 (0.2 µM) and ConA-Alexa 633 (50 µg mL^{-1}). Yoyo-1 stains eDNA (green) and ConA-Alexa 633 EPS (purple). Image size is 100 x 100 µm. 188

Figure 6.5 Quantification of aggregate arrival rate using brightfield DIC microscopy (10×, 0.3) on pNGPDA (blue) and pEGdPEA (pink) with *P. aeruginosa* PAO1-L (left) and *P. aeruginosa* PAO1-N (right) strains. Error bars show ± 1 standard deviation (N=3)..... 189

Figure 6.6 A) Schematic diagram illustrating the conditioned media-exchange experiment. PAO1-W wild-type cells were cultured for 24 h in pNGPDA- or pEGdPEA-coated petri dishes. The cultures were centrifuged at 3,000 rpm for 3 min and filtered through 0.2 µm to remove cells. The centrifuged cells were resuspended in the cell-free conditioned media and further incubated for 1 h at 37 °C prior to LDA. Note: no conditioned media exchange was performed for the respective controls, *i.e.* the cells were resuspended in their original spent media. B) Particle size characterisation of cells upon 1 h incubation in conditioned media exchange using LDA (N = 3). Upon resuspension in the cell-free conditioned medium from pNGPDA, aggregates were observed for the PAO1-W cells grown in contact with pEGdPEA. 191

Figure 6.7 Quantitative analysis of 2-alkyl-4-quinolone (AQ) family signalling molecules (A) and *N*-acylhomoserine lactones (AHLs) (B) in cell-free conditioned medium extracts from cells exposed to pNGPDA or pEGdPEA using LC-MS/MS. Significant differences (One-way ANOVA) are shown as * $p < 0.05$, **** $p < 0.0001$. Error bars show ± 1 standard deviation (N = 6). 192

Figure 6.8 3-oxo-C12-HSL induces aggregate formation. A) Brightfield DIC (10×, 0.45) microscopy time series showing images of PAO1-W cells inoculated in RPMI-1640 medium on pNGPDA (blue) and pEGdPEA with 3-oxo-C12-HSL (1µM) (orange) and without (pink) at 37°C for 12 h (under static conditions). Images shown are at the 12 h mark then from top to bottom every 2-8 h. Settling aggregates were manually identified (yellow objects) and corresponding aggregate areas were measured using ImageJ. Scale bar is 20 µm. B) Quantitative data of area covered by aggregates on pNGPDA (blue) and pEGdPEA with 3-oxo-C12-HSL (1µM) (orange) and without (pink). Significant differences using a one-way ANOVA non-parametric test were found between samples. ** ($p < 0.05$), * ($p < 0.01$). C) Sum of aggregates areas over 12 h of observation on pNGPDA, pEGdPEA with and without 3-oxo-C12-HSL. One-way ANOVA (with post-hoc Tukey test) reveals significant differences expressed as * ($p < 0.05$), ** ($p < 0.01$). Error bars represent ± 1 standard deviation (N=3)..... 194

Figure 6.9 A) Confocal images (10×, 0.3) of *m-cherry* tagged *P. aeruginosa* PAO1-W after 24 h on pNGPDA (blue), pEGdPEA (pink) and pEGdPEA with exogenous 3-oxo-C12-HSL. Samples were washed 2× in PBS and 1× in H_2O. Scale bar is 50 µm. B) Quantification of bacterial biomass for surfaces. Error bars show ± 1 standard deviation (N=3). One-way ANOVA (with post-hoc Tukey test) reveals significant differences expressed as * ($p<0.05$), ** ($p<0.01$). Error bars represent 1 standard deviation (N = 3). 196

Figure 6.10 ESEM representative images of bacteria grown for 24 h on pNGPDA (blue), pEGdPEA with (orange) and without (pink) 3-oxo-C12-HSL (1 µM). Images captured at 10,000× magnification. Scale bar is 2 µm..... 196

Figure 6.11 Diagram outlining the role of 3-oxo-C12-HSL (red dots) in aggregate and biofilm formation..... 197

Figure 8.1 Technical drawing of a custom designed 12 wells holder to run multiple samples (measures are in mm)..... 226

Figure 8.2 Representative colour maps of tracks of *P. aeruginosa* Δ*pilA* (top-left) Δ*fliC* (top-right) and *ΔpilAΔfliC* (bottom) on pEGdPEA measured in situ over 1 h of exposure to surfaces. No motility was observed using *P. aeruginosa* Δ*pilA*. On the contrary, motility was observed using *P. aeruginosa* Δ*fliC*. Thus, motility observed was T4P driven. Scale bar is 10 µm. 232

Figure 8.3 CLSM images captured a t = 0 h (top) and t = 2.5 h (bottom) on pEGdPEA (right) and pNGPDA (left). Scale bar is 10 µm. 232

List of Tables

Table 2.1 List of monomers used in this project. 81

Table 2.2 All strains used in this work. 90

Table 4.1 Young's Modulus values in dry and wet conditions for pNGPDA and pEGdPEA 154

Table 8.1 Sidak's multiple comparison test with different mutants on pNGPDA and pEGdPEA considering the three branching divisions. 228

Table 8.2 Sidak's multiple comparison test with different mutants on pNGPDA and pEGdPEA considering the fraction of cells expressing c-di-GMP. 233

List of Abbreviations

AFM	Atomic Force Microscopy
AMR	Antimicrobial resistance
ANOVA	Analysis of variance
CAP	Covalently attached protein
CLSM	Confocal Laser Scanning Microscopy
DHM	Digital Holographic Microscopy
DIC	Differential Interference Microscopy
DMT	Derjaguin-Muller-Toporov
EPS	Extracellular polymeric substance
ESEM	Environmental Scanning Electron Microscopy
FDR	False Discovery Rate
HCAIs	Healthcare-associated infections
ID	Internal diameter
IMP	Integral membrane protein
INDELs	Short insertions and deletions
LB	Luria Bertani broth medium
LP	Lipoprotein
LPS	Lipopolysaccharide
LTA	Lipoteichoic acid
MCP	Methyl-accepting chemotaxis protein
MRM	Multiple reaction monitoring
MSCRAMM	Microb. surf. components recognising adhesive matrix molec.
OD	Outside diameter
OD_{600}	Optical density at 600 nm
OMP	Outer membrane protein
PCR	Polymerase chain reaction
PDE	Phosphodiesterase
PIA	Polysaccharide intercellular adhesin
PQS	Pseudomonas quinolone signal
QS	Quorum sensing
QSS	Quorum sensing system
Re	Reynolds number
RF	Radio frequency
RMS	Root mean square
RPMI	Roswell Park Memorial Institute Medium-1640
SEM	Scanning electron microscopy
SLIPS	Slippery-liquid infused porous surfaces
SNPs	Single nucleotide polymorphisms

SPR	Surface plasmon resonance
T4P	Type 4 pili
ToF-SIMS	Time-of-Flight Mass Spectrometry
UPEC	Uropathogenic *Escherichia coli*
UV	Ultraviolet radiation
WT	Wild-type
WTA	Wall teichoic acid
XPS	X-ray photoelectron spectroscopy

List of Abbreviations of Molecules

3-oxo-C6-HSL	*N*-(3-oxohexanoyl)-L-homoserine lactone
3-oxo-C12-HSL	*N*-(3-oxododecanoyl)-L-homoserine lactone
AHL	*N*-Acylhomoserine Lactone
BACOEA	2-[[(butylamino)carbonyl]oxy]ethyl acrylate
BnMA	Benzyl methacrylate
cAMP	cyclic adenosine monophosphate
c-di-GMP	3'-5'-cyclic diguanylic acid
DNA	Deoxyribonucleic Acid
EGdPEA	Ethylene glycol dicyclopentenyl ether acrylate
iBMA	Isobornyl methacrylate
MEEMA	2-(2-methoxyethoxy)ethyl methacrylate
NGPDA	Neopentyl glycol propoxylate diacrylate
PAAm	Polyacrylamide
PC	Phosphorylcholine
PDMS	Polydimethylsiloxane
PEEK	Polyether ether ketone
PEGDMA	Poly(ethylene glycol) dimethacrylate
PEM	Polyelectrolyte multilayers
PET	Polyethylene terephthalate
PET-COOH	Carboxylated polyethylene terephthalate
PEG	Polyethylene glycol
PEO	Polyethylene oxide
PI	Propidium iodide
PNIPAAM	Poly(N-isopropylacrylamide)
PPGdA	Polypropylene glycol diacrylate
SAMs	Self-assembled monolayers
SAM	S-adenosyl methionine
TMCHMA	Trimethylcyclohexyl methacrylate
TMPEMEdA	Trimethylolpropane ethoxylate methyl ether diacrylate

TSB Tryptic Soy Broth

List of Abbreviations for Pathogens

P. aeruginosa	*Pseudomonas aeruginosa*
B. subtilis	*Bacillus subtilis*
Pr. mirabilis	*Proteus mirabilis*
E. coli	*Escherichia coli*
A. tumefaciens	*Agrobacterium tumefaciens*
V. cholerae	*Vibrio cholerae*
V. fisheri	*Vibrio fisheri*
S. aureus	*Staphylococcus aureus*
S. epidermidis	*Staphylococcus epidermidis*
C. marina	*Cobetia marina*
C. albicans	*Candida albicans*
C. tropicalis	*Candida tropicalis*

Chapter 1

Introduction

1.1 The Problem: Healthcare-Associated Infections

The rise of antibiotic-resistant bacteria poses a global healthcare threat.[1] In addition to acquiring resistance to antibiotics, many bacteria such as *P. aeruginosa* also form biofilms, *i.e.* surface-associated multicellular communities enmeshed in extracellular polymeric substances (EPS) containing polysaccharides, nucleic acids, proteins, and lipids.[2] It has been estimated that over 80% of microbial infections have a biofilm origin and it has been reported that bacteria within biofilms can resist antimicrobial agents up to 1,000 times more compared to their planktonic counterparts,[3] which makes the eradication of such infections a very challenging task. Consequently, research has mainly focused on the development of new strategies to prevent rather than "cure" biofilm-centred infections.[4-8]

Recently, scientists have made progress in the development of new medical devices and artificial organs that are more adapted to human needs.[9] Notably, almost all of the devices used for medical purposes have been found at risk of bacterial infections and of bacterial biofilm formation (see some examples of medical devices in Figure 1.1).

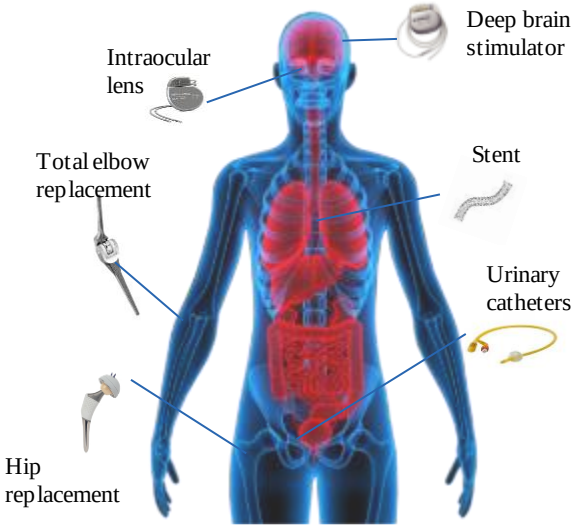

Figure 1.1 Examples of indwelling medical devices. Image adapted from [10].

Healthcare-associated infections (HCAIs) occur in care homes, hospitals or in a patient's own home.[11] A prevalence level of 6.4% and 1,000,000 cases are reported each year in England.[12] The most commonly used materials in medical devices, which differ widely in chemical and mechanical properties, include titanium, stainless steel, cobalt-chromium, and various polymers, including ultra-high molecular weight polyethylene, silicone, and various ceramics.[13] Although, they all have properties that make them ideal for use in specific biomedical applications, such as appropriate modulus of elasticity, resistance and a propensity for tissue integration, they are likely to be the cause and the substrate for developing an infection.[13] A detailed understanding of how these materials increase infection risk is not fully available, but the current problem shows the huge need of developing new biomaterials to prevent such infections.[14]

The massive use of antibiotics associated with HCAIs has led to new multi-antibiotic-resistant strains.[15] In 2014, Lord Jim O'Neill and his team published a review commissioned by the United Kingdom government entitled, "Antimicrobial Resistance: Tackling a crisis for the health and wealth of nations" (the AMR Review).[1] It estimated that, by 2050, worldwide 10 million people will die every year due to antimicrobial resistance (AMR) unless a global response to the problem of AMR is mounted. Figure 1.2 shows deaths annually attributable to AMR (ca. 700,000 in 2014) compared to other major causes of death.

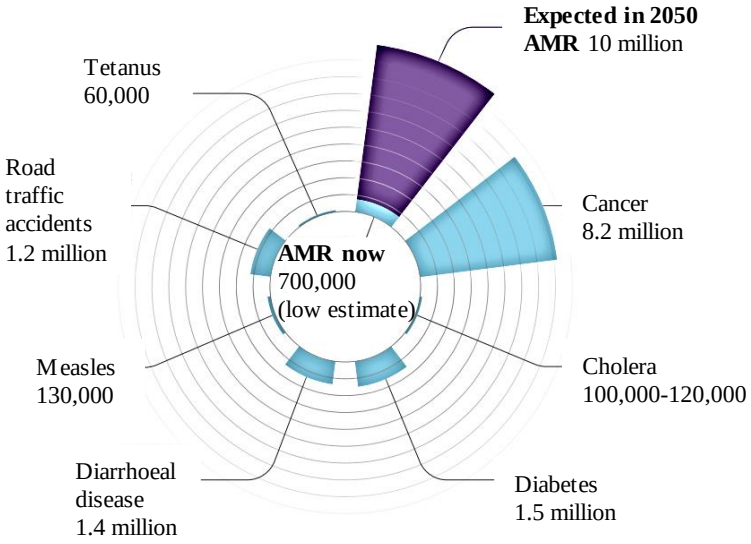

Figure 1.2 Expected mortality caused by AMR. Number of deaths worldwide per year for different causes (blue bars). Expected mortality in 2050 caused by AMR is highlighted in violet. Figure taken from ref. [1].

The risks posed by AMR have continued to intensify in the five years since the report.[16] Numerous funding initiatives have been launched, but concrete successes in addressing the problem remain elusive. We still face two trends that spell potential disaster: only a few numbers of new classes of drugs are currently in clinical phase III trials or already in the clinic, and resistance to existing drugs continues to spread inexorably.[17, 18]

The study of bacteria is of great interest to the scientific world and beyond. The more we learn about bacteria, the more we realise the extent to which they impact on our lives - our health, our habits, and the things around us (both biological and man-made). However, we must not overlook the fact that bacteria can also do much good, especially the ones involved in the microbiome.[19] Bacteria are also used across a range of processes to improve hygiene and fight/prevent contamination, including biodegradation, sewage treatment, cheese and yogurt production, biotechnology, and the manufacture of antibiotics and other chemicals.[20] Given the profound and wide-ranging impact of this crisis on our lives and livelihoods, understanding how and why bacteria attach to materials is important.

The following literature review is aimed at presenting and summarising findings related to bacterial-surface interactions and the development of materials with antimicrobial activity. The importance of studying bacteria is discussed with a focus on the emergence of biofilm production in nosocomial infections in section 1.2. The various steps biofilms are known to include are introduced in section 1.3, whereas the structure and the role of nanomachines such as polar flagella and type 4 pili (T4P) which are bacterial appendages believed to be involved in sensing and exploration of biotic and abiotic surfaces are described in section 1.4. All the key stages from swimming planktonic bacteria able to sense surfaces to biofilm formation are presented in section 1.5, focusing on how these nanomachineries (pili and flagella) interact and trigger bacterial responses upon surface contact. Section 1.6 focuses on the main strategies used to tackle biofilms with an in-depth description of a group of polymers used for preventing bacterial biofilm-centred infections from our laboratories.

1.2 What is a biofilm?

Bacterial biofilms are single or multi-species microbial communities attached to a surface or suspended and covered with an extracellular matrix (Figure 1.3),[21] which are widespread both in nature and in clinical settings. A biofilm can be considered as a prototype multicellular organism.[22-24] Cells in biofilms can differentiate into dormant "persister" cells which resist stress, dividing cells that are vulnerable to stress but reproduce rapidly, stationary cells that build up the biofilm matrix and motile cells which migrate to colonise new areas and form new biofilms, and even cells which die so that the biofilm as a whole can survive.[25]

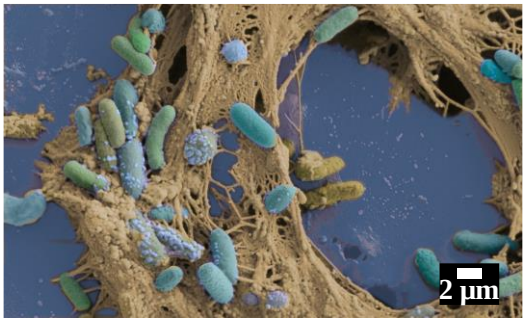

Figure 1.3 Example of a biofilm. EPS matrix is highlighted in yellow. Image adapted from ref. [26].

Bacteria that form biofilms are characterised by a link between localisation and specialisation. In *Bacillus subtilis* (*B. subtilis*) for instance, cells that provide EPS, biofilm, or that express motility, and spore-producing are localised in different regions within the biofilm and similarly in *P. aeruginosa* cells present different patterns in terms of motility and antimicrobial susceptibility.[27, 28]

Bacteria are believed to persist in a biofilm for protection against environmental stresses such as antibiotics, exhibiting either resistance or tolerance.[29] The term "tolerance" is distinguished from "resistance" because the latter is characterised by increased minimal inhibitory concentration (MIC) values and a resistant phenotype also in bacteria dispersed from the biofilm, whereas the former refers to the fact that dispersed planktonic bacteria show sensitivity to antibiotics and display low MIC values.[30] Mechanistically, resistance is due to genetic mutations or resistance gene acquisition which can involve antibiotic-inactivating enzymes, efflux pumps, or affect the molecular target of the antibiotic and allow bacterial survival even if not protected by the extracellular matrix.[31] The most common case of tolerance is physical and it is mediated by restricted penetration of the antibiotics into the biofilm.[32] A number of studies have suggested that biofilm matrices do not inhibit diffusion of antibiotics in general, but that restricted penetration of antibiotics through biofilms may occur in cases where the antibiotics bind to components of the biofilm matrix or the bacterial cell envelope.[30] Biofilms contain bacterial subpopulations characterised by a wide range of metabolic activities. Usually cells in the biofilm core show lower physiological activity in comparison with biofilm-periphery cells. This is due to a gradient and consequently differential consumption of oxygen and nutrients which leaves the cells located in the interior of the biofilm with little or no oxygen and nutrients.[33] Low-metabolic rates are then associated with inactivity of the major antibiotic targets, thus affecting antibiotic efficacy. For instance, either reduced DNA or protein or peptidoglycan biosynthesis alters the efficacy of aminoglycosides, quinolones and beta-lactams respectively.[30]

To successfully form biofilm on a surface, bacteria have to attach and interact with surfaces. However, how bacterial pathogens such as *P. aeruginosa* respond to surface encounters and how they adjust their behaviour to balance virulence, proliferation, and dissemination is poorly understood.

1.3 Bacterial Biofilm Life Cycle

Five distinct phases in the bacterial biofilm's life cycle have been described: first reversible attachment to solid surface, extracellular substrate secretion and irreversible attachment, cell aggregation, biofilm growth and maturation, and biofilm dispersal (Figure 1.4).[34]

The first bacterial surface interaction occurs through either active or passive motion that enables adhering planktonic cells to come closer to solid boundaries. The nature of the initial attachment is not completely clear and it is likely that a variety of physico-chemical and biological factors are involved: surface properties,[35] bacteria appendages[36-38] and species-specific characteristics may all combine with the presence of an organic layer obtained from the growth medium or from bacterial products.[39] Furthermore, in solution there is evidence that adhesion and biofilm formation in some species are influenced by the presence or the depletion of nutrients,[38, 40] variation in temperature or even the absence of oxygen.[23] It is likely that bacteria sense their environment and the specific surface before proceeding to colonisation and biofilm maturation.

After initial reversible and weak attachment, EPS, which contains exopolysaccharides (e.g. for *P. aeruginosa*, Psl, Pel and alginate), nucleic acids, proteins, and lipids, is produced to achieve a stronger adhesion (irreversible attachment) resisting surface removal. In addition to EPS, bacteria display macromolecules on their surfaces (adhesins)- which are either protein or glycan mediated- that are devoted to strengthening the adhesion after the irreversible stage. Adhesins will be described in more detail in section 1.5.3.2. Mutants defective for specific adhesins, like the polysaccharide adhesin β-1,6-*N*-acetyl-D-glucosamine (Δ*pgaC*) in *Escherichia coli* (*E. coli*) were unable to adhere

irreversibly to a surface.[41] Moreover, bacteria are known to use complex networks of intra- and extra- cellular molecules to communicate and to respond to internal and external signals that regulate the irreversible adhesion stage.[42] One of these networks is termed quorum sensing (QS). A second messenger, cyclic-di-GMP (3'-5'-cyclic diguanylic acid) or (c-di-GMP) mediates the switch from reversible to irreversible attachment in many different Gram-negative bacteria. High intracellular concentrations of c-di-GMP regulate EPS production,[43, 44] enhancement of biofilm formation and inhibition of bacterial motility,[36, 45, 46] although the multiple mechanisms involved are not completely understood.[47-49]

After irreversible attachment, bacteria accumulate on the surface, begin to organise themselves into microcolonies[50] and later develop into mature structures composed of hundreds of cells enmeshed within EPS. In addition, biofilms can exist with different topographies (flat, mushroom-shaped stalks and streamers in flow[51-53]) that are species specific and influenced by environmental cues such as nutrient availability and flow. Afterwards, cells are released into the bulk as suspended planktonic forms. Environmental factors and intracellular signalling can trigger or modulate this process.[54, 55]

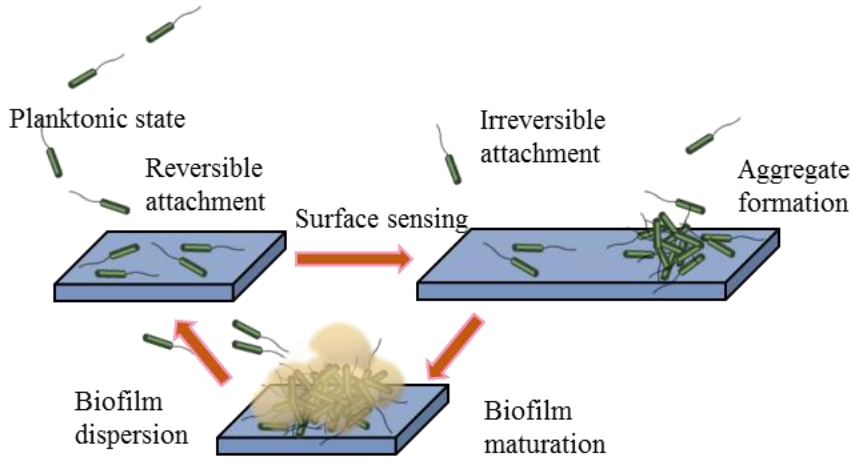

Figure 1.4 Schematic life cycle of *P. aeruginosa* from planktonic to surface sensing, biofilm formation and dispersal. Image adapted from ref. [56].

1.4 Bacterial Surface Appendages

Bacterial motility plays a crucial role in enabling bacteria to reach surfaces and start colonising.[57] However, the switch to a sessile form is a pivotal factor in both bacterial colonisation and biofilm dispersal.[58] In order to evaluate swimming and attachment behaviour it is necessary to understand the bacterial surface appendages involved with these processes.

Filamentous structures have been observed on Gram-negative bacterial surfaces since the introduction of electron microscopy. Bacteria, depending on the species, can deploy two types of protruding appendages (Figure 1.5): thin and unbending "fimbriae" or "pili" and undulating and flexible flagella two or more times longer than the bacterial body length.[59]

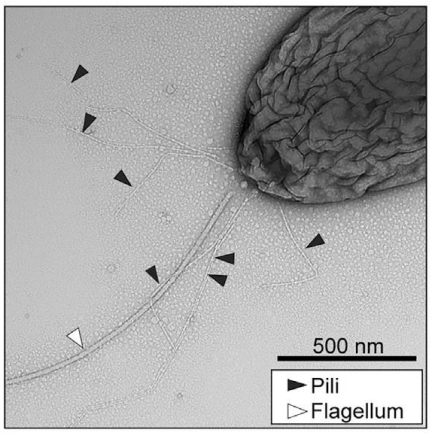

Figure 1.5 Representative electron micrograph of *P. aeruginosa*. Pili (black arrows) and flagellum (white arrow) are highlighted. Image taken from ref. [60].

1.4.1 Pili

Pili are organelles that, together with flagella, can mediate adhesion to biotic or abiotic surfaces. Their activity has been shown in conjugation, bacterial colony formation, and surface motility and biofilm formation.[59] These pili (Latin for 'hair') or fimbriae (Latin for 'fiber') present surface molecules called adhesins at the external apices. Pilins are small 15 – 25 kDa sub-units that are organised

into groups of hundreds or thousands and define the basic structure of pili known as the ‘fimbrial rod’ or ‘pilus shaft’.
Different assembly pathways define categories of pili in gram-negative bacteria. In this chapter, only the two most common pili pathways and curli are described.

a) The bacterial chaperone–usher pathway (Cup) is deployed to construct and release multi-subunits.[61] The type I and P pili, which are expressed by bacteria,[62] especially those involved in colonisation and infection of the urinary tract, are the most well-known pili belonging to this group (Figure 1.6). Notably, fimbriae (PMF) using the same type of chaperone-usher system are produced by *Proteus mirabilis* (*Pr. mirabilis*), an important etiological agent in different urogenital infections.[63] The *fim* and *pap* operons, respectively (Figure 1.6A) are respectively responsible for the assembly and release of P and type I pili.[62, 64] The pilus subunits (pilins) are released into the periplasmic space, whereupon a specific chaperone binds the subunits preventing premature assembly of pilins. The pilin passage through the outer membrane is mediated *via* a pore formed by the usher protein, hence, the assembly is then released into the outer membrane.[65] These fimbriae have different functions such as promoting attachment to inert surfaces or mediating adhesion to host tissues or facilitating escape from host defence systems, e.g. by shielding antigens that can be recognised. In *P. aeruginosa* Vallet *et al.* identified 5 fimbrial (*cup*) gene clusters termed *cupA* to *cupE*.[66] These clusters vary in regulation as well in composition and function. Whereas the *cupC* operon encodes the pilin, chaperone and usher, the other clusters are likely to encode additional fimbrial subunits which contribute to biofilm formation or alter adhesive properties. The expression of *cup* genes is tightly regulated and most are not expressed during growth in liquid culture.[67]

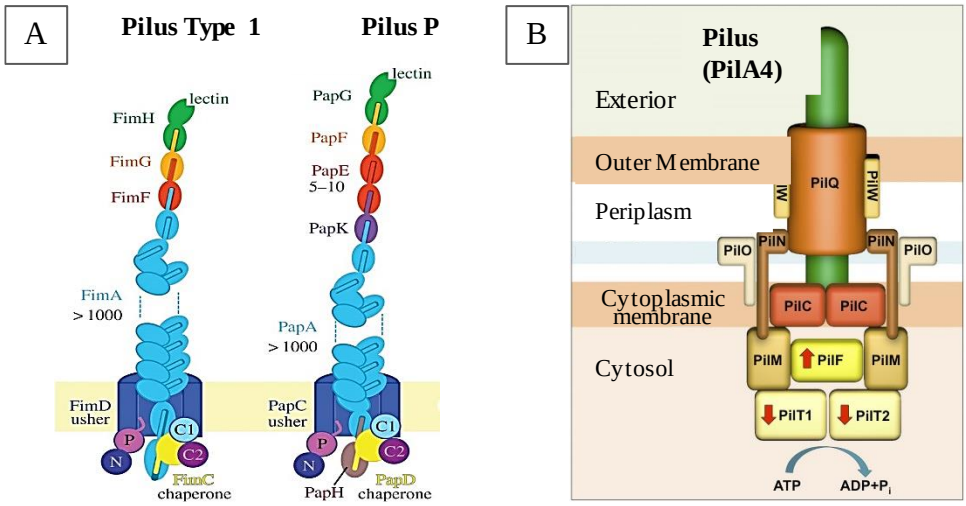

Figure 1.6 A) The type 1 pili and the P pili from uropathogenic *Escherichia coli* (UPEC) obtained from the combination of different subunits (Fim and Pap). Figure from ref. [59]. **B)** Schematic of the T4P machinery in *Thermus thermophilus*. Figure from ref. [68].

b) Type IV pili (T4P) are important in bacterial pathogenesis as they mediate attachment to host cells, aiding bacterial colonisation and supporting biofilm formation.[69] These pili are found in many Gram-negative bacteria, including *P. aeruginosa*. T4P are thin fibres (6 – 8 nm wide)[70] characterised by flexibility and tens of microns in length, which often combine to form characteristic "bundles" at one or both cell poles of *P. aeruginosa*. In addition, T4P are relevant in a non-dependent flagella form of movement termed twitching motility. The movement, as described in the section 1.5.1.2, is due to the ability of T4P to contract, exerting a pulling force on the cell body.[71] Several proteins encoded within *pil* gene clusters include AAA-ATPases that are mainly implicated in the assembly and disassembly of the T4P pilus (Figure 1.6B).[68, 72] T4P are generally composed of a major pilin subunit, PilA, extended by the motor PilB, and retracted by the motors PilT and PilU. With respect to virulence, T4P promote attachment to host cells[73] and induce Vfr, a global regulator of virulence gene expression in *P. aeruginosa* PAO1 lineage strains.[74] PilA is synthesised as a preprotein with an N-terminal type III signal peptide and secreted *via* the Sec system.[75] The signal peptide is then removed by the prepilin peptidase PilD,[76] leaving the mature pilin anchored in the cytoplasmic membrane by an N-terminal hydrophobic α-helix.[77] During T4P extension, PilA is incorporated at the base of a T4P from this cytoplasmic membrane

reservoir; T4P retraction involves the removal of PilA subunits from the base of the T4P and their re-insertion into the cytoplasmic membrane.[78]

c) Bacteria are sometimes protected from unfavourable conditions by expressing another type of protein on their cell surfaces called curli which are extracellular protein fibre analogues of functional amyloids. As observed in 1989 on *E. coli*, curli consist of subunits of the pilin, CsgA (or curlin). The nucleation-precipitation pathway is the model by which soluble curlin is secreted into the extracellular environment through a membrane lipoprotein and thus, deposited in the outer membrane.[79]

Only recently, the structures of pili in Gram-positive bacteria have been described.[80] Flexible and much longer pili (length to 3 mm) than in gram-negative bacteria have been identified in different strains of *Streptococcus* while other gram-positive bacteria present shorter and thinner appendages. Pilins are fibrous proteins that constitute the structures of these organelles and thereupon they have been considered to have adhesive function.[81] As the subject of this thesis is *Pseudomonas*, pili in Gram-positive bacteria will not be discussed further.

1.4.2 Flagellum Structure

As shown in Figure 1.7A, three assembled elements compose a flagellum: a long helical filament, a short curved structure called the hook, and a basal body.[82] The basal body, which is defined by a motor, central rod and several different rings, is implanted in the cytoplasmic membrane, whereas the hook and the filament extent out of the cell. The flagellar filament, which consists of 11 proteinaceous fibrils that form a cylinder, is typically a left-handed helix of normally 5 to 10 μm of length and 20 nm thickness. The filament is linked to the motor through the cylindrical hook. In peritrichous flagellated bacteria such as *E. coli*, the hook also plays a role in organising the filaments in order to create a bundle.

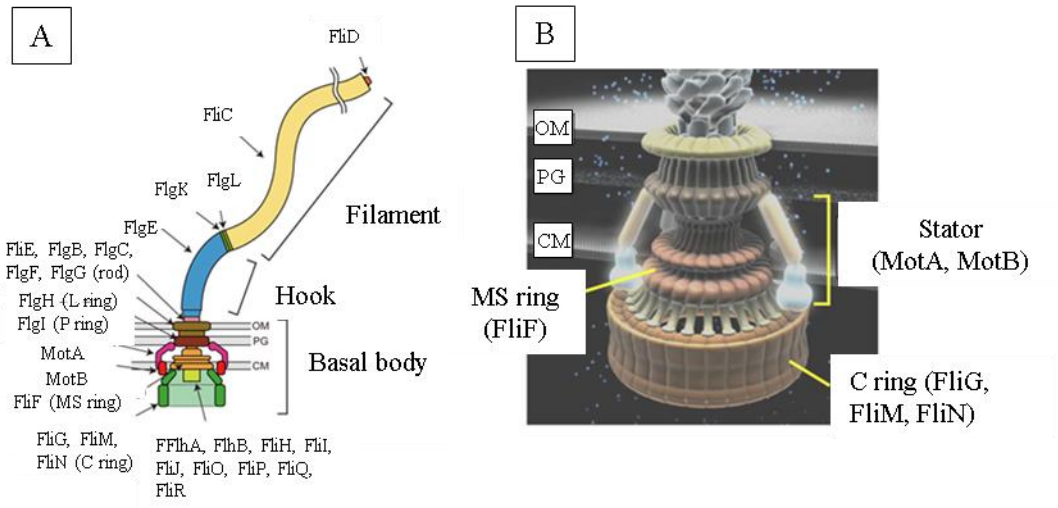

Figure 1.7 Schematic diagram of **A)** a bacterial flagellum and **B)** the flagellar motor. Figure adapted from ref. [82].

The flagellum can rotate in both directions (clockwise and counter-clockwise) which causes a change in swimming direction leading to different motility patterns as described in section 1.5.1. Motility switching is controlled *via* the C ring which is composed, as described in Figure 1.7B, of three proteins.[82, 83] The rotary motor is coupled with membrane ion flux to exert rotation. MotA and MotB are the stator proteins which form the ion-conducting channel complex that generates torque. Although MotB is likely to tether the stator to the cell wall, anchoring is not permanent and there is dynamic turnover of MotB.[84] The stator interacts with FliG, FliM and FliN.[85] The electrostatic interactions between MotA and FliG determines the linkage between ion flow through the $MotA_4B_2$ complex and rotation. The number of stators recruited is variable up to 11 units in *E. coli*.[86] In *E. coli* this number can be increased in conditions of high load. In *B. subtilis*, dual stators function under different conditions, namely H^+ and Na^+ flux that enable either fast swimming at high pH and high viscosity respectively. *P. aeruginosa* possesses a single polar flagellum made of one rotor and two sets of H^+ driven MotAB-like stators, PA1460/1461 and PA4954/4953 encoded in two gene operons (named by Kuchma *et al. motAB* and *motCD* respectively). In contrast with the complete elimination of motility when both MotAB and MotCD are deleted, mutants in either of the two stators have been described to possess slightly diminished wild-type rates of swimming motility in bulk liquid.[87] A single stator is sufficient to underpin swimming motility. However, *motCD* mutants are compromised in swarming/swimming motility

under high load conditions whereas *motAB* mutants display swarming motility similar to the wild-type.[88] Swarming is a rapid multicellular movement of bacteria on solid or semisolid surfaces mediated by flagellar rotation.

1.5 From Swimming to Biofilm Formation: Key Stages in Biofilm Formation

Although numerous studies have focused on either bacteria in the planktonic state or in biofilm state,[89] the transition from one state to the other remains poorly fully understood. This may prove fundamental to determining the best approach to prevent biofilm formation.

Swimming bacteria are found in soil, oceans, biological tissues and organs, which are complex 3D environments. Bacterial motility patterns may provide relevant information about different environments and species: species differences in motility patterns,[90] the mechanism of chemotaxis,[91] the regulatory genes,[92] the network elicited by external chemical stimuli[93] and the mechanism by which bacteria sense surfaces.[94] Motility plays a pivotal role in the life cycle of certain bacteria and is important for biofilm formation, biofilm dispersal and virulence.[95] Thus, studying motility in different types of bacteria may be of crucial relevance not only when it comes to acquiring a new understanding of how surfaces impact on bacterial movement, but also to develop more detailed models of biofilm regulation.

1.5.1 Bacterial Motility

1.5.1.1 Flagellar Motility in Swimming Patterns

The first contribution of flagella motility to biofilm formation is to provide a means to allow bacteria to get close to surfaces and to overcome the eventual near-surface repulsive effect enhancing surface adhesion and contact with other bacteria (more details in section 1.5.3.1). Despite the great number of different bacterial species, only a few flagellation patterns have been observed (Figure 1.8). Localisation of the flagellum is either restricted to the cell pole(s) or along

the lateral side of the cell. Flagellar numbers differ from a minimum of 1 to a maximum of 25 for *B. subtilis* to as many as several hundred in swarming cells of *Pr. mirabilis*.[41] Major flagellation patterns are (a) monotrichous with one flagellum at one cell pole (e.g, *Pseudomonas* and *Vibrio*), (b) amphitrichous with a flagellum for each cell pole (c) lophotrichous with a tuft of flagella at one pole (e.g. *Helicobacter*, other *Pseudomonas* species and *Agrobacterium*) and (d) peritrichous having flagella uniformly distributed over the body surface (e.g. *E. coli* and *Pr. mirabili*s).[96]

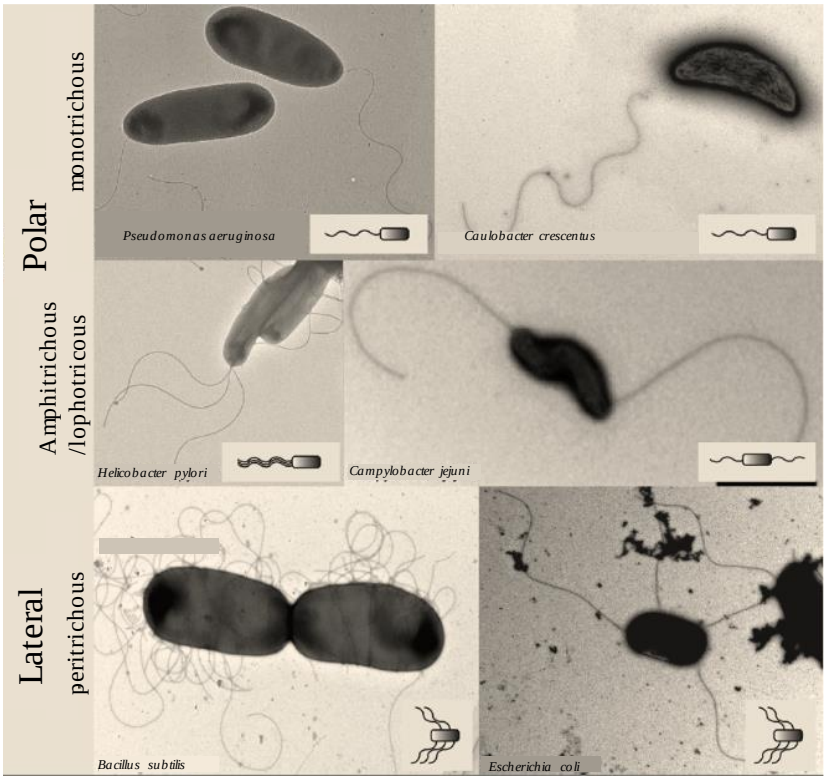

Figure 1.8 Different bacterial species display differences in the position and number of flagella. Electron micrographs and the insets describe the structure of polar-flagellated *P. aeruginosa*, *Caulobacter crescentus* (*C. crescentus*), the lophotrichous *Helicobacter pylori*, the amphitrichous *Campylobacter jejuni* and the peritrichously flagellated *B. subtilis* and *E. coli*. The insets schematically indicate the respective patterns. Figure taken from ref. [96].

Monotrichous bacteria (e.g. *P. aeruginosa*) have been reported to exhibit 5 different motility patterns as meander, oscillation, helix, pseudo-helix, and twisting and can *switch* between them.[97] However, in different environmental conditions, bacteria can adjust their orientation and propel themselves in new directions. Peritrichous *E. coli* and monotrichous *P. aeruginosa* modify direction in their movement by similar mechanisms through reversal of flagellar rotation.

Reversal causes tumbling in *E. coli* or moving forwards in *P. aeruginosa* respectively. During a run, the peritrichous flagella of *E. coli* form a helical bundle rotating counter-clockwise while tumbling occurs *via* the opposite rotation of flagella.[91]

Different studies have demonstrated that physical and chemical properties are implicated in the modification of bacterial motility.[98] Using the analysis of *E. coli* swimming close to generic surfaces, a model in which the physics of swimming is associated with hydrodynamic interactions has been derived.[99] In fact, *E coli* swim in circular trajectories near solid boundaries as a natural consequence of force-free and torque-free swimming and the radius of curvature of the circular paths has been correlated with swimming velocity (Figure 1.9). The flagellar motor is remarkable in its ability to efficiently convert the free energy stored in the transmembrane electrochemical gradient into mechanical work: while man-made engines lose significant amounts of energy to heat, the bacterial flagellar motor operates at close to 100% efficiency.[100] Rotating at approximately 300 Hz (or 18,000 rpm; compared to the upper limit of a typical car engine's rotational speed of 6,000 rpm), the *E. coli* motor can output power of approximately 1.5 x 10^5 pN nm s^{-1}[101] and propel bacterial cells at a speed up to 100 ms^{-1} that is up to 100 body lengths per second!
The motor's fundamental role in bacterial locomotion makes it central for several biological processes, including chemotaxis, surface swarming, biofilm formation and the interaction with host cells and tissues.

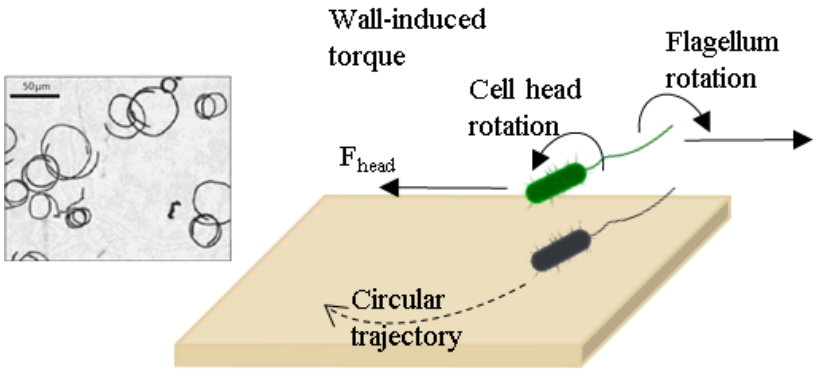

Figure 1.9 Circular trajectories are determined by a wall-induced torque acting on the cell head and flagellar bundle. The inset presents trajectories of a non-tumbling mutant of *E. coli* (HCB437). Figure adapted from [102].

Little is still known about how bacteria modify their movements according to chemically distinct surfaces and how motility patterns are associated with stages in the bacterial life cycle such as attachment and biofilm formation. It is only in recent times, thanks to the advent of the usage of digital holography, that it is possible to acquire new data about how bacteria swim within a 3D space.

Vater *et al.* demonstrated different motility patterns for the highly motile *P. aeruginosa* strain P154.[97] The authors extracted 35 trajectories of swimming *P. aeruginosa* with a track length between 1 and 3 min (Figure 1.10A-B). Figure 1.10C-D show five identified motility patterns and their distribution. The first motility mode was termed "meander", a smooth and continuous trajectory without sharp changes of direction, which, on the contrary, were observed in the "oscillation" trajectory. "Helical" and "pseudo-helical" trajectories displayed consecutive loops that were preferentially left-handed (70%) on a straight axis (helical) or on a curved axis (pseudo-helical). The twisting was characterised by randomly entangled loops without sharp directional changes. More than half of the bacteria (70%) moved with meander and twisting patterns. In order to consider directionality of the motility patterns, Vater *et al.* calculated the ratio between straight line and curvilinear speed for a selected segment. Straight line speed was measured as the distance between the first and the last point of the segment divided by its duration, whereas the curvilinear speed was obtained as the mean speed considering the lengths of all of the trajectories.

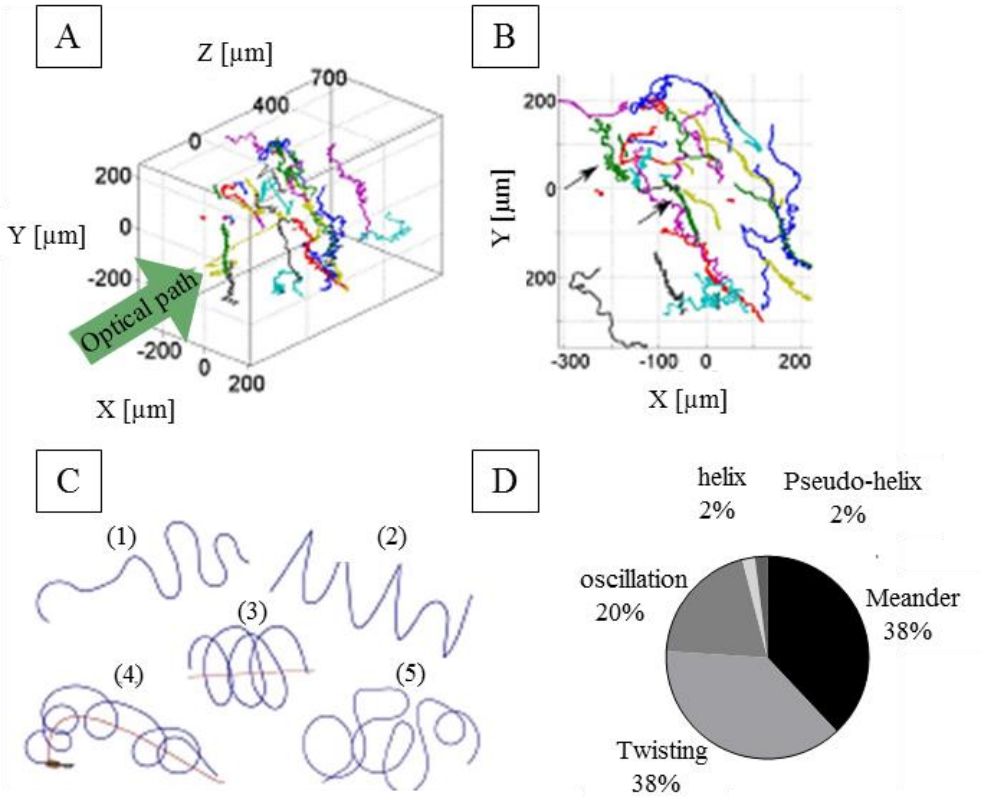

Figure 1.10 3D motility patterns made by *P. aeruginosa*. **A)** 3D schematic of trajectories obtained; **B)** xy-projection of trajectories; **C)** representation of 5 motility patterns; **D)** frequency of each motility mode. Values obtained over 35 trajectories. Figure taken from [97].

Surface-anchored spinning occurs when the flagellum adheres to a surface but continuously rotates on its axis (Figure 1.11). The grounded endpoint of the flagellum causes the bacterial cell to rotate instead. Spinning has been observed to be followed by detachment,[103] whereupon flagella and pili mediate a coordinated sequence of detachment to modify the cell orientation from horizontal to vertical and then detachment. Conrad *et al.* determined that total detachment probability for flagellum-deficient (Δ*fliM*) and T4P-deficient (Δ*pilA*) cells was much smaller than that of the wild-type, suggesting that detachment events decrease in frequency in the absence of appendages.[103] This also shows how pili and flagella may play a crucial role in surface sensing and adhesion.

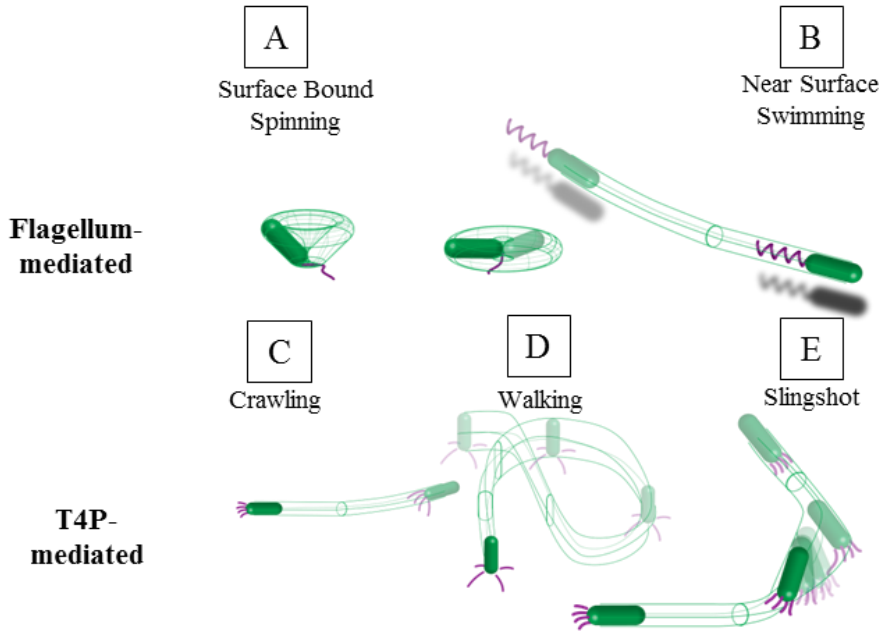

Figure 1.11 Flagella and T4P-mediated motility in *P. aeruginosa*: **A)** spinning; **B)** swimming. T4P mediated motility: **C)** crawling; **D)** walking; **E)** slingshot. Figure adapted from ref. [103].

1.5.1.2 Surface Motility Mediated by Pili

Bacterial motility is not limited to the use of the flagella and can be driven by other organelles, like pili. *P. aeruginosa* and other bacteria use T4P to effectuate bacterial movement by twitching,[69] which has been observed in biofilms.[104] Pili drive cell motility by pulling the bacterium along the surface through cycles of adhesion and retraction. Tensions of at least 10 pN have been shown to be necessary to pull cells forward by pili withdrawal.[105] *P. aeruginosa* movement has been classified into three different motility modes which deploy T4P on surfaces: crawling, walking and slingshot (Figure 1.11).

In 2011, Conrad *et al.* used brightfield and epifluorescence microscopy to individually track cells in 2-dimensions and quantitatively describe these surface-based motility mechanisms. Through a thorough analysis of their data they described two new modes of movement across the surface: horizontal crawling and vertical walking, which differed in bacterial position, speed, distance and directional persistence. These results indicated that there exist two

different modes of travel: one that resulted in long distance travel (crawling), and another used to more rapidly explore local surroundings (walking).

Jin *et al.* used a Δ*fliM* isogenic mutant of *P. aeruginosa* strain ATCC 15692 to clarify the mechanisms of T4P-driven twitching movement.[106] Over 12,000 tracks were observed in sterile flow-cells in FAB medium. They identified slingshots as distinct rapid (20 times faster than crawling speed) directional changes within cells otherwise exhibiting crawling motility. As shown in Figure 1.12 this sudden change in direction was assumed to be due to the fast release of a lateral T4P previously under tension.[106]

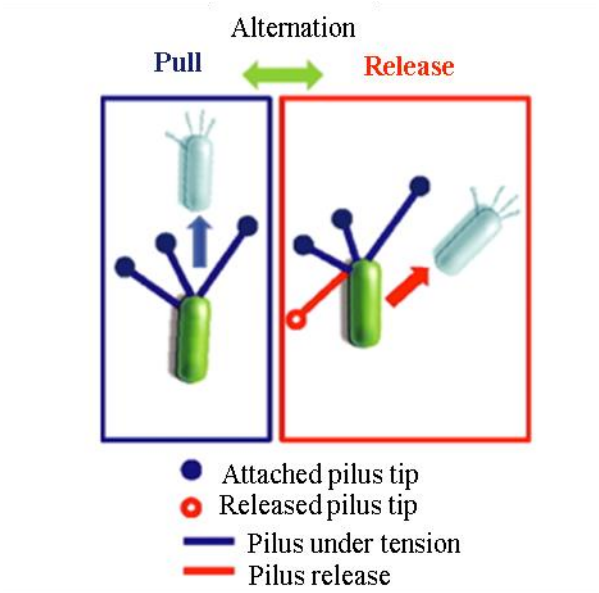

Figure 1.12 Mechanism for *P. aeruginosa* of crawling motility by pili-mediated pulling or by a slingshot obtained by the release of a T4P. Figure taken from ref. [106].

Rodesney *et al.* also compared T4P-driven motility in *P. aeruginosa* PAO1 strain wild-type with an isogenic Δ*pel* mutant which does not produce Pel polysaccharide. They observed that both strains retained surface motility, demonstrating that pilus function is not lost in the absence of *pel*. They further noted that wild-type cells moved about 25% more slowly on glass than the Δ*pel* mutant and that this discrepancy was even greater for cells that spend most of their lifetime lying flat.[107] From these findings they concluded that Pel coated cells and caused friction between the cells and surface. As a proxy readout for tilting, they looked at the projected aspect ratio in each frame. In their experiment

a newly divided cell lying flat on the surface has an aspect ratio of about 2. Therefore, a projected aspect ratio less than 2 indicates unambiguously that a cell is tilting. Interpretation of aspect ratios larger than 2 is ambiguous, because these cells may be either lying flat or longer cells tilted up. For each cell, they then computed the fraction of its lifetime spent unambiguously tilting, with 1 being unambiguously tilted up for the whole trajectory, and 0, lying flat for the whole trajectory.[107]

1.5.1.3 Motility within Biofilms

Flagella driven motion also allows biofilm dispersal where bacteria transit to the planktonic state from sessile structures to spread and colonise other surfaces.[98] Although most bacterial cells in biofilms live in a sessile state without expressing flagella, a subpopulation of microorganisms (0.1-1% of the cells) has been discovered inside a biofilm exhibiting swimming motility. These bacteria infiltrate into the matrix and cause spreading of nutrients by tunnelling.[108] During biofilm maturation the down regulation of flagellar filament genes prevents motility disrupting the microcolony structure.[88] In many bacteria species, c-di-GMP is one of the molecules responsible for the switch from the planktonic state to the sessile.[88, 109]

Flagella are also decisive for the morphology of the structures that bacteria can build as colonies. For instance, flagellar deficient mutants of *Agrobacterium tumefaciens* are unable to form biofilms.[110] In motile bacteria, the homogeneity and uniformity of biofilms can be determined by the cells ability to move. In fact, mutation of flagella regulatory genes in *V. cholerae* causes rugose patterns in colonies instead of the smooth-edge formed by the wild-type strain (WT). However, the role of flagella in bacterial attachment is still not fully understood.

T4P and associated twitching motility also modulates the morphology of biofilms (Figure 1.13), causing highly irregular edges or affecting smooth, rounded microcolonies with T4P defective (Δ*pilA*) strains of *P. aeruginosa* strain ATCC 15692.[36, 111] These data confirm the idea that twitching allows cells to move along surfaces and plays a crucial role in biofilm maturation.

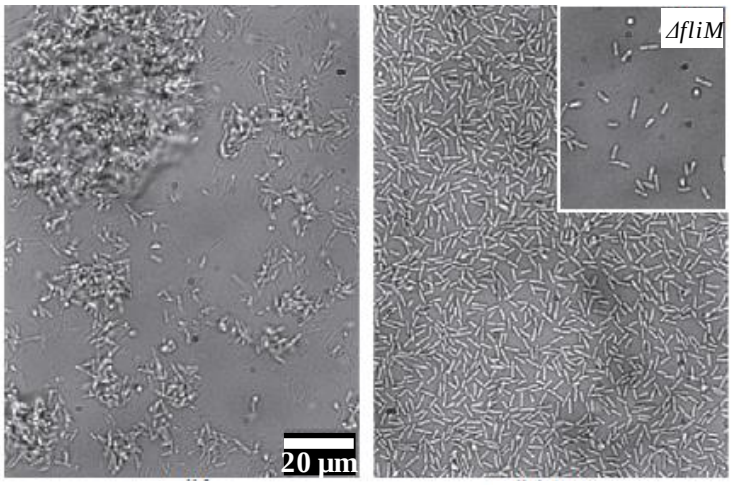

Figure 1.13 Representative micrographs of *P. aeruginosa* strain ATCC 15692 T4P deficient mutant Δ*pilA*, WT, and flagella deficient mutant Δ*fliM* biofilms on glass coverslips. Large cluster are observed with twitching deficient bacteria, indicating that bacteria are not able to cover wider areas. The flagella deficient mutant is not able to create biofilm and cell clusters. Image taken from ref. [103].

1.5.2 Surface Sensing Systems

1.5.2.1 Flagella in Sensing Surfaces and the Role of Motors

Chemotaxis is the description of motility exhibited by bacterial cells towards nutrient rich areas or away from noxious regions. Bacteria are able to sense different types of signals: chemicals, pH, temperature, viscosity and osmolarity. Temporal sensing is the mechanism by which bacteria, considering their very small dimensions, are thought to be able to compare concentrations of a specific compound with its concentration at different times[112] although Thar and Khul provided evidence that bipolar flagellated *Vibrio* can sense chemical gradients spatially.[113] As described in section 1.5.1.1, peritrichous bacteria such as *E. coli* swim with a run and tumble motility pattern; the time interval between two consequent runs is about 1 s. This period is altered by the presence of chemical or physical cues. The direction of flagellar rotation is influenced and regulated by chemosensory systems regardless of the variable position and number of flagella.[114] Bacteria are able to sense environmental signals on solid or semi-solid surfaces, including host-derived cues, and in the literature there are many studies related to the process of chemotaxis (see review from Wadhams and Armitage [115]). Some organisms (*e.g.* quadriflagellated zoospores) can

determine the suitability of a surface for adhesion and decelerate before contact,[116] but there is yet no evidence for bacterial motility correlating with surface chemistries.

Mechano-sensing is an ubiquitous instrument that translates environmental mechanical stimuli into biological responses which bacteria can utilise.[117] In *Vibrio parahaemolyticus* physical contact may cause the cell to switch from a swimming state to an alternative surface mode of translocation such as swarming.[118] Conditions impeding movement of the swimming flagellum, such as contact with surfaces or highly viscous liquid media, may induce the expression of several lateral flagella deployed to induce swarming motility. The same cellular differentiation into specialised swarmer cells has also been shown in *Pr. mirabilis* with either increased viscosity or deletion of flagellar structural genes.[119]

Mechano-sensory flagella are used by *V. cholerae* for initiating biofilm formation. In fact, contact with a solid boundary causes the flagellar motor and the associated ion flow to stop, leading to a temporary hyperpolarisation of the cell membrane. This has been ascribed as a critical event in the transition to permanent adhesion.[120] In *C. crescentus* and *A. tumefaciens*, surface contact stimulates secretion of a specialised adhesive polysaccharide involved in irreversible attachment called ‘holdfast’.[121]

Recent studies have shown the importance of the rotary flagellum in mechano-sensing in *Pseudomonas*.[122-124] The flagellar motor has been shown to play an important role in rapid surface attachment by translating a mechanical signal into a rapid increase in c-di-GMP.[60] The MotAB stator, but not the flagellar filament, is required for tactile responses leading to FimW activation and subsequent T4P assembly and attachment consolidation.[60] MotCD has also been described to disengage from the flagellar motor in the presence of high intracellular c-di-GMP concentrations and to interact with the diguanylate cyclase SadC.[125] This regulation implies a positive feedback loop in which c-di-GMP signalling events cause MotCD stators to disengage from the motor; the latter stimulate c-di-GMP production to reinforce the biofilm mode of growth

promoting the motile-sessile transition by inhibiting flagellar motility and increasing the production of exopolysaccharides to form the biofilm matrix.[126, 127]

In *Staphylococcus aureus*, an example of a non-flagellated bacterium, adhesion force to substratum surfaces have been found to control EPS release and biofilm growth through *icaABCD* regulation. Expression of *icaABCD* genes which are responsible for production of the polyGlcNAc extracellular matrix decreased with increasing adhesion forces.[128]

1.5.2.2 Sensing Surfaces by Pili

P. aeruginosa deploys T4P to interact with surfaces, enhancing cell adhesion, twitching motility and virulence in host tissues.[69, 129] Different mechanisms were proposed for mechano-sensing including the detection of mechanically induced modifications in T4P by the Pil-Chp chemosensory system.[74, 130] This system leads to the activation of another secondary messenger cyclic adenosine monophosphate (cAMP) and subsequent virulence activation.[131] Another mechanism of pili-mediated surface sensing involves the pilin PilY1 either *via* the FimS-AlgR two component sensor regulator system[132] or *via* T4P-dependent activation of the diguanylate cyclase SadC which synthesises c-GMP.[107] These publications contribute to a well-established model wherein, surface contact of motile bacteria *via* few pre-existing T4P mediates adherence and a rapid cAMP response, which, with a positive feedback loop upregulates T4P (and PilY1) production, consolidates attachment, and stimulates virulence gene expression. In a consecutive T4P-dependent step, c-di-GMP would then be upregulated to coordinate all these steps.

1.5.2.3 Cyclic di-GMP: Second Messenger Extraordinaire

Cyclic dinucleotides such as c-di-GMP are versatile signalling molecules that control various important biological processes in many bacteria.[133] Known since 1987, c-di-GMP is now recognised as a second messenger that coordinates

diverse aspects of bacterial cellular processes.[134] The c-di-GMP, as shown in Figure 1.14, is synthesised from two GTP molecules by diguanylate cyclase (DGC) and is degraded by phosphodiesterase (PDE). The genome of *P. aeruginosa* PAO1 encodes 41 c-di-GMP proteins predicted to participate in c-di-GMP metabolism.

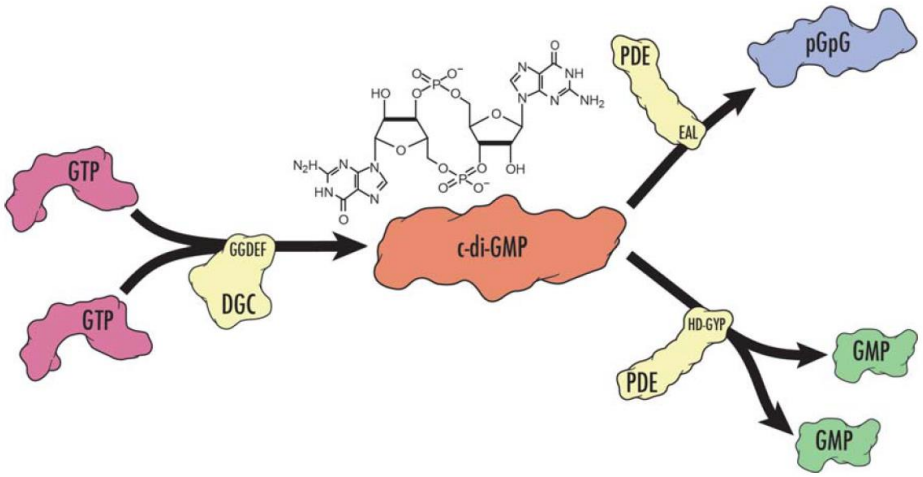

Figure 1.14 The structure of c-di-GMP is shown (center). Enzymes known as DGCs that carry a conserved GGDEF domain, synthesised c-di-GMP from two molecules of GTP. This second messenger can be degraded by two families of PDE: those with an EAL domain which linearise the molecule to pGpG, and other proteins with HD-GYP domain which generate two molecules of GMP. Figure taken from [133].

The enzymatic control of c-di-GMP concentration allows bacteria to more rapidly adapt to environments than signals that engage transcription and translation machineries.[135] c-di-GMP is therefore controlled in time and space by the coordinated control of makers and breakers. However, the c-di-GMP pathways ultimately rely on the respective effectors that bind to c-di-GMP and on their downstream targets.[134] In many bacterial species, including *P. aeruginosa*, high intracellular c-di-GMP level results in the repression of flagellar motility genes and the promotion of gene involved in production of biofilm matrix components, such as Pel, Psl, proteins and eDNA.[136, 137] *Pseudomonas* has at least two distinct surface sensing systems, the Wsp and the Pil-Chp systems as described in section 1.5.2.2, that when activated, lead to biofilm formation. The Wsp system senses an unknown surface-related signal through WspA, which is a membrane-bound protein homologous to methyl-accepting chemotaxis proteins (MCPs). Activation of this system stimulates phosphorylation of the diguanylate cyclase WspR which leads to increase c-di-GMP synthesis.[138]

Many bacterial intracellular regulatory systems, which are involved in the response of bacteria to environment stimuli or in the switch from one lifestyle to another, belong to a large class of proteins called two-component systems (TCSs). TCSs typically consist of two elements: a sensor kinase and a response regulator. The sensor kinase is often a membrane bound protein that enables bacteria to monitor environmental stimuli such as pH, osmolarity, temperature and nutrients. The response regulator receives the signal transmitted from its cognate kinase and then acts as a transcriptional factor. Several TCSs and DGCs are known to cooperate during the transition from planktonic to sessile surface-attached state (Figure 1.15). The DGC SadC, for instance, *via* c-di-GMP affects the RsmA transcription factor of the Gac/Rsm system directing the cell to biofilm state.[139]

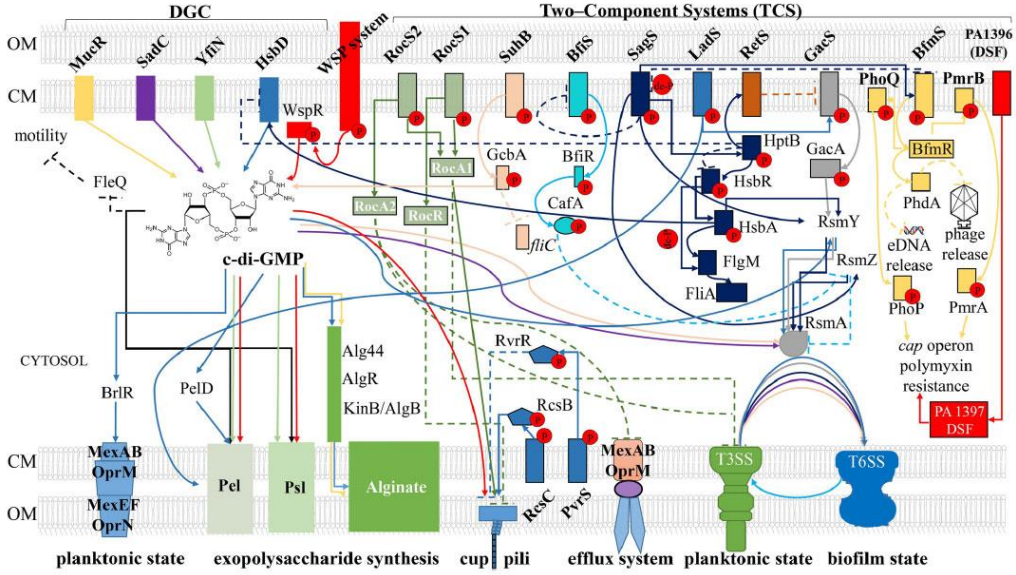

Figure 1.15 Crosstalk regulation between c-di-GMP and TCS / DGC systems during *P. aeruginosa* biofilm formation. The activation and inhibition pathways are marked with solid and dashed lines, respectively. Figure taken from [139].

1.5.3 Bacterial Surface Interactions

Many advantages are gained by bacteria adhering to surfaces. Firstly, nutrients in low concentrations are deposited on surfaces and become more accessible to cells.[140] Secondly, bacteria may obtain necessary metabolites or co-factors directly from the surfaces.[141] Motility observations in experiments under flow

have also shown that *E.coli* swim upstream along a surface. Kaya and Köser used an *E.coli* K12 strain and observed motility in Luria-Bertani (LB) medium with a microfluidic device with three different syringes to pumping at different shear rates, which are gradients of flow velocity.[142] When they increased the flow speed, bacteria aligned to move upstream as shown in Figure 1.16 in contrast with orthogonal movement which was observed at higher shear rates (where bacteria swam towards channel walls).[143]

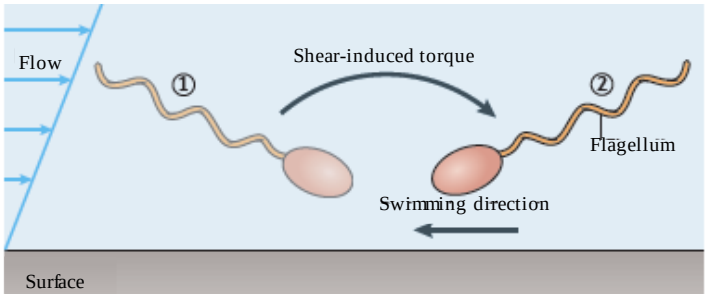

Figure 1.16 Schematic mechanism of upstream motility in *E. coli* under different flow rates. Figure taken from [102].

Outcomes of some experiments have demonstrated that cells adhered to surfaces and not associated with biofilms have antibiotics resistance profiles that are similar to biofilm cells.[144] This function is primarily mediated by two mechanisms: reducing the net charge on the bacterial surface and increasing membrane stability.[145]

1.5.3.1 Mechanisms of Attachment

Bacterial cell size is about 0.5 – 2 µm, nearly in the range of colloidal particles. Therefore, bacterial adhesion has been described by the Derjaguin-Landau-Verwey-Overbeek (DLVO) theory, which originally described the interaction of a colloidal particle with a surface.[146] According to this theory, the interaction between a surface and particles is given by the summation of their van der Waals and Coulomb interactions (Figure 1.17). The former force is dominant in the vicinity of the surface, whereas in contrast, the latter is dominant at distance away from the surface. However, a charged particle in an aqueous solution attracts counter ions against the surface charge forming an electric double layer. Bacteria and natural surfaces in aqueous solutions are naturally negatively

charged, therefore both form electrical double layers which might overlay and generate repulsive electrostatic energy.

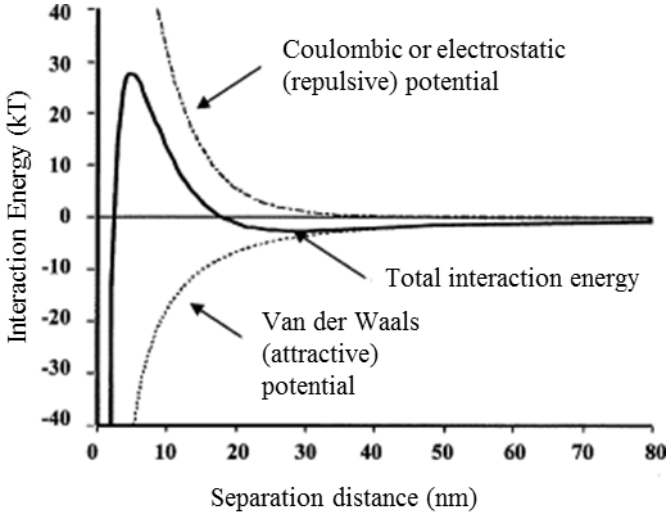

Figure 1.17 Schematic interaction energy versus distance profiles of DLVO interaction. The attractive van der Waals and the repulsive electrostatic potentials form the total interaction energy. Image adapted from ref. [147].

As shown in Figure 1.18, for low ionic strength, both particles have a net repulsion at large and intermediate separations. To approach one another requires that the kinetic energy of the particles due to thermal motion be larger than the finite energy barrier. In contrast, at high ionic strength, up to 0.2 M, conditions common to many *in vitro* experiments, the range of the van der Waals force is larger and the interaction energy is slightly attractive at large separations with a repulsive energy barrier at medium separations.[148] All the experiments described in this thesis were conducted in RPMI-1640 medium (Lonza), which presents an ionic strength of 0.15 µM. In this situation, a secondary minimum is generated. The energy barrier is lower and particles can overcome it more easily either by motility or Brownian motion leading to a reversible surface attachment. Many publications have described links between reduced bacterial adhesion and decreasing ionic strength, which is consistent with the DLVO theory however, it does disregard the dynamic role of the bacterial cell and its appendages in response to the surface.[149]

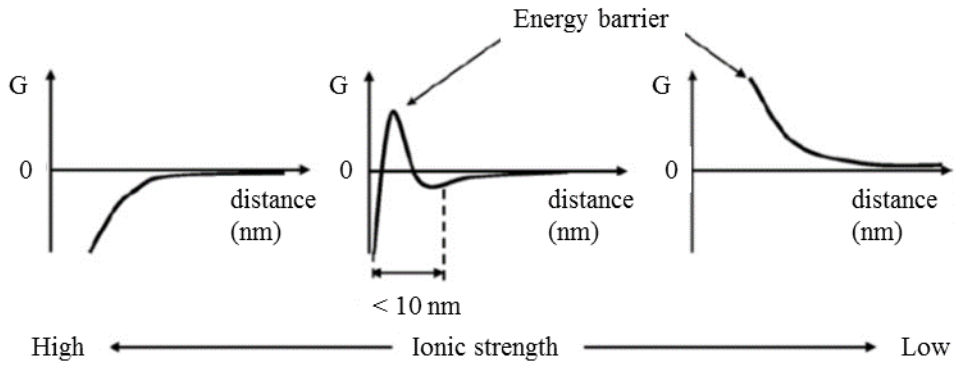

Figure 1.18 Total interaction energy between a bacterial cell and a surface depending on ionic strength. Image taken from ref [149].

The thermodynamic approach provides another model of bacteria-surface interaction based on the surface free energies of the interacting surfaces. Although it principally assumes that the adhesion process is always reversible-which is often not the case,[146] this approach helps to explain a common observation that bacteria with a hydrophobic surface prefer hydrophobic material surfaces.[150]

Two stages in cell attachment upon contacting surfaces have been observed.[151] The initial stage of attachment is a reversible process, which occurs rapidly and involves hydrodynamic and electrostatic interactions.[152] In this first phase bacteria move towards surfaces through physical forces with a different distance range *via* van der Walls forces, hydrophobic interactions, Brownian motion and/or electrostatic charges.

Consequently, as part of transition from reversible to irreversible adhesion, a rapid increase in the adhesive force between bacteria and surfaces has been observed over time. This phenomenon is due to physicochemical effects such as the loss of interfacial water, structural changes in surface molecules and repositioning of the cell body to maximize attachment to the surface.[153] Some bacteria such as *Pseudomonas* deploy appendages to translocate onto surfaces (section 1.5.1.2). The adoption of the sessile mode arises following irreversible attachment.[154]

In the second stage, bacteria can progress to irreversible attachment. It occurs on a time scale of several hours, and involves van der Waals interactions between the hydrophobic region of the outer cell envelope and the surface[155] and specific biological structures, which have only recently been considered in descriptions of bacterial adhesion.[156] Predominantly, some organelles including flagella, pili or fimbriae and curli fibers have been proposed to mediate specific attachment to surfaces. These organelles may be terminated with tip proteins referred to as adhesins, which bind to molecules presented on the surface. Similarly, EPS has been found contribute to increasing the strength of bonds between the cell and the surface.[149]

Strong correlations between bacterial attachment and physical properties, such as water contact angle,[157, 158] stiffness[159, 160] zeta potential, and chemical descriptors,[8, 161] have been observed - but only on a narrow range of substrates- i.e. libraries of poly(ethylene glycol) and poly(dimethylsiloxane) and microorganisms.[158] While a simplistic approach to describe bacterial attachment remains attractive to many, most living cells are not inert particles in a fluid but respond on contact to surface in specific and dynamic ways.

1.5.3.2 Adhesins

The bacterial cell envelope is a complex multi-layered structure that serves to protect these organisms from their unpredictable and often hostile environment. The cell envelopes of most bacteria fall into one of two major groups. Gram-negative bacteria are surrounded by a thin peptidoglycan layer, which itself is surrounded by an outer membrane containing lipopolysaccharide and proteins. Gram-positive bacteria lack an outer membrane but are surrounded by layers of peptidoglycan many times thicker than is found in the Gram-negatives. Long anionic polymers, called teichoic acids, and proteins are woven into these layers of peptidoglycan (Figure 1.19).[162]

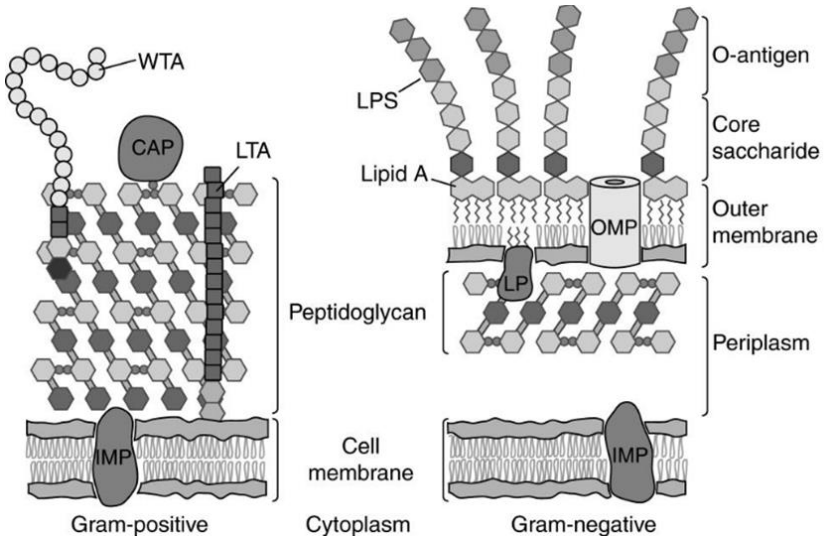

Figure 1.19 Depiction of Gram-positive and Gram-negative cell envelopes: CAP = covalently attached protein; IMP= integral membrane protein; LP= lipoprotein; LPS= lipopolysaccharide; LTA= lipoteichoic acid; OMP= outer membrane protein; WTA= wall teichoic acid. Image taken from [162].

On their outer membrane pathogenic bacteria are endowed with adhesive molecules that promote attachment to biotic or abiotic surfaces. Adhesins are defined proteinaceous adhesive subunits typically but not always exposed at the tips of cell appendages like fimbriae. These proteins have been described with specific affinities for different types of molecules or receptors expressed on the membrane of host cells. In *P. aeruginosa* for instance, there are proteins able to bind fibronectin, fibrinogen in wounds and mucin in airways.[163, 164] Several types of adhesive structures promote attachment and collaborate in the bacterial adhesion.[165]

MrpH is an interesting example of adhesins of mannose-resistant/*Proteus*-like (MR/P) fimbriae that determine virulence in *Proteus* and is a pivotal factor in urinary tract infections.[166] The most common adhesive organelle in *E. coli* is the type I fimbria that specifically binds mannosylated macromolecules and host cell receptors. Carbohydrates play a crucial role also in the surface-attachment of UPEC. The most important fimbrial structures are called P-fimbriae because their Gal-Gal moieties are also included in P-blood group antigens.[167]

Recently, tips functionalised with antibodies in atomic force microscopy (AFM) have been used to investigate the position and distribution of adhesive structures

in the bacterial outer membrane.[168] Through the analysis of specific molecular recognition events Arnal *et al.* built a map of the spatial distribution of adhesins on the surface of a pathogenic bacterial envelope revealing a non-homogenous pattern.

Gram-positive bacteria, such as *S. aureus*, can adhere to components of the extracellular matrix of the host to initiate colonisation. Adherence is mediated by protein adhesins of the MSCRAMM (microbial surface components recognising adhesive matrix molecules) family, which in most cases are covalently anchored to the cell wall peptidoglycan.[169] Non-proteinaceous adhesins comprise the polysaccharide PIA (polysaccharide intercellular adhesin), wall teichoic and lipoteichoic acids.[170]

1.5.3.3 Bacterial Footprint and EPS

During biofilm formation, bacteria excrete macromolecules, which form their EPS comprising DNA, proteins and polysaccharides.[171] Pel, Psl and alginate are three secreted exopolysaccharides produced by *P. aeruginosa.* The structures of alginate and Psl have been chemically described whereas Pel has not been fully characterised although it is likely to have a different composition from the other two bacterial exopolysaccharides.[172] Alginate is a high molecular weight acidic polysaccharide composed of non-repeating subunits of selectively O-acetylated D mannuronic acid and its C5' epimer L-glucuronic acid,[173] whereas Psl is composed of a repeating pentamer containing D-mannose, L-rhamnose, and D-glucose in ratio 3:1:1.[174]

Bacterial footprints have been analysed using different optical techniques: electron scanning and transmission electron microscopy using fluorescently labelled lectins which are carbohydrate-binding proteins. El-Kirat-Chatel *et al.* investigated adhesin protein LapA in *Pseudomonas fluorescens* accumulated onto hydrophobic alkanethiol monolayers coated on glass coverslips.[175]
They analysed bacterial footprints using single-molecule AFM with functionalised tips with anti-HA antibodies able to specifically bind to hemagglutinin (HA) tag in LapA structure. They were able to measure adhesion

force and rupture length (50-900 nm). LapA interaction with hydrophobic materials was confirmed through the use of LapA deficient and LapA hyper-producer mutants.[175]

1.5.4 Bacterial Cell Aggregation, Micro-colony Formation and Surface Exploration

In natural environments, bacteria live mainly in aggregates or in biofilm structures.[31] At this organisational level, cells behave and live as a community that is able to express different functions. Recent studies have shown how several surface appendages (e.g. curli in *E. coli*) and proteins (e.g. Ag43) can amplify colonisation and cell-to-cell aggregation.[176] The kinetics of bacterial colonisation are dependent on the presence of these adhesive structures. Beloin *et al.* coupled a micrometric colloidal system with advanced flow cytometry analysis to describe the expression of three adhesive appendages on single cells in a very short time scale (few seconds). In this study, they were able to identify the appendages expressed in early stages of cell adhesion and in subsequent cell aggregation. In fact, they established that curli and F-pili are the main actors in cell adhesion in the first minutes of attachment, whereas Antigen 43 is likely to be involved in cell-to-cell aggregation. Moreover, they found significant charge changes on the surfaces when exposed to bacterial suspensions for all strains and they showed that different molecules were deposited by bacteria on the surface that can affect the motility of other bacteria. For instance, *P. aeruginosa* leaves trails of the extracellular polysaccharide Psl during its movement on glass borosilicate surface (Figure 1.20).[154] Zhao *et al.* combined a cell-tracking algorithm to analyse the motility of *P. aeruginosa* with a fluorescence staining technique for Psl to demonstrate a correlation between the frequency of cells and the Psl levels deposited on the surfaces. As a consequence (positive feedback), areas with trails of Psl with a hierarchical distribution[154] produce higher bacterial visit frequencies. This is likely to be an exploratory strategy by which cells go where other cells have previously deposited Psl.

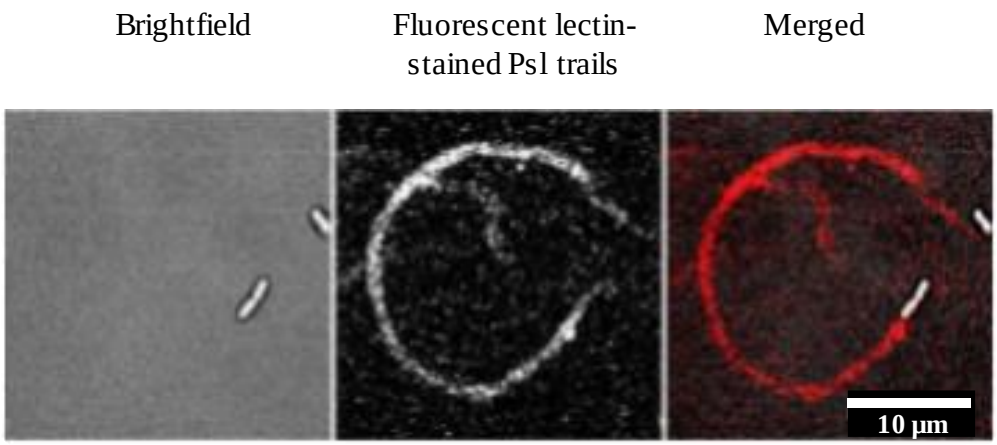

Figure 1.20 Psl trail left behind by bacteria, brightfield microscopy image of the *P. aeruginosa* (left) on glass borosilicate; Psl trail stained by fluorescently conjugated HHA lectin (center); merged image with trail pseudo-coloured in red (right). Scale bar is 10 µm. Figure taken from [154].

Aggregate formation in *P. aeruginosa* has been investigated over the last decade, and the role of aggregates in biofilm formation has been widely described.[177-179] A new model of biofilm formation has been proposed to illustrate the tendency of bacteria to clump as multicellular aggregates during the process of biofilm formation, instead of just seeding a particular surface by individual bacterial cells in the planktonic state. It has also been suggested that planktonic cell aggregation, which occurs in the bulk liquid above surfaces, is mediated by the same mechanisms as those involved in the formation of surface attached biofilms. In common with biofilms, planktonic aggregation is influenced by sub-lethal concentration of antibiotics and cells in the aggregates are protected against several clinically relevant antimicrobial compounds.[180] Therefore, planktonic aggregates are a valid model system to address questions about the mechanisms which underpin the formation, maturation, or dispersal of surface-associated biofilms.[178]

1.5.5 Cell-to-cell Communication

Within biofilm communities cells communicate through a variety of mechanisms including extracellular vesicles,[181] bridges for transferring proteins or for the diffusion of small chemical signals, intercellular nano-wires structures (that act as conduit for redox reactions),[182] vesicle chains with lipid

appendages covered by carbohydrate (possibly lipopolysaccharides LPS, which may play a role in cell-cell recognition and in intercellular material transfer).[183] The term quorum sensing (QS) is now employed to describe the phenomenon whereby bacteria coordinate population density-dependent changes in behaviour.[184] This network is particularly advantageous to bacteria as they are able to exchange nutrients and signals and regulate biofilm development. QS systems rely on the production and sensing of self-generated extracellular signals.

QS bacteria produce and excrete molecules termed autoinducers whose concentration is proportional to bacterial population density. Cells are able to perceive and detect a threshold stimulatory level of these molecules, i.e. when the number of bacterial cells is quorate, through receptor proteins and so modify cell expression and bacterial population behaviour.[185] QS enables bacteria to synchronise their response on a population-wide scale. Although species specific systems often possess unique types of molecules, receptors and mechanisms of transduction, interspecies communication depends on a similar mechanism.[186] In this section, some examples of well-characterised QS systems have briefly been described (Figure 1.21).

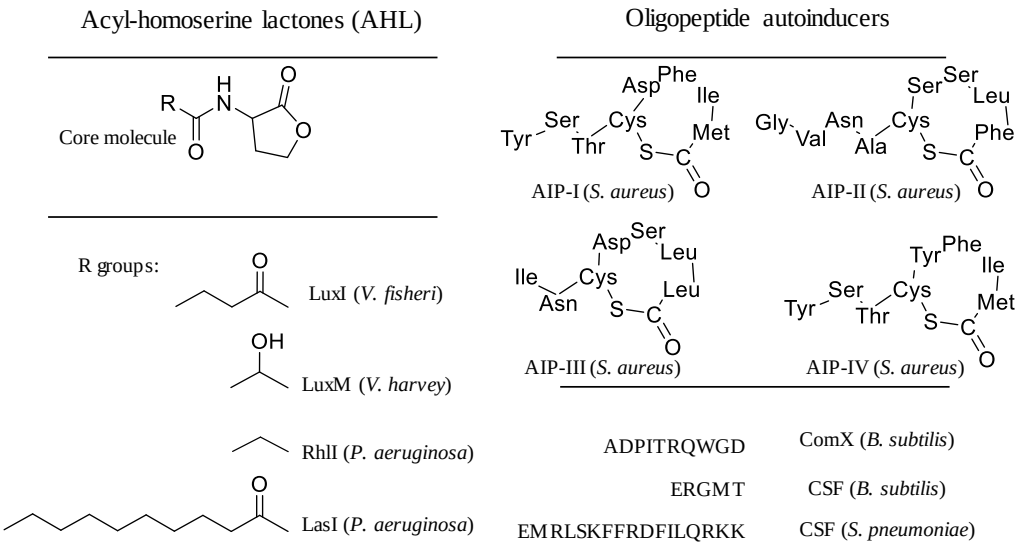

Figure 1.21 Some examples of AHLs and oligopeptide autoinducers in gram negative and gram-positive bacteria respectively. Figure taken from [186].

In many Gram-negative bacteria, LuxI and LuxR are proteins that control expression of different genes not only the luciferase operon (*luxICDABE*) in *Vibrio (Photobacterium) fisheri*.[187] LuxI is the autoinducer synthase which produces the *N*-acyl-homoserine lactone (AHL) autoinducer *N*-(3-oxohexanoyl)-L-homoserine lactone (3-oxo-C6-HSL).[188] LuxR is a cytoplasmic autoinducer receptor/DNA binding transcriptional activator. AHLs diffuses in and out of the cell and its concentration increases with increasing bacterial population density. The binding of AHL to LuxR, which is a complex obtained only when a critical threshold concentration is reached, enables bacteria to activate the target genes (e.g. luciferase in *Vibrio fisheri*).[189] At the same time, through a positive feedback AHL-LuxR complex induces *luxI* expression causing the entire population to switch into a QS mode.

Similar AHL QS systems have since been shown to be widely distributed in *Proteobacteria*, where they control diverse behaviours, such as production of secreted toxins and virulence factors, biofilm matrix components, and DNA conjugation.[190] Species specific signalling differs in AHL molecules for length of the acyl side chain, backbone saturation and incorporated substitutions. LuxI type proteins that generate this AHL diversity have been studied across many different bacterial species. Most LuxI-type AHL synthases produce AHLs from S-adenosyl methionine (SAM) and fatty acyl chains carried provided *via* acylated acyl carrier proteins.[191] Studies on the structure of LuxR type proteins revealed a specificity determined by an acyl binding pocket that precisely fits a specific side-chain moiety. Besides that, LuxR proteins possess specific pockets for selectively binding to its cognate AHL signal. This explains how in environments with mixed species, each species can measure and distinguish their AHLs.

Many Gram-positive bacteria communicate using modified oligopeptides (signals) and two-component type membrane bound sensor histidine kinases (receptors). It is known that QS peptide signals are obtained from cleavage of larger pro-peptide precursors which are modified to contain lactone and thiolactone rings, lanthionines and isopropenyl groups.[192]

QS in *S. aureus* is an example of a mechanism for controlling a biphasic population response. At low densities, cells express and produce factors that promote adhesion and cell aggregation, whereas at high density, bacteria inhibit their expression and initiate secretion toxins and proteases required for invasive disease. This switch is provided by the accessory gene regulator locus (Agr) QS system.[193]

In addition to chemical considerations of the molecules and receptors involved, it is worthy to underline a few examples of the QS circuitry. *P. aeruginosa* is responsive to different AHLs and the regulatory circuits are arranged in series rather than in parallel. In *P. aeruginosa*, QS is mediated by a network of three major pathways: the alkylquinolone system controlled by PqsR, as well as two LuxR/LuxI-type systems, LasR/LasI and RhlR/RhlI, respectively. These systems are organised hierarchically with LasR functioning as a master regulator at the top of the cascade. Two circuits, LasIR and RhlIR interlink with each other in the QS network of *P. aeruginosa*.[194]

LasI, a LuxI homologue, produces an AHL autoinducer ligand, *N*-(3-oxododecanoyl)-L-homoserine lactone (3-oxo-C12-HSL) that binds LasR.[195] The complex activates different genes including *lasI via* positive feedback. The same complex activates *rhlR* and *rhlI* which are responsible of another QS circuit. RhlI produces *N*-butanoyl-homoserine lactone (C4-HSL) which binding its receptor, RhlR regulates the expression of target genes many of which are also regulated by the *las* system.[196]

The quinolone-based QS system acts mainly *via* 2-heptyl-3-hydroxy-4-quinolone, called the *Pseudomonas* quinolone signal (PQS), which connects the LysR-type transcriptional regulator PqsR to stimulate diverse virulence genes.[197] These signaling systems create a global regulatory network and are believed to regulate the expression of up to 12% of the *P. aeruginosa* genome.[198] Hence, this may be crucial for the temporal ordering of certain events in bacterial life cycle.[199].

1.6 Anti-biofilm Strategies

Anti-infective biomaterials have progressively become a primary strategy to prevent medical device-associated infections. A number of different anti-biofilm coatings have been developed to achieve different outcomes based upon their application. Three classes can be distinguished: prevention of protein adsorption, prevention of bacterial adhesion and bacterial killing strategies.

1.6.1 Prevention of Protein Adsorption

Protein adsorption is a crucial parameter that needs to be addressed when designing medical devices such as venous or urinary catheters because the build-up of adherent host material acts as a foothold for bacterial adherence leading to formation of biofilms.[200] In addition, thrombus formation is another example of a phenomenon that can occur when specific blood clotting proteinaceous factors are activated on the contact with foreign surfaces.[201] Furthermore, materials with good anti-bacterial adhesion activity can lose their properties over time because they become masked by a protein layer.[202] The main strategies to prevent protein adsorption on the surface are outlined below.

1.6.1.1 PEG-based Coatings

Immobilising polyethylene glycol (PEG) is one of the most commonly used approaches to avoid protein adsorption on surfaces[203, 204] and has also been applied to prevent biofilm formation. This strategy is based on the generalisation that the extent of protein adsorption is related to the grade of hydrophobicity of the surface. Steric hindrance, high hydrophilicity, high flexibility and hence a large excluded volume of PEG chains are reported in the literature to mediate anti-protein adsorption properties.[205] PEG interacts with water molecules by hydrogen bonding providing steric repulsion for protein adsorption. The surface coating of PEG has been successfully used to prevent opsonisation (protein adsorption) in drug delivery systems.[206]

PEG has also been reported to reduce bacterial adhesion by different species.[207-210] For instance, Kingshott *et al.* found a reduction of up to 2 orders of magnitude of bacterial adhesion if cells were grown for 5 h on PEG immobilised on a carboxylated poly(ethylene terephthalate) (PET-COOH) surface in comparison with control PET.[207] A greater level of resistance to bacterial attachment was achieved for higher molecular weight PEGs. Roosjen *et al.* investigated the effect of chain length on microbial adhesion to poly(ethylene oxide) (PEO) brushes.[211] They produced by grafting three different chains of 526, 2000 and 9800 Da of molecular weight.

After length estimation with water contact angle, ellipsometry and XPS, these chains were evaluated in their anti-adhesion activity for two bacterial species *(Staphylococcus epidermidis* and *P. aeruginosa*) and two yeasts (*Candida albicans* and *Candida tropicalis*). Both bacterial species and *C. tropicalis* showed adhesion reduction with longer chains. *C. albicans* showed the opposite results and, hence, this experiment established PEG chains length as an important factor in preventing bacterial adhesion depending on microbial species.[209]

The influence of PEG architecture on protein adsorption was also assessed by using chain-end tethering of PEG brushes. Michel *et al.* studied the adsorption of three proteins of different sizes, myoglobin (16 kDa), albumin (67 kDa) and fibrinogen (340 kDa) on poly(l-lysine)-*g*-poly(ethylene glycol) (PLL-*g*-PEG) copolymers with various grafting ratios adsorbed to niobium pentoxide-coated silicon wafers. The smallest protein, myoglobin, generally adsorbed in higher concentration than the much larger fibrinogen. Protein adsorption was found to be lowest on the surfaces with the highest PEG chain surface density and increased as the PEG layer density decreased.[212]

Despite PEG coated surfaces being one of the more frequently explored and used approaches in fabricating protein–resistant surfaces, they fail to effectively reduce bacterial colonisation in long-term experiments.[210] PEG coatings also suffer from auto-oxidation in aqueous conditions and form aldehydes and ethers in the presence of oxygen, thus causing the surfaces to lose their activity.[213]

Along with PEG coatings, self-assembled monolayers (SAMs) presenting oligo-(ethylene oxide) groups represent another example of protein-resistant surfaces.[214] SAMs are monolayers of organic molecules (e.g. alkanethiols) formed on inorganic substrates such as gold. Prime and Whiteside produced oligo(ethylene glycol) terminated alkanethiol (OEG-SH) SAMs on gold substrates and measured the level of protein adsorption using Surface Plasmon Resonance (SPR).[214] The end group charge plays an important role in protein adsorption prevention. In fact, Holmlin *et al*. found that the presence of a pair of oppositely charged functional groups produces localised dipoles oriented parallel to the surface plane with a negligible dipole vector oriented perpendicular to the surface.[215]

As reviewed in ref. [89], the polymers with positive results present four common parameters: the presence of polar functional groups, the absence of any net charge, the presence of hydrogen bond acceptor groups and the absence of hydrogen bond donor.[216] Chilkoti and co-workers used poly(oligo ethylene glycol methacrylate) (POEGMA) brushes and proposed a mechanism whereby these materials resist protein adsorption.[217] The disordered and tightly packed structure of POEGMA brushes enables significant penetration of water resulting in a strong hydration of the long macromolecular chains and the generation of a so-called “excluded volume”, which causes a higher conformational entropy and entails strong repulsive forces against biomolecules, thereby protecting the underlying substrate.

Zwitterionic SAMs and polymers are phosphorylcholine (PC) based zwitterionic surfaces that have been widely studied for their protein resistant activity.[218] Their most promising hypothesised mechanism is similar to the PEG mechanism as the PC zwitterions, which do not suffer from auto-oxidation problems, strongly bind water creating a hydrated layer that does not allow proteins to adhere.[219] A similar mechanism has been described by Zhang *et al.* using zwitterionic hydrogels for implants to prevent nonspecific protein adsorption and consequent foreign-body reaction driven by the immune system which

recognises implants as foreign and encapsulates them with a dense collagen.[220]

(PC) moieties are likely to reduce protein adsorption mimicking the lipid component of the external cell membrane believed to resist protein deposition.[221] Although some questions may be raised considering the opsonisation that occurs on bacterial surfaces before being phagocytised, Lu *et al.* explored the protein resistance activity using an organic mono- or bi-layer bearing a PC group anchored on the surface of hydrophilic silicon oxide. These materials were tested using chicken egg white lysozyme, bovine serum albumin and fibrinogen and from the results obtained they concluded that PC bilayers were twice as effective than the corresponding monolayers in protein resistance.[222]

Another example of zwitterions and bacterial adhesion was reported by Smith and co-authors.[223] They modified a vascular catheter with the non-leaching polymeric sulfobetaine (polySB), which directs water molecules to the catheter surface (Figure 1.22). The modified surface effectively reduced protein, mammalian cell, and microbial attachment *in vitro* and *in vivo*. Relative to commercial catheters, polySB-modified catheters exposed to human blood i*n vitro* had a > 98% reduction in the attachment and a significant reduction in activation of platelets, lymphocytes, monocytes, and neutrophils. Additionally, the accumulation of thrombotic material on the catheter surface was reduced by > 99% even after catheters were exposed to serum *in vitro* for 60 days. *In vivo*, in a highly thrombogenic canine model, device- and vessel-associated thrombus was reduced by 99%.

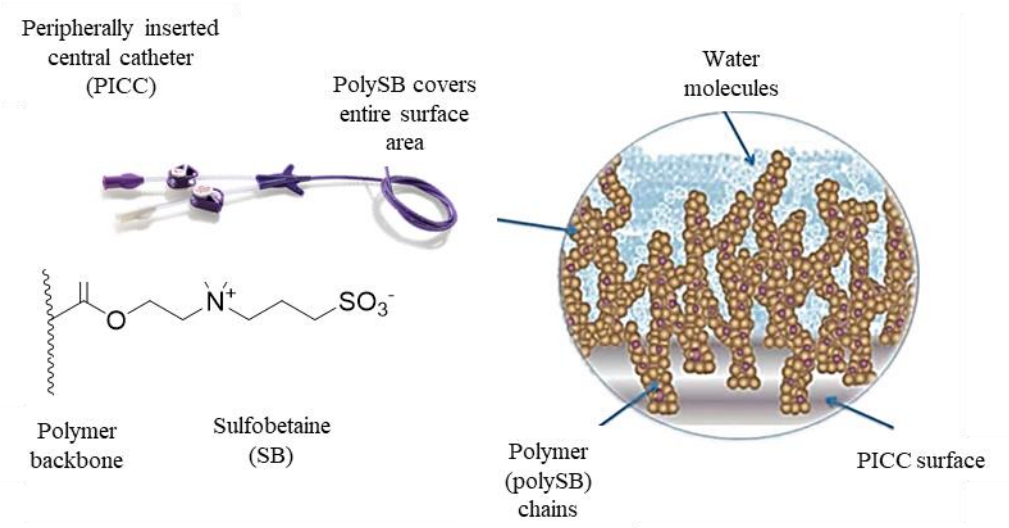

Figure 1.22 PolySB modification of a peripherally inserted central catheter surface (PICC). PolySB is bound to the surface of the PICC to form a conformal polymer surface. The zwitterionic polySB modification coordinates both free and bound water molecules to create a hydrophilic surface. PolySB-modified PICC has reduced thrombus accumulation. Image taken from ref. [223].

1.6.1.2 Protein-Degrading Films

Protein-degrading films are biocompatible matrices used in order to reduce opsonisation and consequent bacterial adhesion. Protein-degrading properties might be obtained through two different approaches.

1) Proteases can be incorporated into coatings. Kim *et al.* described a new method for incorporating hydrolytic enzymes Pronase (the name given to a group of proteolytic enzymes) and α-chymotrypsin by either sol-gel entrapment or by covalent attachment into a polydimethylsiloxane (PDMS) matrix. Protein adsorption was observed to decrease due to the hydrolytic activity of the film.[224] However, the denaturation of the proteases over time limits the long-term activity of these surfaces.

2) Photoactivated self-cleaning coatings have become a major research focus,[225] but although they have been used for their self-cleaning activities, there has been no widespread uptake for biofilm prevention in the healthcare sector despite its potential.[226] These coatings degrade deposits in the presence of ultraviolet or visible radiation which stimulates production of reactive oxygen species (ROS).[226] ROS have no specific targets in terms of microbes.

Therefore, this avoids the potential problems of microbes developing resistance to this microbiocidal treatment.

Other coating materials have also been observed for their protein-degrading activity such as TiO_2 [227] and carbon nanotubes.[228, 229]

1.6.2 Prevention of Bacterial Adhesion

Anti-adhesive strategies do not deactivate/kill the microbes. In fact, if the infection occurs in a body, preventing bacterial attachment and biofilm formation, the subject's host defences will be naturally enabled to clear the planktonic bacteria.

1.6.2.1 Smart Materials

Bacterial attachment depends upon several factors, among which hydrophobic and electrostatic interactions are often invoked to explain bacterial behaviour.

Smart or stimuli-responsive materials present reversible and rapid changes in their physicochemical properties as a response to small changes in environmental conditions (e.g. electrical potential, pH, temperature, light). Poly(*N*-isopropylacrylamide) (PNIPAAM) is one of the most studied and widely-used environmentally sensitive (smart) polymers in order to control the wettability of surfaces.[230] When exposed above a critical temperature, this polymer undergoes a transition phase and presents a hydrophobic surface that facilitates cell attachment and growth. On the contrary, with a temperature decrease, the polymer swells and presents a hydrophilic surface and adsorbed cells are released from the surface. Lopez and co-workers prepared thermally switchable poly(isopropylacrylamide) PNIPAAM-tethered polystyrene (PS) surfaces. The favourable temperatures for attachment were 25°C and 37°C, for *S. epidermidis* and *Halomonas marina* respectively while their respective optimal anti-adhesion activity was detected at 37°C (*S. epidermidis)* and 4°C (*H. marina)*. Detachment studies established *S. epidermidis* attaches preferentially to hydrophilic PNIPAAM surface rather than the hydrophobic surface.[230] Hook *et al.* found that two co-polymers previously identified by high-throughput screening to have thermo-responsive properties caused the detachment of UPEC

after 72 h of incubation by up to 96% when the temperature was reduced from 37 to 4°C. They chose two different copolymers because one exhibited an increase and the other a decrease in WCA when the temperature was reduced. The first co-polymer, which exhibited a decrease in WCA with a reduction in temperature, was a 70:30 cross-linked copolymer of polypropylene glycol diacrylate (PPGdA) and trimethylolpropane ethoxylate (1 EO/OH) methyl ether diacrylate (TMPEMEdA) which was referred to as PPGdA 70:30 TMPEMEdA. The second material, which exhibited an increase in WCA with a reduction in temperature, was a linear 70:30 copolymer of 2-[[(butylamino)carbonyl]oxy]ethyl acrylate (BACOEA) and 2-(2-methoxyethoxy)ethyl methacrylate (MEEMA), referred to as BACOEA 70:30 MEEMA. The chemical structures of the monomers are shown in Figure 1.23. The equivalent response of UPEC to these two materials despite their different change in WCA demonstrated that bacterial attachment cannot be explained by a simple correlation with WCA.[5]

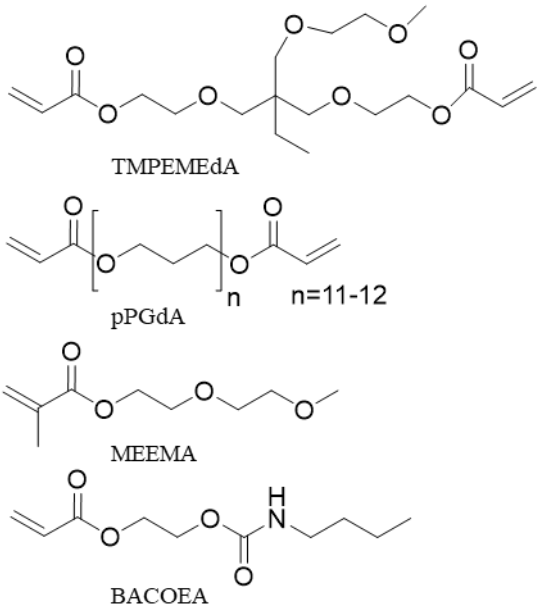

Figure 1.23 Ethylene glycol containing monomers used by Hook *et al*. to create thermally switchable polymers with controlled anti-microbial activity. Figure taken from ref. [5].

1.6.2.2 High throughput discovery of polymers resistant to bacterial attachment

Polymer materials showing an intrinsic resistance to bacterial attachment are a flourishing area in current biomaterials research. Hook *et al*. have applied a high throughput method to simultaneously screen hundreds of materials[231] to investigate their resistance to selected pathogenic bacteria *(P. aeruginosa*, UPEC and *S. aureus*). A library of 22 acrylate monomers with wide chemical diversity (linear, cyclic, aromatic fluorine substituted moieties) was used to create different copolymers. According to this method, a group of five structurally related polymer materials ('hit' materials) consisting of ester and cyclic hydrocarbon groups on the micro array was identified (Figure 1.24). These were then scaled up onto coupons and used as a coating on commercially available silicone catheters.

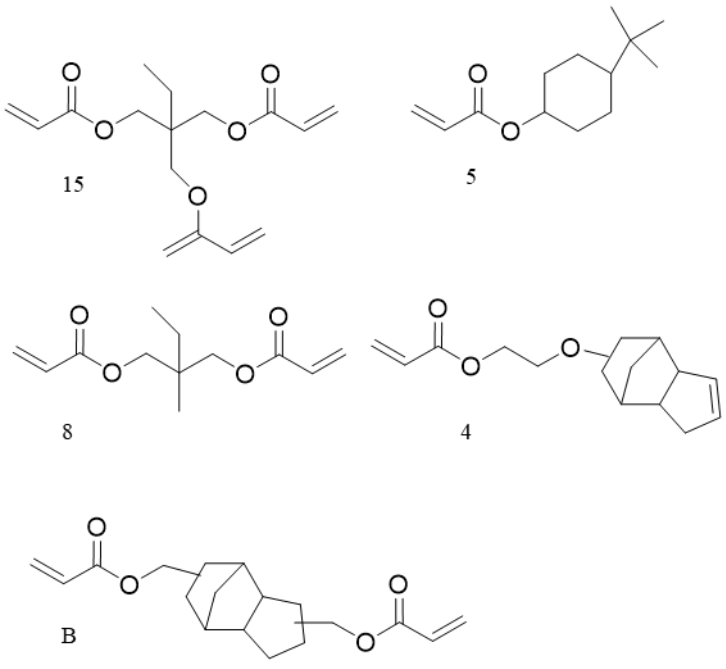

Figure 1.24 Five hit polymers that Hook *et al.* identified. Figure taken from ref. [7].

In-vitro results showed a 67-fold reduction in bacterial attachment and biofilm formation on coated catheters with these polymers as compared to uncoated silicone catheters. In addition, these coated catheters showed a 30-fold reduction in bacterial attachment in comparison with commercially available silver

hydrogel coated catheters. Monomer 4 shown in Figure 1.24 was mixed with di(ethylene glycol) methyl methacrylate (DEGMA) to tune the polymer's mechanical properties and used for coating catheter to be tested *in vivo* in mice with *S. aureus* Xen29 strain injected into the catheter lumen. This polymer has recently been approved for human use as a coating (BACTIGON®) for urinary tract catheters.[232] After 4 days bioluminescence on the infection site showed more than 90% reduction. A correlation was derived for bacterial attachment and a parameter derived from the partition coefficient and the number of rotatable bonds of the material pendant groups.[8] This suggested that bacterial attachment was reduced on surfaces exhibiting rigid hydrophobic chemical moieties in the specific case of poly(meth)acrylates with hydrocarbon pendant groups. The hydrophobic groups of these polymers were always partnered with hydrophilic ester groups providing weak amphiphilic moieties. As shown in Figure 1.25 since none of the currently used strategies used to prevent infections seems to describe the mechanism of this novel class of polymers, it is likely that an active response is involved which might be regulated by bacterial footprints and QS signalling.

Pernagallo *et al.* produced an early report of an array to identify specific bacterial binding/non-binding polymers. The authors used clinically relevant strains and identified polyacrylate materials, which had properties of high binding, low binding and selective binding.[233, 234] They screened a 381 polymer library with up to eleven different clinically relevant strains. Further to their high-throughput screen a number of "hit" polyurethane and polyacrylates/acrylamides were identified. The hit coating, a co-polymer of methylmethacrylate and dimethylacrylamide in a molar ratio of 9:1, generated $\geqslant$ 96% reduction for the bacterial mixtures tested after 24 and 48 h in brain-heart-infusion (BHI) medium.[234]

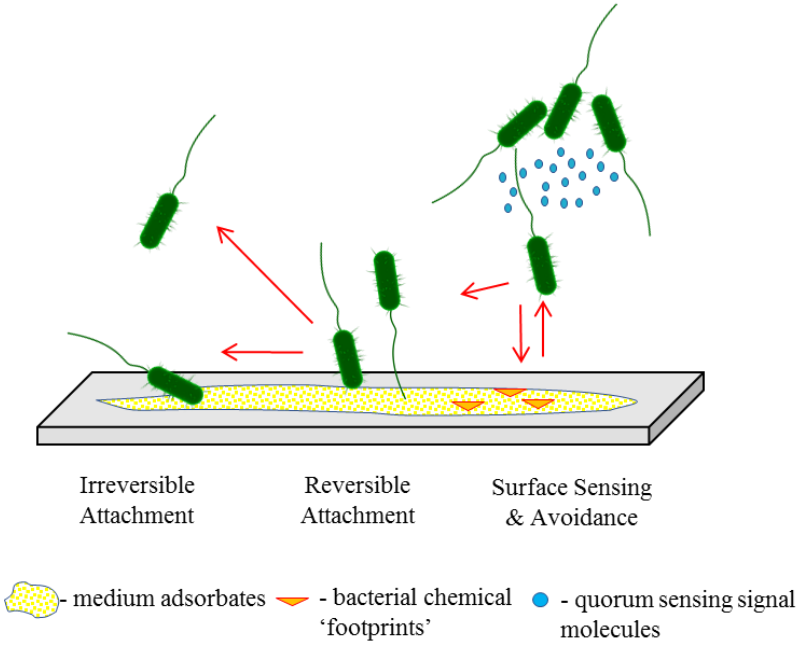

Figure 1.25 Hypothesis of model of how motile bacteria such as *P. aeruginosa* respond to a novel class of polymeric bacteria.

1.6.2.3 Slippery-Liquid Infused Porous Surfaces (SLIPS)

Traditional antifouling surfaces are mainly in solid forms, therefore permanent interactions between the surfaces and biological adhesins can eventually be established on the time scales of the adhesion process. A potential approach to generating dynamic surfaces is to utilise a stabilised liquid interface. Inspired by the *Nepenthes* pitcher plant, a new model of repellent surfaces has been recently developed.[235] A stable, immobilised and smooth liquid surface was locked in place by a porous solid. This novel slippery liquid-infused porous surface (SLIPS) is a material concept that exploits the extreme stability of the fully wetted liquid film to maintain repellence across a broad range of temperatures, pressures, surface tension, and other conditions. SLIPS have been shown to resist fouling by a broad range of micro-organisms, including clinically relevant bacterial and fungal strains.[236] Conventional SLIPS are not designed to either kill or retard the growth of bacteria. SLIPS, in fact, do not have any activity preventing planktonic bacteria from producing virulence factors and forming biofilms on nearby unprotected surfaces. To address these issues, Kratochvill *et al.* loaded into SLIPS QS inhibitors which were gradually released to attenuate

virulence phenotypes in non-adherent cells while maintaining the slippery properties of the SLIPS.[236]

1.6.3 Bacterial Killing Strategies

A great variety of compounds have been incorporated into materials to achieve antimicrobial activity, including electro-conductive polymers, polycation hydrogel carrying positive charges, antiseptics such as chlorhexidine and silver sulfadiazine, broad spectrum antibiotics, photosensitising drugs and essential oils derived from natural products. Silver has been the most widely used compound due to its bactericidal activity.[237, 238] A design of polyelectrolyte multilayers (PEM) containing silver nanoparticles has been demonstrated to exhibit antimicrobial activity.[239] PEMs were impregnated with a range of loadings of silver-nanoparticles and stamped onto the dermis of human cadaver skin (a wound-simulant) that was subsequently incubated with bacterial cultures. Skin dermis stamped with PEMs that released 0.25 ± 0.01 μg cm^{-2} of silver ions caused a 6 $\log_{10}$ reduction in colony forming units of *S. epidermidis* and *P. aeruginosa* within 12 h.[240] Lee *et al.* reported the antibacterial activity of silver nanoparticle-loaded multilayers of poly(acrylic acid) and poly(acrylamide) formed on magnetic microspheres as well as on plain glass.[241] The coatings were resistant to *E. coli* and *S. epidermidis* adhesion. However, silver nanoparticles are toxic to mammalian cells, able to penetrate through the pores and glands of the human skin thus causing damage.[242] Furthermore, bacterial strains with silver resistance are emerging due to the extensive use of silver.[243]

Greenfield *et al*. explored the synergistic antimicrobial activity of two commonly used antiseptic agents (silver sulfadiazine and chlorhexidine) on polyurethane central venous catheters *in vivo*.[244] Clinical studies revealed good antibacterial activity only in short-term implants (7 days at maximum) because of low release rate of the antiseptic agent after 2 days of elution and the absence of intraluminal coatings.[245]

Antibiotics were widely studied for their anti-biofilm activity. One approach was based on the incorporation of Rifampicin and Amoxicillin into a device but the effect was limited by the insufficient amount of antibiotic incorporated and the lack of sustained bactericidal concentrations for the life-time of the device.[246] An impregnation technique was used for incorporating antibiotics into silicone dialysis catheter: tubes were immersed in different antibiotic solutions in chloroform. Bayston *et al.* used an impregnation method for incorporating broad spectrum antibiotics (rifampicin, triclosan and trimethoprim) into peritoneal dialysis silicone catheters for long-duration antimicrobial activity. The impregnation process was carried out by immersing silicone tubing into a chloroform solution containing each antimicrobial at a concentration of 0.2% w v^{-1}, 1% w v^{-1} and 1% w v^{-1} respectively. These impregnated catheters were then challenged with clinically isolated strains of *S. aureus* (methicillin susceptible and methicillin resistant), *S. epidermidis* and *E. coli* to test the duration of activity before test bacteria became resistant.[247] Antimicrobial activity continued until it was stopped at 280 days and the agents prevented the emergence of resistant strains resulting in a >99.9% reduction of attached bacteria. A similar impregnation process was carried out by Fisher *et al.* with other antimicrobials (rifampicin, triclosan and sparfloxacin at 0.2% w v^{-1}, 1% w v^{-1} and 1% w v^{-1} concentration in chloroform respectively). Foley catheters/segments were immersed in solution for 1 h during which the silicone swelled and then returned to original size after solvent evaporation. In flow experiments, these catheters were able to prevent colonisation by common uropathogens *Pr. mirabilis*, *S. aureus* and *E. coli* for 7 to 12 weeks *in vitro* compared with 1 – 3 days for other, commercially available antimicrobial catheters currently clinically used.[4] An alternative approach covalently linked antibiotics onto the backbone of the polymers as a main-chain monomer, from which the medical devices are made. In a study by Woo *et. al.*[248], fluoroquinolone antibiotics (e.g. ciprofloxacin) was covalently linked onto the backbone of degradable polyurethanes. A macrophage-derived cholesterol esterase was used to release the antibiotic from the polymer backbone by degradation of the polymer chains. This approach showed some success in killing the bacteria. However, it was difficult to control the specificity of the cleavage sites in the polymer and further work will be required to determine the

structures of other degradation products released, which could compromise the material biocompatibility.

Limited reservoirs, absence of long-term properties, cytotoxicity, inflammatory responses, and increase in resistance of bacterial strains are some of the issues reported in the literature with respect to release-based antimicrobial coatings.[249] Recently, this research has been focused on the development of sustained-release coatings through two different approaches. The first approach employs several parameters to influence passive release including properties of the antibacterial agent itself (concentration, distribution, size, charge), the carrier matrix (porosity, surface roughness, functional groups), or the overall micro/nanostructure of the antibacterial coating may be tuned. For example, Zarie *et al.* demonstrated the successful solvent-free fabrication of micro-nanostructured pharmaceutical molecules by simple thermal evaporation. The assembly of the molecules from vapour to solid phase, in dimension and shape influences drug dissolution. Moreover, they obtained long term release employing a multilayer system of different drugs in which a highly dissolving drug (metronidazole) is protected by another compound (poly-lactic-co-glycolic acid, PLGA) that need to be dissolved first.[250]

An alternative approach for delivering antimicrobials from devices employs strategies to actively deliver reagents. In this approach the release is mediated by stimuli-response materials that respond to exogenous physical applied stimuli, such as temperature, light, magnetic field, electric field, and ultrasound, enabling the ability to release ‘on demand’ antibacterial effects and extend long-term properties.[251] The dose control in multiple release cycles has been described as a challenge for these coatings. Several other new approaches can be found in the following review.[252]

There is no single reason why the antibacterial approach is the best, in fact several factors need to be examined. First of all, microbicidal coatings have been widely used for their activity but bacterial strains with resistance for these molecules are emerging. Release-based coatings can lose their antibacterial activity as the biocidal substance is released. Moreover, non-release based

antimicrobial systems are bactericidal through a contact mechanism, but these materials have shown some drawbacks (e.g. biomolecules may lose activity upon incorporation into coatings).

In section 1.6 some of the anti-infective biomaterials have been presented describing the main properties and how, if known, these materials prevent protein adsorption, bacterial adhesion and kill bacteria. In this project, a new class of (meth)acrylate polymeric surfaces, described in section 1.6.2.2, will be assessed in order to understand better the mechanism by which they prevent biofilm formation since none of the currently used strategies used to prevent infection has uncovered the biofilm resistance mechanism for this novel class of polymers.

1.7 **Aims and Objectives**

The general aim of this project was to develop methods for spatio-temporal characterisation of bacterial motility at and above surfaces and to investigate the mechanism(s) used by bacteria to sense and respond to surfaces. The experiments were mainly conducted using a custom-designed microscope (chapter 3). Here, two example polymers were selected from a class of acrylate polymers - one that supported biofilm formation (pNGPDA) and another that did not (pEGdPEA).

Bacteria-material interactions are likely to be important in controlling the problem in comparison to antibiotic strategies which rely on the drug activity to kill the bacteria. The bacterial response was characterised considering early stages of the bacterial life cycle by examining changes in bacterial behaviour at a single cell level such as surface motility, lineage and c-di-GMP expression which is discussed in details in section 1.5.2.3.

This involved firstly developing new algorithms to process microscopy images and assessing bacteria interacting with surfaces with divergent biofilm properties (chapter 3). Next in order to verify whether pEGdPEA prevents attachment and therefore biofilm formation, a cell detachment assay has been designed that

follows individual cell removal to investigate bacterial surface adhesion strength using microfluidics (chapter 4). The mechanism(s) to prevent biofilm formation was furtherly studied by investigating the contribution of an intracellular pathway known from the literature to play a crucial role in the switch from reversible to irreversible attachment (chapter 5). Most of the relevant *in vivo* situations are 3-dimensional, and much information is lost due to inadequate methods which are limited to *in vitro* 2-dimensional investigations. In this regard, the presence or not of planktonic aggregates, which progressively seed surfaces, can modulate biofilm maturation. Using microscopy, the role of bacterial planktonic aggregation on surface biofilm formation has been explored making use of pEGdPEA and pNGPDA polymer surfaces as research tools that could produce two different bacterial phenotypes. The different aggregation response observed in the presence of the two distinct polymer surfaces, was examined using liquid chromatography-tandem mass spectrometry (LC-MS/MS) analysis of the cell-free spent medium to identify aggregate-promoting quorum sensing system signal molecules (QSSM) (chapter 6).

Chapter 2

Review of techniques

2.1 Chemicals and Free Radical Chain Reactions

All polymers used in this project were selected based upon previous work by Hook *et al.*[7, 231] and used to coat glass borosilicate coverslips (Gerhard Menzel, Braunschweig, Germany) (Table 2.1). A combination of monomers was used to polymerise a copolymer wherever stated. In order to avoid delamination, glass was treated with oxygen plasma at 100 W incident radio frequency (RF) (13.56 MHz) power for 1 min. Treated coverslips were then methacrylate silanised using 3-trimethoxysilylpropyl methacrylate (Sigma-Aldrich) at 50℃ under argon for 16 h. All monomers were polymerised as described previously[253, 254] with 1% (wv^{-1}) initiator (2,2-dimethoxy-2-phenylacetophenon) (Sigma-Aldrich).[6] A total of 5 µL of each monomer was deposited onto coverslips before irradiating for 60 min using short-wave ultraviolet (UV) light. The polymerisation was carried out under argon with an oxygen concentration below 2000 ppm (to prevent free radical quenching by oxygen), at room temperature (20°C). Coated coverslips were then left at <100 mTorr for 5 days to extract any unpolymerised monomers.

Table 2.1 List of monomers used in this project.

Monomer	Abbreviation	Chemical structure
Ethylene glycol dicyclopentenyl ether acrylate	EGdPEA	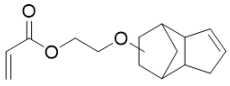
Neopentyl glycol propoxylate diacrylate	NGPDA	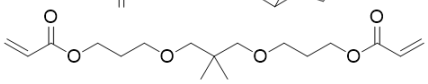
Isobornyl methacrylate	iBMA	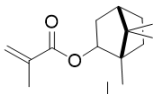
Trimethylcyclohexyl methacrylate	TMCHMA	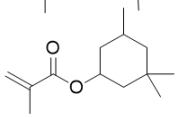
Benzyl methacrylate	BnMA	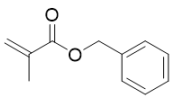

The mechanism of the free radical chain reaction is composed of three primary processes – *initiation*, *propagation*, and *termination* (Figure 2.1). In this case, *initiation* takes place by cleavage of the photo-initiator compound to yield the primary radical. The *propagation* or growth of reaction occurs when monomers add to the primary radical or to the radical at the end of the growing chain. *Termination* occurs primarily by the bimolecular reaction of the two growing polymer radicals.[255]

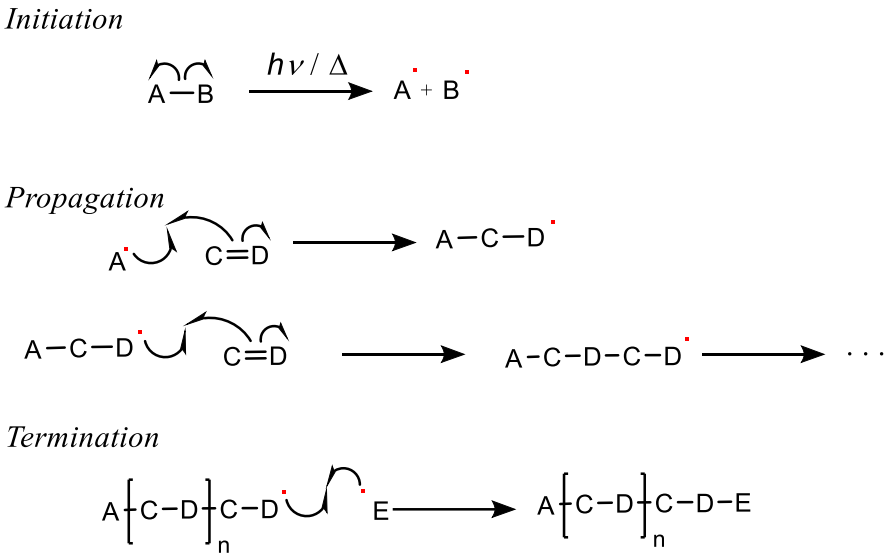

Figure 2.1 Radical chain reactions have three distinct phases: initiation, propagation, and termination.

2.2 Surface Analysis

2.2.1 Time of Flight Secondary Ion Mass Spectrometry

A detailed chemical analysis of a sample can be obtained using SIMS which allows the recording of mass spectra of surfaces in a vacuum environment. This technique is currently deployed to analyse surface contaminants, cells, metabolites and other biological samples with lateral resolution of 100 nm.[256-258] This information is provided by analysing emitted fragments from the top 1-2 nm of a surface after it has been bombarded with primary ions (Figure 2.2A).[259] The primary ions bombard the surface atoms and by the transferring of kinetic energy break the bonds between these atoms through a collision cascade. This fragmentation process liberates secondary molecules and fragments from the surface including neutral species, electrons and charged ions.

Only around 1% of the total are detected and analysed by the mass spectrometer.[260]

The secondary ions are then accelerated through a flight tube and energy corrected using an ion mirror such that they reach the detector at a time corresponding to their molecular weight (Figure 2.2B). The heavier they are, the longer the travel time to the detector. These ions exist initially as packets of surface ions by virtue of the pulsing of the primary ion beams. These packets are withdrawn into a drift tube. It is upon acceleration in the drift tube that the ions separate into their respective masses.

SIMS has two major operation modes: static and dynamic. Static SIMS is the process involved in surface atomic monolayer analysis, or surface molecular analysis, while dynamic SIMS is involved in bulk analysis and closely related to sputtering process.[261] Dynamic SIMS, whilst effective at depth profiling through samples by using a high ion dose, can cause significant damage to surfaces. Dynamic SIMS is useful in the analysis of semiconductor materials. Static SIMS is the mode of choice for more sensitive surfaces. Static mode uses very low ion doses (1 x 10^{12} ions cm^{-2}) to obtain intact molecular ions and fragments which closely represent the structure of the sample by ensuring limited damage by reducing the chance of analysing in the same area as a previous primary ion impact. ToF-SIMS can be operated in positive and negative modes to obtain spectra of the surface with oppositely charged ions.

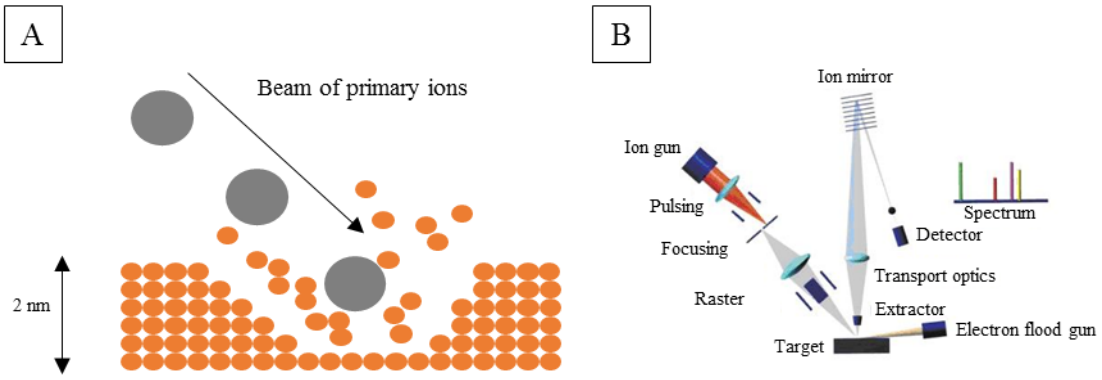

Figure 2.2 A) Schematic of primary ions hitting a surface and releasing secondary ions. **B)** ©IONTOF schematic of a SIMS instrument.

A variety of primary ions are used in ToF-SIMS. They include liquid metals Ga^+ and In^+, polyatomic clusters such as C_{60}^+ and Ar_{5000}^+, surface ionisation sources like Cs^+ or other liquid metal ion sources such as Bi_n^+ (n = 1-7). Using larger clusters offers a wealth of advantages over the monatomic ion sources such as improved mass resolution, secondary ion yields and surface sensitivity. Large clusters also reduce surface damage. For this reason, Bi_3^+ primary ion sources were used throughout this work. When a polymer surface is bombarded with positively charged ions it gains a net positive charge. This is exacerbated by the emission of secondary electrons. This unwanted accumulation of positive charge can affect the function of ToF-SIMS by influencing secondary ion formation and therefore requires neutralising. This is achieved *via* an electron flood gun which provides the surface with a supply of low energy electrons.

ToF-SIMS is capable of providing spatial resolution of the data collected in the form of a chemical map if the incident beam is rastered across several points within a given surface area. On selecting specific ions obtained from the analysis, the distribution of those ions across the surface can be seen. The size of the image depends on the size of the area analysed and each pixel of each image provides individual chemical information. This allows for regions of interest to be analysed. In this work 500 x 500 µm ToF-SIMS images of the polymeric coatings were acquired with 512 pixels/mm resolution (Figure 2.3).

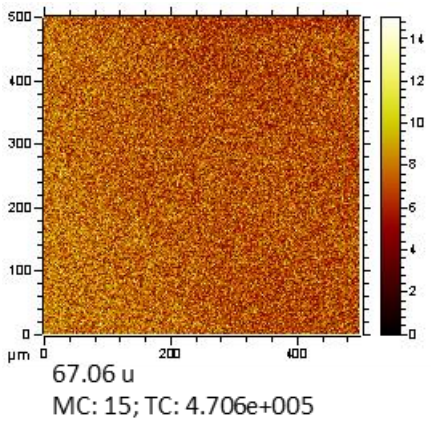

Figure 2.3 500 x 500 µm ToF-SIMS image of $C_5H_7^+$ (*m/z* 67.06) of a copolymeric surface obtained using an IONTOF IV instrument and SurfaceLab6 software.

2.2.2 Water Contact Angle

The wettability of a surface can be quantified using WCA. This hydrophobicity or hydrophilicity information (if water is the solvent used) has been used in an attempt to determine the relationship between biological properties of a surface.[262] Contact angle measurements for each sample were taken using 18.2 Ω·cm miliQ water. A KSV CAM 200 computer controlled Optical Contact Angle Meter was used (Helsinki, Finland). The sessile drop method was employed using 2 µL droplets of water deposited by using a syringe nozzle (Figure 2.4A). The side profile of the droplet extracted from the image was used to determine the contact angle. The profile is curve fitted to the Young-Laplace equation (Equation 1). The angle taken from each side of the droplet was averaged.

$$\sigma_{sg} = \sigma_{sl} + \sigma_{lg} \cdot \cos\theta \quad \text{(Equation 1)}$$

The contact is considered at the thermodynamic equilibrium of the three phases: solid, liquid and gas. This equation assumes a flat, rigid surface.

Because of the influence of evaporation, droplet images were collected, as previously described,[263] using a high-speed camera triggered to record as the droplets were released. It was possible to accurately record the droplet image at time intervals very much shorter than the time scale on which the droplets evaporated. WCA values were then plotted against time. The WCA of droplets decreases slightly with time in a linear manner due to evaporation. An examination of videos revealed they initially decreased in height without movement of the perimeter and then decreased in diameter with a contraction of the perimeter.[263] Subsequently, the WCA that was considered was the WCA at time zero obtained by interpolation of the fitting linear equation (Figure 2.4B).

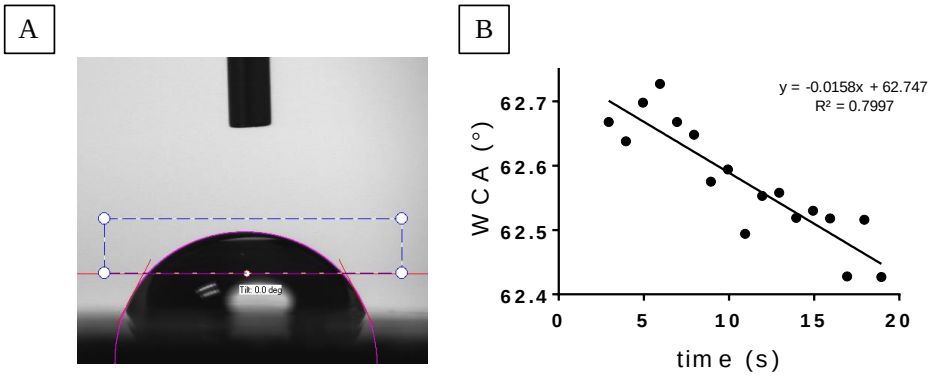

Figure 2.4 A) Example of droplet deposited onto a polymeric surface. **B)** WCA has been plotted against time (dots). Linear regression was fitted with $R^2 = 0.80$. $y_0 = 62.7$.

2.2.3 Atomic Force Microscopy

The atomic force microscope is able to investigate at nanoscale resolution the surfaces of a wide range of samples in both ambient and aqueous environments. This is particularly beneficial in analysing biological samples.

AFM operates by running a nanoscale tip mounted at the end of a flexible cantilever over a surface. Three different modes can be adopted using AFM depending on the interaction between the tip and the surface. The tip can either raster across or near to the surface or intermittently tapped onto it. These are known as contact, non-contact and tapping mode respectively.[264] In the non-contact mode, the tip of the cantilever does not make direct contact with the sample surface. Instead, the cantilever is oscillated at a frequency slightly above its resonant frequency where the amplitude of oscillation is typically a few nanometres (<10 nm). The van der Waals force, which is strongest from 1 nm to 10 nm above the surface, or any other long-range force which extends above the surface decreases the resonance frequency of the cantilever. In the tapping mode, also called intermittent contact mode, the cantilever is driven to oscillate up and down at near its resonant frequency similar to that in the non-contact mode. However, the amplitude of this oscillation is much greater than 10 nm, typically 100–200 nm. Owing to the force (van der Waals force, electrostatic force, etc.) acting on the cantilever when the tip comes close to the surface, the amplitude of this oscillation is decreased as the tip gets closer to the sample. As the cantilever is scanned over the sample, an electronic servo adjusts the height of the cantilever to maintain constant oscillation amplitude or frequency. Vertical

changes of cantilever are detected through an optical lever effect using a laser beam which is reflected off the cantilever (Figure 2.5A-B).

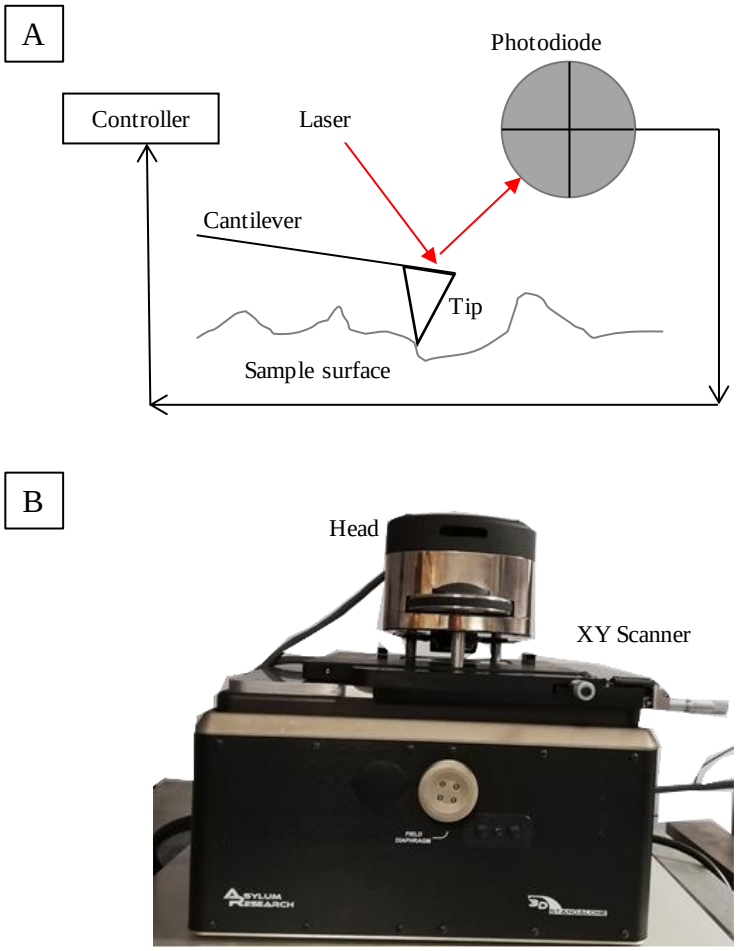

Figure 2.5 A) Schematic of the basic set-up of an atomic force microscope. The movement of the tip across the surface is detected by a laser deflected onto the top of the cantilever. **B)** Photograph of the MFP 3D (Asylum Research) used in this project.

The movement of the laser is then captured by using a photodiode. Changes in height across a surface are then captured by a photodiode which detects the movement of the laser light. This information is then processed into an image of the surface. These images can provide surface characteristics such as roughness and topography. The nature of direct physical interaction between the probe and the surface also allows surface properties such as stiffness and adhesion to be determined at the same spatial resolution.[265]

Polymers and biological samples tend to be softer than other materials and hence can be damaged by the AFM probe during analysis, particularly in contact mode where the tip is in continuous physical contact with the surface.
Tapping mode was developed to circumvent this particular problem and enable such surfaces to be imaged with a reduced chance of permanent damage. In this mode the cantilever resonates at or near to its resonant frequency – this method of excitation often being termed 'acoustic' tapping mode. The amplitude of this oscillation is kept constant. As the tip approaches the surface, the amplitude of oscillation is dampened and a feedback loop is used to maintain tip-sample average separation such that the oscillation reaches a target amplitude (the so-called 'set point'). In tapping mode, the tip tends to touch the surface only at the bottom of each oscillation cycle.

As stated, AFM is also capable of providing quantitative information of the surface such as that of stiffness and adhesion. This can be achieved by recording force-distance curves by driving the tip towards and into the sample surface whilst measuring the cantilever deflection (Figure 2.6). As the tip gets close enough to the sample the tip comes into the range where interacting forces begin to occur and the cantilever bends towards the surface and eventually jumps into contact when the attractive forces exceed the stiffness of the lever. As the tip is driven further into the surface the cantilever straightens until repulsive forces cause further deflection. The cantilever is then removed from the surface, in retraction adhesion may hold the tip onto the surface until the energy stored in the flexed cantilever exceeds this force and the tip jumps away from the surface.

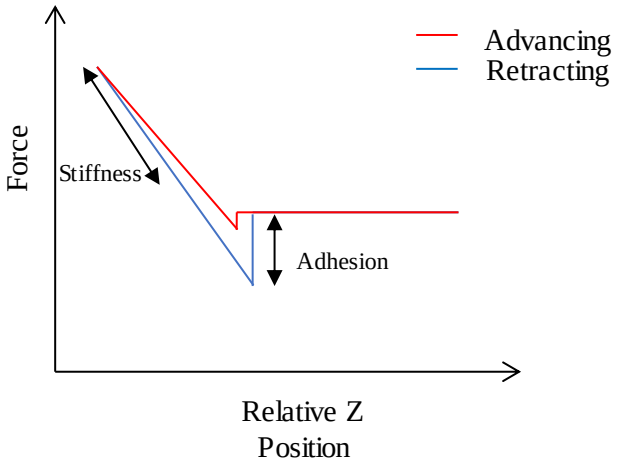

Figure 2.6 Diagram of a standard force *vs* distance curve showing the regions from which stiffness and adhesion of the surface are derived.

The vertical position of the tip against its deflection throughout the process can be plotted as a force *vs* distance curve (Figure 2.6). The force is determined by the magnitude of the deflection of the cantilever, quantified using Hooke's law (Equation 2).

$$F = -kd \quad \text{(Equation 2)}$$

F equates to force, *k* is the cantilever's force constant and *d* is the deflection of the cantilever. This information is then used to determine other mechanical properties. Using the portion of the curve where the tip is driven into the sample, Young's modulus can be calculated. The deflection of the cantilever as it is drawn away from the surface can be converted into force using Equation 3. The spring constant of the cantilever is determined using its resonant frequency and the 'Q factor' or the number of oscillations for the energy of the oscillating cantilever to fall to 0.2% of its original energy (Equation 3). The sensor response is recorded prior to analysis using a known hard surface, usually glass, measuring deflection using the linear part of the curve.

$$k = 2\pi^3 \, l^3 \, w \sqrt{(\rho^3 / E)} \; f_0{}^3 \quad \text{(Equation 3)}$$

In this work, AFM was adapted to characterise polymeric surfaces in term of stiffness.

2.3 Bacterial Strains

A *P. aeruginosa* PAO1 sub-line strain from the University of Washington collection wild-type (WT) (PAO1-W) has been used in this project and any corresponding isogenic mutants were constructed by Dr Jean Dubern. All mutants are reported in Table 2.2.

Table 2.2 All strains used in this work.

Strains	Genotype and/or Relevant characteristic	Source or reference
P. aeruginosa		
PAO1-W	Washington collection wild-type *P. aeruginosa* strain	Washington collection
PAJD431	In frame deletion of *pilA* in PAO1-W	Dr Jean Dubern
PAJD477	In frame deletion of *fliC* in PAO1-W	Dr Jean Dubern
PAJD457	In frame deletion of *fliC* in PAJD431 resulting in a double mutant Δ*pilA* Δ*fliC* in PAO1-W	Dr Jean Dubern
PAJD360	In frame deletion of *motAB* in PAO1-W	Dr Jean Dubern
PAJD552	In frame deletion of *motCD* in PAO1-W	Dr Jean Dubern
PAJD549	In frame deletion of *motCD* in PAJD360 resulting in a quadruple mutant Δ*motAB* Δ*motCD* in PAO1-W	Dr Jean Dubern
PAJD544	In frame deletion of *sadB* in PAO1-W	Dr Jean Dubern

2.4 Microscopy

2.4.1 Multimode Microscope Description

Bacteria can use a number of different mechanisms for moving across surface and through liquids (section 1.5.1).[266] To gain novel insights into the interplay between cells in bulk and the interaction with different surfaces, we have developed a novel multimode 2/3D microscope with interlaced acquisition of 2D surface differential interference contrast (DIC) images with in-line 3D digital holographic microscopy (DHM). To determine bacterial cell orientation, the spatial and temporal resolution of the DIC images at the surface were sufficient. To enable imaging of a higher density bacterial population than is possible for DHM, an optical relay was incorporated to virtually recreate the sampling area, enabling it to be rapidly scanned in the z-dimension using a remote piezo-driven objective to avoid sample disturbance.[267] Figure 2.7 shows a schematic of the multimode 2/3D microscope setup.

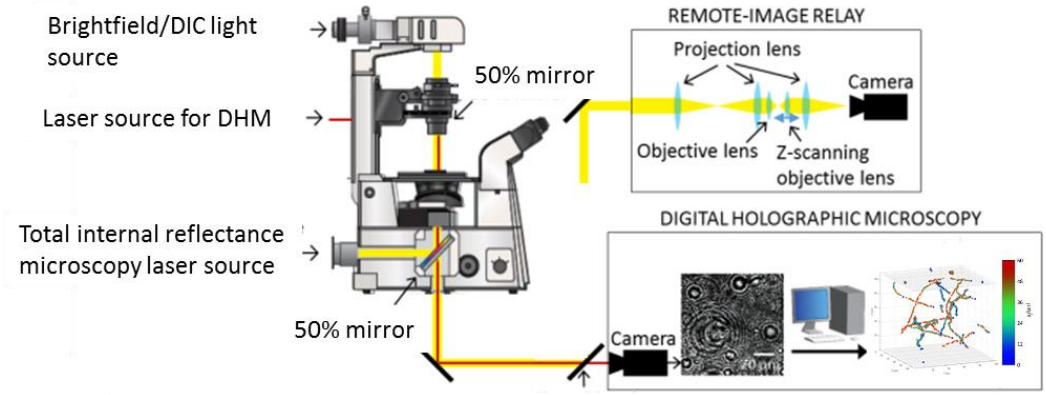

Figure 2.7 Schematic of the multimode 2/3D microscope used in this study including the optical ensemble for the remote-image relay. The remote image relay allows scanning of the focal plane to acquire and reconstruct z-stacks without disturbing the sample. The microscope is also equipped with lasers to enable DHM. Image taken from [268].

2.4.1.1 Differential Interference Contrast Microscopy

Differential Interference Contrast (DIC) Microscopy or Nomarski Interference Contrast microscopy is an optical microscopy technique able to distinguish features in biological samples by exploiting differences in the refractive index of the components that comprise it. This variation is detected by using a specimen and a reference light ray and determining the phase difference between the two.

This method ensures that clear images can be produced when analysing thick samples as well as improved overall resolution as compared to phase microscopy. The fact that the samples do not need to be stained or prepared in any particular way means that biological processes are less impeded than if they were to be altered in such a way prior to analysis.

Initially unpolarised light from a 100 W tungsten-halogen lamp enters the microscope and is polarised at 45°. It then enters the first prism a 'Normaski-modified Wollaston Prism' made of quartz and the two rays of light are separated polarised perpendicular to each other (Figure 2.8A-B-C)). These are the specimen and reference lights. The condenser focusses these two points onto the sample such that they pass through points adjacent to each other, one through

the sample and one through the background. The separation of these two points is usually similar to the resolution of the microscope's objective lens (~0.2 µm). This alters the optical path length of the sample if there are differences in sample thickness or refractive index. These rays then travel through an objective lens and are focussed onto a second prism. This combines the two light rays into a single polarised beam at 135°. This is known as differential interference.

After polarisation, the beams of light can interfere with each other. The rays of light have different phases with each other due to the differences in optical path lengths from the different sample points. Recombining this light generates the observed image which displays a contrast between the optical path lengths. This is usually displayed as differences in brightness between different points with the sample appearing brighter than the background. The image often presents a 3D appearance, but this does not necessarily represent the true situation, it is more an optical feature than true geometric relief (Figure 2.8D).

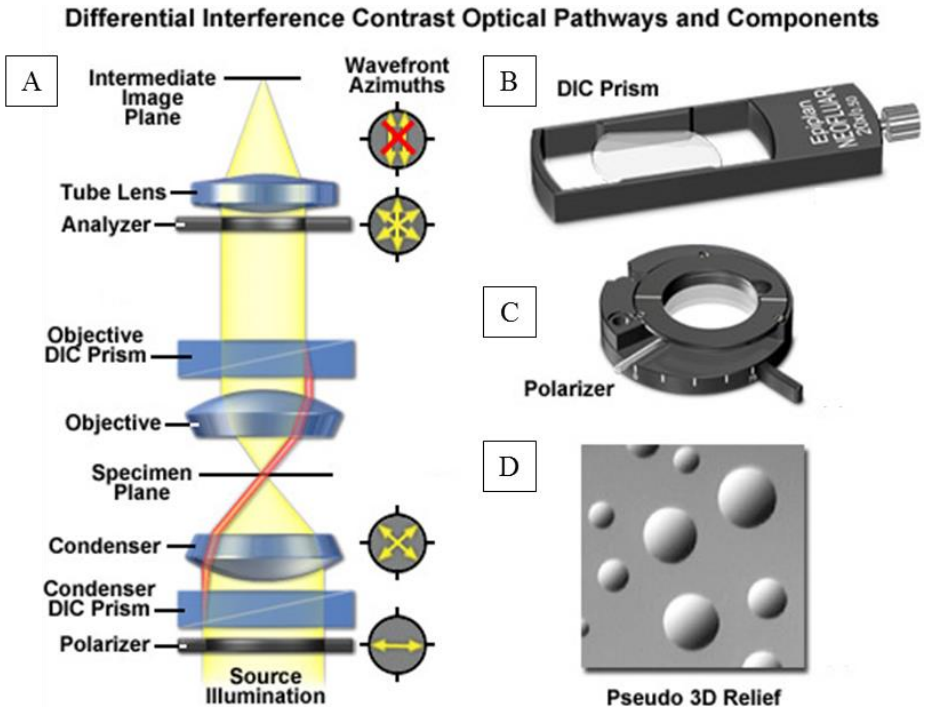

Figure 2.8 DIC principle. **A)** Beam path. **B)** Birefringent prisms. **C)** Condenser prism which performs a vectorial decomposition of the linearly polarised light into two vibration directions that are perpendicularly polarised to each other. Image taken from [269].

DIC is capable of investigating bacteria-surface interaction as an imaging technique by tracking real time changes in bacterial colonisation and movement through stack of frames.[269, 270]

2.4.1.2 3D-Holographic Microscopy and Remote-image Z-stacking Relay System

3D volumes have been imaged using optical techniques with narrow focal planes such as confocal microscopy to acquire z-stacks, but this approach is limited by low light transmission and consequently low acquisition rates. Most recently, 3D tracking of bacteria has been achieved using DHM where the x, y, z-position of individual cells is encoded in recorded diffraction patterns and determined computationally after the acquisition of data.[97] The key advantage of DHM is its ability to observe the 3D trajectories of many cells in a bacterial population simultaneously; however, features such as their orientation and shape are difficult to ascertain from the holograms.

A *hologram* is created by dividing the illuminating laser light in two beams. One beam illuminates the sample and it is referred to as the *sample beam*. The other one bypasses the sample instead and it is known as the *reference beam* (Figure 2.9A). By either reflection or transmission, the sample will interact with the illuminating sample beam. The resulting interference pattern between the two beams is the hologram (Figure 2.9B).

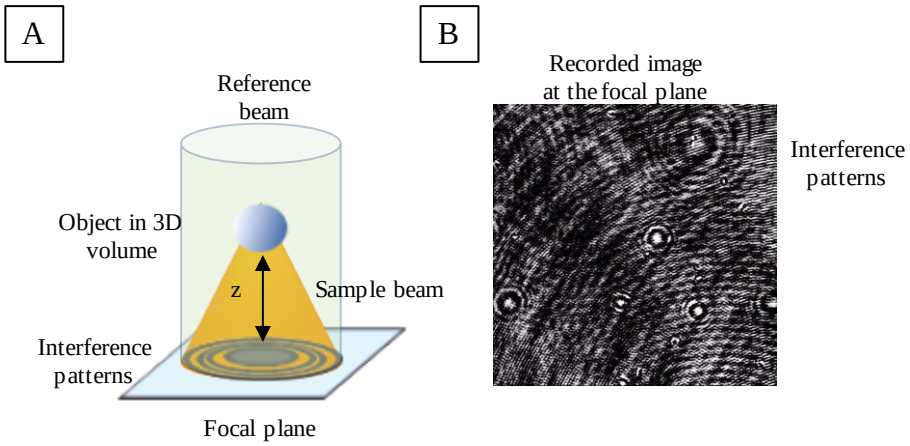

Figure 2.9 A) Schematic of the principle behind the holographic microscope. **B)** Example of recorded image at the focal plane showing the interference patterns of PAO1 in LB medium.

After acquisition, image intensity across a stack was normalised, then the median image over the stack was subtracted to remove background signal, also including attached cells. DHM image output sequences were reconstructed using a bespoke Python algorithm[271] making use of Rayleigh-Sommerfeld formalism to determine bacterial X-Y-Z coordinates. Bacterial trajectories were then determined using bespoke Matlab scripts written by Dr Andrew Hook.[268, 272] To exclude noise, a voxel size limit was set and applied to each image such that a similar number of objects were identified in each frame. Visual inspection of interferogram image sequences enabled an estimate of the number of bacteria per frame to ensure the voxel limit was set so as not to exclude bacterial cells.

Single cell bacterial trajectories in 3D volumes were determined using DHM at cell densities of up to 1.7×10^4 cells μL^{-1}, but above this, overlapping interference patterns inhibited digital holographic reconstruction. To measure the 3D distribution of cells at higher populations, the remote image relay was used to acquire a series of DIC images separated in the z-axis, referred to as *z-stacks*. Analysis of the z-stack data enabled the position of each bacterium to be determined at a population density of 3.7×10^5 cells μL^{-1}, greater than an order of magnitude improvement over holography, with a maximum population density within any one image of 8.0×10^5 cells μL^{-1}.

The remote image relay consists in the design of a microscope system as the result of two separate microscope systems juxtaposed so that the first magnifies the object by a factor M_1 and the second de-magnifies by M_2 (Figure 2.10).This results in a system in which a virtual image is created, another objective lens can scan and move back and forward to focus different plane in the virtual image without any problems for the specimen and for the objective. Until now, nobody has ever used this method to track bacteria in a 3D space.

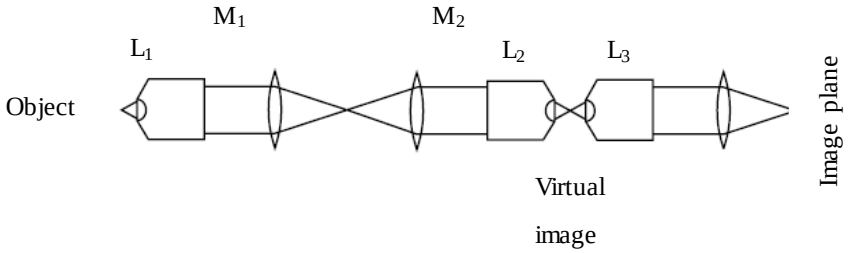

Figure 2.10 Remote image relay system.[267]

Given the limit of the scan speed using the remote image relay system which is 16 ms, only slow movement can be tracked. In addition, the objects in the 3D volumes were found to be affected to flow (Figure 2.11A). A bespoke Matlab script (DriftCorrection Appendix 1) was designed to remove the collective motion associated with bulk drift. Objects that were found in multiple slices following the flow direction were defined as new objects with coordinates the centre of mass of all the position of points in tracks (Figure 2.11B).

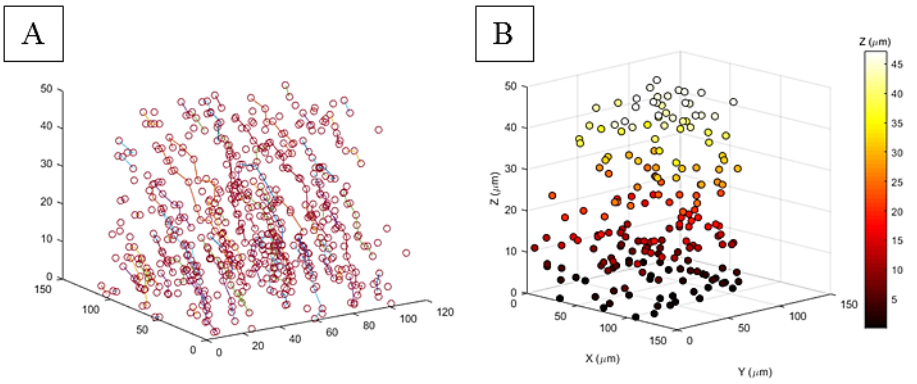

Figure 2.11 A) Identified objects before drift corrections (dots). Lines connect the same object found in multiple z planes due to drift. **B)** Objects in 3D volume after drift correction.

2.4.1 Image Processing and Segmentation

Images of bacteria captured using a microscope have to be processed in order to track bacteria. The aim of tracking is to associate objects across consecutive video frames. Automated tracking is a generic problem that is applicable to many research areas including biology, fluid dynamics, security and surveillance and ecology. There is a variety of imaging modes, types of objects and types of motion, therefore there is also a need to develop tracking algorithms which are suitable to specific investigations and as user-friendly as possible.

Tracking is mainly achieved in two steps: target objects are identified in each frame of a video to create a list of objects which are characterised (x, y, z, and other parameters); then the same objects in different frames are linked together to create a trajectory/track. Algorithms have to be developed to transform objects into tracks. The problem is usually complicated by the presence of spurious objects (caused by false positives during the detection step), missed detections (false negatives), track crossing, object occlusion (full or partial overlapping of two or more objects) and track spawning (where an object splits into two).

In order to decrease the possibility of these problems it is relevant to improve the accuracy of the object detection stage. For instance, either fluorescent labelled bacteria or dark field or phase contrast microscopy can be used to improve the contrast in the microscope image. Similarly, in this project it has been decided to use DIC images and fluorescently labelled bacteria. Despite the fact that there are several algorithms available to track bacteria, to our knowledge none of them can process DIC images. For this reason, we developed our own MATLAB scripts package.

DIC images were processed using a bespoke MATLAB script (StackMaster respectively).[272] Each image was flattened by a line-by-line polynomial fit. A threshold was then applied to binarise the image to segment pixels with bacteria. Threshold was set as $signal^2 : noise^2 > 10$. The square of the signal was measured so as to identify both bright and dark regions associated with the DIC image. Objects less than 20 pixels were excluded as noise. Holes within objects were

filled using the MATLAB function ‘imfill’. Bright and dark regions were paired based upon proximity and a common directional vector between objects within the same frame. The centre of mass of objects was calculated giving equal weighting to bright and dark regions. The length and width of the smallest rectangle around an object and the orientation of the bacterial cells was determined using a bespoke MATLAB script (ParticleAnalysisDIC).[272]

To exclude noise a pixel limit was set and applied to each image such that a similar number of objects were identified in each frame. Visual inspection of DIC image sequences enabled an estimate of the number of bacteria per frame to ensure the pixel limit was set so as not to exclude bacterial cells. Bacterial trajectories were determined using the bespoke MATLAB script (TrackingAnalysis, Appendix 2). Objects were matched with their nearest neighbour within the next frame, applying a distance limit based upon the maximum speed of bacteria (100 μm s^{-1}). The script looked up to 4 frames ahead for a matching object. All tracks were also visually inspected using a bespoke MATLAB script (VideoMaker Appendix 3) to ensure trajectories skipping more than 4 frames could be joined.

Experiments were conducted under the microscope in static conditions using a custom designed 1/12 well(s) holder in polyether ether ketone (PEEK) (Figure 2.12A-B). The holder allows a coated coverslip to be inserted and filled with 4 ml of culture medium. To avoid leaks, coverslips were sealed using a silicone and halogen free high-vacuum grease (Apiezon M). The technical drawing for the 12 wells holder is shown in Appendix 4.

A

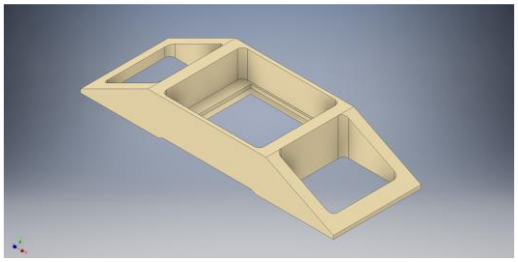

B

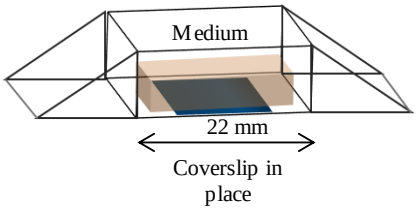

Figure 2.12 A-B) Schematic of bespoke holder to use coverslips coated with different polymers. The 22 × 22 mm coverslip was sealed at the bottom using a silicone and halogen free high-vacuum grease (Apiezon M).

2.4.2 Fluorescence Confocal Laser Scanning Microscopy

Samples which are not entirely flat such as coated catheters can pose problems for conventional widefield optical systems because bright fluorescent signals from objects outside the focal plane can affect the background images. Confocal microscopy fixes this problem by not accepting signals coming from sources which are not in the focal plane. Using Confocal microscopy this is achieved by illuminating the sample with a focused scanning laser beam and by placing a pinhole aperture in the image plane in front of an electronic photon detector. This allows to improve the signal-to-noise ratio (SNR) and to achieve high resolution and better contrast imaging with a small depth of field. By using a stepper motor system that changes microscope focus in small step defined by the user, confocal microscopy allows the acquisition of z-stacks of images and to generate 3D view of specimen.[273]

Initially a laser light source of a certain wavelength illuminated the sample and a dichromatic mirror reflects the laser light towards the sample (Figure 2.13). This mirror allows longer wavelength emitted light to pass through to the detector. The objective lens focusses the excitation light onto the sample and the emitted light onto the detector. In order to stop scattered light potentially causing unwanted photo-bleaching, confocal microscopes use pinholes to block the scattered light from above and below the focal planes. [214]

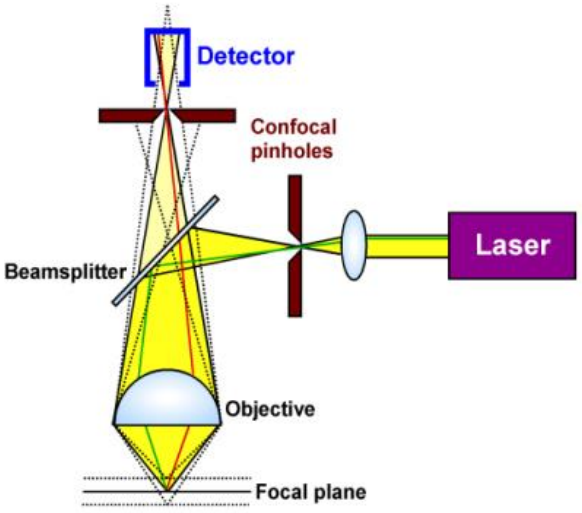

Figure 2.13 Schematic of the basic components of a confocal microscope.[216]

If the pinholes are too small a large portion of the total fluorescence signal may be blocked, too large and the resolution decreases. Therefore, an intense light source like a laser and a photomultiplier is used to amplify the total amount of fluorescence signal from the sample. At this point gain and exposure time must be used wisely in order to increase sensitivity sufficiently without increasing background noise or photobleaching the sample. Cross sections of a sample can be taken and combined in the z axis to construct 3D images of the total sample.

2.4.3 Environment Scanning Electron Microscopy

Environmental scanning electron allowed us to avoid conditions that are typically used with Scanning Electron Microscopy (SEM) which can adulterate biological samples. Typically, SEM imaging requires a high vacuum, $\leq 10^{-8}$ Torr having first been chemically fixed, dehydrated, and coated with a conductive material (e.g. gold) to prevent charge build-up from the electron beam.[274] Few biological specimens tolerate these conditions without rapid collapse. ESEM technique allows overcoming these obstacles. It is a modified, low-vacuum scanning electron microscopy technique for biofilm monitoring that enables imaging of hydrated specimens.[275]

2.5 **Quantification and Statistical analysis**

Average values and standard errors were determined by using GraphPad PRISM 8 and Microsoft EXCEL 2016. All the error bars represent 1 standard deviation (SD) except where stated. For each figure, the number of technical replicates and biological repeats are described by *n* and N and together with other relevant information are included in the corresponding legend.

A t-test analysis and one-way analysis of variance (ANOVA) were performed to compare two or more samples respectively. Multiple comparison was performed by using Tuckey's correction. For the statistical analysis of multiple polymers and multiple mutants two-way ANOVA was performed and Sidak's method was used for multiple comparison.

Chapter 3

How Single Cell Behaviour and Biofilm Formation is Influenced by the Nature of the Polymer Substrate

3.1 Introduction

Microbiologists have traditionally focussed on microbial investigation at the population level which has provided information about, for instance, how bacteria collectively respond to their environment, communicate at both intra- and inter- species levels, or regulate the expression of genes.[276] However, great heterogeneity has been reported in terms of genetic composition, physiology, biochemistry or behaviour, even in cells in supposedly "clonal" populations.[277] This variability has crucial importance in the study of antibiotic resistance and the rise of potential pathogenic species.[278] Microbial heterogeneity is a hallmark of biological systems and allows bacteria to display a multitude of genetic and non-genetic differences from each other enabling them to have an inherent plasticity and capacity to adapt which creates a successful life strategy.[279] Microbial genomes can undergo remarkable changes within very short periods of time.[280] Asymmetries in the distribution of genetic material between daughter cells has been shown to drive processes of differentiation in several bacterial species.[281] Cell aging, accumulation of DNA damage, gene loss or variability in gene expression are only few examples of genetic heterogeneity between single-celled bacteria.[282] Behavioural variability is the consequence of single-cell heterogeneity in genetic (epigenetic phenomena) and biochemical characteristics. Observation of individual cellular responses to environmental stimuli, measurement of swimming speed and direction, number of reversals, analysis of flagella motor bias indicate some of the possible means through which bacterial heterogeneity can be investigated.[283]

Microscopy represents the master tool available for single-cell analysis and to study dynamic bacterial properties associated with bacterial motility such as cell speed, the number and duration of runs and tumbles, residence time.[276] Biofilms are an important part of the bacterial lifestyle of bacteria, and it is

assumed that there is a motility-to-biofilm transition wherein the cessation of motility promotes biofilm formation.[88] Here we developed a multimode microscope (section 2.4.1) to assess bacterial behavioural heterogeneity at surfaces with different chemistries. This chapter focuses on how different surfaces might affect *Pseudomonas* motility. Flagella and T4P have been widely described to be involved in bacteria motility in *Pseudomonas* in section 1.5.1. Recently, Oliveira *et al.* showed, for the first time, surface-attached cells perform chemotaxis on a surface (using T4P) where bacteria adjust their favoured positions on a surface and regulate their movements with remarkable sub-micron precision.[284] Little is still known about the potential for these cells to respond to surface chemical environments. To successfully colonise medical devices, and generic surfaces, some bacterial species control motility and EPS production *via* the second messenger c-di-GMP (section 1.5.2.3) which is known to play a crucial role in biofilm formation.[285]

3.1.1 Aims

Multimode microscopy was used to explore bacterial-material interactions and to gain novel insights into differences in cell behaviour within the bulk and at the surface. A biofilm formation assay at different time points and confocal scanning method allowed us to follow biofilm formation over time. Single cells were tracked to assess bacterial motility near and across surfaces and to investigate whether surface chemistries influence pili and flagella-mediated motility. New MATLAB scripts have been developed to process DIC and fluorescence images and to track bacteria at the presence of different surfaces. This chapter focuses on describing changes in surface chemistry and how such different surfaces might affect bacterial motility. Two different polymeric surfaces previously identified were considered.[253] The biofilm resistant polymer ethylene glycol dicyclopentenyl ether acrylate (pEGdPEA) and the pro-biofilm polymer neopentyl glycol propoxylate diacrylate (pNGPDA) were used to assess bacterial behaviours during initial surface interactions. c-di-GMP and EPS production were then combined with bacterial motility assays in order to assess how this secondary messenger plays a role in bacterial motility on these polymeric surfaces.

3.2 Experimental

3.2.1 Polymer Preparation

Two polymers were selected as anti-biofilm and pro-biofilm polymers based upon previous work by Hook *et al.*[7, 231] and used to coat glass borosilicate coverslips (Gerhard Menzel, Braunschweig, Germany) (Figure 3.1). A combination of the respective monomers was also used to produce a 1:1 copolymer. In order to avoid delamination, glass was treated with oxygen plasma at 100 W incident RF (13.56 MHz) power for 1 min at 0.5 mbar working pressure by using a custom built reactor as previously shown.[286] Activated coverslips were then methacrylate silanised by immersion in 3-trimethoxysilylpropyl methacrylate (Sigma-Aldrich) 2% v v^{-1} at 50℃ under 1 atmosphere of argon for 16 h. Biofilm resistant polymer pEGdPEA was polymerised from ethylene glycol dicyclopentenyl ether acrylate (EGdPEA) monomer (Sigma-Aldrich) and pro-biofilm pNGPDA from neopentyl glycol propoxylate diacrylate (NGPDA) (Sigma-Aldrich) as described previously.[6, 253, 254] A total of 5 µL of each monomer containing 1% (w v^{-1}) initiator 2,2-dimethoxy-2-phenylacetophenone (DMPA) (Sigma-Aldrich) was deposited onto each coverslip before irradiating for 60 min using short-wave ultraviolet (UV) light 365 nm, 2 x 15 W. The polymerisation was carried out under argon maintaining an oxygen concentration below 2000 ppm (to prevent free radical quenching by oxygen) at room temperature (20°C). Homopolymer coatings as well as a copolymer pEGdPEA-co-NGPDA (1:1) (v v^{-1}) coating were prepared. Coated coverslips were then dried at <100 mTorr for 5 days to extract any unpolymerised monomers.

The same procedure was used to polymerise three other polymers known to have biofilm resistance properties: benzyl methacrylate (BnMA) (Sigma-Aldrich),[8] isobornyl methacrylate (iBMA) (Sigma-Aldrich),[6] trimethylcyclohexyl methacrylate (TMCHMA) (Sigma-Aldrich).[6]

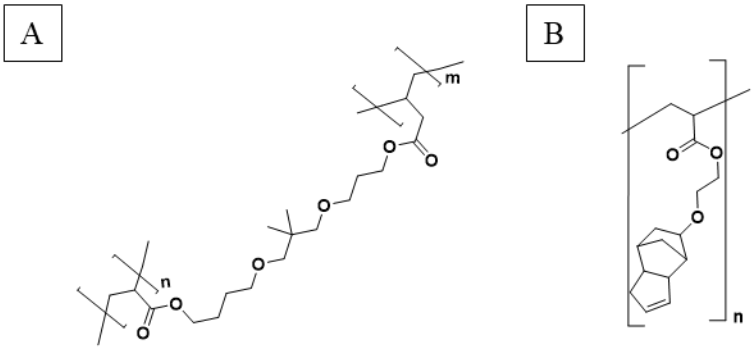

Figure 3.1 Chemical structure of **A)** pNGPDA and **B)** pEGdPEA.

3.2.2 Time-of-Flight Mass Spectrometry

ToF-SIMS data were acquired from pEGdPEA and pNGPDA homopolymer and pEGdPEA-co-NGPDA (1:1) copolymer printed spots with hyperspectral image data acquisition employed resulting in an image with a full spectrum at each pixel. The ToF-SIMS data were acquired using a ToF-SIMS IV instrument (ION-TOF GmbH., Münster, Germany) equipped with a bismuth liquid metal ion gun and a single-stage reflectron analyser. Operating conditions utilised Bi_3^+ with primary ion energy of 25 kV and a pulsed target current of approximately 1.0 pA. Low-energy electrons (20 eV) were used to compensate for surface charging caused by the positively charged primary ion beam on the insulating surfaces. Individual spots were analysed rastering areas of 500 × 500 μm at a resolution of 256 × 256 pixels. The total primary ion beam dose for each analysed area was kept below 1 × 1012 ions cm^{-2}, ensuring static conditions. Both positive and negative secondary ion spectra were collected (mass resolution of >6,000), over an acquisition period of 15 scans (the data from which were added together). Owing to the non-conductive nature of the samples, charge compensation was applied *via* a low energy (20 eV) electron floodgun. Data analysis were performed using SurfaceLab 6 (IONTOF GmBH, Germany). Positive ion spectra were calibrated against peaks for CH_2^+, CH_3^+, $C_3H_2^+$ and $C_4H_3^+$ before further analysis. Negative ion spectra were calibrated against peaks for CH^-, C_2H^-, $C_2H_5O^-$ and OH^- before further analysis. The calibrated data were used to generate a peak list comprising all secondary ions of significant intensity. The peak list was generated using the search function in the SurfaceLab 6

software with a selection threshold of >100 counts, >1 SNR, max background 0.8. pEGdPEA substrate coating uniquely contained $C_5H_5^+$, whereas $C_3H_5O^+$ was used as characteristic marker for pNGPDA. The copolymer showed intermediate intensities for the two ions.

3.2.3 Bacterial Growth Conditions and Biofilm Assay

Biofilms were cultivated on borosilicate glass slides treated as above on which the polymers pNGPDA and pEGdPEA were spotted in triplicate. *mCherry*-labelled *P. aeruginosa* PAO1-W wild-type and isogenic mutants were grown at 37ºC for 16 h in 5 ml Luria-Bertani broth. Cultures were diluted 1:100 in fresh medium until OD_{600} of 0.01 was reached in 5 ml RPMI-1640 and inoculated into petri dishes containing UV sterilised spotted glass slides or coverslips. Bacterial cells were seeded at 37ºC under static conditions for 2 h before dishes were moved to a shaker at 60 rpm and 37ºC for 24 h to form mature biofilms. The slides were examined under a Laser Scanning fluorescent Microscope (LSM2, Zeiss). Biofilms were visualised using *mCherry* or green fluorescence protein (*gfp)* mode at an excitation wavelength of 587/ 509 nm. Images were obtained using 40×/1.3, 20×/0.8 or 10×/0.3 Plan-Apochromat objective lens with a pinhole size of 70 µm, 555 and 488 nm lasers and filters at 560 and 555 nm for *mcherry* and *gfp* respectively. Lasers power was set at 2% power. Imaging was carried out using Zen 2011 imaging software (Zeiss). A total of 5 z-stacked images were collected per polymer spot. Sampling was conducted at random from the central portion of each spot. Biomass was calculated using Image J and Comstat 2.1 which indicates biofilm thickness (µm) although the convention is to quote a volume um^3 over an area um^2.[287]

To visualise eDNA/dead cells all seeded coated coverslips were exposed to propidium iodide (PI) (600 nM) for 30 min and gently washed 2× in PBS and 1× in H_2O. eDNA coverage was quantified using ImageJ. Since PI has an excitation maximum at 535 nm and fluorescence emission maximum at 617 nm, therefore *gfp*-labelled *P. aeruginosa* was used.

3.2.4 Microscope and Bacterial Tracking

Time-lapse imaging was achieved using a bespoke multimode microscope (Cairn Ltd.) (section 2.4.1). Samples were analysed at 37°C using a Nikon Eclipse Ti inverted microscope using a 40×, N.A. = 1.4, W.D. = 0.13 mm oil objective. The microscope was fitted with an environmental chamber (Okolab) to regulate temperature and relative humidity. Images were acquired using an Orca-Flash 4.0 digital CMOS camera (Hamamatsu) at different acquisition rates (from 0.03 to 100 Hz) depending on the experiment. DIC imaging was achieved using a single channel white MonoLED (Cairns) light source. Experiments were conducted using a custom designed 1 well holder under the microscope in static conditions (Figure 2.12).

To obtain bacterial track data, a script was developed to analyse captured trajectory data (TrackingAnalysis in Appendix 2). Tracks were then converted into videos (VideoMaker in Appendix 3). Bacterial particles were characterised in terms of length of two axes, orientation and circularity. This latter was obtained in Equation 4 where *A* and *p* are the area and perimeter of the object.

$$circularity = {}^{4\pi A}/_{p^2} \qquad \text{(Equation 4)}$$

Mean squared displacement (MSD) was calculated in accordance to Equation 5 where $\vec{x}(t_j) = \vec{R}_j$ and was vector of the jth point on the trajectory and the angled brackets indicated an average over all time t_i.[288] The *MSD* gave information about the average displacement between points in the trajectory separated by a fixed time lag.[289] A value of k_{MSD} = 1.0 corresponded to random diffusive motion, whereas k_{MSD} = 2.0 corresponded to directional ballistic motion.

$$\Delta x^2(t) = \langle(\vec{x}(t_{i+1}) - \vec{x}(t_i))^2\rangle \qquad \text{(Equation 5)}$$

The instantaneous speed was calculated as a function of the displacement vector as shown in Equation 6 where $\Delta t = t_{i+1} - t_i$ while the average speed was calculated according to Equation 7 where n is number of points in the track.

$$\vec{v}_i = |\vec{x}(t_{i+1}) - \vec{x}(t_i)|/_{\Delta t} \quad \text{(Equation 6)}$$

$$\vec{v}_{average} = \frac{1}{n}\sum_{i=1}^{n}(\vec{v}_i) \quad \text{(Equation 7)}$$

The sum of distance from mean was obtained as Equation 8 where $\vec{R}_i$ is the position vector of the ith point on the trajectory and $\vec{R}_{mean}$ is the mean of all points.

$$\overrightarrow{SDM} = \frac{1}{n}\sum_{i=1}^{n}\left(\left(\vec{R}_i\right) - \left(\vec{R}_{mean}\right)\right) \text{(Equation 8)}$$

The radius of curvature $\vec{R}$ from centre of mass was calculated as described in Equation 9, where $\vec{R}_i$ is the position vector of the ith point on the trajectory and $\vec{R}_{cm}$ is the centre-of-mass of all points as used before.[288]

$$\vec{R} = \frac{1}{n}\sum_{i=1}^{n}\left(\left(\vec{R}_i\right) - \left(\vec{R}_{cm}\right)\right) \quad \text{(Equation 9)}$$

This parameter gives information about the average displacement together with *MSD*.

Residence time was measured as the time between the start and the end of tracks between t = 1 h to t = 2 h from inoculation.

The division events were determined by searching for cases where one mother cell in frame *i* became two daughter cells in frame i^{+1}. These events (n=100 for each surface and each type of bacteria over 3 independent replicates N=3) were manually assessed to avoid possible misreading of the automatic algorithm. Each daughter cell was assigned a new identification. The states of post-division cells were defined as follows with three types of division branching. “Two-legged” (d=2) branching occurs when both daughter cells detach, “one-legged” (d=1) when one daughter cell detaches, and “zero-legged” (d=0) when both daughter cells remain surface-attached.

Intracellular levels of c-di-GMP were explored using a *cdrA*::*gfp* reporter gene fusion transformed into wild-type *P. aeruginosa* PAO1-W and the isogenic *mot* mutants. Tracks were obtained from images acquired using widefield epifluorescence microscopy (40×, 1.3) every 30 s for 3h and then processed

through a custom single-cell tracking algorithm. Evaluation of average fluorescence (*F* values) that correspond to *cdrA* expression levels in stationary cells was considered for cells with average speed < 1 nms^{-1} onto polymers. Tracks obtained using DIC images were combined with fluorescence images using FluorescenceIntensity script (Appendix 5).

3.2.5 Bacterial Matrix Visualisation

Environmental scanning electron micrographs were obtained using a Quanta 200FEG ESEM (FEI Company, Eindhoven, the Netherlands). Samples of polymers coupons incubated with *P. aeruginosa* were glued to the holders using die-cut carbon conductive adhesive discs (SPI Supplies/Structure Probe, Inc., West Chester, PA, USA). About 20 different measurement positions on the surface of each sample were chosen randomly to obtain representative images of biofilm formation. Images were obtained using Peltier Stage and gaseous secondary electron detector and captured at 1,000, 5,000 and 10,000× magnification. The chamber parameters were settled to 2°C temperature and 600 Pa pressure, at 10-15 kV. With these parameters the samples retain 85% of relative humidity. Then the chamber parameters were settled to <-10 °C temperature and 238 Pa pressure, at 5-15 kV in order to progressively sublimate the water content of the sample.

3.2.6 Investigation of Bacterial Footprints and Trails

Footprint trails were visualised using Concanavalin A, Alexa Fluor™ 633 Conjugate (ThermoFisher Scientific) at 50 $\mu g\ ml^{-1}$. Concanavalin A (ConA) is a lectin (carbohydrate-binding protein) which binds specifically to certain moieties found in various sugars, glycoproteins, and glycolipids, mainly internal and nonreducing terminal α-D-mannosyl and α-D-glucosyl groups.[290]

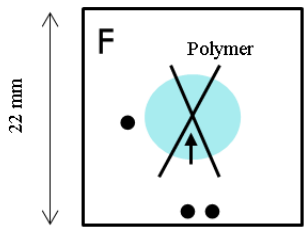

Figure 3.2 Schematic of glass coverslip (22 x 22 mm) with polymer spotted onto it. A cross with two and one dot in two corners were drawn with a marker pen in order to have reference of areas visualised through microscopy.

PAO1-W wild-type was grown in RPMI-1640 to an OD_{600} 0.002 and pipetted onto a surface, image in DIC mode for 2.5 h before being furtherly imaged using a confocal microscope (LSM2, Zeiss) without being washed. Samples were prepared as in Figure 3.2 with a cross on the back of the surface to facilitate assessment of the same area during tracking and for EPS visualisation. Trails were visualised at an excitation wavelength of 633 nm. Images were obtained using 63×/1.4, Plan-Apochromat objective lens, pinhole size of 70 µm, 639 nm laser and filter at 640 nm. EPS levels at the surface were measured as fluorescence intensity *F* using Zen 2011 imaging software (Zeiss) following Equation 10 where Fb and Ft are the intensities measured over an area of 100 µm^2 on polymers at t = 0 h (background) and t = 2.5 h respectively.

$$F = \frac{1}{3}\sum_{i=1}^{3}(Ft) - \frac{1}{3}\sum_{i=1}^{3}(Fb) \quad \text{Equation 10}$$

Similar background fluorescence levels for the polymeric surfaces were observed at t = 0 h at the presence of ConA staining and no cells. In particular, we detected an *Fb* equal to 3360 ± 1250 (a.u.) and 2452 ± 1564 (a.u.) on pNGPDA and pEGdPEA respectively (N=3).

3.3 Results

3.3.1 Time-of-Flight Mass Spectrometry

In a previous study, polymer microarrays were used for the discovery of a novel class of amphipathic acrylate polymers that were resistant to *P. aeruginosa* attachment.[254] Two polymers with opposite biofilm properties were prepared

by catalytic chain transfer radical polymerisation (section 2.1): the pro-biofilm pNGPDA and the anti-biofilm pEGdPEA.

To ascertain the chemistries of the polymers and copolymer, chemical fragment information of the surfaces was collected using ToF-SIMS. Figure 3.3A shows representative mass spectrum of pNGPDA, pEGdPEA and pNGPDA-co-EGdPEA highlighting particularly intense peaks at 67.06 m/z and at 59.05 m/z which were assigned to $C_5H_7^+$ and $C_3H_7O^+$ as respective fragments for pEGdPEA and pNGPDA.

These peaks were then normalised to the total intensity ion counts and compared between samples (Figure 3.3B-C). The coverage of the chemistry across polymers was also analysed using ToF-SIMS imaging. Figure 3.3D demonstrates homogenous coverage of pNGPDA-co-EGdPEA.

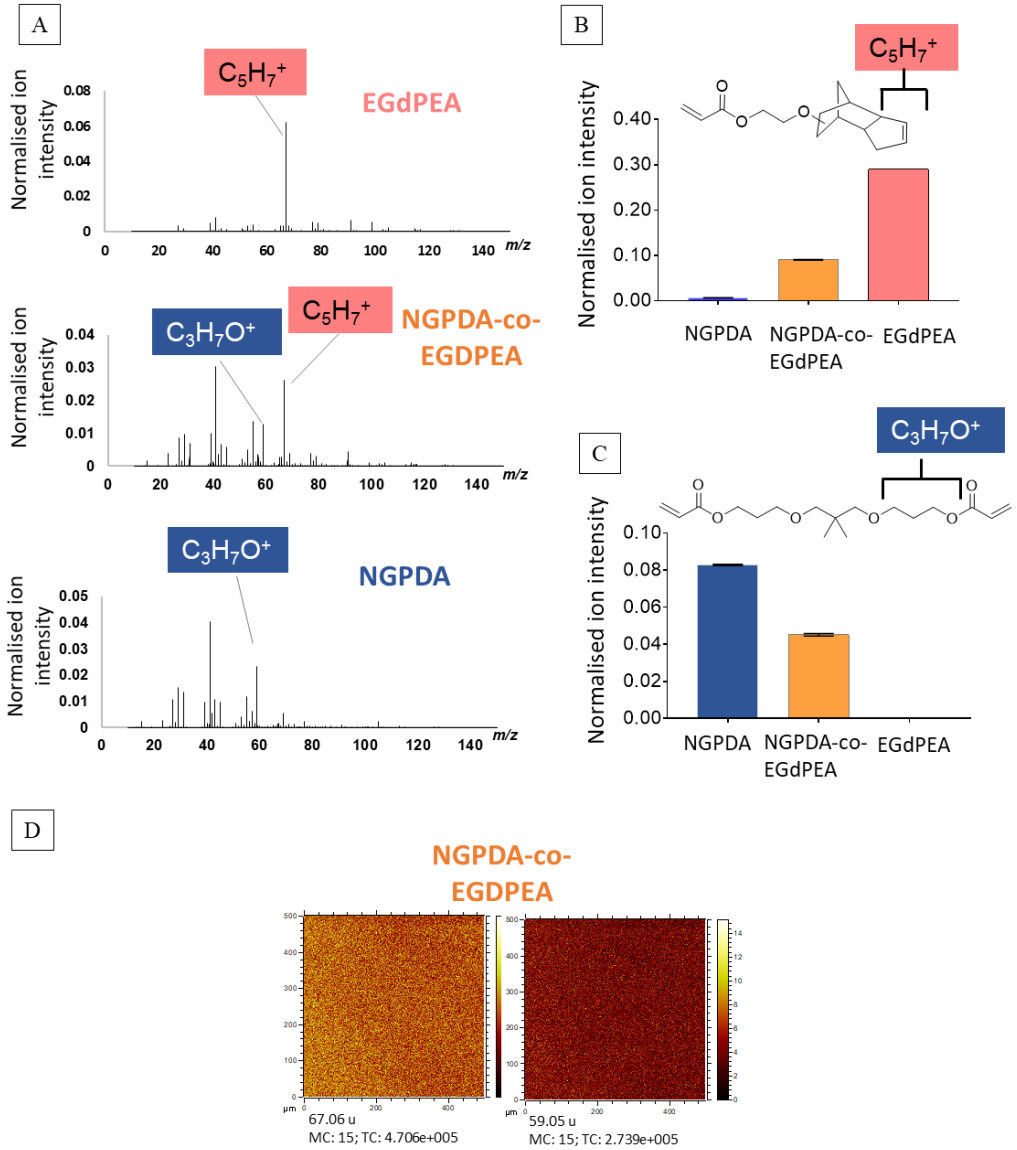

Figure 3.3 Surface characterisation. ToF-SIMS characterisation of polymer-coated coverslips. Positive ion ToF-SIMS spectra of pEGdPEA (pink), NGPDA-co-EGdPEA (1:1) (orange), pNGPDA (blue). $C_5H_7^+$ (*m/z* 67.06) and $C_3H_7O^+$ (*m/z* 59.05) are characteristic ions for pEGdPEA and pNGPDA respectively **(A)**. Comparison of normalised ion intensities for $C_5H_7^+$ **(B)** and $C_3H_7O^+$ **(C)** for the 3 polymers. **D)** An example corresponding secondary ion image (500 x 500 µm) for both $C_5H_7^+$ (m/z 67.06) and $C_3H_7O^+$ (m/z 59.05) ions using pNGPDA-co-EGdPEA. The two monomers polymerised homogeneously.

3.3.2 *P. aeruginosa* Fails to Form Mature Biofilms on pEGdPEA

Initially biofilm formation of *P. aeruginosa* PAO1-W *m-cherry* tagged was assessed on pEGdPEA, pNGPDA and a 1:1 (v v^{-1}) copolymer pNGPDA-co-EGdPEA. Representative confocal images from the coated coverslips after bacterial incubation for 24 h in RPMI-1640 are shown in Figure 3.4A and the biomass was quantified using COMSTAT 2.1 (ImageJ) in Figure 3.4B. Bacterial

biomass was observed to reduce from 23.8 ± 2.8 μm^3 μm^{-2} for pNPGDA to 0.2 ± 0.1 μm^3 μm^{-2} for pEGdPEA. This is consistent with bacterial coverage previously observed on these polymers.[6] An increase in bacterial biomass was measured for pNGPDA-co-EGdPEA (12.3 ± 1.8 μm^3 μm^{-2}) compared with pEGdPEA.

After 72 h PAO1-W biofilm on pEGdPEA and pNGPDA-co-EGdPEA (1:1) was 0.4 ± 0.2 μm^3 μm^{-2} and 0.7 ± 0.1 and μm^3 μm^{-2} respectively, whereas pNGPDA exhibited much higher biofilm coverage (47.8 ± 7.9 μm^3 μm^{-2}) (Figure 3.4).

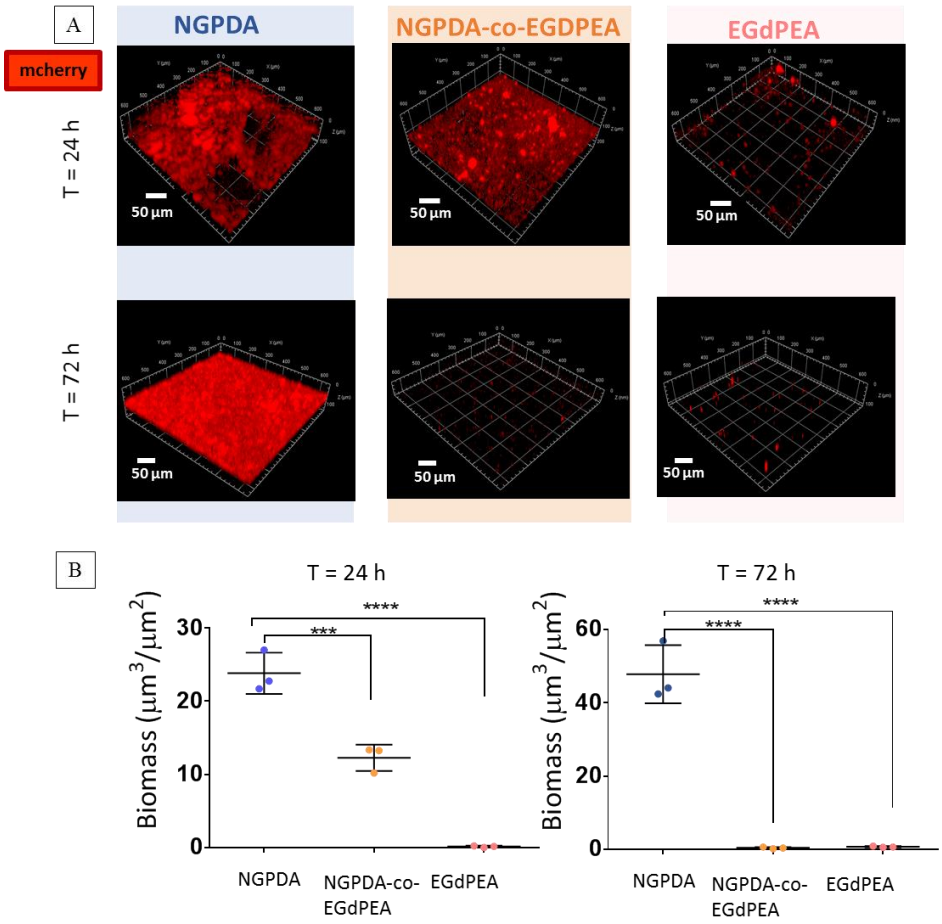

Figure 3.4 A) Confocal images (10×, 0.3) of *P. aeruginosa m-cherry* tagged after 24 h (top) and 72 h (bottom) on pNGPDA (left), pNGPDA-co-EGDPEA (middle), and pEGdPEA (right). Samples were washed 2× in PBS and 1× in H2O. Scale bar is 50 µm. **B)** Quantification of bacterial biomass for the 3 polymer surfaces. Error bars show ± 1 standard deviation (N=3). Significance was determined by analysis of variance One-way ANOVA and Tukey's post-test comparison for differences between the indicated samples. **** p<0.001, *** p<0.001.

3.3.3 Biofilm Characterisation

Biofilms are composed of cells embedded in an EPS which is mainly composed of eDNA, polysaccharides and proteins. Bacterial extracellular matrix is visualised using ESEM in Figure 3.5 showing representative images of bacteria attached to the surface of pNGPDA (left) and pEGdPEA (right) incubated for 24 h in RPMI medium. EPS encapsulating sessile bacteria was clearly observed on pNGPDA whereas no extracellular matrix was observed with the few clusters of cells attached to pEGdPEA. Together with biofilm assay data (Figure 3.4), these results demonstrate that pEGdPEA prevents bacterial biofilm formation.

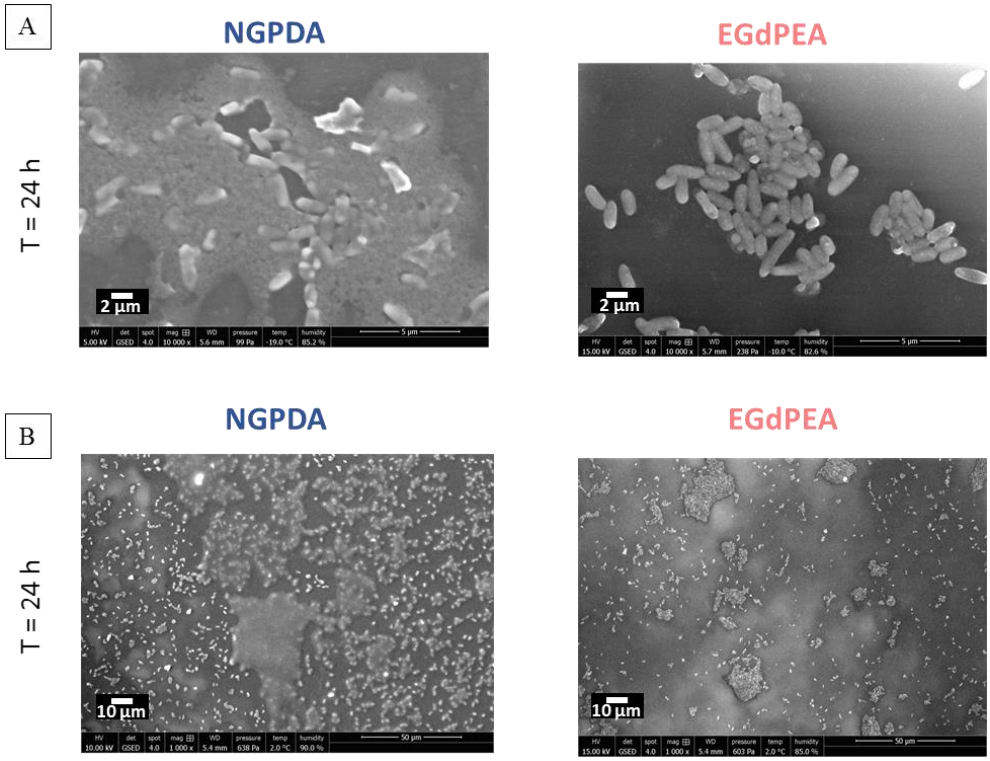

Figure 3.5 ESEM representative images of *P. aeruginosa* grown for 24 h on pNGPDA (left) and pEGdPEA (right). Images captured at 10,000× **(A)** and 1,000× **(B)** magnification. Bacteria were found embedded in the biofilm matrix on pNGPDA, whereas no matrix could be observed when grown on pEGdPEA. Scale bar is 2-10 µm respectively.

To visualise eDNA within cells grown on pNGPDA and pEGdPEA, PI was used. PI is a red-fluorescent acid nucleic staining and since it does not permeate live cells membrane, it only detects dead cells or extracellular DNA. PI binds to DNA by intercalating between bases. Once the dye is bound, the fluorescence

excitation maximum is shifted ~30–40 nm to the red and the fluorescence emission maximum is shifted ~15 nm to the blue, resulting in an excitation maximum at 535 nm and fluorescence emission maximum at 617 nm.[291]

Given these emission parameters *gfp*-labelled *P. aeruginosa* also permitted visualisation of viable bacterial cells. Figure 3.6A shows representative CLSM images of biofilm where cells are in green and dead cells/eDNA in red on pNGPDA, pEGdPEA and pNGPDA-co-EGdPEA. As shown in Figure 3.6B it has been observed a higher eDNA coverage, associated with the production of EPS, on pNGPDA (12.8 ± 1.0%) compared with both pNGPDA-co-EGdPEA (5.1 ± 1.6%) and pEGdPEA (1.9 ± 0.5%) (p<0.0001). This further confirmed the ability of pEGdPEA to prevent bacterial biofilm formation.

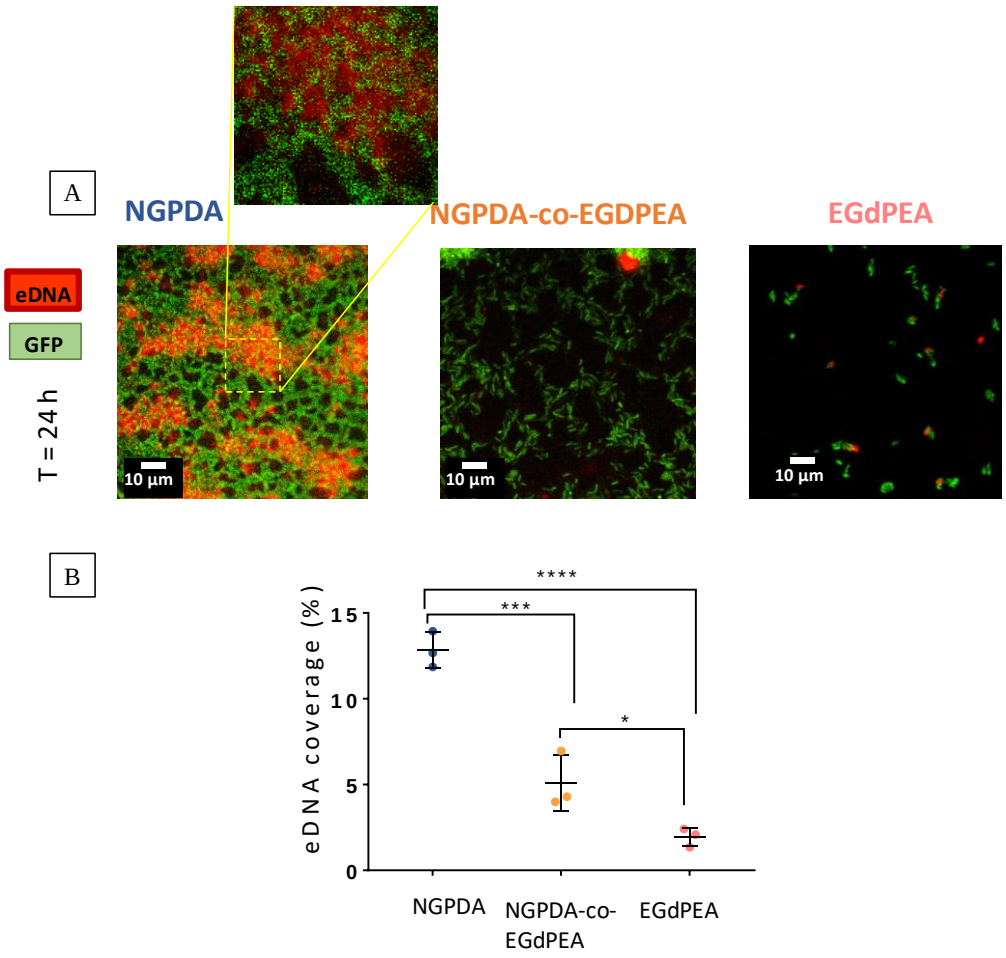

Figure 3.6 A) Confocal images (40×,1.2) of *P. aeruginosa gfp* tagged after 24 h on pNGPDA (left), pNGPDA-co-EGDPEA (middle), and pEGdPEA (right). eDNA was stained through propidium iodide (red) after samples were washed 2× in PBS and 2× in H_2O. Top-square shows higher magnification of biofilm on pNGPDA. Single cells are resolved but dead cells are not indicating it might be eDNA. Scale bar is 10 µm. **B)** Quantification of eDNA coverage on pNGPDA (blue), pEGdPEA (pink) and NGPDA-

co-EGdPEA (orange). Error bars show ± 1 standard deviation (N=3). **** p<0.0001, *** p<0.001, * p<0.05.

In order to verify whether the mechanism observed with pEGdPEA was conserved using other polymers belonging to the same class of poly(meth)acrylates, other three polymers with molecularly rigid hydrophobic chemical side-groups previously discovered were considered: BnMA,[8] iBMA,[6] TMCHMA polymers.[6] Figure 3.7 shows ESEM representative images of PAO1-W wild-type grown for 24 h on BnMA, iBMA, and TMCHMA and no matrix and few clusters of isolated cells were found on all three polymeric surfaces.

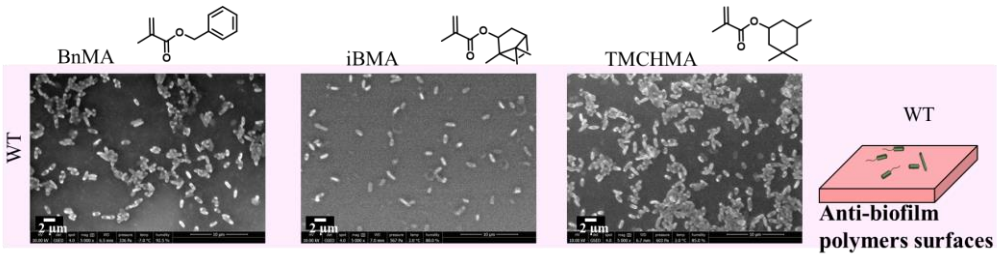

Figure 3.7 ESEM representative images of PAO1-W wild-type grown for 24 h on 3 hit polymers: BnMA and iBMA (monomer E in [8] and monomer 7 in [6]) and TMCHMA (monomer 12 in [6]). Images captured at 5,000× magnification. No matrix could be observed when grown on anti-biofilm surfaces as shown in the schematic (right). Scale bars are 2 µm.

3.3.4 *P. aeruginosa* Behaviour During Early Stage Surface Interactions

Having observed differences in biofilm formation on pEGdPEA and pNGPDA after 24 and 72 h, bacterial behaviour on the two polymers at the earlier stages of biofilm development was investigated. DHM enabled the 3D trajectories of bacteria swimming in the bulk phase above pEGdPEA and pNGPDA surfaces to be captured (Figure 3.8). The measured trajectories are shown in Figure 3.9A-B. No differences were observed in the average speed or directionality (K_{MSD}) of bacteria swimming in the liquid phase above either surface during the first 10 min of exposure.

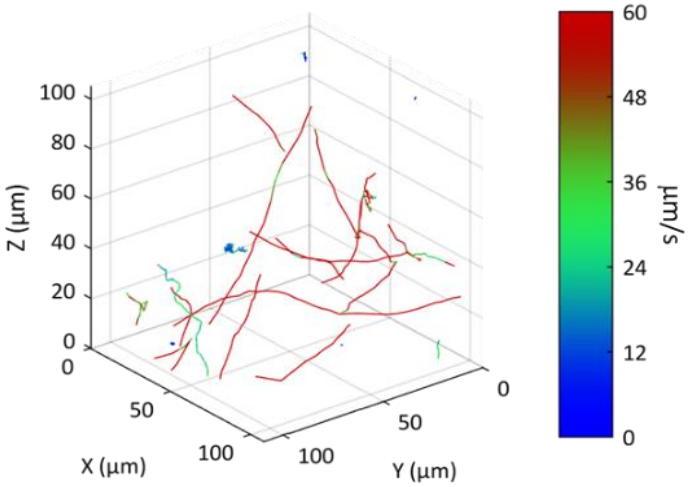

Figure 3.8 Examples of 3D swimming motility tracks obtained using DHM microscopy with PAO1-W on pNGPDA. Colourmap shows average speed of tracks.

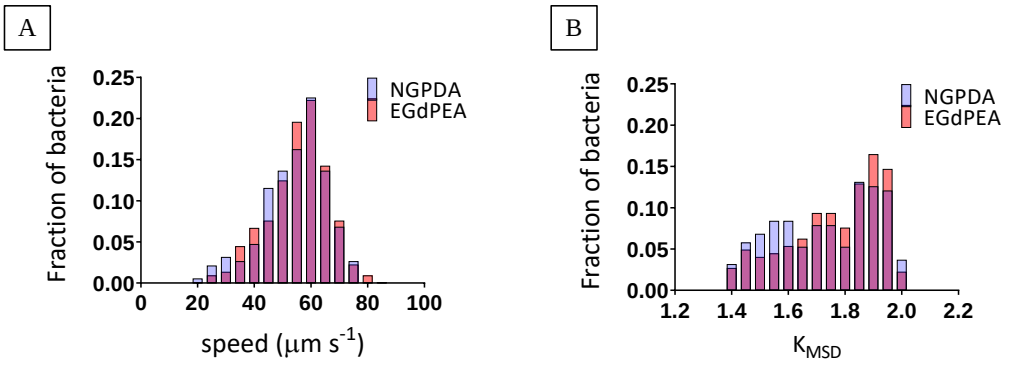

Figure 3.9 Histogram of average speed **(A)** and K_{MSD} **(B)** of tracks at the presence of pNGPDA (blue) and pEGdPEA (pink) (N=9) considering more than n>200 tracks for each sample. Bin is 5 and 0.5.

In order to assess the early stages of biofilm development DIC images were taken over a 3 h period from the inoculation at 0.5 Hz frequency (for a total of ≈ 48,600 images) for 3 biological replicates.

Similar numbers of surface-associated cells were found after the first hour after inoculation on both the pNGPDA and pEGdPEA coatings (Figure 3.10), suggesting that pEGdPEA did not significantly influence the initial bacterial surface interactions.

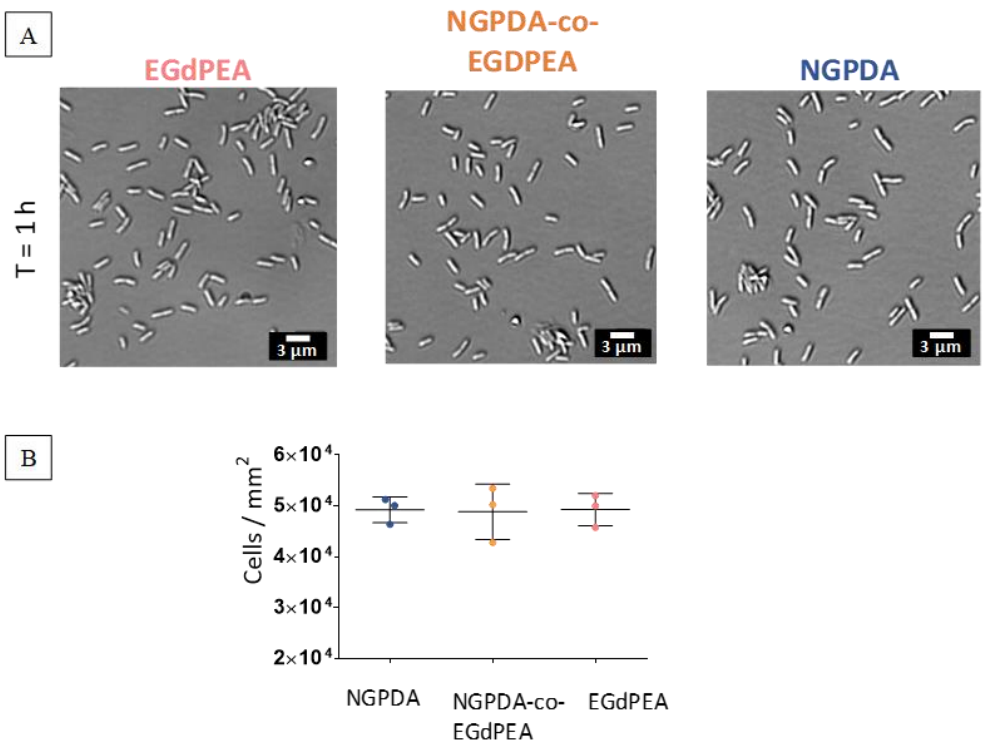

Figure 3.10 Quantification of *P. aeruginosa* coverage of the polymers. **A)** DIC brightfield (40×,1.3) images of PAO1-W on pNGPDA, pNGPDA-co-EGdPEA and pEGdPEA after 1 h from inoculation. **B)** Categorical scatter plot of bacterial coverage. Error bars show ± 1 standard deviation (N=3). Scale bar is 3 µm.

The number of bacteria on pNGPDA increased from 4.2 x 10^3 ± 6.9 x 10^2 to 5.4 x 10^4 ± 6.4 x 10^3 over the time period of 1 - 3 h (Figure 3.11), whereas on pEGdPEA increased from 4.4 x 10^3 ± 4.0 x 10^3 to 4.7 x 10^4 ± 2.2 x 10^3 showing a slight delay in surface growth.

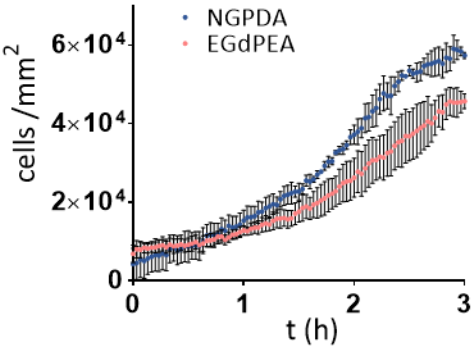

Figure 3.11 Number of bacteria per frame *vs* time increases much faster for pNGPDA (blue) than pEGdPEA (pink). Dots represent mean ± 1 standard deviation (N=3).

After t = 3 h the pNGPDA surface was completely covered by bacteria whereas on pEGdPEA there were still areas not covered by bacteria (Figure 3.12). As cell numbers at the surface can change either by cell division or by cells arriving from or departing to the bulk, a cell tracking algorithm was utilised to quantify the division rates and the residence of all the cells on the two polymer surfaces between t = 1 h and t = 2 h. As shown in Figure 3.13 PAO1-W was observed to have longer residence time on pNGPDA than pEGdPEA (p<0.001).

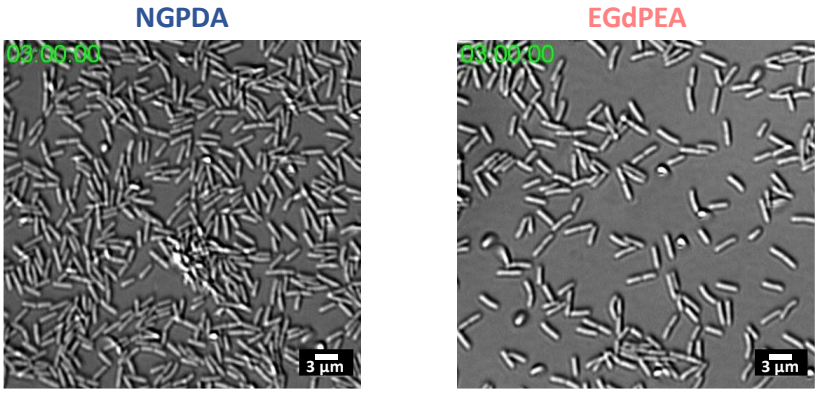

Figure 3.12 DIC brightfield (40×,1.3) images of PAO1-W on pNGPDA (left) and pEGdPEA (right) after 3 h from inoculation. Scale bar is 3 µm.

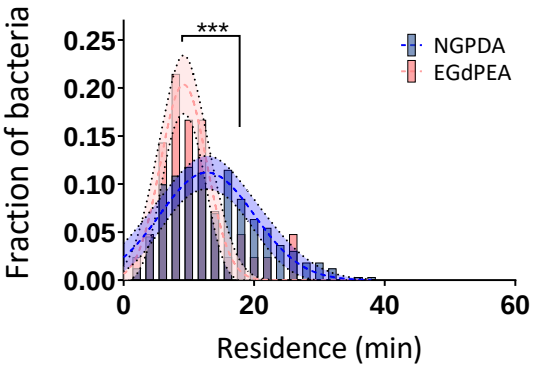

Figure 3.13 Histogram of residence time of PAO1-W on pNGPDA (blue bar) and pEGdPEA (pink bar) between t = 1 h to t = 2 h after inoculation. Solid bars represent fraction of bacteria at different residence times (bin = 2 min). Dashed lines represent data fit to Gaussian functions for pNGPDA (blue) and pEGdPEA (pink). Shaded areas represent 95% CI of the fit deviation. R^2=0.86 for pNGPDA and R^2=0.91 for pEGdPEA (N=3 considering more than 700 bacteria). Welch's t test was applied to compare distribution assuming different variance. *** p<0.001.

PAO1-W replicated on the two polymers with a similar doubling time (59 ± 8 and 58 ± 6 (N=3, n=20) min for pNGPDA and pEGdPEA respectively). Consequently, the fate of cells after division was explored, specifically to determine whether the two daughter cells detached (zero-legged branching),

only one detached (one-legged branching) or both remained (two-legged branching) on the surfaces (Figure 3.14A).[292]

As shown in Figure 3.14B, zero-legged branching of PAO1-W was significantly higher on pNGPDA (83 ± 1%) compared with pEGdPEA (53 ± 10%), whereas one-legged branching was significantly higher on pEGdPEA (44 ± 7%) than on pNGPDA (17 ± 1%) (p<0.001).

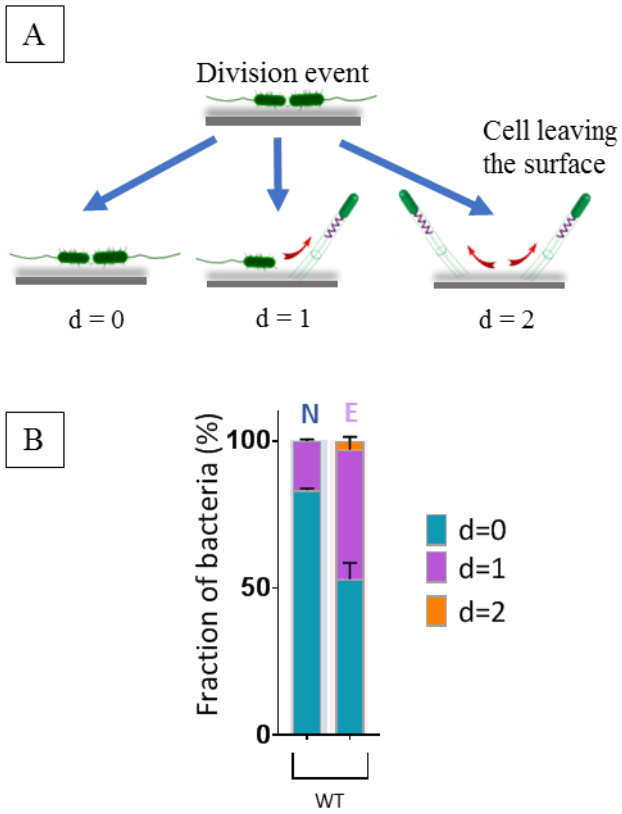

Figure 3.14 A) Schematic of the branching division events. **B)** Bar graph shows proportion of the population for PAO1-W in different branching divisions where pNGPDA (blue) and pEGdPEA (pink). Values obtained considering n>100 doubling events (N=3) between t = 1 h to t = 2 h from inoculation. PAO1-W branching distribution for the two polymers were found to be different (p<0.001) through two-way ANOVA and Sidak's multiple comparison.

3.3.5 The Role of the Bacterial Appendages on the Ability of Bacteria to Leave the Polymer Surfaces

To investigate why the bacterial cells were differentially leaving pNGPDA and pEGdPEA mutants with or without pili (Δ*pilA*) and flagella (Δ*fliC*) or without flagellum stators (Δ*motAB* and Δ*motCD*) were used. This allowed us to ask certain questions about the role of bacterial appendages in the surface launch mechanism. Pili and flagellum deleted mutants showed mainly zero-legged

branching (Figure 3.15). This is consistent with previous studies showing both pili and flagella necessary for detachment.[293] In contrast, Δ*motAB* cells showed a greater likelihood for leaving both surfaces (p<0.0001, compared to PAO1-W), with 36 ± 5% and 24 ± 11% for both daughter cells leaving after division on pNGPDA and pEGdPEA, respectively. The Δ*motCD* strain also showed a significant (p<0.0001) reduction in the number of branching division events leading to 0-order branching compared with the PAO1-W wild-type, however, most Δ*motCD* cells underwent one-legged branching. The increased surface departure of the stator mutants suggests these cells lost their ability to sense the surface, possibly through a mechano-sensing mechanism,[60] and therefore were less likely to engage in behaviour that would cause the cells to remain surface attached. Notably, both stator mutants showed no significant differences in their branching behaviour observed on either pNGPDA or pEGdPEA. This suggests that the surface sensing lost by the removal of the stators also reduced the ability of the cells to differentiate and respond to the chemical/physical differences between the two polymer surfaces.

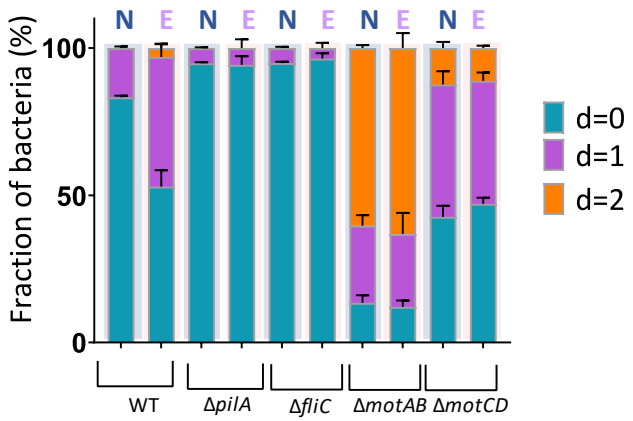

Figure 3.15 Bar graph shows proportion of population for each bacterial strain in different branching division considering pNGPDA (blue) and pEGdPEA (pink). Values obtained considering n>100 doubling events for 3 independent replicates (N=3) between t = 1 h to t = 2 h from inoculation. Sidak's multiple comparison has been used to find statistical differences (**Appendix 6**).

3.3.6 *P. aeruginosa* Motility Across Different Surfaces

Since no differences were observed in the density or directionality of bacteria interacting with either surface using DHM (Figure 3.9), T4P-driven motility was

investigated. *P. aeruginosa* undergoes T4P-mediated twitching motility when at a surface (section 1.5.1.2).[60] Thus, bacterial surface motility was also assessed, measuring twitching speed and residence time. To confirm that the observed movement was T4P driven, single and double pili and flagella mutants (Δ*pilA*, Δ*fliC*, and Δ*pilA*Δ*fliC*) were used. No motility was observed using Δ*pilA* and the double mutant. On the contrary, motility was observed using Δ*fliC*. Figure 3.16 presents colourmaps of tracks on pNGPDA of pili and flagella mutants showing speed. Similar results were found when cells were exposed to pEGdPEA (Appendix 7).

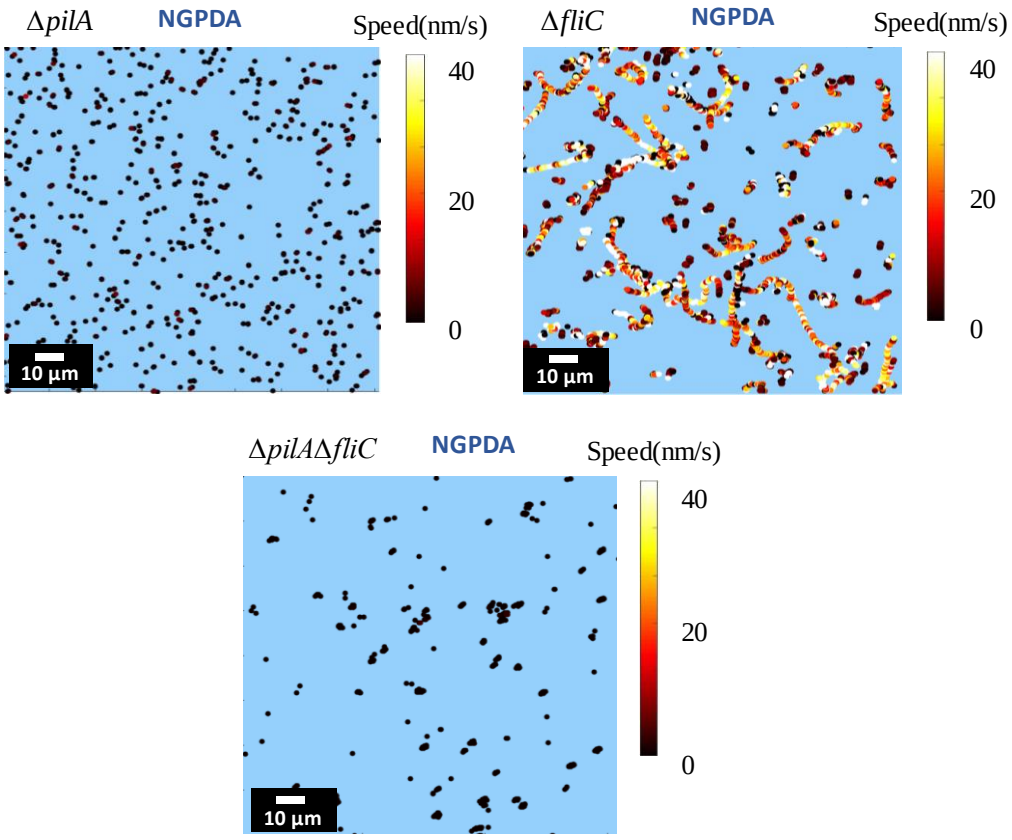

Figure 3.16 Representative colour maps of tracks of *P. aeruginosa* Δ*pilA* (top-left) Δ*fliC* (top-right) and Δ*pilA*Δ*fliC* (bottom) on pNGPDA measured over 1 h of exposure to surfaces. No motility was observed for *P. aeruginosa* Δ*pilA* or Δ*pilA*Δ*fliC mutants*. On the contrary, motility was observed using *P. aeruginosa* Δ*fliC*. Thus, the surface motility observed was T4P driven. Scale bar is 10 µm.

Figure 3.17A shows example maps of bacterial tracks of PAO1-W on the two polymeric surfaces. Track curvature was evaluated by considering the radius of curvature. Higher values of this parameter correspond to more linear trajectories.[288] The fraction of motile cells (55 ± 16% and 58 ± 3% on

pNGPDA and pEGdPEA respectively) and directionality on the two polymers were similar (Figure 3.17B), however, the average speed of twitching cells on pNGPDA was significantly (p<0.0001) slower (9 ± 4 nm/s) than on pEGdPEA (11 ± 6 nm/s) (Figure 3.17C).

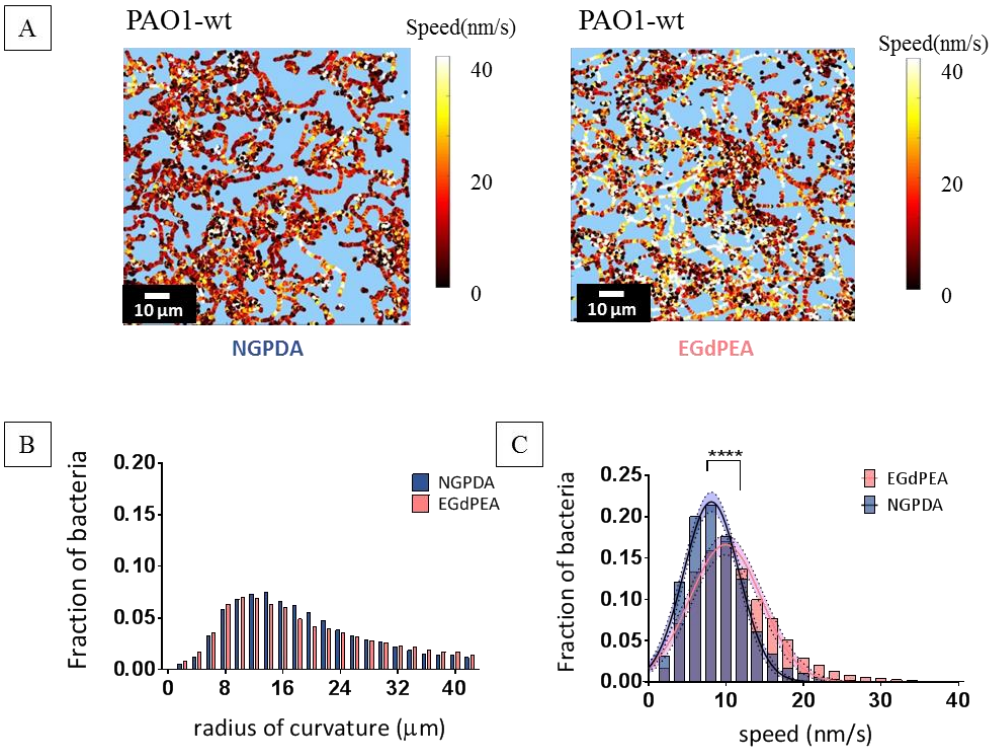

Figure 3.17 A) Representative colour maps of PAO1-W twitching tracks on pNGPDA and pEGdPEA measured over 1 h of exposure to surfaces. Colours show different speeds as indicated by the intensity scale. Scale bar is 10 µm. **B)** Histogram of radius of curvature for all tracks on different polymers. n>12,000 (N=3). Higher radius of curvature corresponds to more directional motility.[288] Bin is 2. **C)** Histogram of PAO1-W speeds on pNGPDA and pEGdPEA (N=3). Bin = 2. Dashed lines represent data fit to Gaussian functions. Shaded areas represent 95% CI of the fits. **** p<0.0001 using Welch's t test assuming different variance.

The T4P-driven twitching motility of *P. aeruginosa* can take on two distinct modes: flat "crawling," where the cell is lying flat on the surface or upright "walking," where the cell is in contact with the surface at only one pole (section 1.5.1.2). Walking cells have been described as faster than crawling cells.[103] In order to examine walking and crawling distributions, the method developed by Rodesney *et al.*[294] was used by considering the lifetime tilting fraction as the time bacteria spend in a vertical position (section 1.5.1.2). As shown in Figure 3.18, PAO1-W was found to be faster on pEGdPEA than pNGPDA

independently from the cell body position (either vertical or horizontal). For each cell, the fraction of its lifetime spent unambiguously tilting was computed, with 1 being unambiguously tilted up for the whole trajectory, and 0, lying flat for the whole trajectory. Because the force-generating capabilities of T4P are intrinsic to the proteins that generate the pulling force, it has been assumed that bacteria have the same pilus machinery and function on the polymers. Thus, the reduced twitching speed observed on pNGPDA is likely the result of a stronger interaction between the cell body/flagella and pNGPDA that would oppose the pulling force.

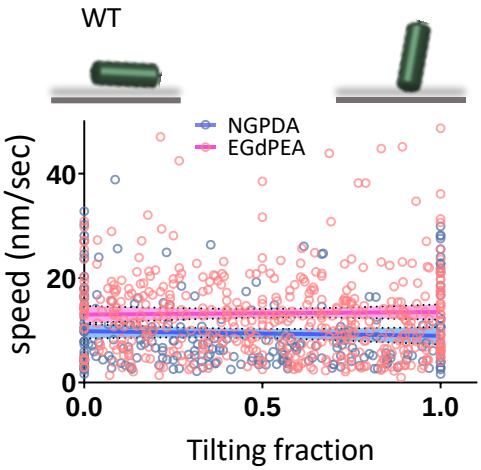

Figure 3.18 Scatter plot showing the mean speed of cells during an entire trajectory as a function of the fraction of the cell's tracked lifetime that was spent tilting (vertical position). Linear fits (y = m*x + b) to each dataset yield: for pEGdPEA, m = 0.5 ± 1.3, b = 13.0 ± 0.8; for pNGPDA, m = -0.9 ± 3.0, b = 9.8 ± 1.2. As a proxy readout for tilting, the projected aspect ratio in each frame has been examined as described in section 1.5.1.2.

3.3.7 pNGPDA but not pEGdPEA Stimulates an Increase in c-di-GMP

Having identified some differences in the initial interactions of *P. aeruginosa* with the pEGdPEA and pNGPDA polymers, the research next focussed on the mechanisms that bacteria use to switch between motile and sessile behaviour. Biofilm formation and the dispersal of PAO1 are regulated *via* the intracellular secondary messenger c-di-GMP, which is synthesised by DGC enzymes and degraded by PDE enzymes (section 1.5.2.3). A high intracellular content of c-di-GMP inhibits *P. aeruginosa* motility and induces exopolysaccharide (Pel, Psl

and alginate) biosynthesis, which are important in the switch from reversible to irreversible attachment and biofilm formation.[295]

Traditional bulk culture-based biochemical measurements cannot determine the variation of second messenger levels in single cells. Here c-di-GMP dynamics have been followed over time using time-lapse epifluorescence microscopy of bacteria containing the plasmid *pcdrA*::*gfp*. The *cdrA* promoter is a validated reporter for c-di-GMP in *P. aeruginosa*. Figure 3.19 shows colour maps of PAO1 *cdrA*::*gfp* tracks on pNGPDA (left) and on pEGdPEA (right) obtained from frames captured every 30 s over the first 60 min of exposure to the two surfaces. Colours show measured instantaneous fluorescence intensity (*F*). Here we found that bacteria showed lower fluorescence levels when they were moving in comparison to more stationary cells for either polymers in agreement with recent published data.[296] Cells were classified as stationary or motile depending on twitching speed with cut-off 1 nm s^{-1}.

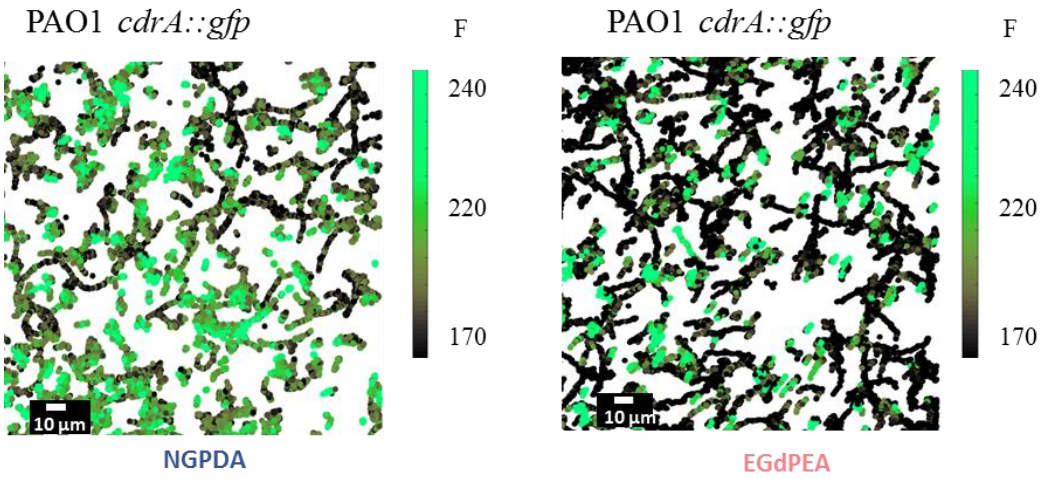

Figure 3.19 Representative colour maps of tracks of *P. aeruginosa cdrA*::*gfp* on pNGPDA (left) and pEGdPEA (right). Colours show instantaneous fluorescence intensity measured (*F*) according to the intensity scale shown. Tracks were obtained from images acquired using widefield epifluorescence microscopy (40×, 1.3) every 30 s for 60 min and then processed through a custom single-cell tracking algorithm. Scale bar is 10 µm.

The fluorescence distribution for bacteria on the two polymeric surfaces were significantly different (p<0.0001) with a decrease of 10% of the average fluorescence when cells were exposed to pEGdPEA for 1h (Figure 3.20A). As biofilm development is accompanied by a loss of motility,[295, 297] two

populations of motile and non-motile cells with speeds of either ≥ or <1 nm s^{-1} are highlighted in Figure 3.21. A significant (p<0.0001) reduction in the average F on pEGdPEA (194.7 ± 4.6) compared with on pNGPDA (207.4 ± 4.0) was observed for stationary cells (Figure 3.20B). Similarly, a significant inhibition was observed also for motile cells at the presence of pEGdPEA (p<0.0001) (Figure 3.20C). These results suggest that contact with pEGdPEA inhibits the intracellular production of c-di-GMP.

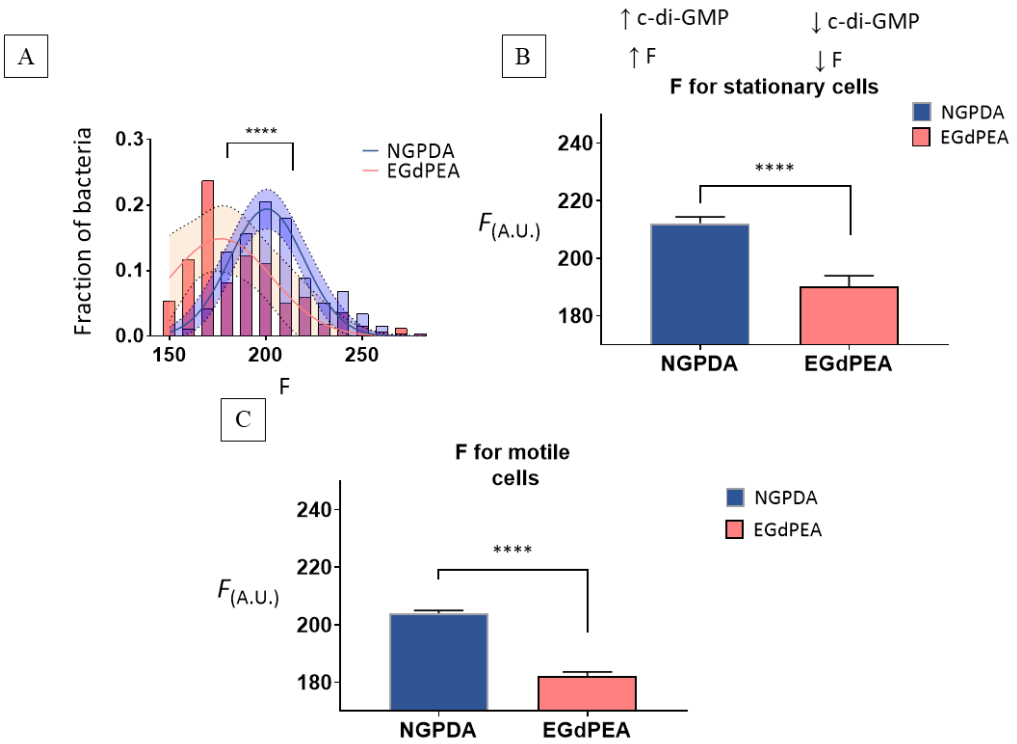

Figure 3.20 A) Histogram of F for all tracks on different polymers. n> 1,000 for three independent experiments (N=3). Dashed lines represent data fit to Gaussian functions. Shaded areas represent 95% CI of the fits. **B)** Evaluation of single-cell mean (F values) *cdrA* expression by stationary (speed < 1 nm s^{-1}) and **(C)** motile cells (speed > 1 nm s^{-1}) on each polymer. Error bars show ± 1 standard deviation (N=3). Unpaired t-test with Welch's correction was used to compared curves (****p<0.0001).

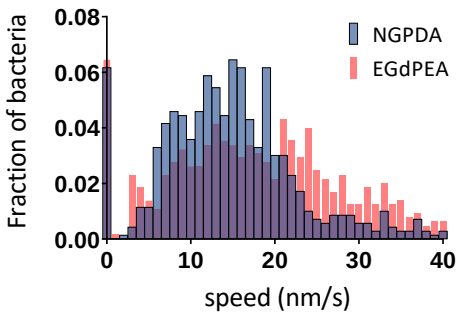

Figure 3.21 Histogram of speeds for all the tracks on pNGPDA (blue) and pEGdPEA (pink) respectively. Bin=1.

3.3.8 pEGdPEA Affects ExoPolysaccharide Production of *P. aeruginosa*

A high intracellular content of c-di-GMP represses *P. aeruginosa* cell motility and induces exo-polysaccharide synthesis, which are important in biofilm formation *in vitro*.[295, 297, 298] An analysis of the EPS derived from biofilm-grown *P. aeruginosa*, as described in section 1.5.3.3, revealed that the primary carbohydrate constituents are glucose, rhamnose, and mannose, not mannuronate or guluronate (which are mainly present in alginate).[299] In addition, alginate is generally not produced by environmental strains other than in the cystic fibrosis lung.[172] Pel is a positively charged exopolysaccharide composed of partially acetylated 1'-4' glycosidic linkages of *N*-acetylgalactosamine and *N*-acetylglucosamine and it is likely to cross-link eDNA in the biofilm stalk *via* ionic interactions.[300]

In order to evaluate whether different levels of c-di-GMP might correspond to differential exopolysaccharide production on our polymeric surfaces, samples were exposed to ConA-Alexa 633 staining (50 μg ml^{-1}) which is known to stain bacterial EPS.[301] PAO1-W was grown in RPMI-1640 in the presence of pNGPDA and pEGdPEA for 2.5 h and DIC images were acquired every 10 s. After 2.5 h samples were imaged using CLSM to assess EPS production. Figure 3.22 shows tracks obtained from processing DIC images acquired on pNGPDA. Using CLSM it has also been observed that bacteria left EPS trails on the surface and that these overlaid the cell paths.

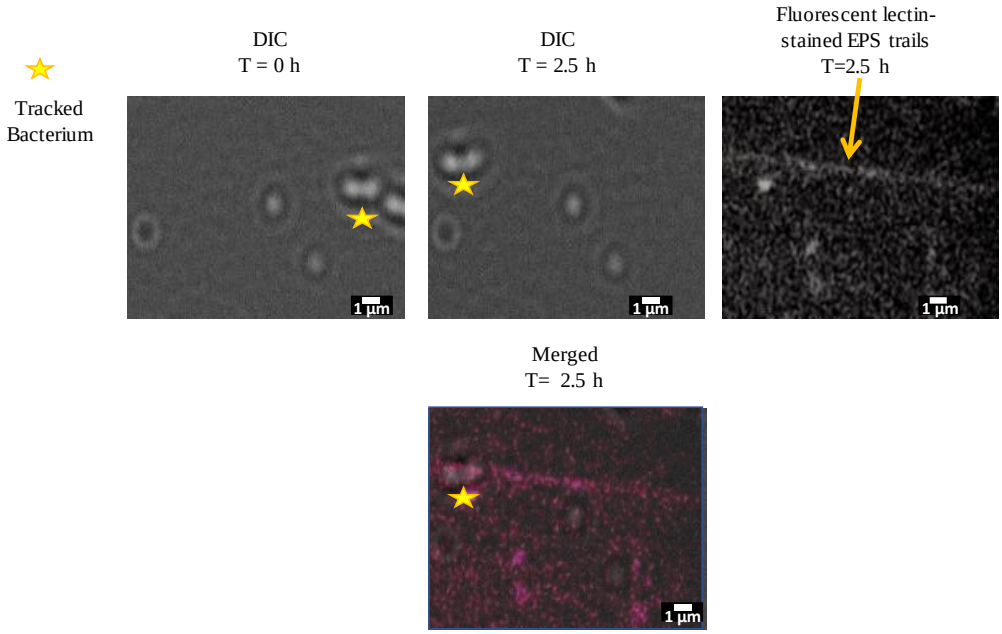

Figure 3.22 DIC images of tracked *P. aeruginosa* at t = 0 h and t = 2.5 h (highlighted with a star; fluorescent lectin stained EPS trails after 2.5 h and a merged image of the 2 channels. Scale bar is 1 µm.

pNGPDA and pEGdPEA samples were therefore compared, and CLSM images of background at t = 0 h and after 2.5 h of exposure to surfaces were acquired in order to consider only EPS produced by bacteria and attached to surfaces. Representative images are shown in Figure 3.23, whereas images of the background can be found in Appendix 8.

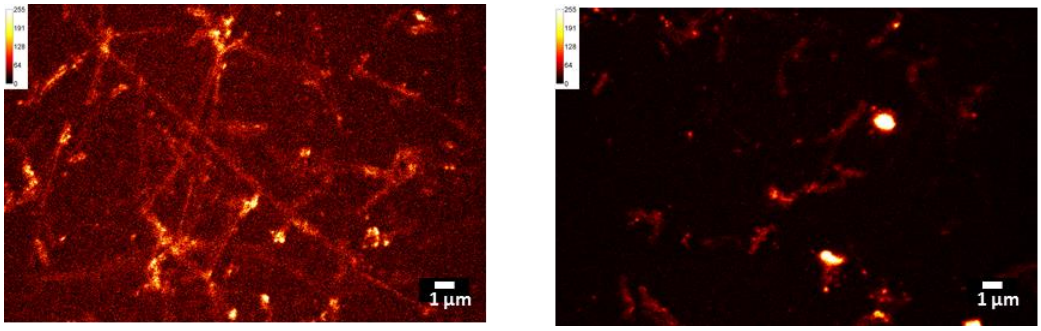

Figure 3.23 CLSM images captured at t = 2.5 h on pEGdPEA (right) and pNGPDA (left). Colourmap shows fluorescence level of ConA bound to EPS at surfaces. Scale bars are 10 µm.

A higher level of EPS on pNGPDA than pEGdPEA was measured at t = 2.5 h (Figure 3.24), specifically, EPS coverage on pEGdPEA was reduced by ≈ 76% (p<0.01). Therefore, EPS was observed to be more abundant on pNGPDA than on pEGdPEA.

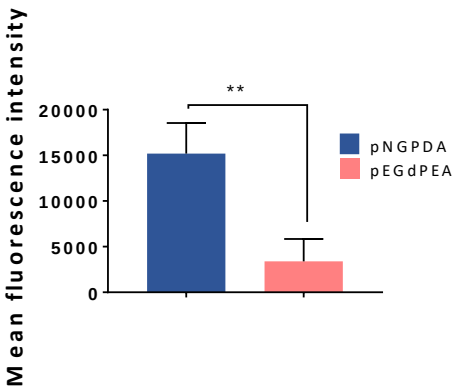

Figure 3.24 Mean fluorescence intensity measured on pNGPDA and pEGdPEA after 2.5 h from inoculation and after background subtraction. Unpaired t-test (**p<0.01). Error bars show ± 1 standard deviation (N=3).

3.4 Discussion

In order to define the mechanism(s) used by bacteria to respond to chemically distinct surfaces, here two surfaces that showed differential biofilm formation properties were employed: biofilm-resistant (pEGdPEA) and pro-biofilm (pNGPDA) acrylate polymers. In particular, in this chapter, investigations of the early stages of bacterial interactions with different polymer surface chemistries are described. These data were obtained using custom designed algorithms developed to track motile bacteria.

Although similar numbers of surface-associated PAO1-W cells were observed on pNGPDA and pEGdPEA at the early stages of bacterial colonisation, more cells accumulated on pNGPDA than on pEGdPEA. This was a consequence of longer bacterial residence times on pNGPDA and a higher number of wild-type single daughter cells leaving the pEGdPEA surface after cell division. Asymmetric growth and distinct daughter cell morphologies and/or physiologies are well-recognised and understood in eukaryotic biology.[302] The role and the prevalence of asymmetric behaviours in prokaryotes are less appreciated. However, in the last decade it has become evident how complex and organised bacteria are.[303] The poles of rod-shaped bacteria serve as a localisation hub and dynamic changes at the poles have been described to have a critical control of cellular physiology.[304] In addition, the cell poles are a common site for

production and assembly of surface organelles such as flagella, pili and adhesins allowing proper orientation before swimming and attachment to/detachment from surfaces. Since cells were observed leaving or remaining at the surface, this immediately raises the question about differences in ages. The cell poles are known to be not identical (one is relatively older), giving rise to asymmetry even in seemingly symmetric rod-shaped cells.[281] Bacteria have been shown to use multigenerational memory based on coupled oscillations of cAMP levels and T4P activity to adaptively respond and adhere to surfaces, but no-one has described a surface sensing memory for different surface chemistries.[305] Laventie *et al.* described asymmetric division of *P. aeruginosa* at a surface as an event caused by an increase in c-di-GMP levels after a surface encounter which induces surface adherence in one daughter cell by stimulating pilus assembly through activation of the c-di-GMP receptor FimW.[60]

The *cdrA* gene reporter that has been adopted in our experiments is able to differentiate between samples giving an estimation of the intracellular c-di-GMP levels but it is not able to report on c-di-GMP localisation. Pili and flagella have been previously described to play crucial roles in cell surface attachment and detachment.[292] *P. aeruginosa pilA* and *fliC* mutants were observed not leave either pNGPDA or pEGdPEA surfaces. This contrasts with what Lee *et al* found.[305] A Δ*pilA P. aeruginosa* PA14 mutant, which lacks T4P, was shown to exhibit predominantly one-legged branching which does not contribute to surface population growth. One possible explanation is the fact that their experiment was carried over a longer period (>20 h) and considered less cell division events (about 70 division events). Also, they used a different growth medium (M63 supplemented with 1 mM $MgSO_4$, 0.05% glucose, and 0.125% casamino acids (CAA)) and the experiments were conducted at 30°C under flow conditions (3 mL h^{-1}) instead of RPMI-1640 medium at 37°C in static conditions. Nutrients and temperature changes are likely to be responsible for differential transcriptional regulation in *Pseudomonas*.[306] Additionally, bacterial detachment from a new class of polymeric surfaces has been explored, whereas Lee *et al.* adopted a flow cell prepared with a glass borosilicate surface.

Here it has also been shown that the flagella motor stators influence surface detachment. Although *mot* mutants exhibited a higher proportion of leaving daughter cells than the wild-type, more *motCD* mutants stayed on both surfaces than *motAB mutants*. Hence, mutation of *mot* stators resulted in an inability to remain surface-associated on either surface despite their ability to produce flagella filaments. This is in agreement with Laventie *et al.* who investigated FimW polarity in *Pseudomonas* wild-type and *mot* mutants using a yellow fluorescent (Venus) fusion to FimW. FimW was used as a valid marker for dynamic assembly of T4P at the cell poles which are responsible of surface attachment.[60] Mutants lacking the MotAB stator units were observed to lack FimW localisation leading to cell detachment from glass borosilicate surface. In contrast, Δ*motCD* was observed to have a stronger polar localisation of Venus-FimW which is confirmed by our experiments where a higher proportion of cells remain at the surface.

It has been found that PAO1-W wild-type cells deployed T4P in twitching mode and moved faster on pEGdPEA than on pNGPDA. Ni *et al.* described how *P. aeruginosa* differently deploys T4P to alter motility types depending on nutrient availability on glass borosilicate surface.[307] They showed that bacteria in nutrient-limited conditions preferentially use more directional (higher K_{MSD}) motility types, whereas under nutrient-supplemented conditions bacteria preferentially arrest motility selecting a suitable place to form a microcolony. This raises questions about the presence of different nutrient adsorption on our polymeric surfaces which could modify bacterial responses. In addition to that, Laventie *et al.* described how c-di-GMP levels induce surface adherence in daughter cells by stimulating pilus assembly through activation of the c-di-GMP receptor FimW.[60] Since a higher c-di-GMP production on pNGPDA was found over the first hour of exposure, the stronger interaction between pNGPDA and PAO1 might be due to multiple pili pulling in different directions resulting in un-coordinated movements.

It is known that c-di-GMP is an intracellular secondary messenger that plays a role in switching cells to the sessile state and therefore towards biofilm formation by increasing EPS production.[308] Regulation of extracellular matrix and

biofilm formation *via* c-di-GMP is well documented.[133] Since the motile to sessile switch does not occur on pEGdPEA, how and why this happens is unknown. A possible explanation comes from studies on c-di-GMP heterogeneity in *Pseudomonas*. Recently, Kulasekara *et al.* correlated c-di-GMP levels with a specific PDE Pch which was shown to move towards poles cells after cell division and be dependent on the histidine kinase component of the chemotaxis machinery CheA.[309] The c-di-GMP signalling network links environmental stimuli to specific adaptive responses:[47] including oxygen,[310] blue light,[311] nutrient starvation,[312] and antibiotics.[313] However, little is known about how surfaces might affect *in situ* localised c-di-GMP production.

3.5 **Conclusions**

Previously, using a high-throughput screen a polymer pEGdPEA that resists bacterial biofilm formation was identified. No extracellular matrix and lower eDNA release were observed with a few clusters of isolated cells attached to pEGdPEA after 24 h of exposure to the surface. To understand how pEGdPEA prevents biofilm formation the early stages of *P. aeruginosa*-pEGdPEA interactions were investigated. Although, DHM revealed no obvious differences in the density or directionality of bacteria interacting with either pEGdPEA or the biofilm-promoting polymeric surface pNGPDA, using time-lapse experiment it has been found that pEGdPEA affects bacterial colonisation and surface residence time during the first few hours of colonisation. A higher number of PAO1-W cells were also observed to leave pEGdPEA after cell division in comparison with pNGPDA showing different behaviours in the daughter cells after exposure to polymers. Asymmetrical phenotypes have been described in bacteria and in particular c-di-GMP has been recently shown to play a crucial role in cell detachment and pili expression in *Pseudomonas* after cell division. Here, it has been shown that the prevention of biofilm formation on pEGdPEA was characterised by downregulation of the expression of *cdrA* indicating reduced c-di-GMP production in the first hours of surface exposure and consequently an EPS production. In addition, the increased departure of the stator mutants from the polymer surfaces suggest that these cells have lost their

ability to sense the surfaces. Our studies define a completely new mechanism by which a polymeric surface prevents biofilm formation avoiding the transition from reversible to irreversible attachment.

In order to evaluate in more detail how pEGdPEA influences bacterial attachment, the next stage will be to develop an assay to quantify bacterial adhesion strength to surfaces to ascertain whether the ability of the polymer to prevent biofilm formation is given by its ability to affect how strongly bacteria attach to surfaces. In particular this will help to examine more closely the links between bacterial appendages and surface adhesion strength on pEGdPEA and pNGPDA.

Chapter 4

Development of a P. aeruginosa Surface Detachment Assay on Different Polymers under Flow Stress

4.1 Introduction

Microfluidics have become a particularly important tool for exploring biological behaviour in controlled environments, in which small (10^{-9} to 10^{-18} L) amounts of fluids are processed or manipulated using channels with dimensions of 10^{1} to 10^{2} µm. This field combines the exploitation of both its most obvious characteristic - small size – together with less obvious ones of fluids in microchannels, such as laminar flow. Flow is present during biofilm formation for a number of different medical and non-medical parameters and it is, thus, important to be able to understand bacterial cell and biofilm responses to flow. Microfluidics, therefore, offers fundamentally new opportunities for the study of cells in space and time.[314]

Bacterial cell attachment has been investigated for decades.[315] Bacterial adhesion to a solid surface is a crucial step in the process of biofilm formation.[316] As described in section 1.5.3, bacteria move towards a solid surface and initially reversibly attach, where long and medium range forces govern the interaction between the cell and the surface (primarily van der Waals and electrostatic forces), followed by an irreversible attachment where EPS and adhesins are produced and play a crucial role. Hoffman *et al.* recently determined the timescales and frequencies of reversible and irreversible adhesion events of *C. crescentus* by using fluorescence microscopy to track the polar adhesive 'holdfast', which is well-known to be responsible for the irreversible surface attachment of this bacterium.[317] The adhesion strength of holdfast increases logarithmically with time upon surface contact,[318] and is likely to be due to a curing mechanism.[319] Single-cell adhesion depends on three main factors: the liquid environment, the solid surface and the nature of bacterium.[320] Nutrient availability in the liquid environment can either promote or impair bacterial adhesion. For example, for *A. tumefaciens*, iron and manganese limitation independently affect cell adhesion,[321] whereas phosphate limitation triggers

cell attachment.[322] Also, the effect of surface rigidity on bacterial attachment has been recently studied although no consistent trend has emerged.[160]

Adhesion strength has been probed with various techniques including microfluidics.[323] Centrifugation and spinning disk assays,[324] micromanipulation of single cells using AFM,[325] are two further examples. AFM can provide an accurate measure of adhesion, but sufficient single cell debonding events to achieve acceptable statistics requires many experimental repeats.

The microfluidic detachment assay is another valid technique to measure adhesion strength. It was developed by prof. Axel Rosenhahn and his group and it measures the shear force necessary to detach cells.[326-330] Its uniqueness is related to the capacity to simultaneously assess bacterial adhesion under different conditions e.g. different surfaces and changes in nutrient availability and to stepwise shear forces *via* rapid exchanges of substrate over short experimental times. Their microfluidic device consisted of a glass window (lid), the channel made of PDMS and the coated surfaces. Window, channel, and sample of interest were mechanically held together by two disks connected by screws. They investigated, for instance, the effect of undecanethiol SAMs with $-CH_3$, $-NH_2$, $-OC_7F_{10}CF_3$ termination and PEG terminated SAMs on the adhesion strength of the gram-negative marine bacterium *Cobetia marina* (*C. marina*). A ten-fold reduction in attachment strength was observed in the case of SAMs with PEG supporting the general notion that hydrophilic, highly hydrated ethylene glycol surfaces have the ability to reduce the attachment of marine biofouling microbes.[329]

4.1.1 Microfluidics: Flow Rate in a Channel

Liquids go through channels of any shape or geometry at a *volumetric flow rate*, *Q* (Figure 4.1). Equation 11 shows *Q* as derived from mean velocity *u* of the liquid for a volume *V* which passes through a specific cross-sectional area *A* in a time *t*.

$$Q = uA = V/t \quad \text{Equation 11}$$

Following Bernoulli's principle of continuity of momentum and mass, Q is constant, so that u and A are inversely proportional.[331]

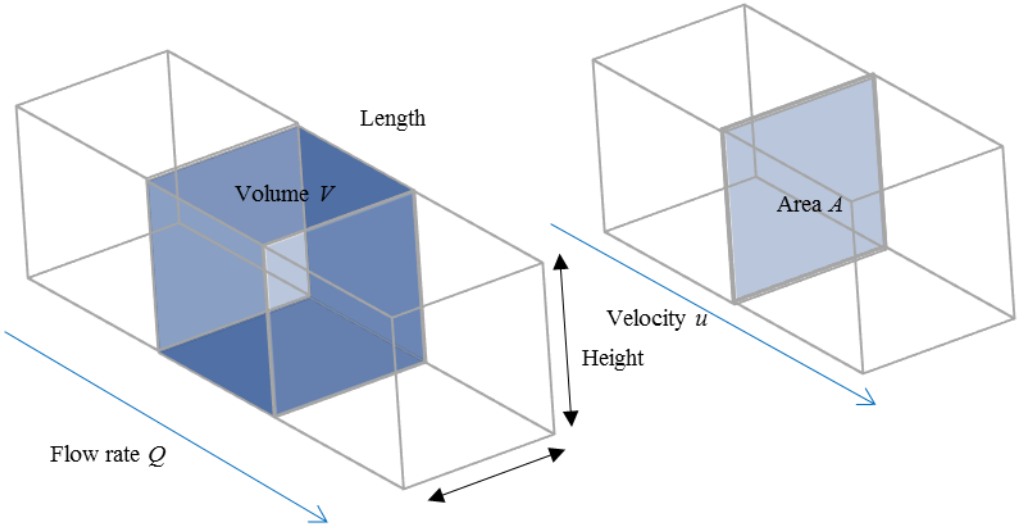

Figure 4.1 Different ways to describe the flow rate Q as either a volume per unit or the product of area and velocity. Figure adapted from [294].

4.1.2 Poiseuille Flow and Shear Stress

In reality, the velocity is not constant across the width of the microfluidics channel because the surface of the channel does not move and any liquid in direct contact with this surface is defined as having zero velocity. This is the *no-slip* condition.

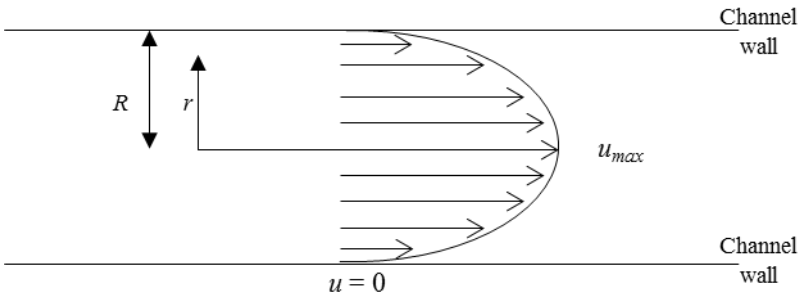

Figure 4.2 Schematic of the velocity profile of a liquid in a microfluidics channel showing a different velocity u depending on the distance from the centre (r). Velocity increases away from the wall and reaches its maximum at the centre of the channel where $r = 0$ and its minimum at the wall where $r = R$ in which R is the half dimension of the channel (either width or height). Image adapted from [294].

Under these conditions, the maximum velocity u_{max} of the flow is reached at the centre line with distance $r = 0$, whereas when $r = R$, where R is half radius of the channel (either width or height), the velocity is zero (Figure 4.2). Equation 12 describes liquid speeds depending on the position and the dimension of the channel.

$$u(r) = u_{max}\left(1 - \frac{r^2}{R^2}\right) \quad \text{Equation 12}$$

The flow velocity profile is then described as a parabola in which liquid in adjacent regions moves at different speeds. For this reason, a shearing force is exerted on any object which extends from the wall, as in the case of adherent bacteria.

The shear stress τ is described as in the Equation 13 where μ is the dynamic viscosity of the fluid (units Pa · s) and the shear rate is the rate change of u at distance y from the channel wall.

$$\tau = \mu \frac{du}{dy} \quad \text{Equation 13}$$

In a channel of square cross-section, the shear stress τ is idealised as shown in Equation 14 where w and h are the channel width and height respectively (Poisseuille equation).[329]

$$\tau = \frac{6\,\mu\,Q}{wh^2} \quad \text{Equation 14}$$

4.1.3 Microchannel and Laminar Flow

In a laminar regime, viscous forces dominate over inertial forces and the kinetic energy associated with the liquid movement is reduced. This means that adjacent regions remain distinct, as described by the Poisseuille flow.[332] The opposite condition, named the turbulent regime, is characterised by the dominance of inertial forces; here, the liquid movement is reduced by inertial forces in a way

that can result in both pressure and velocity changing unpredictably over short distances. Although the turbulent system is closer to that observed in real life, given the unpredictability of the changes in pressure and flow speed, this type of condition is less desirable within a controlled physiochemical environment.

The key parameter for establishing whether a system is operating under a laminar or turbulent regime is the Reynolds number (*Re*) which is defined as described in Equation 15. This dimensionless number is given by the ratio of viscous to inertial forces: *Q* and *A* are the volumetric flow rate and cross-sectional area of the channel respectively; the kinematic viscosity *v* of a fluid is the ratio of the density and dynamic viscosity, both temperature-dependent properties intrinsic to the fluid.

$$Re = \frac{Q\, D_H}{\nu A} \quad \text{Equation 15}$$

D_H is the wetted perimeter of the channel which is for a rectangular shaped channel as calculated in Equation 16.

$$D_H = \frac{2wh}{w+h} \quad \text{Equation 16}$$

The flow regime in an enclosed channel is considered laminar if the Re is below 2,000, and turbulent if above 2,000. In our system h = 50 µm, w = 1000 µm, Q_{max} ≈ 30 mL min^{-1} and v = 1.02 cSt, thus $Re \approx 1$.

4.1.4 Materials Used for the Preparation of the Microfluidic System

All the materials have to be optically transparent to some extent to be used with brightfield imaging and microscopy. Glass, silicon, the elastomer PDMS, thermosets as photoresist SU-8, and thermoplastics such as polymethylmethacrylate (PMMA), polystyrene, or cyclic olefin polymers such as hydrogel[333] (based on alginate, collagen, agarose, and cross-linked PEG) have all been used for the preparation of microfluidic systems.[314] Glass and silicon are restricted to special applications because, due to their flat and hard nature, they have a high cost of machining. Polymers, by contrast, are relatively

easy to fabricate and inexpensive. PDMS is the most popular material used for microfluidic chips. Moreover, PDMS also provides an easy integration of valves and pumping units into the microfluidic chip.[334]

The microfluidic channels are usually designed and printed onto a high-resolution transparency which is used as a photomask in 1:1 contact photolithography (usually using SU-8 or PMMA as photoresist) to produce a master. This latter became a mold for PDMS, which is cured for 1 h at 70°C. The PDMS is then peeled from the master and sealed to a surface to create the final device after plasma oxidation. The overall process takes approximately 24 h. Details of this method termed soft-lithography are widely available.[335] However microfluidics fabrication is often defined as a time-consuming and costly process and one of the main important issues is leakage, especially in condition of high pressure. In addition, the surface chemistry of polymers like the ones have been used in this project would be modified after oxygen plasma treatment.

4.1.5 Aims

Since in chapter 3 it has been described how pEGdPEA affects *P. aeruginosa* transition from the reversible to the irreversible attachment, in this chapter, a microfluidic detachment assay previously developed[330] has been modified to assess bacterial adhesion strength to the pEGdPEA and pNGPDA polymeric surfaces in more detail. A PDMS window (lid) and a double-side tape were used to create the microfluidic device instead. In addition, several *P. aeruginosa* motility mutants have been used to explore the role of pili and flagella structures in the adhesion process.

4.2 Experimental

4.2.1 Polymer Preparation

Materials were prepared according to section 3.2.1.

4.2.2 Microfluidics Device

4.2.2.1 PDMS Mixing

PDMS is formed from the thermal curing of a silicone elastomer mixture base and curing agent. The Sylgard 184 kit (Dow Corning) consists of a base (part A) and curing agent (part B) that was mixed in a ratio of 10:1 w w^{-1}. The chemical composition of part A and B can be found in [336]. The mix was then de-gassed in a desiccator unit attached to a vacuum pump. The resulting viscous liquid was poured into a polystyrene petri-dish (90 mm ϕ). The PDMS was cured at 60°C for 2 h and cut before assembly.

4.2.2.2 Silicone Tape Excision and Adhesion

Microfluidics channels were created using a silicone tape cut using Xurography or "razor writing". This technique is a very simple and cheap alternative to soft-lithography and it is obtained with ultra-rapid prototyping (Figure 4.3A-C). A double-sided tape of known thickness (50 μm), which is cut by a knife plotter, is embedded between a PDMS lid and a surface. The channel is the result of the removal of the cut portions (14 mm × 1 mm × 50 μm). This versatile technique can be used to produce a wide variety of microfluidic device prototypes within just a few hours. Although, the accuracy of the razor is an important issue (~ 10 μm), this method is a useful and inexpensive research tool.[337]

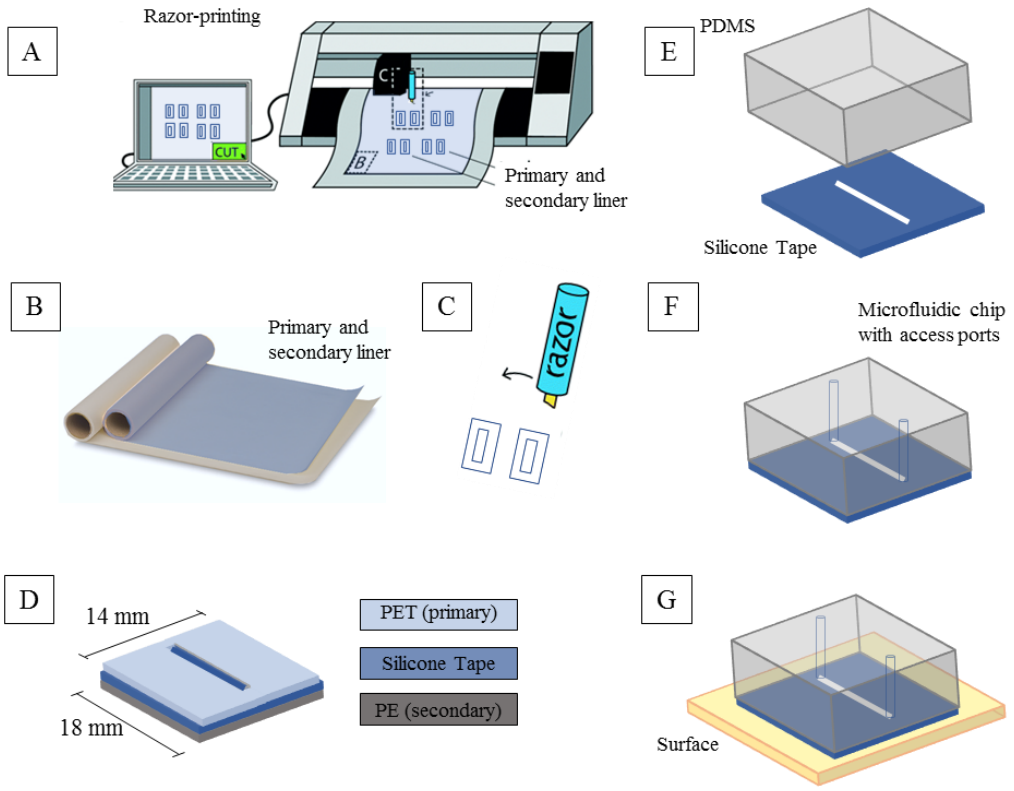

Figure 4.3 A-B-C) Schematic of the "cutting edge" technology for cell biology provided by tape-based devices. A computer device is associated to a razor printer to cut a biocompatible double-side adhesive tape. **D)** Representative microfluidic channel geometry is cut into the primary liner and silicon tape but not into the secondary liner. The microchannel obtained is 14 mm × 1 mm × 50 µm. **E)** The secondary liner is removed and the silicone tape flipped over to adhere to the PDMS. Once adhered, access ports are cut with a biopsy punch **F)**, before the primary liner is removed and the device attached to a surface of interest **G)**.

Silicone-based adhesive transfer tapes (catalogue number ID B40065869) with a thickness of 50 µm (3M^{TM}, USA) were used. The tapes are provided with a white polyethylene terephthalate (PET) primary release liner (Figure 4.3D)) and were backed onto an optically clear polyester (PE) secondary release liner (catalogue number 5053 also 3M^{TM}). Geometries were designed in Autodesk Inventor Professional^{TM} and exported in *.dxf* format to the plotter cutter (Silhouette Cameo, Graphtec^{TM}), which excised them from the liner-tape-liner stack. Devices were assembled starting with a bulk PDMS layer. PDMS was mixed, cast and cured as described in section 4.2.2.1. The secondary release layer was removed from the tape and the exposed silicone adhesive was brought into contact with the lid (PDMS) (Figure 4.3E). Fluid access ports were then created with a 500 µm biopsy punch (Harris Uni-core) (Figure 4.3F), flushed with deionised water to remove debris and nitrogen dried. The moulded face of the

PDMS lid was then cleaned three times with scotch tape to further remove any remaining debris. The primary release liner was then removed, and the adhesive surface brought into contact with the polymer surface of interest (Figure 4.3G). Initial contact was performed at room temperature. Curing to improve the bond strength was carried out at 45°C on a hotplate.

4.2.2.3 Tubes and Connectors

The tubing used in these experiments was selected for material properties and dimensions; fluid dead volume, tubing compliance, fluidic resistance, chemical inertness and gas permeability properties. The dead volume is given by the tube diameter and length; it affects the reagent transport and volume replacement times and the volume of reagents consumed. Larger tubing diameters result in larger volumes for any given length. Tubing length was selected to bridge the system components with minimal tension and small internal diameter tubing (ID = 0.5 mm) was preferred over larger alternatives. Small diameters provide high fluidic resistances. This ensures that small changes in pressure caused by noise and flow rate instabilities do not translate to high variation in liquid flow rate.[338] The tubing compliance relates to the elasticity of the tubing and can cause undesirable flow effects by altering pressure flow rates.[339, 340] Polyether ether ketone (PEEK) (Part Number 18111368 supplied by Scientific Laboratory Supplies Ltd.) was selected for its resistance to high pressure and its chemical resistance. Since the duration of these experiments was in minutes, little consideration was given to the gas permeability of the tubing. The connections were chosen to allow the integration of a macro sized liquid handling system with microfluidic devices. These were as follows: 23G steel tube connectors (Elveflow, steel connector OD = 0.5 mm, h = 20 mm) that were bridged to the PEEK tubes using pieces of Tygon tubing (ID = 0.5 mm) steel connectors (Figure 4.4). PEEK Luer adaptors (Thames Restek) and connectors were used to connect syringes to the tubing.

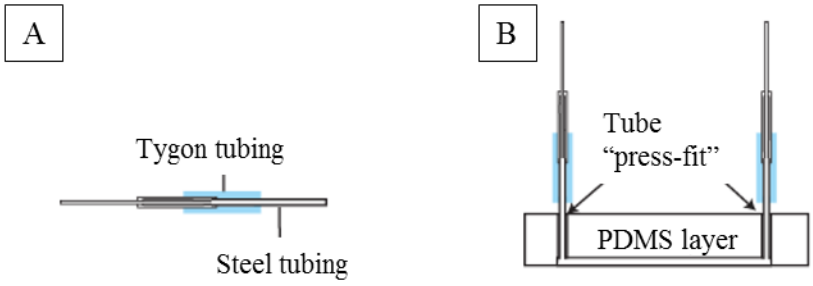

Figure 4.4 A) To hold the tubing in place, steel tubes were preferred for connections. **B)** Tygon tubing was used to bridge the sleeved tubing with the steel tube for connection with the PDMS layer/microfluidics channels.

4.2.2.4 Microfluidics Detachment Assay

Figure 4.5A shows an enlarged view of the microfluidics system where the walls of channels are made of double tape embedded between PDMS and the surface of interest. Cells were then cultured in the channel and the microfluidics chip positioned under an inverted microscope to assess the changes in the number of cells adhering to the surface as the flow rate is increased (Figure 4.5B).[341] Increased flow exerts a shear stress at the surface that on reaching a certain rate was able to detach the bacterial cells (Figure 4.5C). The shear stress necessary to detach bacteria from a surface was used as a measurement of the adherence strength of a bacterial cell (wild-type or mutant) to a particular surface.[329, 330, 342]

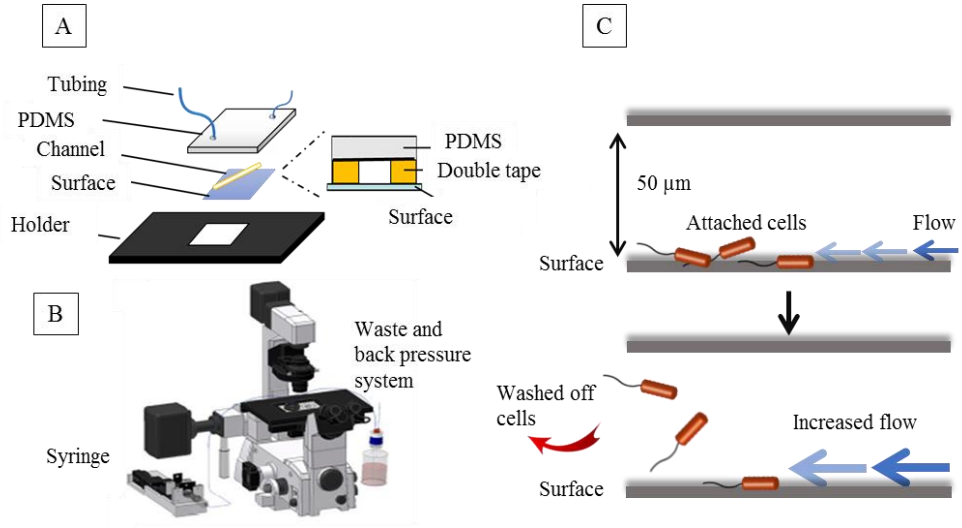

Figure 4.5 Microfluidics detachment experiment. **A)** Enlarged view of the microfluidics channel system. **B)** Microscope set-up with pump, microfluidics, injector and medium. **C)** Schematic of the removal process of adhered cells. Figure readapted from [341].

An neMESYS low pressure precision syringe pump (Cetoni GmbH, Germany) controlled *via* an neMESYS user interface in-built computer was used to aspire media and generate flow inside the channel. The shear stress (τ) was described through Poiseuille's equation as the force exerted onto channel walls which can be calculated using Equation 14 (section 4.1.2). The removal process was carried out by applying a weak flow (0.0276 mL min^{-1}), which was subsequently increased stepwise by 26% in 5 s intervals until a maximum shear stress of $\tau \approx$ 630 Pa was reached. The critical shear stress τ_{50} is defined as the shear stress when 50% of bacterial cells are removed. This parameter was used to compare different surfaces and bacterial strains/mutants.

Although rod-shaped cells are known to attach to a surface either along the cell body (horizontal) or on one of the poles (vertical),[292] surface area was not considered because all cells at very low flow rates (0.0276 mL min^{-1}) showed only horizontal attachment.

4.2.3 Microscope

Experiments were conducted as described in section 3.2.4. A time series of images was collected with a 40×/1.3 and 10×/0.5 objective lens at 1 frame per s.

4.2.4 Bacterial Growth Conditions

P. aeruginosa wild-type and a number of isogenic mutants and the corresponding complemented strains (Table 2.2) were grown at 37°C for 16 h in 5 mL LB broth. Cultures were diluted 1:100 in RPMI-1640 (5 mL) until an OD_{600} of 0.03 was reached. 10 µL samples were inoculated into the microfluidics system before connection the tubing. Surfaces were incubated with bacteria for 10 min before the detachment assay was started.

4.2.5 Bacterial Biofilm Assay

Bacterial biofilm assay was conducted according to section 3.2.3.

4.2.6 Water Contact Angle

A KSV CAM 200 computer controlled optical contact angle meter was used to determine the wettability of the polymer surfaces. The sessile drop method was employed. 60 frames 5 s apart were recorded for a 2 µL 18.2 Ω cm miliQ water droplet placed on the surface. Each image was analysed computationally on the CAM200 software using Young's equation[263] which requires the three phase boundary values: γ_{lg}, γ_{sg} and γ_{sl} with *l* denoting liquid, *s* solid and *g* for gas as described in section 2.2.2. This was recorded 9 times across 3 surfaces. The temperature and humidity remained stable for the ambient run, between 22.2 ± 0.5^{o}C and 35 ± 2% respectively. For the variable temperature experiments a Fisher Isotemp stage temperature controller was used.

4.2.7 Atomic Force Microscopy

Polymer surfaces were analysed using a Bruker Dimension Icon® AFM using PeakForce QNM® mode. Bruker MSNL-F tips were used (silicon tip/nitride lever) with a 0.97 N/m spring constant (calculated *via* the Sader method) and resonant frequency of 116.29 kHz. 1 µm^2 areas were recorded. All images were flattened to remove curvature and slope using *Gwyddion – SPM Data Analysis* software. Images were carried out in dry and liquid PeakForce mode after immersing the sample in 18.2 Ω cm miliQ water for at least 5 min. Root-mean-square (rms) values for roughness were calculated using an average of > 4 measurements over areas of 1 µm^2, 100 µm^2 and 400 µm^2 respectively.

For force measurements, an RTESPA tip with a 30.6 N/m spring constant and 314.47 kHz resonant frequency functionalised with a 21 µm diameter glass bead was used. 169 force curves were taken over three separate 60 µm^2 areas with an Asylum MFP-3D AFM. Nanomechanical attributes were calculated using a Microsoft Excel macro designed by Xinyong Chen (Nottingham, UK). The The Derjaguin-Muller-Toporov (DMT) model was used to calculate Young's modulus *via* the slope from the retraction curves in order to remove contributions by plasticity.

4.3 Results

4.3.1 How Strongly Do *P. aeruginosa* Cells Attach to pNGPDA and pEGdPEA Surfaces?

Since *P. aeruginosa* shows different colonisation rates and daughter cell fates on the two different polymer surfaces (section 3.3.4), a detachment assay was deployed to compare cell adhesion strengths. Bacteria were incubated on each polymer for 10 min, then growth medium was pumped through the flow cell at rates designed to exert a shear stress τ between 0.6 and 630.0 Pa. The attached bacteria were observed for the duration of the experiment and the flow rate at which the cells detached was used to determine the strength of adhesion. The critical shear stress τ_{50} (shear stress when 50% of bacteria were removed) measured for bacteria on pNGPDA was 87.6 ± 15.0 Pa, whereas the τ_{50} was significantly (p<0.0001) reduced to 3.2 ± 0.8 Pa for bacteria grown on pEGdPEA (Figure 4.6). An intermediate τ_{50} of 31.2 ± 15.0 Pa was observed for the copolymer of NGPDA and EGdPEA. Thus, these results suggest that *P. aeruginosa* is unable to adhere to pEGdPEA

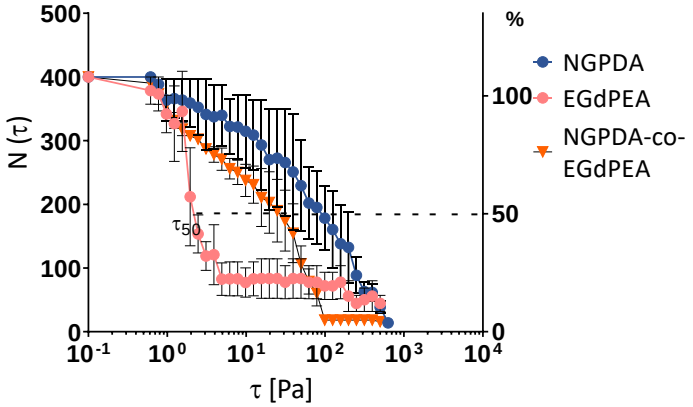

Figure 4.6 Measurement of bacterial adhesion strength to pNGPDA and pEGdPEA. surfaces. The number of PAO1-W surface associated cells on pNGPDA (blue-circles), pEGdPEA (pink-circles) and NGPDA-co-EGdPEA (orange-triangles) surfaces with increasing shear stress τ (Pa) applied through an increase in flow rate. Error bars represent ± 1 SEM (N=3).

4.3.2 Bacterial Surface Appendages Involvement in Adhesion

To understand the contribution of flagellar and T4P surface appendages to *P. aeruginosa* attachment the adhesion force of Δ*pilA* and Δ*fliC* mutants was also determined. Figure 4.7 shows the detachment curves for *P. aeruginosa* WT, Δ*pilA* and Δ*fliC* mutants on pNGPDA. Detachment curves for both polymers are shown in Figure 4.8. The shear stress τ_{50} determined for the Δ*pilA* mutant was similar on both polymers (10.0 ± 2.3 and 9.4 ± 3.1 Pa for pNGPDA and pEGdPEA respectively) and lower than the wild-type (108.6 ± 15.0 Pa) confirming that T4P are involved in the initial surface adhesion events. Similarly, the Δ*fliC* mutant was tested and surprisingly, the bacterial cells were not detached by flow for the range of shear stresses applied. The adhesion strength observed with the Δ*fliC* mutant was higher than for wild-type. Thus, the absence of flagella resulted in increased adhesion strength on both polymer surfaces.

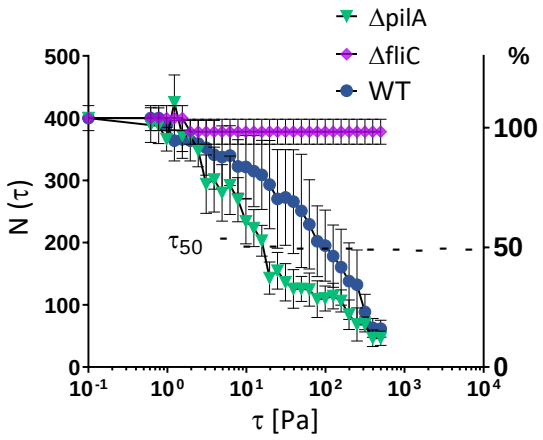

Figure 4.7 Number of *P. aeruginosa* Δ*pilA* cells (green), Δ*fliC* (purple) and PAO1-W WT (blue) on pNGPDA with increasing shear stress τ_{50} (Pa) applied through an increase in flow rate; shear stress τ_{50} indicates the shear stress necessary to detach 50% of cells.

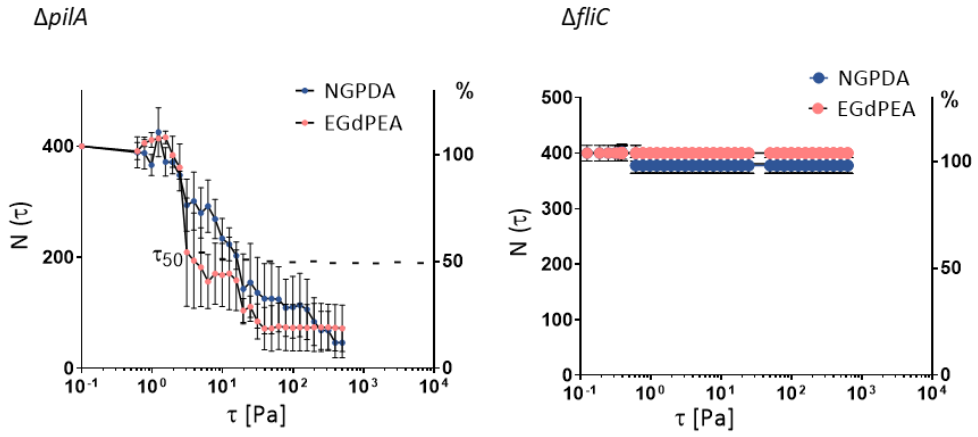

Figure 4.8 Number of *P. aeruginosa* Δ*pilA* (left) and Δ*fliC* (right) cells on pEGdPEA (pink) and pNGPDA (blue) surfaces with increasing shear stress τ_{50} (Pa) applied through an increase in flow rate; shear stress τ_{50} indicates the shear stress necessary to detach 50% of cells.

As previously described (section 1.4.2), the *P. aeruginosa* chromosome encodes two different stators, MotAB and MotCD, that provide the torque required to propel the bacterial cells forward. The recruitment of the two stators to the flagella motor differs in a load-dependent manner,[88] and recent studies have described the importance of the rotary flagellum in mechano-sensing.[122-124] To determine whether the flagellar stators affect bacterial adhesion, strains with either *motAB* or *motCD* or both deleted were tested in the microfluidic detachment assay (Figure 4.9). The adhesion strength of the *mot* mutants to pNGPDA was reduced compared with the wild-type with τ_{50} values of 8.2 ± 7.3 and 18.9 ± 6.2 Pa for *motAB* and *motCD* mutants respectively. *P. aeruginosa* without both stators i.e. the *motABCD* mutant presented the weakest adhesion (with τ_{50} = 0.5 ± 0.1 Pa on both polymers). On pEGdPEA, although the *motAB* mutant presented similar attachment strength to PAO1-W (10.0 ± 9.5 Pa), the *motCD* mutant showed the strongest attachment of 31.3 ± 16.0 Pa ($p<0.05$ in comparison to the wild-type). This suggests cell surface adhesion is weak on pEGdPEA and both T4P and flagellar stators are required to adhere to pNGPDA.

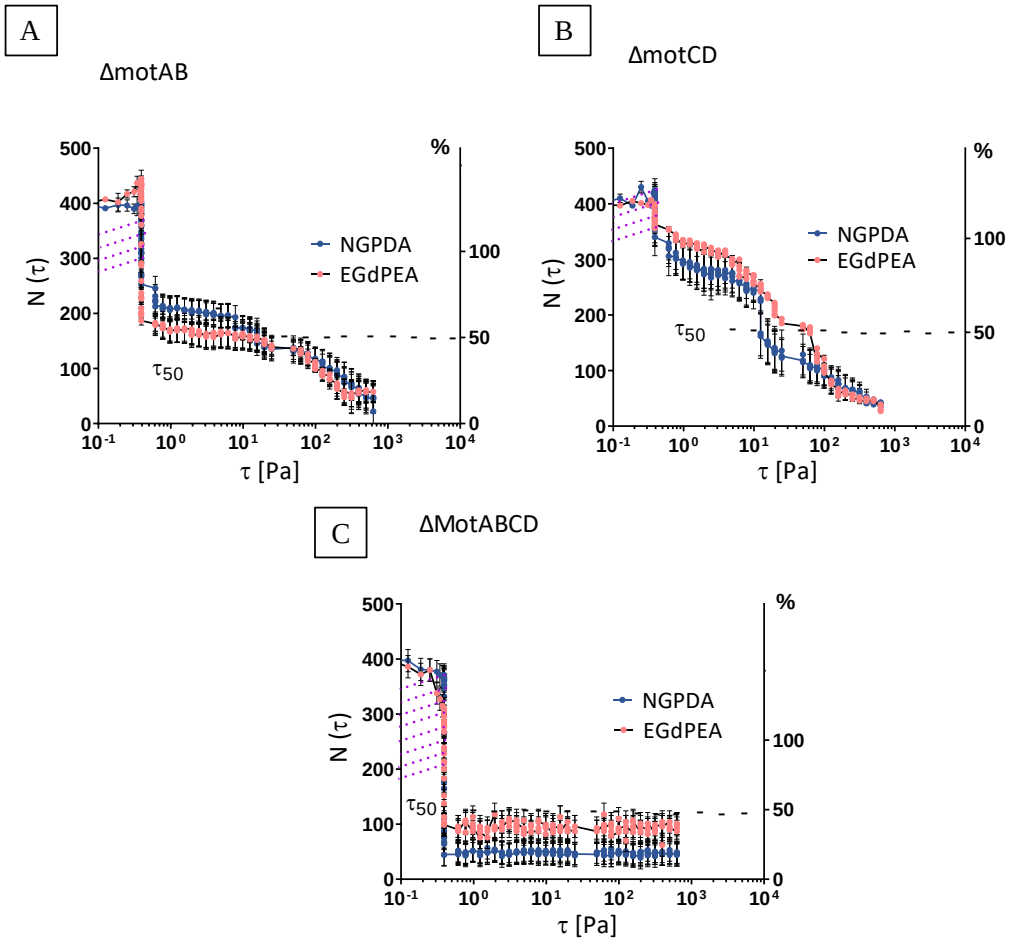

Figure 4.9 Involvement of the flagellar stators in adhesion onto pNGPDA and pEGdPEA. Number of *P. aeruginosa* Δ*motAB* **(A)**, Δ*motCD* **(B)** and Δ*motABCD* **(C)** cells on pEGdPEA (pink) and pNGPDA (blue) surfaces with increasing shear stress τ; shear stress τ_{50} indicates the shear stress necessary to detach 50% of adhered cells. The *mot* mutants differently from wild-type and and *pilA* mutant, presented also cells at the surfaces which were not surface adhered and washed off at low shear stress $\tau < 0.6$ Pa as evidenced with violet dots. Error bars show ± 1 SEM (N=3).

A summary figure of the shear stress (τ_{50}) necessary to detach 50% of *P. aeruginosa* wild type, Δ*pilA*, Δ*motAB*, Δ*motCD* and Δ*motABCD* cells on pEGdPEA (pink) and pNGPDA (blue) are shown in Figure 4.10. 2-way ANOVA analysis by using Sidak's corrections was used for multiple comparisons to establish statistical differences between the samples. This allowed us to observe the influence of both the strain and the surface on bacterial surface attachment strength.

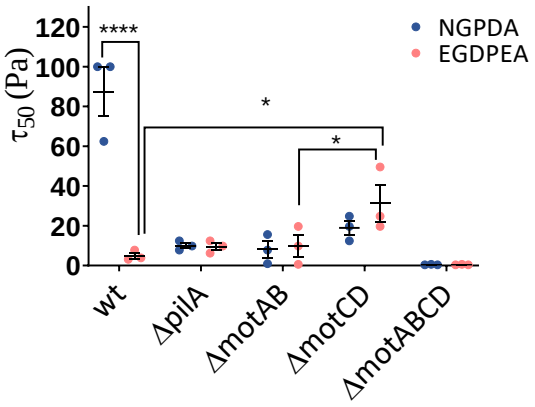

Figure 4.10 Shear stress τ_{50} of PAO1-W, Δ*pilA*, Δ*motAB*, Δ*motCD* and Δ*motABCD* cells on pEGdPEA (pink) and pNGPDA (blue). Error bars represent ± 1 standard deviation (N=3). ****p<0.0001, *p<0.05. Significance was determined by 2-way Anova analysis using Sidak's method for multiple comparisons of differences between the indicated samples.

4.3.3 Do T4P and Functional Flagella Contribute to Biofilm Development on pNGPDA and pEGdPEA?

To determine whether there is a relationship between adhesion strength and biofilm coverage, biofilm formation was assessed after 24 h after inoculation using T4P (Δ*pilA*) or flagellum stator (Δ*motAB,* Δ*motCD* and Δ*motABCD*) mutants. Figure 4.11A shows representative confocal microscopy images of biofilm formation on pNGPDA and pEGdPEA comparing wild-type with the respective mutants. In the absence of pili, MotAB or both sets of flagellar stator units (Δ*motABCD*), *P. aeruginosa* was unable to form biofilms on either polymer confirming the importance of both appendages for both attachment and biofilm formation over the first 24 h. Biofilm biomass quantification revealed that the Δ*motCD* mutant exhibited higher biofilm coverage on pEGdPEA (19.0 ± 3.3 $\mu m^3/\mu m^2$) than the wild-type (6.0 ± 3.4 $\mu m^3/\mu m^2$) (Figure 4.11B) (p<0.001). This result is in accordance with higher adhesion strength observed for the *motCD* mutant suggesting that MotAB is preferred during early attachment to surfaces.

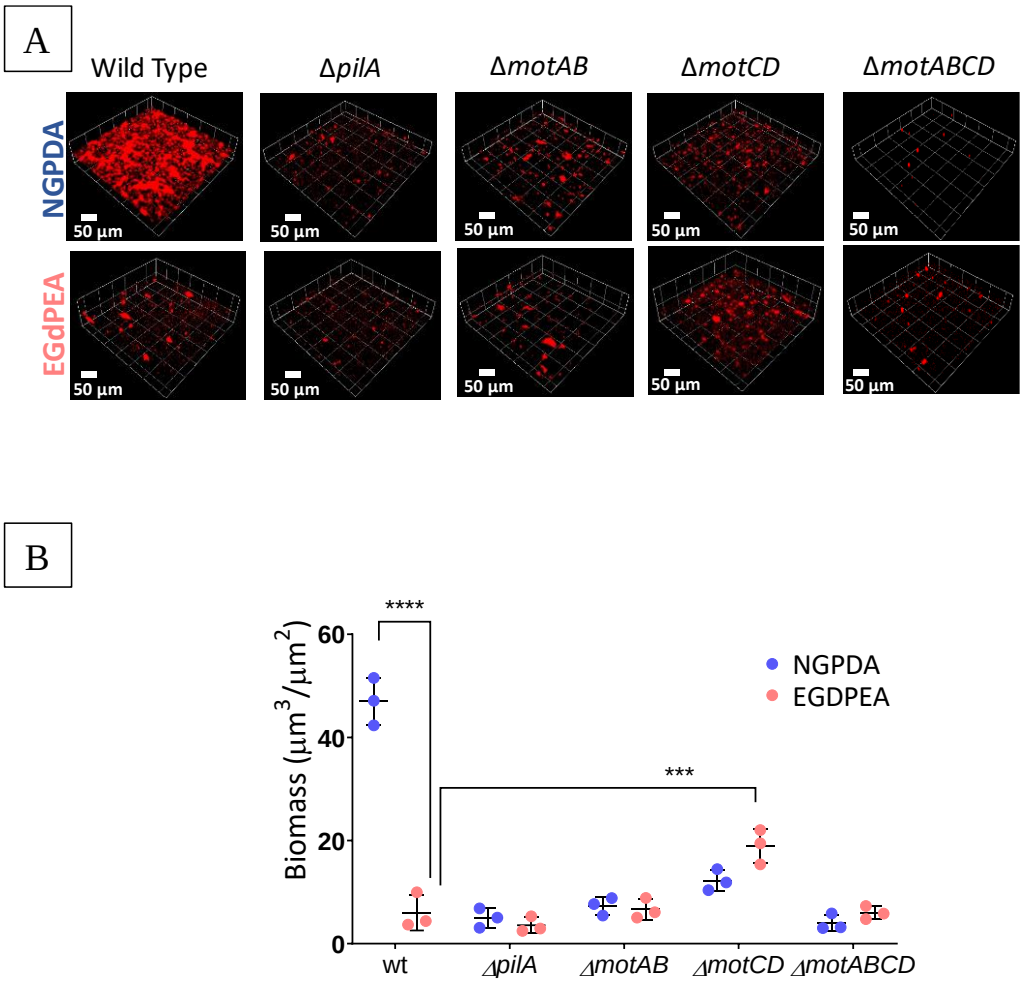

Figure 4.11 A) Confocal images (10×, 0.3) of *P. aeruginosa m-cherry* tagged PAO1-W, Δ*pilA*, Δ*motAB*, Δ*motCD and* Δ*motABCD* after 24 h on pNGPDA (top) and pEGdPEA (bottom). Samples were washed 2× in PBS and 1× in H_2O. Scale bar is 50 µm. **B)** Quantification of bacterial biomass for surfaces. Error bars show ± 1 standard deviation (N=3). Significance was determined by 2-way ANOVA multiple comparison with Sidak's correction for differences between the indicated samples. ****p<0.0001 and ***p<0.001. Data provided by Dr Jean Dubern.

4.3.4 Water Contact Angle

WCA measurements were used to determine how the different chemical groups that are present on the polymer surfaces may be responsible for the reduced bacterial adhesion observed when bacteria are exposed to pEGdPEA. Previous publications have described the influence of wettability and hydration on cell adhesion strength on different surfaces, and hydrophilic and super hydrophobic surfaces have been shown to affect adhesion of several different bacterial species.[328-330, 341, 343] Our polymers possess amphiphilic (pNGPDA) and relatively hydrophobic properties (pEGdPEA). As shown in Figure 4.12

pEGdPEA has a higher WCA (86.3 ± 2.2°), than pNGPDA (69.8 ± 2.7°), an intermediate value was found for the copolymer pNGPDA-co-EGdPEA (77.7 ± 1.7°). The pNGPDA polymer therefore represents an amphipathic surface, with pEGdPEA being relatively hydrophobic.

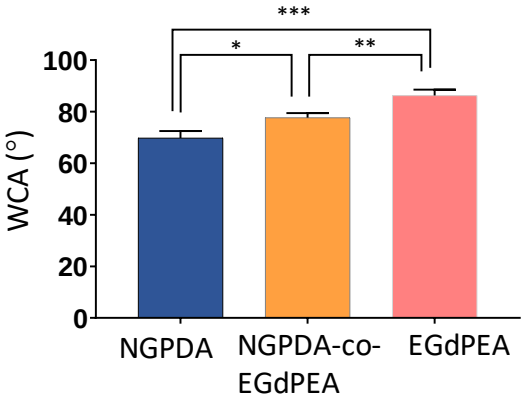

Figure 4.12 WCA measurements on pNGPDA (blue), pEGdPEA (pink) and pNGPDA-co-EGdPEA (orange). Error bars show ± 1 standard deviation (N=9). ***p<0.001, **p< 0.01 and *p<0.05. Statistics assessed using One-way ANOVA with Tukey's multiple correction**.**

4.3.5 Atomic Force Microscopy

Several publications have shown how engineered surface topographical features with well-defined shapes and dimensions in the micro to nanometer range can affect bacterial adhesion.[344, 345] AFM was adopted to investigate any differences in topography at the nanoscale as well as providing mechanical information for the polymers. Figure 4.13 shows a comparison of the topographic details of the polymer surfaces in dry conditions when scanned using AFM. Although under this condition both surfaces present a fine network structure, the texture in pEGdPEA was observed to be smooth as previously noted.[7] A few sporadic artefacts of increased height were detected on the polymers that were attributable to surface dust contaminants.

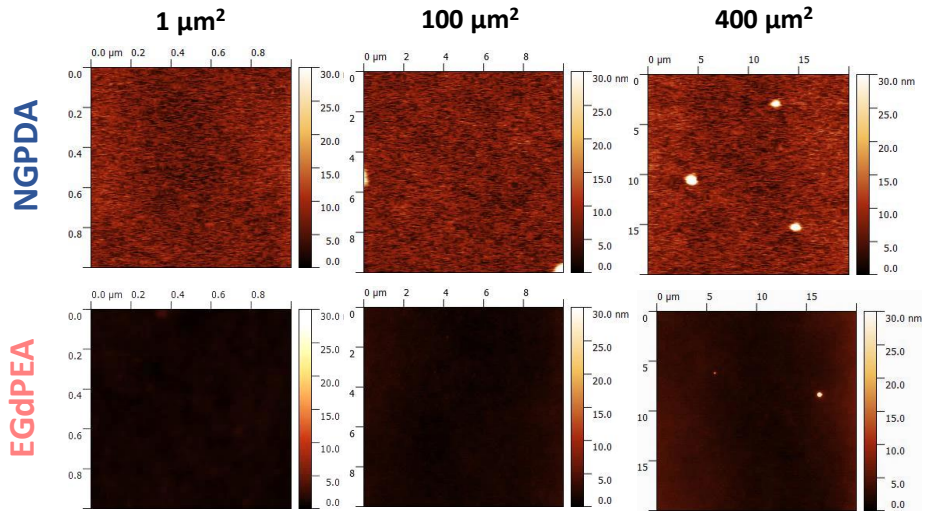

Figure 4.13 AFM height images of pNGPDA (blue) and pEGdPEA (pink) for areas of 1×1, 10×10 and 20×20 µm^2. Images were previously line flattened to remove surface curvature and slope.

The variation in height across the surface of each polymer was quantitatively mapped. This was translated into root mean square (RMS) roughness data. Considering three area sizes (1×1, 10×10 and 20×20 µm^2) the RMS of the samples were not statistically different (Figure 4.14).

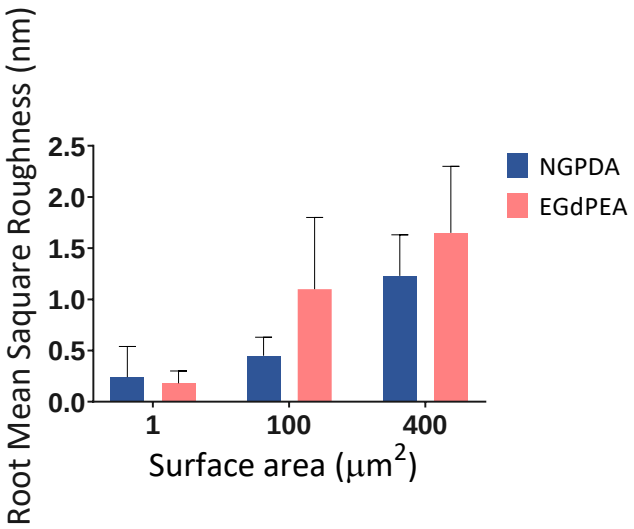

Figure 4.14 Determination of the root mean square roughness (nm) of the at 1 µm^2, 100 µm^2 and 400 µm^2 from the surfaces in dry conditions. Values are the mean of four images taken over 4 different samples. The error bars equal ± 1 standard deviation (N=4). Significance was determined by analysis of variance 2-way ANOVA and Sidak's post-test comparison for differences between the samples.

Another parameter that can be assessed by AFM which is relevant to bacterial adhesion is stiffness, although conflicting results have been published on

different surfaces and pathogens.[159, 346-348] Mechanical data were therefore also obtained in the form of force curves. These curves describe the forces that the AFM probe experiences as it approaches, indents and then retracts from the polymer surfaces. Representative F-D (Force-Displacement) curves for the retraction parts of both polymers under dry conditions are shown in Figure 4.15. The initial low force retraction of the pNGPDA curve is interpreted as a softer surface. This may be explained by the fact that, although pNGPDA is a cross-linked polymer, pEGdPEA presents a cage like moiety which is very rigid. pNGPDA on the other hand has more rotatable bonds resulting in a softer material.

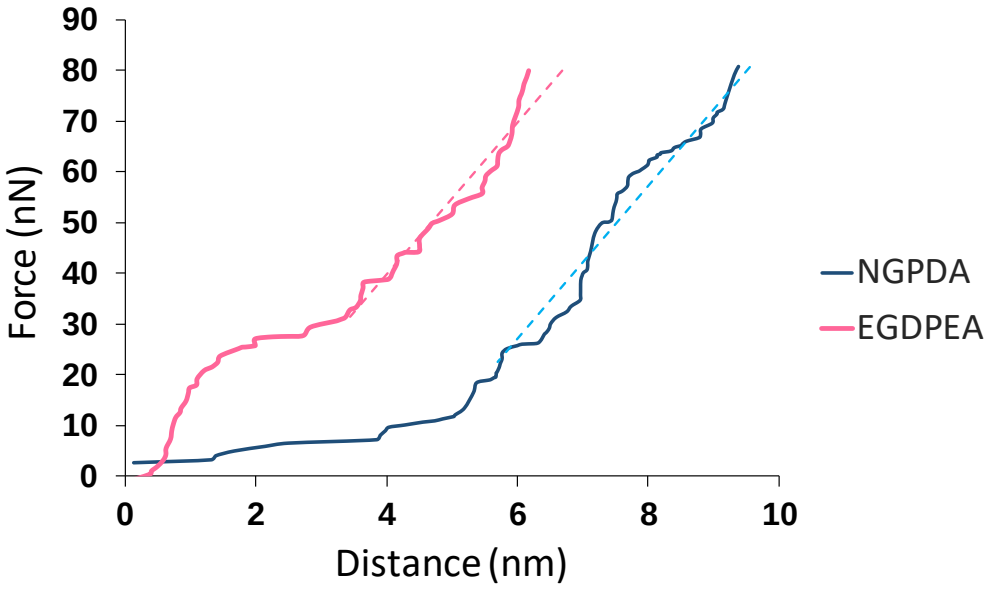

Figure 4.15 F-D curves of representative experimental runs showing the different degrees of deformation for pNGPDA (blue) and pEGdPEA (pink) in dry conditions (n=169).

The entire length of the trace, or the total distance moved forward and backward by the tip was less than 10 nm. Extracting the quantitative data from the curves showed that the Young's Modulus was 456 ± 75 MPa and 735 ± 103 MPa for pNGPDA and pEGdPEA respectively. pEGdPEA was found to be stiffer than pNGPDA (n=169, N=3) (p<0.0001). To explore the effect of water on surface stiffness, Young's Modulus values in wet condition were also extracted and softer values were found for pNGPDA in wet conditions of 203 ± 44 MPa but not for pEGdPEA (793 ± 168 MPa) (Table 4.1).

Table 4.1 Young's Modulus values in dry and wet conditions for pNGPDA and pEGdPEA

		E [MPa]
NGPDA	dry	455.8±75.33
	wet	202.7±44.35
EGDPEA	dry	735.2±102.8
	wet	793.6±167.5

4.4 Discussion

To understand whether and how bacterial adhesion is affected on pEGdPEA, microfluidics was used in combination with live imaging *via* microscopy. The use of microfluidic devices in microscopy of bacterial cell behaviours has recently increased because they enable the precise manipulation of certain environmental parameters such as flow rate and surface chemistry.[320] Our results showed that the *P. aeruginosa* wild-type attachment differed on the two polymer surfaces in accordance with the principle that cell adhesion is a surface-dependent process.[320] However, this contrasts with a report by Lecuyer *et al.* that provided evidence to suggest that the adherence of *P. aeruginosa* strain PA14 is not surface-specific by comparing bacterial adhesion on glass and PDMS surfaces.[349] Our experiments differ from those of Lecuyer *et al.* in a number of important ways. Firstly, the surfaces considered are not the same and may influence the findings; Lecuyer *et al.* investigated attachment to glass and PDMS, which are chemically distinct from pNGPDA and pEGdPEA. Secondly, they explored adhesion by studying the residence time of bacterial cells at the surfaces for increasing shear stress in a range from 1 to 10 Pa. They considered the detachment probability of bacteria over 100 s at constant shear rate or after a shear reduction and their results showed a significant increase in the detachment probability of bacteria when compared to a control where the shear stress was kept constant on either surface. These observations were explained as the result of a shear-sensitive mechanism at the cell level. The system described in this thesis is able to explore shear stress in a range of two orders of magnitude

(1- 600 Pa) greater than previously reported. If Lecuyer *et al.* had explored higher shear stresses they may have observed progressive detachment of bacteria from the surface which could have been linked to how strongly the bacteria were attached. *P. aeruginosa* strains adhered much less strongly to pEGdPEA than to pNGPDA (Figure 4.6). The adhesion strength measured at the presence of hydrophobic pEGdPEA is similar to that observed on hydrophilic PEG2000-OH coated surfaces by Arpa-Sancet *et al.* using *C. marina.*[329] This cannot be explained by considering the wettability of the acrylate surfaces alone, and WCA is not to be a good predictor of bacterial adhesion on acrylate amphiphilic polymers.[158] It is also likely that the pEGdPEA biofilm-resistance mechanism is different from that described for well-known anti-fouling polymers such as PEG.[350, 351] pEGdPEA is characterised by a rigid cyclic hydrocarbon pendant group, whereas pNGPDA (and PEG) constitutes a more linear and flexible structure composed of ethylene glycol groups and exhibits a lower WCA (Figure 3.1). There have been conflicting findings regarding bacterial adhesion trends with respect to surface chemistry. The reasons for this might be surface roughness[352] and texture, as well as material porosity.[353] For example, with respect to *C. marina* Arpa-Sancet *et al.* found that the strength of adhesion with undecanethiol SAMs with $–CH_3$, $–NH_2$, $–OC_7F_{10}CF_3$ termination was ten times higher than with PEG.[329] Using a slightly different chemistry, Pranzetti *et al.* reported for same bacterial species that adhesion was higher on 11-aminoundecanethiol hydrochloride surfaces than on 1-hexadecanethiol surfaces which are more hydrophobic.[354]

Topography is another important parameter to be assessed in investigations of bacterial adherence.[262] Although large surfaces areas with rough topography increase adhesion of gram-positive bacteria,[355] for the study of this parameter it is necessary to consider the shape and size of bacterial cells which also play roles in material surface interactions.[356-358] Using AFM measurements, polymer topography was assessed, and similar values for RMS roughness were found for both pNGPDA and pEGdPEA. Although the impact of stiffness on bacterial adhesion is still under-explored,[159] an emerging body of evidence suggests that this material property might affect bacterial attachment.[31, 159, 348, 359] Here, although before drawing any firm conclusions, more surfaces

need to be compared. Surface stiffness in dry and wet conditions on the acrylate polymers was assessed and pNGPDA was found to be softer (≈500 and 200 MPa, in dry and wet respectively) than pEGdPEA (≈700 MPa in either condition) (Table 4.1). The pNGPDA data are consistent with absorption of water into the surface and in agreement with its higher hydrophilicity given by the flexible structure composed of ethylene glycol groups and low WCA. Lichter *et al*. found that adhesion of *S. epidermidis* to weak polyelectrolyte multilayer (PEM) thin films increased with the stiffness of these hydrated surfaces (ranging from 0.8 to 80 MPa).[348] Increasing evidence suggests that the correlation between stiffness and bacterial attachment is also strongly dependent on the substrate surface hydrophobicity. There are few publications on stiffness of hydrophobic surfaces, but they seem to suggest reduced attachment with increasing surface stiffness. This is likely to be linked to the fact that stiffer materials correspond to a reduced level of internal water. Song *et al.* reported that the initial attachment of *E. coli* and *P. aeruginosa* cells was lower on stiffer PDMS surfaces in dry conditions ranging from, 0.1 to 2.6 MPa.[159] Two follow-up studies from the same group reported that cells attached to soft PDMS surfaces were less motile than those attached to the stiff surfaces, which was attributed to the expression of *motB,* and that c-di-GMP was higher when *P. aeruginosa* attached to soft PDMS surfaces compared to stiff ones (*via* the outer membrane protein, OprF).[360-362] Our data apparently confirm the hypothesis of lower attachment on the more hydrophobic pEGdPEA. However, greater stiffness has been shown to increase bacterial attachment and biofilm formation in several studies employing hydrophilic surfaces.[347, 363] The opposite trend has also been reported: polyacrylamide (PAAm) and poly(ethylene glycol) dimethacrylate (PEGDMA), two hydrophilic surfaces with different stiffnesses, were incubated with *S. aureus* in two separate studies. Bacterial biomass negatively correlated with the stiffness of PAAm, but positively for PEGDMA.[363, 364] This conflicting result might be explained by a different range of substrate stiffnesses used, different polymer surface chemistries and different culture media and bacterial strains. For example, PAAm was incubated in nutrient rich Tryptic Soy Broth (TBS) whereas PEGDMA experiments used a minimal M9 medium. Another important, yet little understood, aspect of the

stiffness-adhesion relationship is the relative contribution of external surface *vs* subsurface stiffness.[365]

The role of bacterial surface appendages in polymer surface attachment was also investigated. In particular, the consequences of the lack of T4P and a functional flagellum on *P. aeruginosa* attachment was determined. Adhesion of *pilA* and *mot* mutants to pNGPDA was observed to be very much weaker than the wild-type on pNGPDA (Figure 4.10) although the *motABCD* mutant was the weakest (Figure 4.10). On pEGdPEA, the *motABCD* mutant showed the weakest adhesion and *motCD* the strongest suggesting that although both *mot* stators are important in bacterial adhesion, *motAB* is primarily involved in the early attachment to surfaces. This confirms the recently proposed hypothesis, that flagella or T4P serve as mechano-sensing nanomachineries to detect surface signals.[60, 124, 293, 366] In addition, our results are in good agreement with the observation that MotAB participates in irreversible attachment.[367] The data presented suggest that cell surface adhesion is weak on pEGdPEA and both T4P and an active flagellum are required for adherence to pNGPDA. Laventie *et al.* reported that the membrane-embedded MotAB stator is likely to act as mechano-sensor and be required for the rapid response of *P. aeruginosa* to surface upon contact.[60] Since stators as described in section 1.4.2 are proton-conducting membrane channels that generate torque, Hug *et al.* proposed that the flagellar motor acts as a sensor reminiscent of mechanosensitive channels.[124] Laventie *et al.* also described the *P. aeruginosa* tactile response in a timescale of a few seconds, similar to that observed in other bacterial species.[60, 317] In our flow detachment experiments cells were incubate for 10 min, that means that *Pseudomonas* stators are likely to generate a cascade of events to respond to our surfaces over that range of time. The nature of the factors involved in this bacterial response to our surfaces is yet unknown, but *motA* and *motB* genes (PA4954/PA4953) cluster with genes responsible for pilus assembly. This leads the hypothesis proposed by Laventie *et al.* in which stators and c-di-GMP influence T4P localisation and activity.[60]

It is well established that bacterial adhesion to surfaces is the first step in biofilm formation.[368] Here *P. aeruginosa* surface attachment and biofilm biomass for

wild-type, T4P and flagellar mutants were studied at the single-cell level. Interestingly, as shown in Figure 4.16, a high correlation (R^2 = 0.98) was observed between 24 h biofilm biomass of all the strains used on pNGPDA and the adhesion strength measured at the early stages of bacterial contamination. This confirms that the initial attachment correlates well with subsequent bacterial community behaviour.

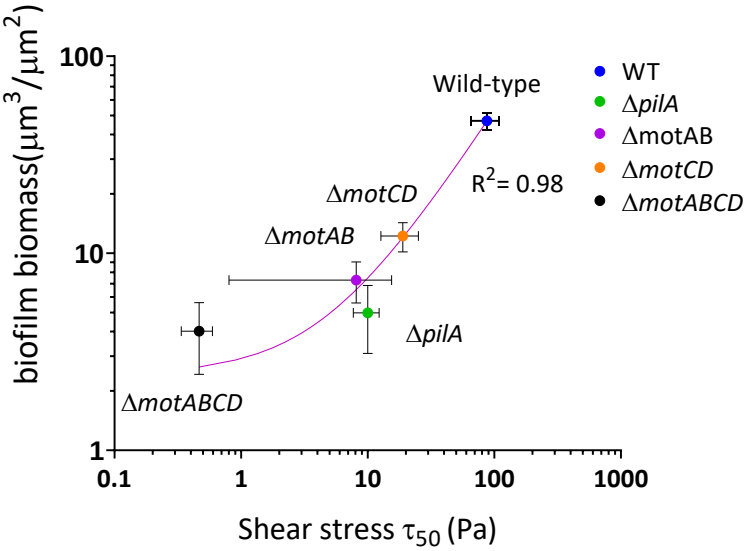

Figure 4.16 Biofilm biomass *vs* shear stress τ_{50} of PAO1-W wild-type (blue), pili (green) and flagella stators mutants (violet, orange and black, for *ΔmotAB*, *ΔmotCD* and *ΔmotABCD* respectively) on pNGPDA. The error bars equal ± 1 standard deviation (N=3). Linear fit (y = m*x + b) yields m = 0.5 and b = 2.4. R^2 = 0.98.

4.5 Conclusions

A microfluidic detachment assay has been used to assess bacterial attachment to the two polymer surfaces, pNGPDA and pEGdPEA which were compared in this study.

The measured attachment strength on biofilm-promoting pNGPDA was determined by a functional T4P and flagellum. In the absence of either, bacterial adhesion was disrupted, confirming the importance of these appendages in surface attachment. Since higher adhesion strength was measured in cells expressing the *motAB* stator genes (i.e. Δ*motCD* mutant background) on pEGdPEA than either the Δ*motAB* mutant or wild-type as shown in Figure 4.10,

these data also suggest that the stator units are necessary for the mechano-sensing system and required for a rapid response to surfaces.

A strong correlation was also observed between bacterial attachment during the early stages of bacterial contamination and 24 h biofilm biomass on pNGPDA. Bacterial adhesion strength was also far weaker on pEGdPEA than on pNGPDA. After surface characterisation, it was noted that surface roughness is not the single most important determining factor because two materials with the same roughness produced a very different biological response.

pEGdPEA affects bacterial adhesion strength and the transition from a reversible to an irreversible attachment by reducing intracellular c-di-GMP level and EPS production (section 3.3.7 and 3.3.8), but how *Pseudomonas* cells sense and respond to pEGdPEA is still not understood. For this reason, the next stage will be to discover the intracellular sensory pathway(s) used by *P. aeruginosa* to control this response (see chapter 5) as this would be ideal to fully understand the mechanism used by bacteria to discriminate between different surface chemistries. Such knowledge would possibly allow the direct, rational design of other bacterial targets to prevent biofilm formation.

Chapter 5

The Role of the SadB in Bacterial Surface Sensing

5.1 Introduction

The tactile and sensory mechanisms used by bacteria such as *P. aeruginosa* to sense whether they are near or on a specific surface are not fully understood but are likely to involve flagella and T4P.[369] It has been proposed that the flagellum does not act simply as a propulsive force, but that it is also functions as a sensor or adhesin to initiate biofilm formation upon contact with the surface,[370] and for exploring the surface topography to find micro-crevices on which to anchor.[371] Chapters 3 and 4 as well as other recent studies have shown the importance of the rotary flagellum in mechano-sensing of different surfaces.[122-124] The flagellar motor plays an important role in promoting the rapid surface attachment of *P. aeruginosa* by translating a mechanical signal into a rapid increase of c-di-GMP.[60] The MotAB stator but not the flagellar filament, is required for tactile responses leading to FimW activation and subsequent T4P assembly and attachment consolidation.[60] MotCD was also shown to disengage from the flagellar motor in the presence of high intracellular concentrations of c-di-GMP coincident with population shift to a biofilm formation phenotype.[125, 372] The mechanisms *via* which c-di-GMP mediates regulation of downstream cellular functions include signal-receptor interactions as effectors and transcriptional regulators.[298] As shown in section 1.5.2.3, the role c-di-GMP signalling plays is complex and involves a multiple signalling pathways. PelD for instance works as a receptor for c-di-GMP and the signal-receptor complex is necessary for Pel production in *P. aeruginosa*.[373] Alg44, a membrane-associated protein, activates alginate polymerisation by allosteric binding of c-di-GMP to its PilZ domain.[374] The second messenger molecular c-di-GMP, at high concentrations, also indirectly activates the expression of *pel, psl* and *cdr* genes in *P. aeruginosa* by interacting with the flagella master transcriptional regulator, FleQ.[375, 376] Flagellar biosynthesis is an expensive process that requires co-ordinated expression of many genes and therefore is tightly controlled.[377] FleQ initiates a regulatory cascade which starts the production and assembly of the flagellar components.[378, 379]

The initiation of this regulatory cascade is influenced by diverse environmental cues and as-yet unknown signals, and involves a signal transduction pathway in *P. fluorescens* initiated by SadB (Figure 5.1).[377] About 20 years ago, O'Toole and Kolter reported the isolation and characterisation of mutants of *P. aeruginosa* PA14 defective in the initiation of biofilm formation on polyvinylchloride surfaces. These mutants were named surface attachment defective (*sad*).[36] Few years later, one of these strains that carries a mutation in the *sadB* gene was furtherly characterised by Caiazza and O'Toole.[380] In particular, it was shown that *sadB* mutant could initiate surface attachment but failed to form microcolonies despite being able to twitch and swim. Closer examination of early attachment revealed an increased number of the *sadB* mutant cells arrested at reversible attachment, functionally defined as adherence *via* the cell pole. SadB is a cytoplasmic protein reported to be modulated by c-di-GMP and inversely regulates bacterial transition from a reversible to an irreversible attachment by altering flagellar reversals *via* CheIV[380, 381] and increasing Pel exopolysaccharide production.[382, 383] However, SadB function and how it interacts with c-di-GMP is yet unknown.

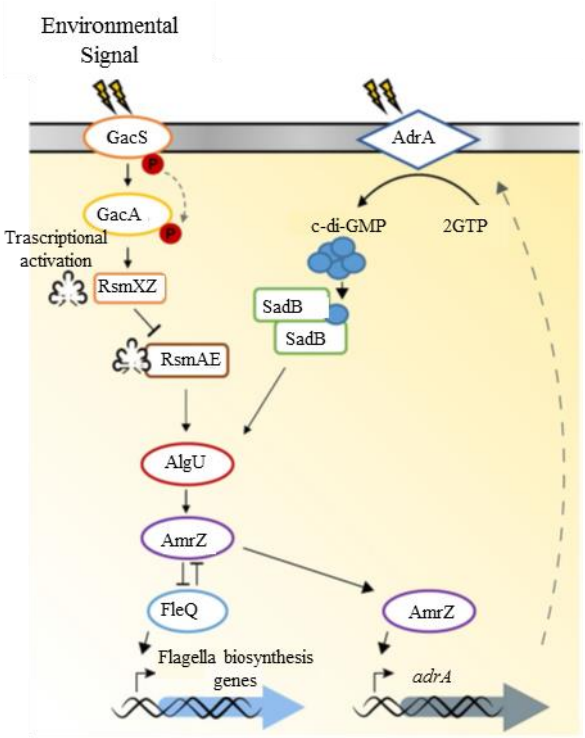

Figure 5.1 Possible SadB involvement in flagellar regulation upon environmental signal in *P. fluorescens*. Image taken from [377].

As described in section 1.5.2.2 several studies have also indicated that T4P are responsible for mechano-sensing.[60] Mechanically induced modifications in T4P have been recently observed to be mediated by the Pil-Chp chemosensory system encoded by cluster IV.[74] When cells encounter and attach to a surface by using T4P, as proposed by Persat *et al.*, the tension generated by the retraction induces an unknown modification in the T4P and a response which is controlled by the PilA-PilJ.[74] The chemotaxis cluster IV (CheIV) contains the *pilGHIJK* and *chpABCDE* genes which control T4P pili activation and include homologues of genes for chemosensory pathways.[384] PilJ, a methyl-accepting chemotaxis protein (MCP),[385] inversely regulates biofilm formation and is positively regulated by SadB.[381]

Tuson and Weibel summarised a list of materials that have been used to study bacteria-surface interactions in the last few decades.[141] However, only few different surface chemistries have been deployed to investigate bacterial surface sensing. Most of these studies have been run on biotic and abiotic surfaces such as agar, glass and polystyrene, which are chemically very different and not meaningfully comparable.[60, 369, 386, 387] Laventie *et al.* exposed *P. aeruginosa* cells to glass borosilicate and agar surfaces and showed that FimW re-localised to the poles in response to surface contact in a process taking only a few seconds.[60] However, the two surfaces might not be sufficient to conclude that this is what occurs when bacteria encounter all surfaces. In addition, most of the surfaces used are biofilm-promoting, which makes it more difficult to exclude the possibility that other surfaces e.g. biofilm resistant surfaces might differentially affect intracellular pathways involved in surface sensing.

5.1.1 Aims

The aim of this chapter was to investigate the intracellular pathway(s) used by *P. aeruginosa* to respond to pEGdPEA coated surfaces that prevent *P. aeruginosa* transitioning from reversible to irreversible attachment. In particular the primary objective was to explore whether SadB affects biofilm formation, bacterial attachment strength, daughter cell fate and c-di-GMP production on the

biofilm-resistant polymer pEGdPEA. The *sadB* gene is required for cells to become irreversibly attached to surfaces *via* a mechanism that is not fully understood. Since *P. aeruginosa* does not form biofilms on pEGdPEA and fails to adhere strongly, it can be hypothesised that *P. aeruginosa* is unable to irreversibly attach to pEGdPEA. Since *sadB* appears essential for the reversible to irreversible attachment switch, it is possible that *P. aeruginosa* is unable either (a) to express *sadB* on pEGdPEA or (b) that a substrate required to activate SadB is not produced when *P. aeruginosa* is exposed to pEGdPEA. Consequently, we investigated the impact of *sadB* overexpression from a non-native promoter by expressing a plasmid-borne copy of the gene in the *P. aeruginosa* wild-type strain. In addition, given the contribution of the *mot* stators to biofilm formation, the impact of *sadB* on biofilm formation in the *mot* mutants was determined.

5.2 Experimental

5.2.1 Polymer Preparation

Materials were prepared according to section 3.2.1.

5.2.2 Bacteria Growth Conditions and Biofilm Assay

P. aeruginosa wild-type and isogenic mutants were grown according to section 3.2.3. Where specified *P. aeruginosa* strains were transformed with a plasmid-borne copy of *sadB (*pME6032::*sadB*). Biofilm assays were conducted as described in section 3.2.3.

5.2.3 Environmental Scanning Electron Microscopy (ESEM)

ESEM micrographs were obtained as described in section 3.2.5.

5.2.4 c-di-GMP Production

Intracellular levels of c-di-GMP were quantified indirectly using a *P. aeruginosa cdrA*::*gfp* bioreporter transformed into wild-type, *sadB* and motility mutants. Fluorescent level for each bacterium was obtained from images acquired using

widefield epifluorescence microscopy (40×,1.3) every 30 s for 3 h and then processed using ImageJ (NIH). The surface bacterial coverage for the different bacterial mutants varied. For this reason, time-lapse frames in DIC and widefield mode were processed using ImageJ to quantify the fraction of cells expressing *cdrA* obtained by the ratio between the number of cells at the surface (from DIC images) and the number of *cdrA* expressing cells (from widefield epifluorescence images). The latter was measured considering cells with higher *gfp* values than an intensity threshold which was set to the 10th percentile of the histogram intensity of *P. aeruginosa* PAO1-W *cdrA*::*gfp* on pNGPDA.

5.2.5 Microfluidic Bacterial Detachment Assay

The adhesion strength of *P. aeruginosa* and the corresponding isogenic mutants on surfaces was assessed using the microfluidic assay based upon the method described in chapter 4.

5.2.6 Microscopy

Experiments were conducted using a custom designed one well holder placed in the microscope under static conditions (Figure 2.12) and as described in section 3.2.4. See chapter 2 for all details of the microscope used.

5.3 Results

5.3.1 Overexpression of *sadB* Enables *P. aeruginosa* to Form Biofilms on pEGdPEA

To understand the contribution of *sadB* to biofilm formation, biofilm assays were performed on the *P. aeruginosa* wild-type overexpressing *sadB* (PAO1-W pME6032::*sadB*) and compared with the wild-type transformed with the empty plasmid vector as well as with a Δ*sadB* mutant with and without a plasmid-borne copy of *sadB*. Figure 5.2 shows representative CLSM images of the strains grown on pNGPDA (top) or pEGdPEA (bottom). The biomass of *P. aeruginosa* pME6032 decreased from 9.8 ± 1.2 $\mu m^3\ \mu m^{-2}$ on pNPGDA to 0.9 ± 0.3 $\mu m^3\ \mu m^{-2}$ on pEGdPEA (Figure 5.3). Although biofilm biomass on pNGPDA was for

PAO1-W pME6032 was lower than that previously quantified for PAO1-W (chapter 4; 23.8 ± 2.8 μm^3 μm^{-2}) a clear difference between the biofilm biomass on the two polymers was observed (p<0.0001). The Δ*sadB* mutant was unable to produce biofilm formation on either surface (Figure 5.2 and Figure 5.3). Conversely, when *P. aeruginosa* overexpressed *sadB*, biofilm formed on pEGdPEA as well as on pNGPDA (Figure 5.2 and Figure 5.3). In fact biofilm biomass on pEGdPEA was 14.5 ± 0.7 μm^3 μm^{-2} for PAO1-W pME6032::*sadB*. When an empty vector with PAO1-W and PAO1 Δ*sadB* was used biofilm formation remained unchanged, confirming that the results were mediated only *via sadB* and not by the plasmid vector itself. In addition, at the presence of pME6032::*sadB*, Δ*sadB* restored its ability to form biofilm on both surfaces confirming the importance of SadB in biofilm formation.

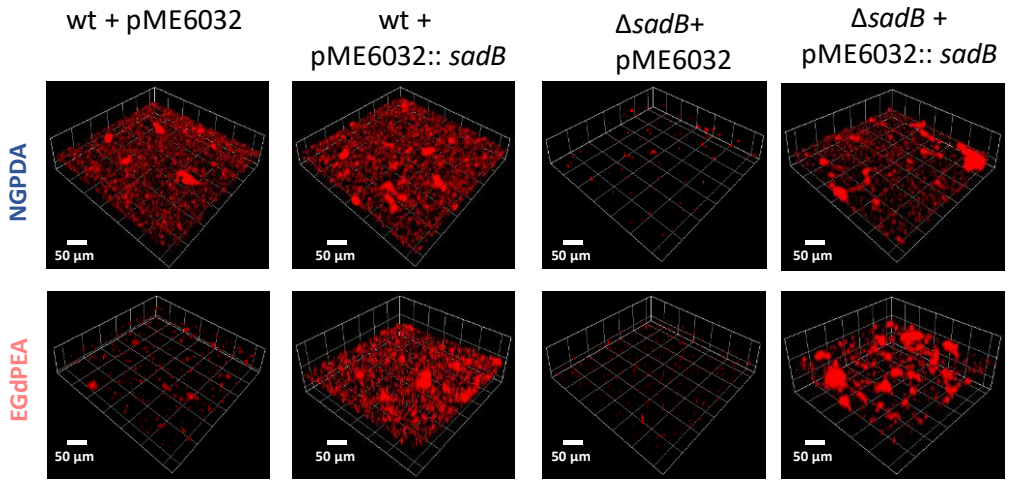

Figure 5.2 Confocal images (10×, 0.3) of *m-cherry* tagged *P. aeruginosa* PAO1-W pME6032 (empty vector), PAO1-W pME6032::*sadB*, Δ*sadB* pME6032 (empty vector) and Δ*sadB* pME6032::*sadB* after 24 h on pNGPDA (top) and pEGdPEA (bottom). Samples were washed 2× in PBS and 1× in H_2O. Scale bar is 50 µm**.** Data provided by Dr Jean Dubern.

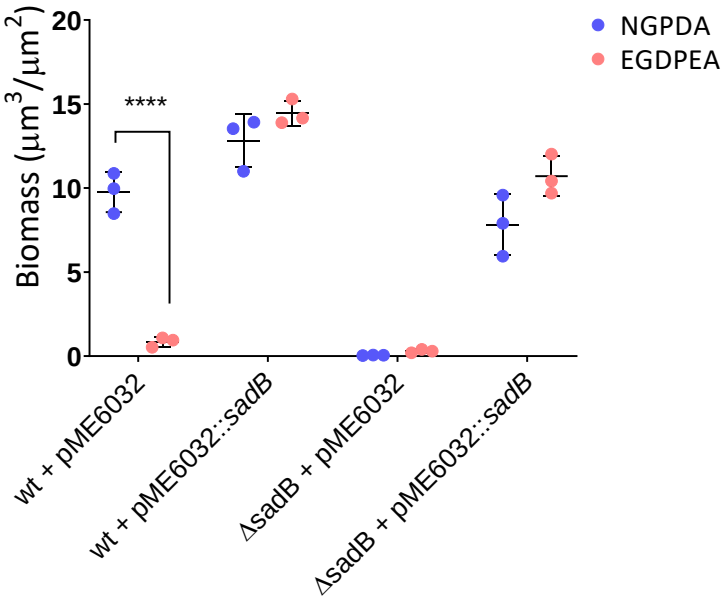

Figure 5.3 Quantification of bacterial biomass for surfaces of *P. aeruginosa* m-cherry tagged PAO1-W pME6032 (empty vector), PAO1-W pME6032::*sadB*::, Δ*sadB* pME6032 (empty vector) and Δ*sadB* pME6032::*sadB*: after 24 h on pNGPDA (top) and pEGdPEA (bottom). Error bars show ± 1 standard deviation (N=3). ****p<0.0001. Significance was determined by Two-way Anova analysis using Sidak's multiple comparison for differences between the indicated samples**.**

Biofilm formation and EPS production was also observed for these strains on three other weakly amphiphilic polyacrylates previously shown to prevent bacterial biofilm formation (Figure 3.7).[8, 388] Figure 5.4 shows ESEM representative images of PAO1-W and PAO1 pME6032*::sadB* grown for 24 h on BnMA,[8] iBMA,[388] TMCHMA.[388] The *sadB* overexpressing strain was able to colonise more and to form biofilms on all of the hit polymers as shown in the ESEM images by the formation of a biofilm matrix and in CLSM images of biofilms in Figure 5.5.

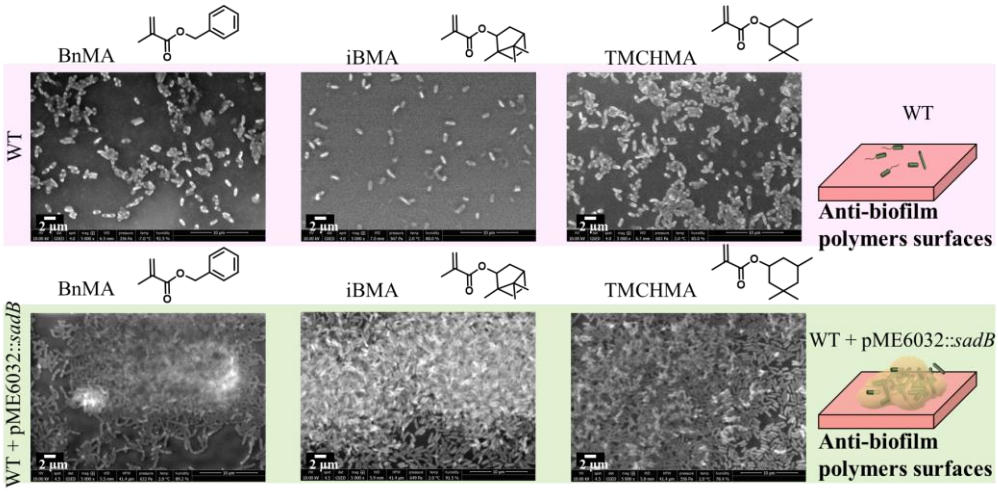

Figure 5.4 The impact of *sadB* overexpression on biofilm formation on resistant polymers BnMA, iBMA and TMCHMA respectively. ESEM representative images of PAO1-W pME6032 (empty vector) and PAO1-W pME6032::*sadB*, grown for 24 h on the 3 polymers. Images captured at 5,000× magnification. Overexpression of *sadB* results in the production of biofilm matrix on biofilm resistant surfaces (lower panel) whereas no matrix could be observed when grown on anti-biofilm surfaces as shown in the upper panel. Scale bars are 2 µm.

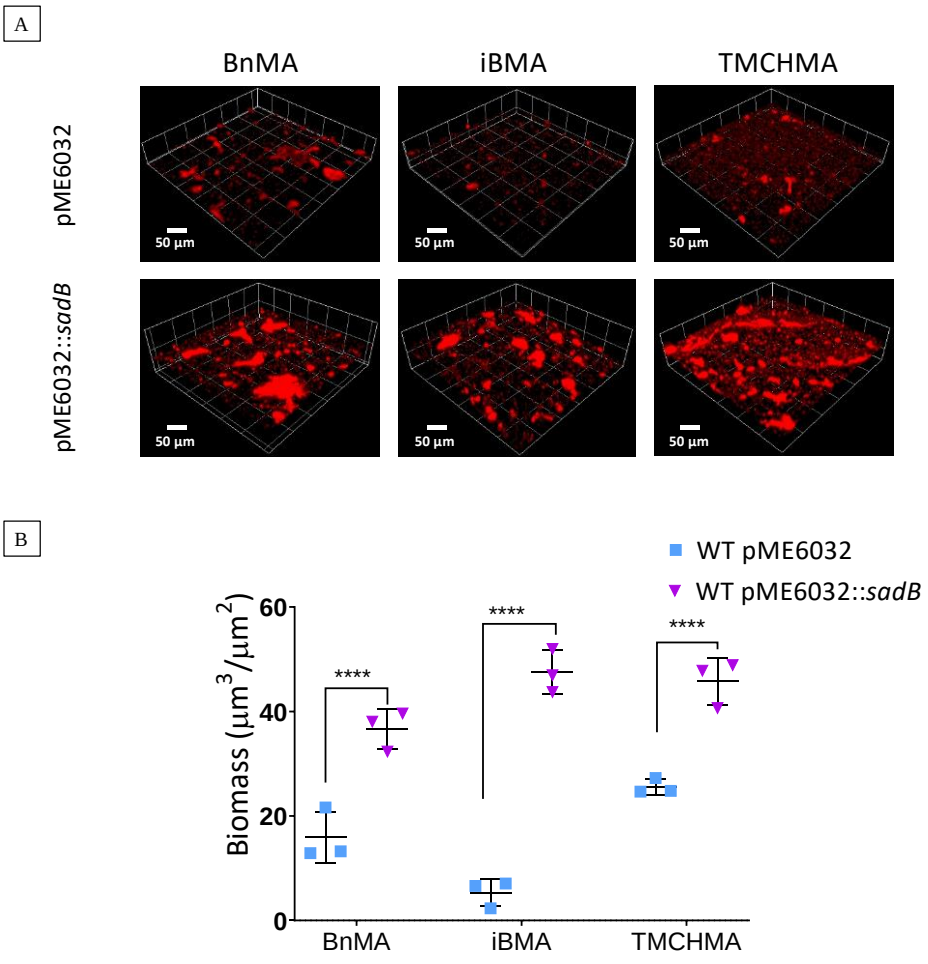

Figure 5.5 Confocal images (10×, 0.3) **(A)** and quantification **(B)** of *m-cherry* tagged *P. aeruginosa* PAO1-W pME6032 (empty vector- blue square) (top), PAO1-W

pME6032::*sadB* (bottom- violet triangle), after 24 h on BnMA, iBMA and TMCHMA. Samples were washed 2× in PBS and 1× in H_2O. Scale bar is 50 µm**.** Data provided by Dr Jean Dubern.

5.3.2 Can *sadB* Restore Biofilm Formation by *motAB* and *motCD* Mutants?

Having previously observed a role for the flagella stators in sensing the different surface chemistries (section 4.3.3), experiments to determine whether *sadB* was epistatic to the *mot* stators were undertaken. Representative CLSM images and quantification of biofilm biomass are shown in Figure 5.6 and Figure 5.7. The presence of the plasmid pME6032 determined a 4× lower biofilm coverage in all the strains than what observed without the plasmid (Figure 4.11). The *mot* mutant with the empty vector pME6032 showed the lowest biofilm biomass. Δ*motAB* pME6032 presented 1.1 ± 0.6 μm^3 μm^{-2} and 0.5 ± 0.3 μm^3 μm^{-2} biomasses on pNGPDA and pEGdPEA respectively. As described in Figure 4.11, a higher biofilm biomass was observed with Δ*motCD* pME6032 which presented 2.5 ± 0.3 μm^3 μm^{-2} and 3.6 ± 0.7 μm^3 μm^{-2} on pNGPDA and pEGdPEA respectively. Overexpression of *sadB* partially restored biofilm formation on pNGPDA for the *motCD* mutant but not for the *motAB* mutant and no biofilm formation was observed for either mutant on pEGdPEA. This result suggests that SadB is upstream of MotAB in the signalling pathway leading to biofilm formation.

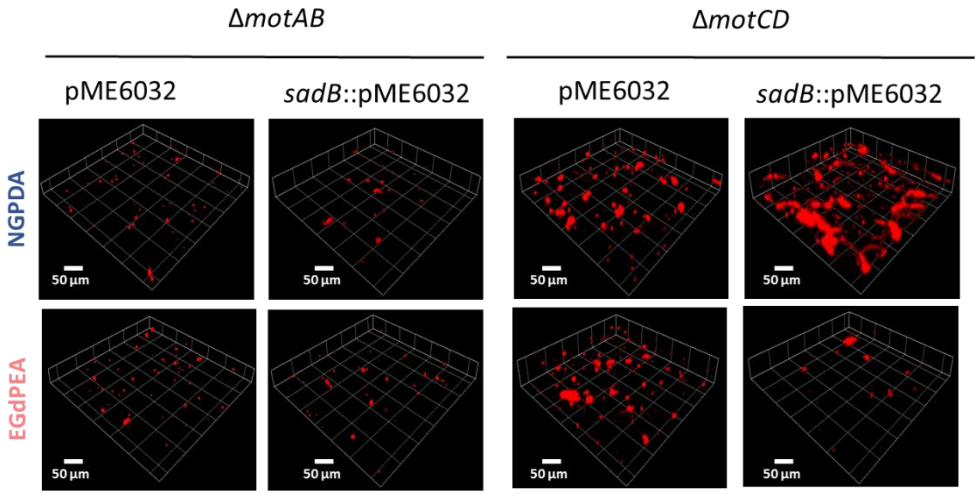

Figure 5.6 Comparison of *P. aeruginosa* biofilm formation on polymer surfaces by using *mot* mutants overexpressing or not *sadB.* Confocal images (10×, 0.3) of m-cherry

tagged *P. aeruginosa* PAO1 Δ*motAB* and Δ*motCD* transformed with pME6032 (empty vector) or pME6032::*sadB* after 24 h on pNGPDA (top) and pEGdPEA (bottom). Samples were washed 2× in PBS and 1× in H_2O. Scale bar is 50 µm.

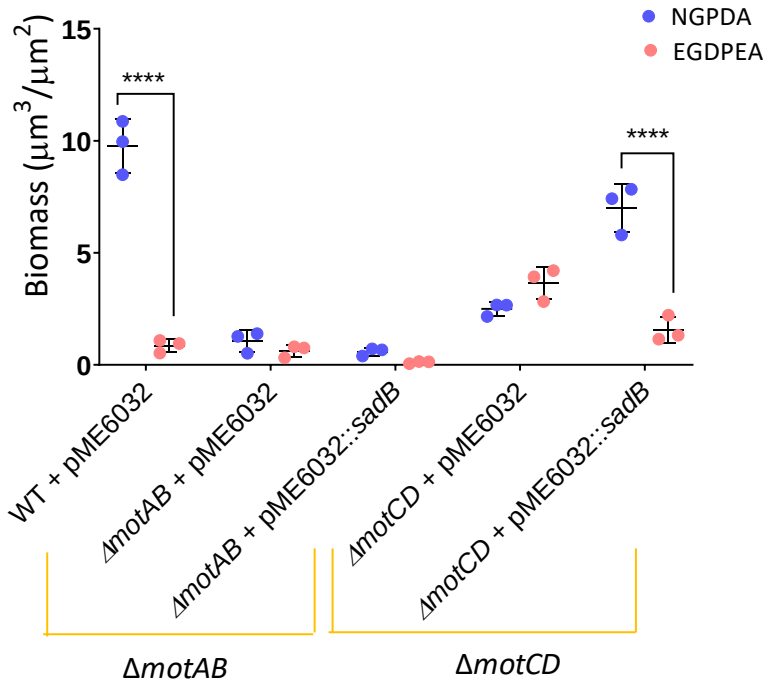

Figure 5.7 Quantification of bacterial biomass for surfaces of *m-cherry* tagged *P. aeruginosa* PAO1-W Δ*motAB* and Δ*motCD* pME6032 (empty vector) or pME6032:: *sadB* after 24 h on pNGPDA (top) and pEGdPEA (bottom). Samples were washed 2× in PBS and 1× in H_2O. Error bars show ± 1 standard deviation (N=3). Significance was determined by Two-way Anova analysis using Sidak's multiple comparison for differences between the indicated samples. ****p<0.0001.

5.3.3 The *sadB* Gene and Daughter Cell Fate

To begin to understand how *sadB* overexpression restores biofilm formation on pEGdPEA, the fate of daughter cells post cell division was investigated. Cells were classified as d = 0 if the two daughter cells remained on the surface, d = 1 if only one detached or d = 2 if both left the surface.[292] Figure 5.8 presents the relative proportions of cells for each bacterial strain belonging to d = 0, 1 or 2 on either pNGPDA or pEGdPEA. As already described in chapter 3 and Figure 3.14, it was observed that the proportion of PAO1-W wild-type cells belonging to d = 0 was significantly higher on pNGPDA (83 ± 1%) compared with pEGdPEA (53 ± 10%), whereas d = 1 was significantly higher on pEGdPEA (44 ± 7%) than on pNGPDA (17 ± 1%) (p<0.001). It was also discovered that the increased surface departure of the *mot* stator mutants (Figure 3.15) suggests that

these cells have lost their ability to remain at the surface and so may be unable to sense the surface,[60] and therefore less likely to engage in behaviour that would lead to biofilm formation.

Wild-type cells overexpressing *sadB* were more likely to stay on both pNGPDA and pEGdPEA surfaces (as shown in Figure 5.8, 94 ± 1% and 93 ± 3% cells respectively were d = 0) after cell division than the wild-type and no cells belonged to d = 2. In the Δ*sadB* mutant, both cells were much more likely to leave the surface (94% were d = 2 on both pNGPDA and pEGdPEA) when compared with the WT. These data suggest that *sadB* is essential for ensuring that cells stay on the surface.[380]

When *sadB* is overexpressed in the *mot* mutants and the daughter cell fate is quantified, an increase of d = 1 cells in the Δ*motAB* pME6032*::sadB* mutant was observed ($p<0.0001$) i.e. more cells remained on the surface when compared with the Δ*motAB* mutant. However, overexpression of *sadB* does not restore the behaviour of the *motAB* mutant to wild-type. These data provide further evidence that SadB functions upstream of MotAB.

Overexpression of *sadB* in the *motCD* mutant however had little impact on the number of cells, leaving or remaining at the surface compared, which were very similar to the *motCD* mutant. This is in contrast with biofilm data where overexpression of *sadB* in the Δ*motCD* mutant increased biofilm biomass on pNGPDA but not on pEGdPEA. This might be explained by the fact that SadB might improve Δ*motCD* attachment at later stages (t > 2 h of exposure to surfaces).

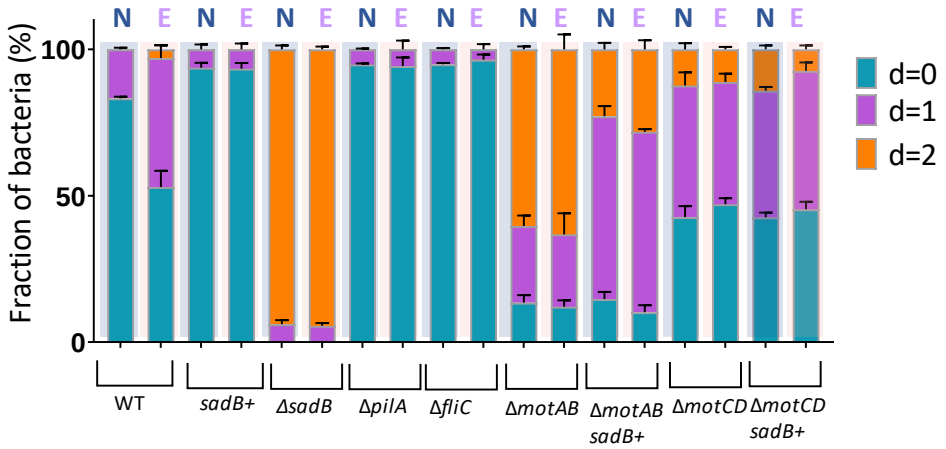

Figure 5.8 Bar graph shows proportion of population for each bacterial strain in different branching division considering pNGPDA (blue) and pEGdPEA (pink). Values obtained considering n>100 doubling events for each of 3 independent replicates (N=3) between t = 1 h to t = 2 h after inoculation. Tukey's multiple comparison test for the different strains on pNGPDA and pEGdPEA considering the three branching divisions is reported in **Appendix 6.**

5.3.4 SadB and Adhesion Strength

The impact of *sadB* on adhesion strength was assessed using microfluidics (Figure 5.9A-B) during the early stages of exposure to the polymers. The shear force required to detach the wild-type overexpressing *sadB* cells from pEGdPEA was τ_{50} = 31.3 ± 16.0 Pa, which was significantly higher than the wild-type (**p<0.01) but still much reduced in comparison with that of the wild-type on pNGPDA (87.5 ± 21.6 Pa). The Δ*sadB* mutant exerted the weakest attachment (0.5 ± 0.1 Pa) (Figure 5.9D).

Since a slight increase in the number of surface-associated cells was observed in *motAB* pME6032::*sadB* in comparison with the *motAB* mutant (on both surfaces), the adhesion strength for these mutants was also assessed.

However, as shown in Figure 5.9C-D no statistical differences between the PAO1-W wild-type and overexpression of *sadB* in Δ*motAB* mutant were observed.

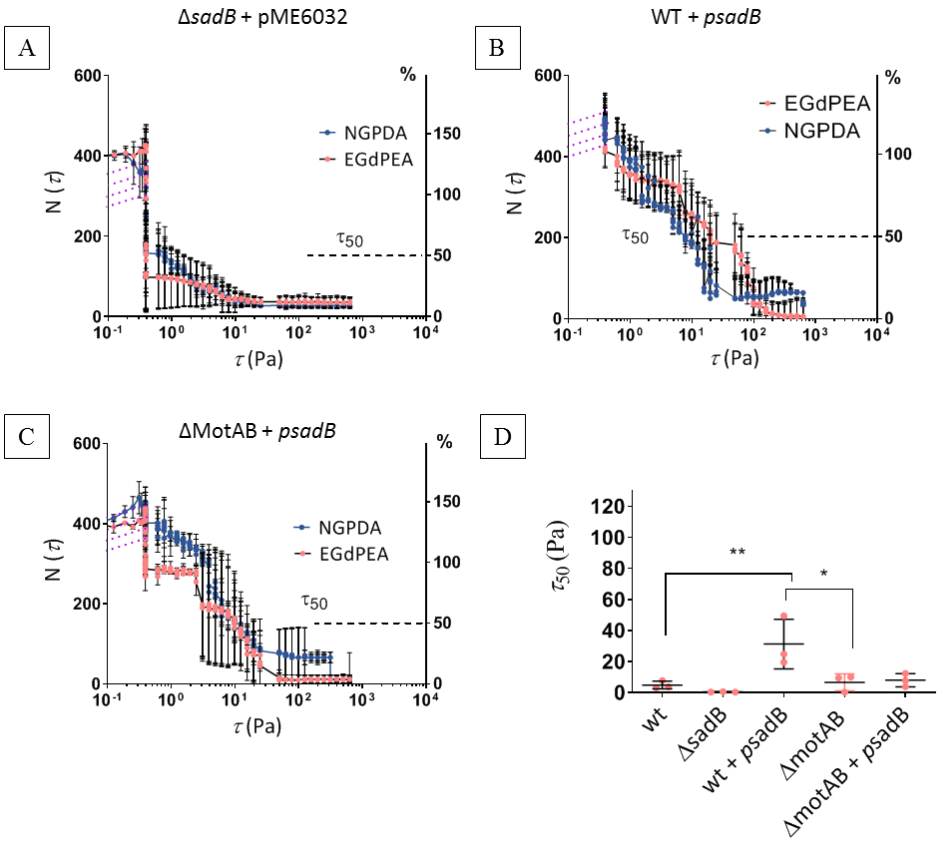

Figure 5.9 Number of *P. aeruginosa* Δ*sadB* **(A)**, *pME6032::sadB* **(B)**, Δ*motAB pME6032::sadB* **(C)** cells on pEGdPEA (pink) and pNGPDA (blue) surfaces with increasing shear stress applied through an increase in flow rate. **D)** Shear stress τ_{50} necessary to detach 50% of PAO1-W wild-type, PAO1-W pME6032::*sadB*, Δ*sadB* pME6032 (empty vector) cells on pEGdPEA. Error bars represent ± 1 standard deviation unit (N=3). Significance was determined by Anova analysis using Tuckey's multiple comparison for differences between samples.

5.3.5 Impact of *sadB* on c-di-GMP Levels

To determine the impact of SadB on c-di-GMP production, we used time-lapse epifluorescence microscopy of *P. aeruginosa* containing the plasmid *pcdrA*::*gfp*. As already described the *cdrA* promoter is a validated reporter for c-di-GMP in *P. aeruginosa*.[389] The focal plane was at the surface and as shown in Figure 5.10 the bacterial population was expressing *cdrA::gfp* heterogeneously.[296]

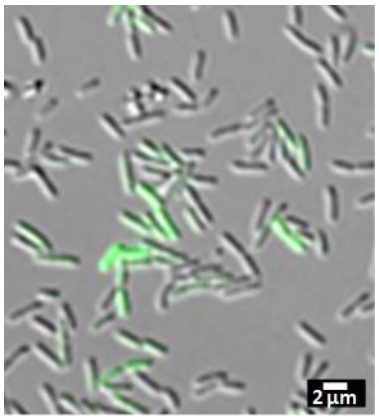

Figure 5.10 Combined DIC and widefield epifluorescence image of *P. aeruginosa* PAO1-W p*cdrA::gfp* after 1 h of exposure to pNGPDA. Scale bar is 2 µm.

Figure 5.11 shows images of the expression of *cdrA*::*gfp* in the wild-type, flagellar (*motAB* and *motCD*) and *sadB* mutants as well as when overexpressed (*sadB*+) in the wild-type and *mot* mutants on pNGPDA (left) and on pEGdPEA (right) obtained from frames captured every h up to 3 h of exposure to either polymer surface. The *gfp* fluorescence output was confirmed to be always intracellular even when in cell aggregates were observed.

The fluorescence output over time for each bacterial strain varied. For this reason, time-lapse frames in DIC and widefield mode were processed using ImageJ to quantify the fraction of cells expressing *cdrA* obtained by the ratio between the number of cells at the surface (from DIC images) and the number of *cdrA* expressing cells (from widefield epifluorescence images). The latter was measured considering cells with higher *gfp* values than an intensity threshold which was set to the 10th percentile of the histogram intensity of PAO1-W *cdrA*::*gfp* on pNGPDA.

Figure 5.12 presents the fraction of bacteria expressing *cdrA::gfp*. An area of 6,400 μm^2 was considered over 3 biological replicates. The *P. aeruginosa* PAO1-W wild-type p*cdrA::gfp* exhibited a differential response on pNGPDA and pEGdPEA during the first 60 min of exposure (section 3.3.7). Here, more remarkable differences were observed after 3h of exposure. In particular, 63 ± 7.2% cells on pNGPDA were observed to express c-di-GMP. In contrast, a significant reduction of cells expressing *cdrA::gfp* was found on pEGdPEA (41 ± 7.2%) ($p<0.001$). The *mot* mutants showed a lower percentage of cells expressing *cdrA::gfp* at the surfaces. This is in agreement with the report of Baker *et al.* where they found that the loss of stators impacts cellular c-di-GMP

levels.[126] The lowest fluorescence values were observed for the Δ*motABCD mutant* (5.9 ± 3.9% and 7.7 ± 9.5% on pNGPDA and pEGdPEA respectively). These results suggest that the flagellar motor plays an important role once *P. aeruginosa* encounters a surface by translating a mechanical signal into a rapid increase in c-di-GMP, as in the absence of the stators no c-di-GMP increase was observed in single cells on either polymer (Figure 5.11).

Conversely, when *sadB* was overexpressed in the wild-type (*sadB+;* Figure 5.12) similar levels of *cdrA::gfp* expression on pNGPDA to the wild-type was observed (64 ± 7% compared with 63 ± 7%) whereas on pEGdPEA a significant increase (>65%) was observed with 68 ± 8% of cells expressing c-di-GMP in comparison with 41 ± 7% of PAO1-W wild-type ($p<0.001$). SadB is known to be regulated upstream by c-di-GMP.[390] Here it has been shown that, when overexpressed, *sadB* induces higher levels *cdrA::gfp* expression and therefore likely to be reflected by an increase in c-di-GMP production on a surface where biofilm formation is otherwise prevented. It can therefore be hypothesised that either *sadB* expression is inhibited on pEGdPEA or that SadB is not activated on pEGdPEA and so cannot serve as a positive feedback mechanism to enhance c-di-GMP production when cells are surface associated.

The expression of *cdrA::gfp* was also investigated in the *mot* mutants and in *mot* mutants transformed with pME6032::*sadB.* No statistical differences were found between Δ*motAB* and Δ*motAB sadB+*, and between Δ*motABCD* and Δ*motABCD sadB+*. In accordance with the biofilm assay (Figure 5.7), an increase in the percentage of c-di-GMP expressing cells was found in Δ*motCD sadB+* with a change from 19.0 ± 6% to 47 ± 7% on pNGPDA ($p<0.01$) and from 18 ± 2% to 43 ± 5% on pEGdPEA ($p<0.05$).

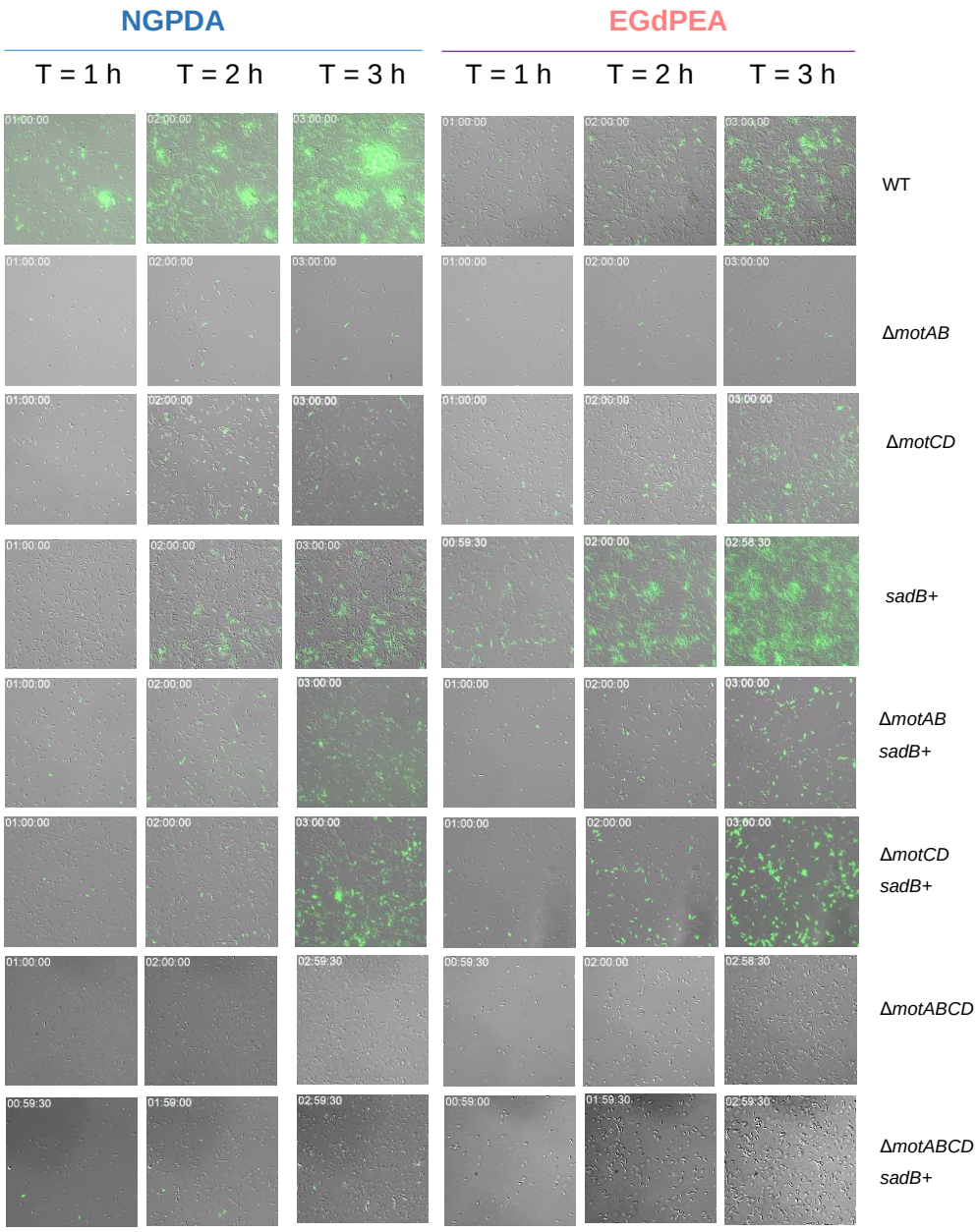

Figure 5.11 Representative epifluorescence microscopy time series images of *P. aeruginosa* PAO1-W wild-type, *sadB* and *mot* mutants transformed with *cdrA*::*gfp* with or without pME6032::*sadB* over the first 3 h of incubation. Image size is 150 x 150 µm.

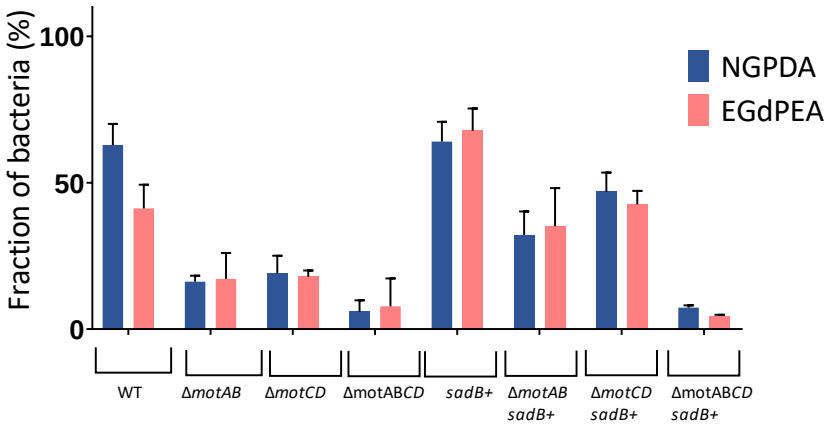

Figure 5.12 Fraction of *P. aeruginosa* wild-type, stator and *sadB* mutant/overproducing cells expressing *cdrA::gfp* 3 h after inoculation. Images were processed using ImageJ (NIH). A threshold was used to identified bacteria which were expressing c-di-GMP (section 5.2.4). Data are obtained from DIC and epifluorescence microscopy images of bacteria grown on pNGPDA (blue) and pEGdPEA (pink) respectively. Two-way ANOVA with Sidak's multiple comparison has been used to find statistical differences (**Appendix 9**).

5.4 Discussion

Regulation of extracellular matrix and biofilm formation *via* the second messenger molecule c-di-GMP is well documented.[391, 392] In Figure 5.11 using time lapse microscopy c-di-GMP production was observed to be much more strongly stimulated in *P. aeruginosa* wild-type cells exposed to pNGPDA than on pEGdPEA. When considered alongside the reduced surface adhesion described in 4.3.1, this indicates that the transition from a reversible to irreversible attachment does not occur on pEGdPEA and so *P. aeruginosa* cannot switch to a biofilm state. Here a possible intracellular pathway that might be involved in this response has now been identified. The switch from a motile to a sessile mode, due to a likely functional inactivity of flagella and T4P is the first step towards an irreversible attachment which is further mediated by EPS molecules. Since swimming motility and twitching motility were observed at the presence of both surfaces (section 3.3.4 and 3.3.6), the secretion of biofilm matrix is likely to be involved in the response that *Pseudomonas* showed at the presence of pNGPDA and pEGdPEA.

The *sadB* gene is required for cells to become irreversibly attached *via* an unknown mechanism.[380] Here, it has been found that *sadB* mutants failed to form biofilms on either pNGPDA or pEGdPEA, whereas the overexpression of *sadB* in the *sadB* mutant restored biofilm formation on pNGPDA and enabled biofilms to form the biofilm resistant polymer pEGdPEA. Similar results were observed on several other biofilm resistance polymers which were previously identified.[7, 8, 388] Daughter cell fate after division was also studied and SadB, when overexpressed, was observed to direct bacteria to remain at the polymer surface (Figure 5.8). A possible explanation of this phenotype, as shown by attachment strength data (section 5.3.4), might be that cells overexpressing *sadB* are unable to detach because of the presence of EPS.[381] Muriel *et al.* recently described an intracellular regulatory cascade which involves SadB and the down-regulation of flagellar genes in *P. fluorescens*.[377] Our microfluidics data also suggests that the overexpression of *sadB* increases the adhesion strength of the wild-type to pEGdPEA. Overexpression of *sadB* in the *motAB* mutant failed to restore biofilm formation on either surface (Figure 5.3). Therefore, SadB must be operating upstream of *motAB* in the signalling pathway. This is in agreement with Laventie *et al.* who recently reported that MotAB but not MotCD is required for surface sensing.[60] Moreover, the inability of the *motCD* mutant (which still has *motAB*) to form a biofilm despite the overexpression of *sadB* implicates *motAB* within the signalling pathway activated upon the interaction of *P. aeruginosa* with pEGdPEA. The recruitment of MotAB and MotCD to the flagellar motor differs in a load-dependent manner.[88] The results presented in this thesis may be explained by different mechanical loads on bacterial flagella experienced by bacteria at the polymer surfaces. Muriel *et al.* showed through epistasis analysis that the diguanylate cyclase AdrA acts upstream of SadB, linking SadB with environmental signalling in *P. fluorescens*. To date no studies published suggested that *P. aeruginosa* responds to flagellar stalling like in *C. crescentus*, but some earlier papers have linked changes in the frequency of flagellar reversals with defects in biofilm formation.[58]

Our results indicate that *sadB* might serve as a positive feedback mechanism to increase c-di-GMP levels and to drive irreversible attachment and therefore

biofilm mode on pEGdPEA. Muriel *et al.* reported the AdrA-SadB pathway incorporated a positive feedback system (Figure 5.1) by which bacteria increase c-di-GMP levels in *P. fluorescens*.[377] SadB contains two domains that might be implicated in c-di-GMP binding: a HDOD domain and an Ybak like domain. The former resembles the HD-GYP domain but lacks its characteristic phosphodiesterase activity, and the latter has an unknown function and resembles the active sites of deacylases.[393] Other examples of proteins with HDOD domains have been reported to be involved in attachment in other bacterial species.[394] Merritt *et al.* and Navazo *et al.* hypothesised that this domain might be a binding site for c-di-GMP.[382, 395]

5.5 Conclusions

The observed prevention of biofilm formation on a class of acrylate polymers recently discovered was characterised by the downregulation of the expression of *cdrA::gfp* that in turn reflects a reduction in the production of c-di-GMP, a key regulator of biofilm formation in *P. aeruginosa* and other microbes. Concomitantly, cells that reversibly attached formed weaker surface interactions and showed more motile offspring that leave the surface.

Overexpression of SadB enabled more surface-committed *P. aeruginosa* progeny, stronger surface adhesion and biofilm formation on biofilm-resistant polymers *in vitro.* These data suggest that the SadB signalling pathway is not activated on biofilm resistant polymers such as pEGdPEA. Having previously described the importance of flagellar stators in surface adhesion (chapter 4 and 5), using the *sadB* overexpression vector in *mot* mutants revealed how SadB requires the presence of both stators to form biofilm. The absence of c-di-GMP producing cells in the Δ*motABCD sadB+* strain confirms the importance of the stators in the surface sensing mechanism since c-di-GMP is a key regulator in the transition from planktonic growth to biofilm formation.

Here it has also been observed that SadB increases c-di-GMP levels in the *P. aeruginosa* wild-type on the surface of pEGdPEA and in *motCD* mutants in the presence of either polymer surface. This indicates that MotAB and SadB, if

expressed, can regulate through a positive feedback involving intracellular c-di-GMP levels as proposed in Figure 5.1 for *P. fluorescens*.

Chapter 6

Investigating the Effect of Chemically Distinct Polymer Surfaces on P. aeruginosa Aggregation

6.1 Introduction

Single-cell bacterial responses to different surfaces have been described in the previous chapters. However, bacteria are known to exhibit community behaviours such as swarming, biofilm formation and cell aggregation. Surface aggregate formation in *P. aeruginosa* has been investigated over the last few decades, and the role of aggregates in biofilm formation has been established.[177-179] A new model of biofilm formation has been proposed by Kragh *et al.* to illustrate the tendency of planktonic bacteria to cluster as multicellular aggregates during the process of biofilm formation. [179] It has also been suggested that planktonic cellular aggregation is mediated by the same mechanisms as those involved in the formation of surface-attached biofilms.[178] Therefore, planktonic aggregates are an integral component of biofilm formation and an important consideration when addressing questions about the mechanisms which underpin the formation, maturation and dispersal of surface-associated biofilms.[178] Aggregation is a community-level behaviour and in this regard, as shown in section 1.5.5, QS plays a crucial role.[396] In fact, a recent study has shown that exogenous 2-heptyl-3-hydroxy-4-quinolone (also known as the *Pseudomonas* Quinolone Signal, C7-PQS) induces aggregation of *P. aeruginosa* cells in suspension.[397] The production of the siderophore pyoverdine, responsible for obtaining extracellular iron (a nutrient essential for biofilm formation in pseudomonads), occurs before biofilm formation, and is likely induced by the aggregation of the cells due to PQS, itself an iron chelator.[398] *P. aeruginosa* mutants defective in exopolysaccharides, T4P, or flagellar biosynthesis (which are all components of biofilm formation) all failed to properly form these aggregates in the biofilm matrix and also had impaired pyoverdine production.[399] In addition, large aggregates ($> 5 \times 10^{-6}$ mm^3) engage 3-oxo-C12-HSL QS to communicate within and between *P. aeruginosa* aggregates.[400] Addition of this QS signal allowed the

development of bacterial clusters as packed cells.[24] However a full understanding of the nature of these clusters is still required.

As presented in section 5.1, Tuson and Weibel's report listed the materials that have been used to study bacteria-surface interactions over the last few decades.[141] Although these studies focussed on most of the crucial aspects of bacterial colonisation of surfaces such as cell adhesion, biofilm formation, protein adhesion and exopolysaccharide production, none considered the effect mediated by surfaces on planktonic aggregation. The possibility of discovering materials which affect bacterial aggregation offers us the potential of a new tool to investigate the stages in biofilm formation.

6.1.1 Aims

To study the role of *P. aeruginosa* cell aggregation in biofilm formation, bacteria were exposed to pNGPDA and pEGdPEA acrylate polymers, which present different pendant groups and opposing biofilm formation properties.[7, 388] Planktonic aggregate formation was observed using microscopy and laser-diffraction particle-size scanning (LDA) in order to probe the relationship between aggregates and biofilm formation. The different rates of aggregation in the presence of pNGPDA and pEGdPEA were further investigated to identify molecules which might drive the differential community behaviour observed. For this reason, liquid chromatography tandem mass spectrometry (LC-MS/MS) [401] was exploited to explore whether aggregate formation following exposure to different surfaces was QS-dependent.

6.2 Experimental

6.2.1 Polymer Preparation

Materials were prepared according to section 3.2.1. The two polymers (pNGPDA and pEGdPEA) were also used to coat plasma-treated Nunc® polystyrene petri dishes (ø = 35 x 12 mm). Each monomer (200 µL) was deposited into each petri dish, before irradiating for 60 min using UV light

6.2.2 Bacterial Culture

Bacteria cultures were prepared according to section 3.2.3. In addition to *P. aeruginosa* PAO1-W wild-type, other sublines have been used PAO1 Lausanne (PAO1-L) and PAO1 Nottingham (PAO1-N).

6.2.3 Quorum Sensing Signal Molecule (QSSM) Extraction

To extract the QSSMs, 1 mL ethyl acetate (acidified with 0.1% v v^{-1} acetic acid for pronation) was added to 1 mL of the spent culture medium and vortexed at 1,500 rpm for 2 min to increase QSSM solubility in the organic phase and remove salts. The samples were centrifuged at 13,000 rpm for 5 min, 20°C. The organic (upper) layer was removed and the extraction process repeated twice, and the extracts combined. The combined extracts were dried under vacuum using a centrifugal evaporator, prior to being reconstituted in 50 µL methanol for LC-MS/MS analysis.[401]

6.2.4 Analytical Methodologies

Laser diffraction analysis (LDA) was employed to quantify the mean size and size distribution of *P. aeruginosa* aggregates using a Coulter LS230 particle size analyser (Beckman, UK) based on previous work.[178] Particle size distribution was determined as a function of the particle diffraction using the Coulter software (version 2.11a) and plotted as a function of the percentage of distribution volume. Size distributions of bacterial clusters were determined under moderate stirring (default speed 5 setting). The final size distribution for each sample was obtained as an average of 3 runs per sample.

In the cell-free spent media-exchange experiment (section 6.3.4), spent media were centrifuged at 3,000 rpm for 3 min, 20°C. The spent media were filtered through 0.2 µm filter to remove the cells. The resulting cell-free spent media were used to resuspend the centrifuged cells exposed to the opposite polymers. After 1 h of incubation at 37°C, samples were assessed using LDA. Control samples were resuspended in their original spent medium after centrifugation.

Spent media were analysed to ascertain the absence of cells and cell debris through microscopy.

6.2.5 Microscopy

Bacteria were observed with using an inverted brightfield differential interference contrast (DIC) microscope as described in section 3.2.4 with minor variations. Time series of images were collected with a 40×/1.3 and 10×/0.5 objective lens at 1 frame per 1 min. Glass coverslips (uncoated or coated with the two polymers) were mounted in a custom designed 12-well PEEK dish (Appendix 4). Aggregates rates were quantified using ImageJ software (version 1.44) (National Institute of Health, USA) and an automatic threshold was set to ascertain the pixel that contain aggregates (>10 µm).

In order to investigate EPS and eDNA content in aggregates, bacteria were grown in the presence of either polymer in RPMI-1640 at a starting OD_{600} 0.01 with YOYO-1 (0.2 µM) and ConA (50 µg mL^{-1}). After 4 h samples were imaged using a confocal microscope (LSM2, Zeiss) without being washed. EPS and eDNA were visualised at an excitation wavelength of 633 and 488 nm respectively. Images were obtained using 63×/1.4, Plan-Apochromat objective lens, pinhole size of 70 µm, 639 nm laser and filter at 640 nm for EPS and 488 nm laser and filter at 555 for eDNA.

6.2.6 Liquid Chromatography-Tandem Mass Spectrometry (LC-MS/MS)

The QS extracts were further quantified using LC-MS/MS as previously described[401] using a LC-10AD VP system (Shimadzu, Japan) coupled to Applied Biosystems QTRAP 4000 hybrid triple-quadrupole linear ion trap MS (MSD Sciex, Canada) equipped with an electrospray ionisation (ESI) interface or a Agilent 1100 LC system (Agilent Technologies, Germany) coupled to Micromass Quattro Ultima triple-quadrupole MS (Waters, UK).

LC was performed on either a Phenomenex Gemini C18 column (100 x 3 mm, 3 µm particle size) or Phenomenex Gemini C18 column (50 x 3 mm, 3 µm particle size) with appropriate guard column, with a mobile phase consisted of A: 0.1% (v v^{-1}) formic acid in water and B: 0.1% (v v^{-1}) formic acid in methanol. Compounds were separated using a binary gradient, initially at 10% B for 1 min, increased linearly to 50% B over 0.5 min, then to 99% B over 4 min. The composition remained at 99% B for 1.5 min, decreased to 10% B over 0.1 min, and stayed at this composition for 2.9 min. The flow rate was 450 µL min^{-1} and sample injection volume was 5 µL. For the analysis of alkyl quinolones, 2 mM 2-picolinic acid was supplemented to mobile phase A.

Mass spectrometry was performed in the electrospray positive ion mode. For the QTRAP 4000, the instrument was configured to the following parameters: curtain gas: 20, ion source potential: 5,000 V, temperature: 450°C, nebuliser gas: 20, and auxiliary gas: 15. The multiple reaction monitoring (MRM) transitions were based on previously described protocol.[401] Data analyses were performed using commercial vendor software respectively, *i.e.* Analyst (version 1.6.3) and Masslynx (version 4.1).

6.3 Results

6.3.1 Exposure to a pNGPDA Influences *P. aeruginosa* Aggregation

The *P. aeruginosa* PAO1-W wild-type was exposed to biofilm-promoting (pNGPDA) and biofilm-resistant (pEGdPEA) polymers and observed microscopically for 24 h to compare the cell behaviours. Planktonic bacteria aggregated in the bulk medium and settle on surfaces under the influence of gravity by sedimentation or convective-diffusion,[402] where they can be detected using surface microscopy (Figure 6.1).

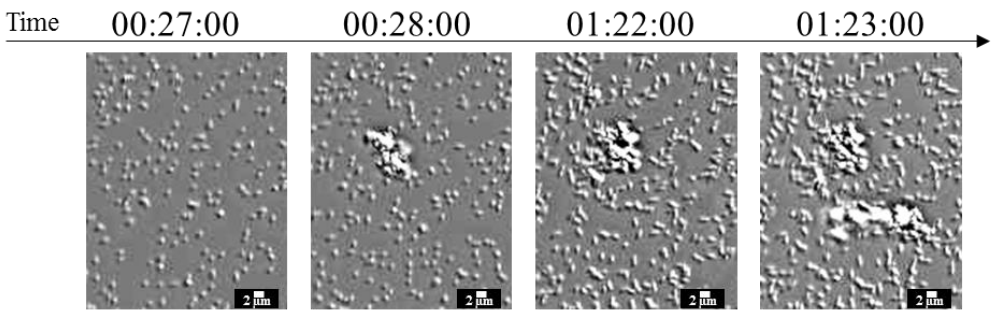

Figure 6.1 Sequence of DIC images (10×, 0.3) after 27, 28, 82, 83 min of *P. aeruginosa* exposure to pNGPDA. The aggregates observed derived from planktonic cells and deposited onto the polymer surface.

The arrival of aggregates at the polymer surfaces was clearly visible for both polymers after the initial inoculation of bacteria, likely due to the presence of aggregates in the overnight culture.[177] Figure 6.1 depicts a sequence of DIC brightfield images of PAO1-W aggregates after settling onto pNGPDA. These aggregates were observed by using microscopy to consist of about 50-100 cells. During the early stages of bacterial colonisation, within the first 3 h after inoculation, planktonic aggregates were observed to be more likely to disperse after landing on pEGdPEA than on pNGPDA. At later time points (after t = 5 h) a higher rate of aggregate arrivals was observed on pNGPDA (28 ± 7 per mm^2) than on pEGdPEA (3 ± 2 per mm^2) from t = 4 h to t = 5 h after inoculation (Figure 6.2) (p<0.01). It has also been observed that the coverage area of planktonic seeded aggregates was higher on pro-biofilm surface pNGPDA than pEGdPEA 33,254 ± 3,216 and 4,751 ± 2,278 μm^2/ mm^2 respectively at t = 24 h (**p<0.01).

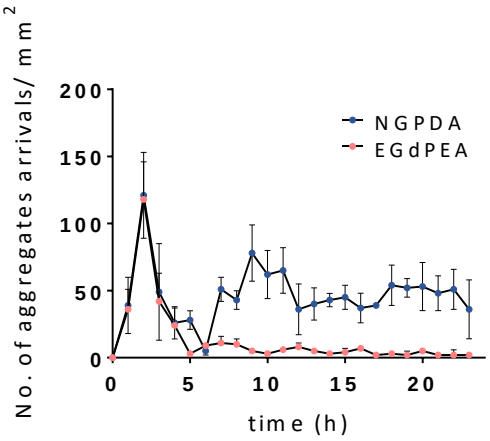

Figure 6.2 Quantification of *P. aeruginosa* aggregate arrival rate using brightfield DIC microscopy (10×, 0.3) on pNGPDA (blue) and pEGdPEA (pink). Aggregates rates were quantified using ImageJ software (version 1.44) (NIH, USA) and an automatic threshold was set to ascertain the pixel that contain aggregates (> 10 μm). Note that the cells were grown under static conditions. Error bars show ± 1 standard deviation (N=3).

To quantify the impact of settled aggregates on surface biomass, the average size of the observed aggregates and the cumulative number of aggregate arrivals over 24 h on pNGPDA was considered. The settled aggregates were found to contribute up to 40% of the surface biomass on pNGPDA assuming none of the settled aggregates left. This observation is consistent with previous studies suggesting that multicellular aggregation is one mechanism used by bacteria to form mature biofilms.[178] Incubation of *P. aeruginosa* PAO1-W with pEGdPEA showed no evidence of planktonic growth inhibition.[7]

The arrival of aggregates originating away from the solid-liquid interface was initially evaluated using microscopy. As an alternative approach, LDA was used to assess *P. aeruginosa* aggregate formation in the bulk phase after 24 h incubation. This approach confirmed the presence of aggregates within the bulk phase of planktonic cultures in contact with pNGPDA. Figure 6.3 shows the size distribution of bacterial aggregates in the presence of pNGPDA, pEGdPEA and pNGPDA-co-EGdPEA. Two major aggregate size fractions were observed. Approximately 20% of the total biomass consisted of particles in the range of 2–

30 µm, which corresponds to multicellular aggregates, whereas particles in the range of 0–2 µm, represent single cells that contribute to the remaining 80% of the total biomass. However, when *P. aeruginosa* was grown in contact with pEGdPEA, the contribution of multicellular aggregates (2–30 µm) to the total biomass reduced to 1% and the biomass predominantly consisted of single cells (99%). An intermediate cell size distribution of planktonic cells and aggregates (up to 10 µm) was observed for the pNGPDA-co-EGdPEA copolymer, with 12% of total biomass consisting of particles of 2-30 µm and 88% of 0–2 µm.

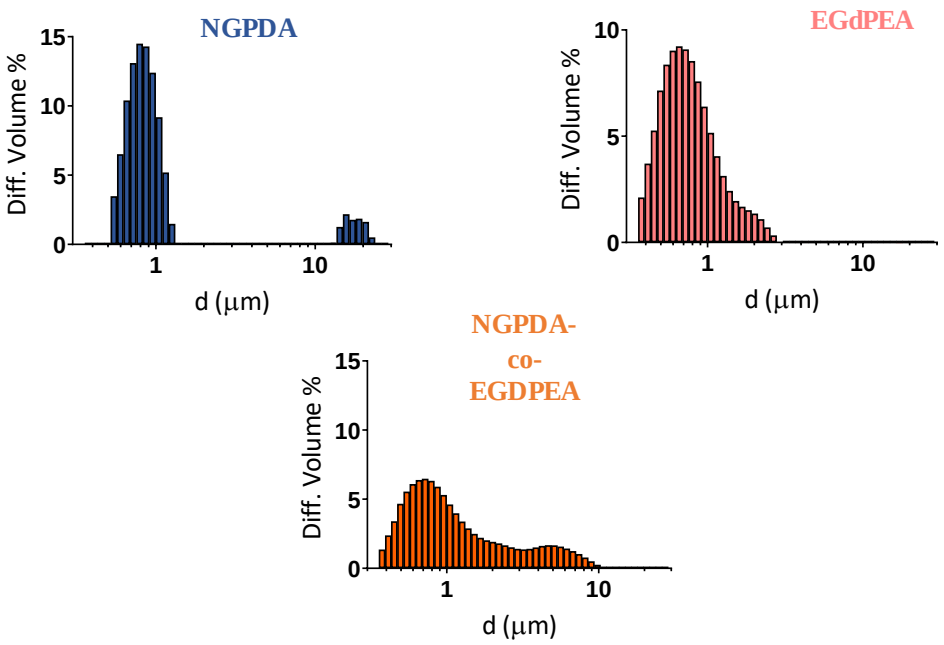

Figure 6.3 LDA characterisation of *P. aeruginosa* cells and aggregates after 24 h incubation and exposure to pNGPDA, pNGPDA-co-EGdPEA or pEGdPEA (N = 3). Aggregates (>10 µm) were observed for cells cultured in contact with pNGPDA (blue), whereas the cells were predominantly in the planktonic state upon contact with pEGdPEA (pink). An intermediate cell size distribution of planktonic cells and aggregates (up to 10 µm) was observed for the pNGPDA-co-EGdPEA copolymer (orange).

6.3.2 *P. aeruginosa* Aggregates are Rich in eDNA and EPS

To understand the extracellular macromolecular composition of aggregates, two different staining were used. YOYO-1 is cell-impermeant and used to stain dsDNA. ConA-Alexa 633 selectively, as described in section 3.2.5, binds to alpha-mannopyranosyl and alpha-glucopyranosyl residues. Both residues are present in *P. aeruginosa* EPS. Bacteria were grown in the presence of either

polymer in a custom designed holder (previously described in Figure 2.12) in RPMI-1640 at a starting OD_{600} 0.01 with YOYO-1 (0.2 µM) and ConA (50 µg mL^{-1}).

CLSM microscopy was used to assess the area above surfaces in order to visualise planktonic aggregates above the polymers after 4 h of exposure.

Figure 6.4 presents 3D images of aggregation in the presence of pNGPDA and pEGdPEA. Aggregates above surface were found to be rich in eDNA (green) and EPS (purple), which are commonly found in biofilms.[403] Conversely above the biofilm-resistant polymer pEGdPEA, few aggregates and less eDNA (<76%) and EPS (<99%) were imaged and quantified by using normalised integrated fluorescent density for each channels after manual selection of aggregates areas (N=3) with ImageJ (NIH). This led us to hypothesise that bacteria above pEGdPEA were unable to switch to EPS production and eDNA release which are both characteristic of surface associated biofilm formation.[404, 405]

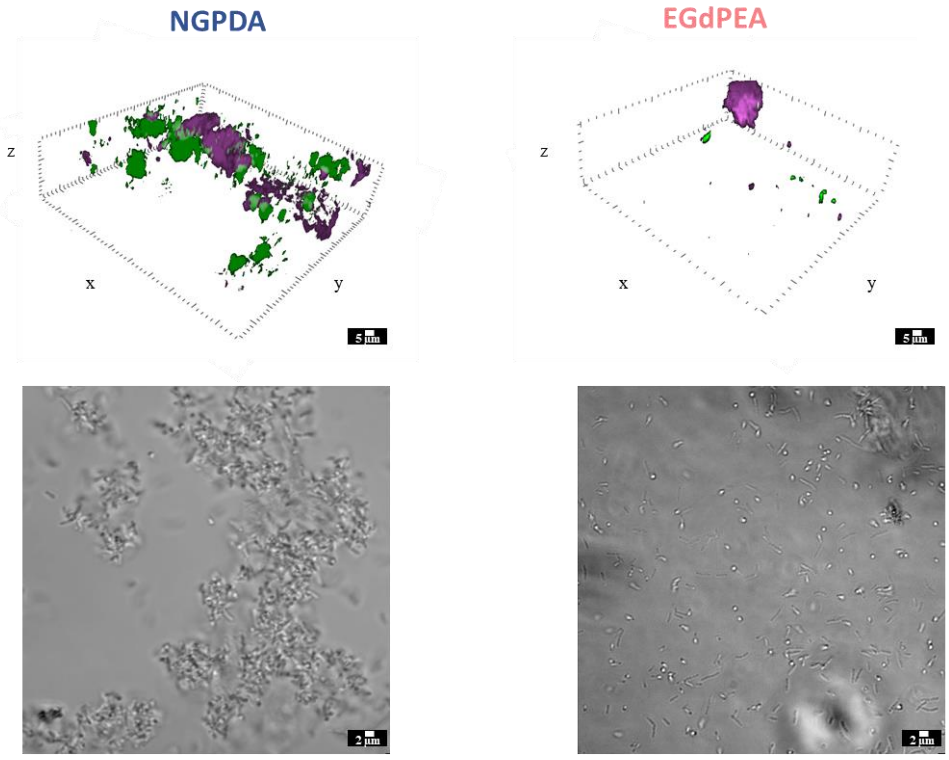

Figure 6.4 Confocal (top) and brightfield (bottom) images (63x, 1.4) of *P. aeruginosa* after 4 h on pNGPDA (left), and pEGdPEA (right). Samples were imaged directly in a custom designed holder with YOYO-1 (0.2 µM) and ConA-Alexa 633 (50 µg mL^{-1}). Yoyo-1 stains eDNA (green) and ConA-Alexa 633 EPS (purple). Image size is 100 x 100 µm.

6.3.3 Aggregate Formation by Different *P. aeruginosa* PAO1 Sublines

To determine whether the differences observed in cell aggregation were apparent in different *P. aeruginosa* PAO1 sub-lines we adopted the time-lapse microscopy experiment to be able to quantify the number and size of aggregates seeding the polymer surfaces. Figure 6.5 shows the results obtained over a 24 h period of exposure to the polymers for the PAO1 Lausanne (PAO1-L) and PAO1 Nottingham (PAO1-N) sublines. PAO1-L showed a significant reduction in aggregate arrival rate when cells were exposed to pEGdPEA (p<0.001) (Figure 6.5). In contrast, PAO1-N was unable to distinguish between the two surfaces aggregated in a similar manner to PAO1-W (Figure 6.2) and PAO1-L on pNGPDA. Comparison of PAO1 genome sequences has revealed that the chromosome of this *P. aeruginosa* strain has diversified into different sub-lines during storage and maintenance in different laboratories.[406] Single nucleotide polymorphisms (SNPs), short insertions and deletions (INDELs) unique to individual PAO1 sublines have been identified. These changes will be helpful in determining the identity of gene(s) that are responsible for the different phenotypes observed on the two polymers.

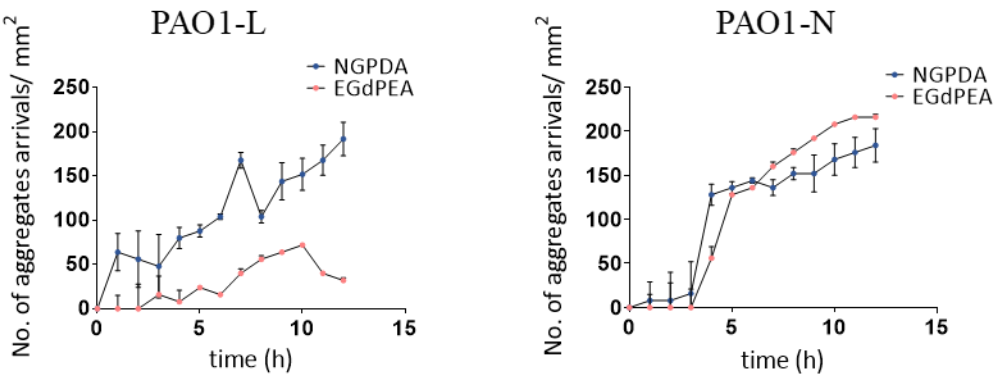

Figure 6.5 Quantification of aggregate arrival rate using brightfield DIC microscopy (10×, 0.3) on pNGPDA (blue) and pEGdPEA (pink) with *P. aeruginosa* PAO1-L (left) and *P. aeruginosa* PAO1-N (right) strains. Error bars show ± 1 standard deviation (N=3).

6.3.4 Does *P. aeruginosa* Produce Aggregation-Inducing Factors on pNGPDA but not on pEGdPEA?

To gain further insights into aggregate formation during the culture of PAO1-W in contact with pNGPDA, a cell-free conditioned medium exchange experiment was devised (Figure 6.6A). Bacteria were incubated for 24 h on polymer-coated petri dishes (pNGPDA or pEGdPEA), after which, the conditioned media were centrifuged and filtered (0.2 µm) to remove the cells. The resulting cell-free conditioned media was then used to resuspend the centrifuged cells exposed to the other polymers, *i.e.* cells on pNGPDA were resuspended in cell-free conditioned medium from pEGdPEA and vice-versa. The cells were then incubated for 1 h at 37°C prior to LDA. The control samples were resuspended in their original conditioned medium.

Aggregate formation was observed for cells incubated with pEGdPEA but exposed to the medium conditioned by pNGPDA exposed cells (Figure 6.6B). Approximately 95% and 5% of the total biomass consisted of 2-100 µm and 0-2 µm size particles respectively, showing a significant (p<0.001) shift in aggregate formation. In contrast, no changes were observed in the particle size distribution for cells grown in contact with pNGPDA and exposed to pEGdPEA conditioned medium. Control experiments were conducted resuspending cells from either pNGPDA or pEGdPEA with their own (filtered) conditioned medium. Approximately 90% of the total biomass consisted of particles in the size range of 2–100 µm, whereas particles in the 0–2 µm size range, contributed 10% for cells from pNGPDA samples. Conversely, 90% of the total biomass corresponded to single cell size (0–2 µm size range), and only 10% to small cells aggregates (2-100 µm) with cells exposed to pEGdPEA. These observations suggest the presence of aggregation-inducing factor(s) in pNGPDA conditioned media.

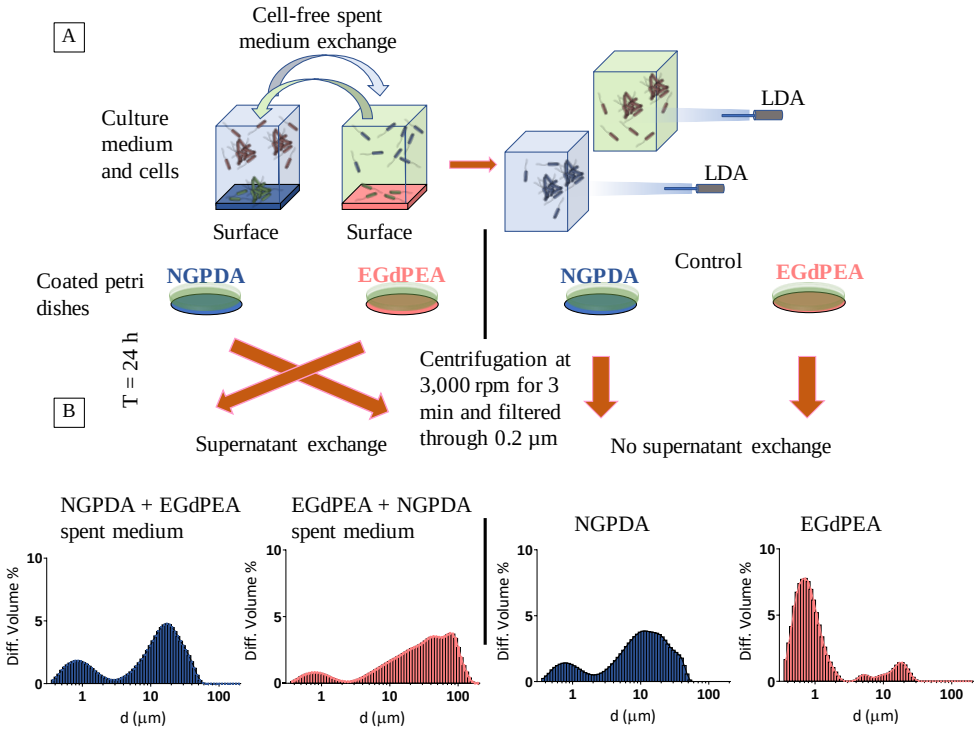

Figure 6.6 A) Schematic diagram illustrating the conditioned media-exchange experiment. PAO1-W wild-type cells were cultured for 24 h in pNGPDA- or pEGdPEA-coated petri dishes. The cultures were centrifuged at 3,000 rpm for 3 min and filtered through 0.2 µm to remove cells. The centrifuged cells were resuspended in the cell-free conditioned media and further incubated for 1 h at 37 °C prior to LDA. Note: no conditioned media exchange was performed for the respective controls, *i.e.* the cells were resuspended in their original spent media. **B)** Particle size characterisation of cells upon 1 h incubation in conditioned media exchange using LDA (N = 3). Upon resuspension in the cell-free conditioned medium from pNGPDA, aggregates were observed for the PAO1-W cells grown in contact with pEGdPEA.

6.3.5 3-oxo-C12-HSL is a Key Factor Promoting Bacterial Planktonic Cell Aggregation

To identify small molecules within the conditioned media that could induce aggregation, cultures were analysed by LC-MS/MS, targeting QS signal molecules since QS plays a role in population density-dependent regulation of virulence factor production [407] and biofilm formation in *P. aeruginosa*.[408, 409]

The concentration of eight different QS molecules was quantified in conditioned media (after 24 h of exposure to pNGPDA and pEGdPEA surfaces in RPMI-1640) originating from either planktonic cultures or biofilms using a previously established LC-MS/MS method.[410] As shown in Figure 6.7, 2-heptyl-4-

quinolone (C7-HHQ) which is a precursor of 2-heptyl-3-hydroxy-4-quinolone (also known as C7-PQS) and 3-oxo-C12-HSL were found to be statistically significantly more abundant (p<0.05 and p<0.0001, respectively) in the spent media of pNGPDA. On the other hand, C7-PQS (p<0.05) was found to be statistically significantly more abundant in the spent media of pEGdPEA.

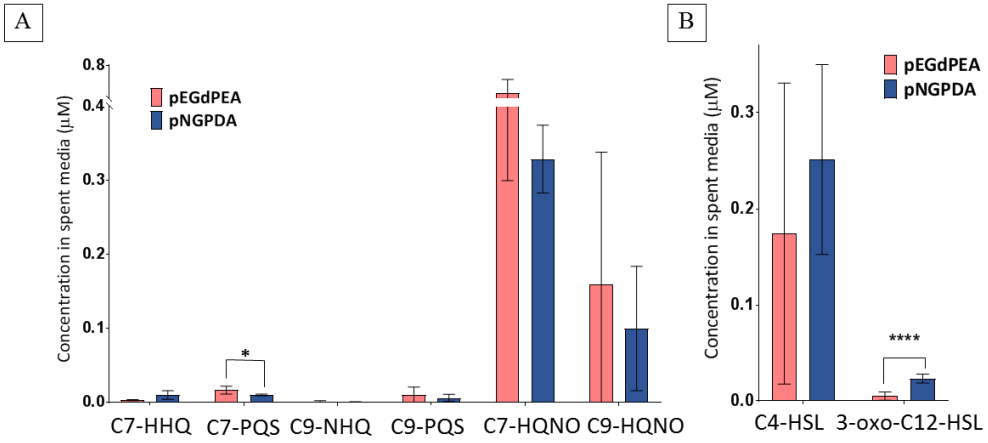

Figure 6.7 Quantitative analysis of 2-alkyl-4-quinolone (AQ) family signalling molecules **(A)** and *N*-acylhomoserine lactones (AHLs) **(B)** in cell-free conditioned medium extracts from cells exposed to pNGPDA or pEGdPEA using LC-MS/MS. Significant differences (One-way ANOVA) are shown as * p < 0.05, ****p < 0.0001. Error bars show ± 1 standard deviation (N = 6).

Some of the detected QSSMs were relatively low (in the nanomolar range) in the conditioned media. For instance, 2-nonyl-4-hydroxyquinoline (NHQ) concentrations of 0.5 ± 0.5 nM and 1.3 ± 1.1 nM were quantified in pNGPDA and pEGdPEA conditioned media, respectively. In contrast, 3-oxo-C12-HSL has a nanomolar EC_{50} to induce LasR-dependent QS.[411] 3-oxo-C12-HSL was however present in concentrations of 23.3 ± 4.7 and 5.1 ± 4.3 nM on pNGPDA and pEGdPEA respectively, 4.6 times higher on the former. This led us to postulate that 3-oxo-C12-HSL may play a role in aggregate formation.

6.3.6 Exogenous 3-oxo-C12-HSL Increases Aggregation and Biofilm Formation on pEGdPEA

To determine whether 3-oxo-C12-HSL is an aggregate-promoting factor it was added at a saturating concentration of 1 µM. This concentration was selected due to previous observations showing an effect on *P. aeruginosa* at 1-5 µM.[412]

Figure 6.8A shows a brightfield DIC microscopy time image series, showing the deposited aggregates on pNGPDA, and on pEGdPEA with and without the addition of 3-oxo-C12-HSL (yellow rings mark the aggregate borders). It has been observed that PAO1-W formed more aggregates on pEGdPEA when exposed to exogenous 3-oxo-C12-HSL than in its absence (Figure 6.8B). The average surface coverage areas of the seeding aggregates over a period of 12 h increased on pEGdPEA samples (>125%) with exogenous 3-oxo-C12-HSL (Figure 6.8C). After 5 h the aggregate arrival rate was 9 ± 3 compared with 2 ± 1 on pEGdPEA with and without 3-oxo-C12-HSL. As controls, the carrier solvent methanol was added instead and although different aggregate rates were detected in the presence of the two polymers, fewer aggregates formed on both surfaces than in the absence of methanol. This might be due to an increase in swimming motility at the presence of the solvent, which has previously been reported.[413] Notably a larger coverage area of aggregates deposited on pNGPDA, in comparison to pEGdPEA with or without 3-oxo-C12-HSL. This means that PAO1 might have different signals pathways to form aggregates in addition to the ones mediated by 3-oxo-C12-HSL which determines more aggregates at the presence of pNGPDA. Considering the coverage area of aggregates depositing on the two different surfaces, the calculated sum of areas of aggregates settling over the first 12 h upon inoculation was compared. The aggregates contributed to a coverage of 13,474 ± 1,148 μm^2 per mm^2 on pNGPDA, whereas on pEGdPEA, the aggregate coverage was 4,284 ± 552.6 (without the addition of 3-oxo-C12-HSL) and 9,915 ± 2,399 μm^2 (with the addition of 3-oxo-C12-HSL) per mm^2 respectively (Figure 6.8C). One-way ANOVA (with post-hoc Tukey test) yielded a *p* value of < 0.01 and 0.05 between pNGPDA and pEGdPEA, and between pEGdPEA with and without 3-oxo-C12-HSL, indicating that the two populations were significantly different (N=3).

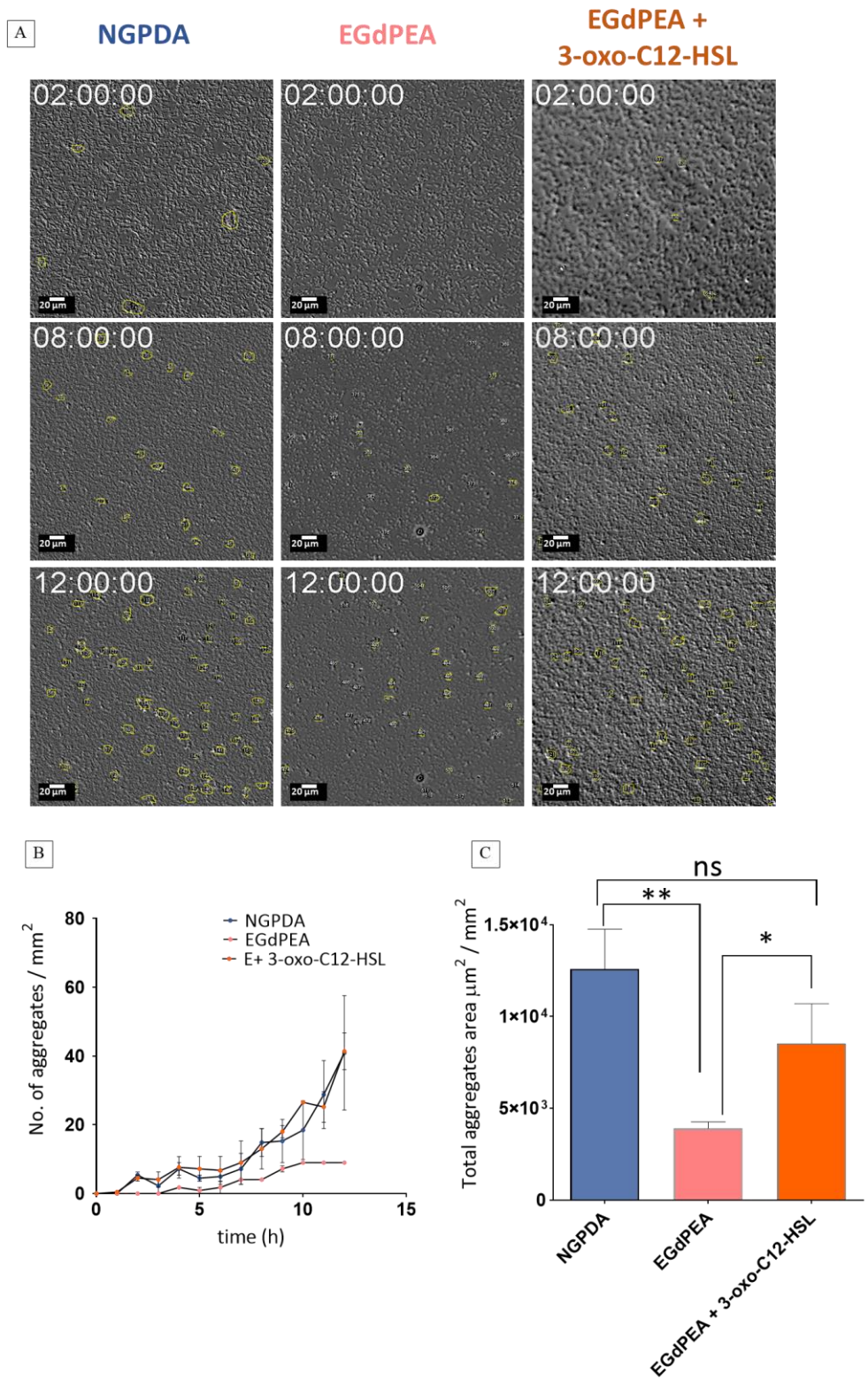

Figure 6.8 3-oxo-C12-HSL induces aggregate formation. **A)** Brightfield DIC (10×, 0.45) microscopy time series showing images of PAO1-W cells inoculated in RPMI-1640 medium on pNGPDA (blue) and pEGdPEA with 3-oxo-C12-HSL (1µM) (orange) and without (pink) at 37°C for 12 h (under static conditions). Images shown are at the 12 h mark then from top to bottom every 2-8 h. Settling aggregates were manually identified (yellow objects) and corresponding aggregate areas were measured using ImageJ. Scale bar is 20 µm. **B)** Quantitative data of area covered by aggregates on

pNGPDA (blue) and pEGdPEA with 3-oxo-C12-HSL (1µM) (orange) and without (pink). Significant differences using a one-way ANOVA non-parametric test were found between samples. ** ($p < 0.05$), * ($p < 0.01$). **C)** Sum of aggregates areas over 12 h of observation on pNGPDA, pEGdPEA with and without 3-oxo-C12-HSL. One-way ANOVA (with post-hoc Tukey test) reveals significant differences expressed as * ($p < 0.05$), ** ($p < 0.01$). Error bars represent ± 1 standard deviation (N=3).

To determine whether the exogenous 3-oxo-C12-HSL could restore biofilm formation in the presence of pEGdPEA, PAO1-W was grown in RPMI-1640 for 24 h and biofilm assays performed as previously described.[7] Biofilm formation by *mcherry*-labelled PAO1-W was assessed on pEGdPEA, pNGPDA and pEGdPEA with or without exogenous 3-oxo-C12-HSL. Representative confocal images from the coated coverslips after bacterial incubation for 24 h in RPMI-1640 are shown in Figure 6.9A where the biomass was quantified using COMSTAT 2.1 (ImageJ) and shown in Figure 6.9B. Bacterial biomass was observed to decrease from 37.3 ± 2.8 $\mu m^3\ \mu m^{-2}$ for pNGPDA to 3.5 ± 0.1 $\mu m^3\ \mu m^{-2}$ for pEGdPEA. This is consistent with bacterial coverage previously observed on these polymers (section 3.3.2). An increase in bacterial biomass was measured for pEGdPEA with 3-oxo-C12-HSL compared with pEGdPEA (18.1 ± 7.3 $\mu m^3\ \mu m^{-2}$) ($p<0.05$). The presence of extracellular matrix associated with bacteria on pEGdPEA supplemented with 3-oxo-C12-HSL was also shown by ESEM images of the samples, which facilitated observation of the EPS production, demonstrating that the addition of the QS molecule initiates biofilm formation on pEGdPEA (Figure 6.10).

This is a further confirmation of the importance of aggregates in biofilm formation (Figure 6.11).

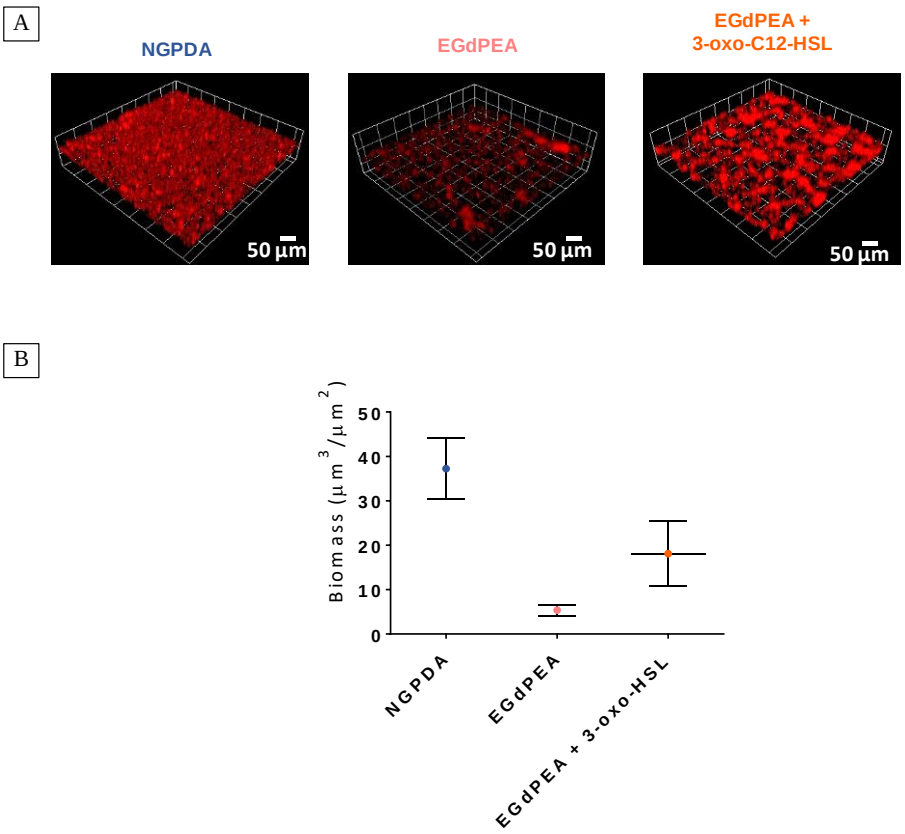

Figure 6.9 A) Confocal images (10×, 0.3) of *m-cherry* tagged *P. aeruginosa* PAO1-W after 24 h on pNGPDA (blue), pEGdPEA (pink) and pEGdPEA with exogenous 3-oxo-C12-HSL. Samples were washed 2× in PBS and 1× in H_2O. Scale bar is 50 µm. **B)** Quantification of bacterial biomass for surfaces. Error bars show ± 1 standard deviation (N=3). One-way ANOVA (with post-hoc Tukey test) reveals significant differences expressed as * (p<0.05), ** (p<0.01). Error bars represent 1 standard deviation (N = 3).

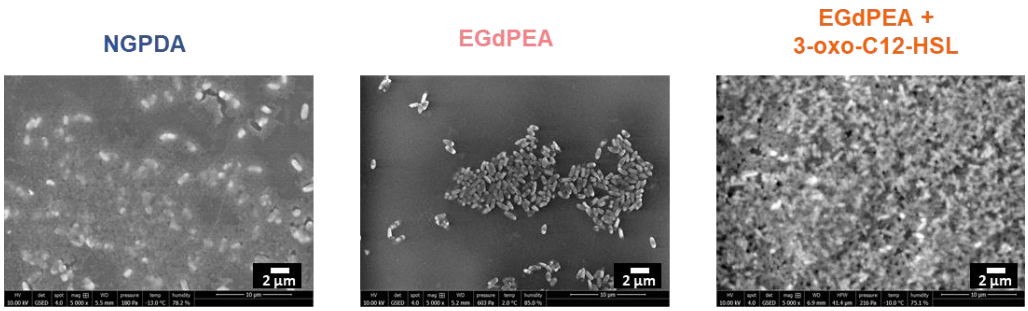

Figure 6.10 ESEM representative images of bacteria grown for 24 h on pNGPDA (blue), pEGdPEA with (orange) and without (pink) 3-oxo-C12-HSL (1 µM). Images captured at 10,000× magnification. Scale bar is 2 µm.

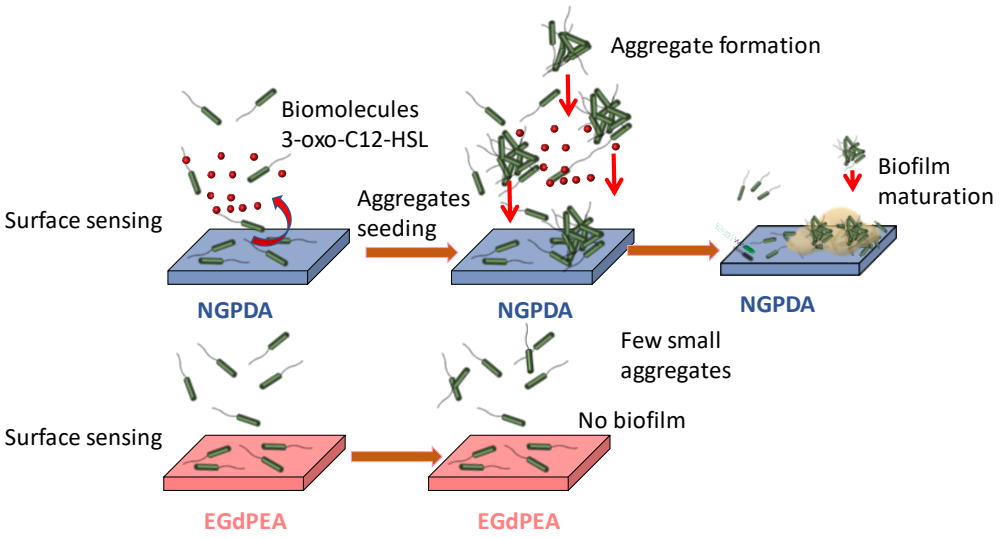

Figure 6.11 Diagram outlining the role of 3-oxo-C12-HSL (red dots) in aggregate and biofilm formation.

6.4 Discussion

The presence of *P. aeruginosa* aggregates in suspension was observed within the bulk culture above pNGPDA but not pEGdPEA. Biofilm maturation has traditionally been envisaged as a result of bacterial cell division, migration, cell death and cell recruitment on the surface together with adhesive processes that link bacteria together during proliferation.[414] Conditioned growth media exchange experiments demonstrated that excreted small molecules from the biofilm samples could induce aggregation within a sample (Figure 6.6). Using LC-MS/MS, 3-oxo-C12-HSL was identified as a key signalling molecule that could instigate bacterial aggregation and biofilm formation, even on samples grown on pEGdPEA. Notably, high levels of eDNA and EPS expression were observed on aggregates arriving at the polymer surface, suggesting that these bacteria could be regarded as being biofilm-like. The complex between 3-oxo-C12-HSL and its receptor LasR activates transcription of target genes including those encoding virulence factors such as elastase, proteases, and exotoxin A.[415] Connell *et al.* confined bacteria in micro-3D printed bacterial "lobster traps" and showed that few hundreds of bacteria were capable of producing QS-controlled exoproduct pyocyanin.[416] It has, thus, been proposed that through QS signalling, bacteria cells in biofilms are able to signal to planktonic bacteria to instigate the transition to biofilm-like cells despite these cells not being

surface bound. These cells, as planktonic aggregates, are then able to readily integrate with the surface-bound biofilm upon exposure to the surface and may also contribute to seeding new sites for bacterial biofilm formation Thus, *P. aeruginosa* has developed a mechanism by which biofilms are able to recruit new planktonic aggregates from the bulk phase. Our observations suggest that the difference in aggregate formation between the two polymers takes about 5 h to be observable. This is after the cells move from reversible to irreversible attachment (as described in chapters 3 and 4). That decision is influenced by the nature of the polymer surface.

In *P. aeruginosa*, QS is mediated by a network of three well established pathways: the alkylquinolone system controlled by PqsR, as well as two LuxR/LuxI-type systems, LasR/LasI and RhlR/RhlI, respectively. These systems are organised hierarchically with LasR functioning as a master regulator at the top of the cascade.[197] When in complex with its autoinducer ligand, 3-oxo-C12-HSL, which is synthesised *via* LasI, LasR functions as a transcriptional activator. A *lasI* deletion mutant, is known to form flat, undifferentiated biofilms,[24] and our results showed how 3-oxo-C12-HSL is important in biofilm maturation affecting planktonic aggregation.

Interestingly, it has been noted that the addition of 3-oxo-C12-HSL requires 5 h before observing an effect on aggregation. From our data it is apparent that, although exogenous 3-oxo-C12-HSL increases aggregation on a biofilm resistant polymer, multiple signaling pathways are likely to be involved in promoting and inhibiting *P. aeruginosa* aggregation.

These observations demonstrate the utility of LC-MS/MS for screening chemical compounds present in the conditioned media of cells that are involved in sensing different surface chemistries. This LC-MS/MS technology can be used for metabolite profiling to quantify intracellular metabolites involved in surface interactions and to investigate specific pathways identified in the current study.

6.5 Conclusions

P. aeruginosa PAO1-W cell aggregates that form in the bulk liquid above a surface are an important component of biofilm development. How surfaces affect aggregation is yet unknown. Here, using microscopy and LDA, a reduction in bacterial aggregate formation was observed for bacteria grown in the presence of the biofilm resistant polymer pEGdPEA in comparison with cells grown with the pro-biofilm stimulating polymer, pNGPDA. Intermediate results were also obtained using a 1:1 copolymer. The reduction in aggregate size in response to pEGdPEA was also observed for PAO1-L but not with PAO1-N. The genomes of these two PAO1 lineage isolates have been sequenced and a number of genes involved in biofilm development in PAO1-L have been deleted or mutated in PAO1-N through natural evolution. These include *bifA*, a cyclic-di-GMP phosphodiesterase that inversely regulates biofilm formation and swarming motility.[390] BifA is known to participates with SadC in the inverse regulation of biofilm formation and swarming motility in a SadB-dependent manner and hence likely to be involved in the switch from reversible to irreversible surface attachment.

Aggregates above pNGPDA were found to have adopted a biofilm growth mode i.e - rich in eDNA and EPS which are commonly found in biofilms. Lower levels of eDNA and EPS were also observed in pEGdPEA aggregates. Although planktonic aggregation started after 1 h of incubation, our observations suggested that difference between the two polymers takes about 5 h to become apparent highlighting a possible mechanism mediated by QS signal molecules by which bacteria induce aggregate formation. For this reason, cell-free conditioned media exchange experiments were developed, and an aggregate-inducing factor(s) was detected in the conditioned medium from cells previously exposed to pNGPDA.

In order to identify the nature of this factor(s), the conditioned media were investigated using LC-MS/MS analysis which revealed significant differences in the QS signal molecules observed upon exposure to the two polymers. 3-oxo-C12-HSL was present at a significantly higher concentration in conditioned media from cells previously exposed to the biofilm-promoting polymer

compared to anti-biofilm control. This molecule induced aggregate and matrix rich biofilm formation on the pEGdPEA anti-biofilm polymer, suggesting that this molecule plays a key role in the ability of a population of surface-associated cells to recruit planktonic cells as aggregates that subsequently seed a site favourable to biofilm formation.

This new insight into bacterial behaviour provides a possible new route for targeting biofilm formation for the prevention of device associated nosocomial infections.

Chapter 7

Conclusion and Future Work

7.1 Conclusions

Biofilm formation on medical devices is a major healthcare problem causing a significant mortality and morbidity in hospitalised patients. Furthermore, the replacement of an infected device may prove costly as well as a significant discomfort for the patient. The current clinical practice measures, such as the use of antibiotics, are insufficient to tackle the problem. Due to ever increasing multi-antibiotic resistance and a fear of the arrival of a post-antibiotic era, novel biomaterials that resist bacterial contamination and biofilm formation are needed. Previously, an acrylate microarray was screened in high-throughput for biocompatible polymers that prevented biofilm formation by multiple bacterial pathogens including *P. aeruginosa*. This resulted in the discovery of pEGdPEA which has recently been approved for human use as a coating (BACTIGON®) for urinary catheters. Although the anti-biofilm properties of pEGdPEA were established, it was unclear as to the mechanism by which this polymer acted upon bacteria. For this reason, the aim of this work was to discover the mechanism used by bacteria to sense surfaces with different chemistries and biofilm forming properties and to describe bacterial responses at both single cell and population levels.

To understand how pEGdPEA prevents biofilm formation, the early stages of bacteria-surface interactions have been described in chapter 3. DHM experiments showed PAO1 cells interacting indistinguishably with both biofilm-promoting (pNGPDA) and biofilm inhibiting (pEGdPEA). From time-lapse experiments pEGdPEA was found to influence bacterial colonisation and surface residence time over the first hours of surface interaction. A slight delay in bacterial surface growth and shorter dwell times were observed on pEGdPEA than on pNGPDA. A higher number of cells were also observed to leave pEGdPEA after cell division in comparison with pNGPDA showing how materials can impact on cells programmed (a)symmetry. c-di-GMP has recently been shown to play a crucial role in determining whether cells are motile or

sessile through the control of cell attachment, detachment and pilus formation and flagellar mediated motility in Gram-negative bacteria including *Pseudomonas*.[139] For this reason, it was decided to explore the changes in intracellular levels of c-di-GMP on either surface. This secondary messenger is a key regulator of biofilm formation in *P. aeruginosa* and other microbes, and it is important in the transition from a reversible to an irreversible attachment activating T4P biogenesis and inducing virulence *via* a cAMP-dependent program.[60] The prevention of biofilm formation on pEGdPEA was found to be accompanied by reduced c-di-GMP production and consequent EPS production which corresponds with a more motile rather than sessile state. This is the converse for the increased production of c-di-GMP noted for bacteria on the pro-biofilm polymer pNGPDA. Bacteria either deposited less EPS on pEGdPEA or the material retains less EPS at the surface than the pro-biofilm pNGPDA. This clearly shows that pEGdPEA inhibits the transition from single cell to biofilm.

In chapter 4 a microfluidic detachment assay was optimised and deployed to assess the strength of bacterial attachment to surfaces and was successfully used to measure the adhesion strength of bacteria to polymers with different surface chemistries. *P. aeruginosa* showed to adhere much more weakly on pEGdPEA than on pNGPDA, while an intermediate adhesion strength corresponded to 1:1 co-polymer. The measure of adhesion strength correlated with the biomass of biofilm observed on these polymers. T4P and a functional flagellum were both found to be necessary in the adhesion of PAO1-W to surfaces. Mutants lacking either component exhibited reduced attachment strength and a concomitant reduction in biofilm formation. A strong correlation was also found for the contribution of pili and flagella to bacterial attachment and biofilm formation in the early stages and after 24 h on pNGPDA. This chapter provides evidence that pEGdPEA does not support the adherence of PAO1 through interactions with T4 pili and flagella.

To identify the intracellular pathway involved in the response of *P. aeruginosa* to pEGdPEA, the role of SadB, an intracellular protein important for irreversible attachment was explored. In chapter 5 it was shown that the *sadB* mutant was

unable to form biofilm, whereas *sadB* overexpression enabled cells to form a matrix rich biofilm on pEGdPEA and other polymer surfaces which were reported to prevent biofilm formation. It has also been shown that cells overexpressing *sadB* cells were more likely to stay on the surface after cell division in contrast to that observed with the *sadB* mutant which showed the highest proportion of daughter cells leaving the surface. The adhesion strength of the *sadB* mutant cells was assessed using microfluidics. PAO1-W Δ*sadB* showed the weakest attachment, whereas overexpressing *sadB* attached more strongly than PAO1-W on pEGdPEA. A more surface-committed progeny, a stronger adhesion to the surface and biofilm formation on biofilm-resistant polymers (like pEGdPEA), observed *in vitro* experiments, suggest these polymers are likely to interact with the *sadB* signalling pathway. Taken together, these results suggest that PAO1 cells programme either their surface colonisation or surface detachment upon surface contact *via* a sensory pathway involving SadB.

Having previously observed a role for the flagella stators in sensing the different polymer surface chemistries (section 4.3.3), the combined influence of both SadB and stator mutants was assessed. In particular, it was shown that the overexpression of *sadB* in a Δ*motAB* mutant was unable to restore the ability to form biofilm on surfaces leading to the hypothesis that SadB operates upstream of MotAB in the signalling pathway. From the literature SadB is also known to be upregulated upstream by the secondary messenger c-di-GMP,[390] here it has also been observed that SadB is able to increase c-di-GMP levels in PAO1-W in contact with pEGdPEA and in *motCD* mutants on either surface. These studies help define the biofilm prevention mechanism exerted by some polymer surfaces, with molecularly rigid hydrophobic chemical side-groups, to prevent the switch from reversible to irreversible attachment.

In chapter 6, the role of bacterial aggregation on surface biofilm formation was described making use of pEGdPEA and pNGPDA polymer surfaces as research tools that could drive the emergence of two different phenotypes. Aggregate arrival at the surface was presumed to originate away from the solid-liquid interfaces. Planktonic aggregates were monitored at the surface by using

microscopy and in the bulk with LDA. After 5 h of exposure to surfaces, a higher number of aggregate arrivals was observed to colonise pNGPDA than pEGdPEA with a much higher percentage of total bulk biomass after 24 h on pNGPDA consisting of particles in the 2-30 μm range compared with pEGdPEA. Aggregate settlement was found to contribute up to 40% of the surface biomass on pNGPDA and to be rich in eDNA and EPS. Studies with different PAO1 strains revealed that pEGdPEA prevented aggregation by *P. aeruginosa* PAO1-W and PAO1-L strains but not PAO1-N. The genome of these two PAO1 linage isolates have been sequenced and a number of genes involved in biofilm formation and in proteins which play a role in *sadB* pathway have been deleted or mutated in PAO1-N. In order to gain further insights into the preferential formation of aggregates when PAO1-W was cultured in contact with biofilm-promoting pNGPDA a cell-free conditioned media exchange experiment was devised which showed that cells previously exposed to pEGdPEA, and then to media conditioned by cells incubated on pNGPDA were able to form aggregates confirming a presence of aggregates-promoting factor(s) in the pNGPDA media. LC-MS/MS analysis of the cell-free spent media revealed significant differences between samples in the bacteria excreted QS molecules observed upon exposure to pNGPDA and pEGdPEA. The aggregation-inducing signal 3-oxo-C12-HSL was identified and found to induce aggregates and increase biofilm formation on the biofilm-resistant pEGdPEA, suggesting that this signalling molecule plays a key role in the ability of a population of surface-associated cells to recruit planktonic cellular aggregates to a site favourable to biofilm formation. This insight into bacterial behaviour at the early stages of biofilm formation provides a new route to target for the prevention of device associated nosocomial infections.

7.2 **Future work**

Strategies for reducing biofilm formation traditionally focus on the incorporation of antimicrobials which have been shown to increase the challenges associated with multi-antibiotic resistance. Here it has been demonstrated that a new class of materials (i.e. pEGdPEA) able to prevent biofilm formation *via* a unique mechanism, by preventing bacteria switching from a planktonic to a biofilm state

through SadB signalling pathway *in vitro* experiments. Future research should investigate whether this pathway influences biofilm formation within the *in vivo* environment where there is a complex milieu of host proteins and biomolecules that can adsorb onto the surface of a device. The next stage in this work would therefore be to use *in vivo* mouse infection models in order to verify the importance of *sadB* pathway and biofilm formation in animal infections with anti-biofilm pEGdPEA coated catheters. This mouse model is a subcutaneous foreign-body infection model which has previously been used to test the *in vivo* biofilm resistance performance of bacteria-resistant materials.[254] Results showing that the cells overexpressing *sadB* are able to overcome *in* vivo the biofilm-resistance properties of pEGdPEA, with the converse being observed for the *sadB* mutant, may provide the basis for the development of a new target for new narrow spectrum anti-biofilm drug.

With regards to *sadB* expression, even if evidence for its involvement in the surface-sensing process have been provided, it would be interesting to use a reporter fusion for *sadB* to observe the effect of polymers on its expression in real-time. Considerably more work will need to be done to determine the position of this protein in the cell by constructing and using a translational fusion. This will allow us to establish whether SadB localises to the cell poles upon surface contact to drive cells asymmetric behaviour as observed for daughter cell fates. It has been observed that daughter cell destiny in the overexpressing *sadB* strain was shifted towards a more surface-associated state. It would be ideal to fully explain the full mechanism of surface detachment. Such knowledge would allow the direct, rational design of other surfaces that do not support bacterial colonisation. From the literature it has been shown that pili and flagella are both required in the detachment process.[292] SadB is likely to be involved in the activity of stators and pili. The use of interferometric scattering microscopy which has been shown to be a powerful tool for label-free sensitive detection and imaging of T4P activity, would allow us to visualise T4P activity in *sadB* mutants.[417]

A greater interest should be put on SadB function and its relationship with c-di-GMP. As highlighted in Figure 1.15 the sensory signalling processes involving

c-di-GMP are complex and involve multiple proteins. The two polymer surfaces used in this thesis have been demonstrated as excellent experimental tools that produce different phenotypes. Constructing other mutants such as the ones involved in EPS production and incubating them with the 2 surfaces would allow the complex interaction to be better understood revealing which factors are downstream the interaction between SadB/c-di-GMP. In order to screen multiple mutants, it will be necessary to develop a high-throughput screening approach. A robotic contact (pin) printer might be a helpful tool to answer this need. Robotic printers have extensively been used in polymers microarrays.[233, 234, 253] Another possible use would be to rapidly print the two polymers in 96/384 wells plates where each well will be incubated with a different bacterial mutant. After 24 h of incubation a fluorescence scanner could generate biofilm formation data for each well corresponding to each strain. Combinatorial mutants could be also applied to establish interconnections between different pathways.

Exogenous 3-oxo-C12-HSL at 1 µM restored aggregation and biofilm formation (confocal, ESEM) on pEGdPEA. These results suggest the existence of a previously unknown target for *P. aeruginosa* QS regulation. Further research might explore the possibility that surface association, which is necessary for many of the same group behaviours as QS, could be a cue that promotes different QS responses for different surface chemistries. A natural progression of this work would be to analyse QS molecules at the surface using mass-spectrometry based techniques. 3D OrbiSims might be the right instrument to combine the high spatial resolution of secondary ion mass spectrometry (SIMS) with the high mass-resolving power of an Orbitrap. [418] This will allow us to visualise QS in 3D with cellular resolution in the aggregates. All these data will be combined with QS signal molecule detection in the bulk phase by using LC-MS/MS at multiple time points during bacteria surface-interaction. More information about QS production in surface-associated bacteria would help us to establish a greater degree of knowledge of how bacteria respond to surface at a community level.
The precise mechanism by which 3-oxo-C12-HSL mediates aggregation remains to be elucidated. Further investigation on the 3-oxo-C12-HSL receptor (LasR) and synthase (LasI) involved is recommended. In order to understand *lasR* and *lasI* involvement in aggregation, it is necessary to construct mutants for both

genes and determine the aggregation phenotype with or without 3-oxo-C12-HSL. *P. aeruginosa lasR*::fluorescent protein fusion is also required to visualise the expression of LasR in the aggregates. Furthermore, in many other systems, small RNAs (sRNAs) have emerged as QS regulators, and LasR is known to regulate at least one sRNA, Lrs1.[419] However, the regulation of LasR expression by sRNAs in aggregates has not been examined. It would be interesting to examine aggregation upon deletion of the sRNA universal RNA chaperone Hfq, which is required for the stability and function of most sRNAs.[420]

Since the contribution of cell aggregation in biofilm formation has been demonstrated, another possible area of future research would be to investigate whether there is a relationship between the properties of materials and aggregation. Machine learning and other statistical methods (i.e partial least-squares regression analysis) have been reported to provide a better understanding of the details of the molecular interactions (ToF-SIMS spectra) and mechanisms underlying biological phenomena (cell adhesion), and to be able to predict biological response of materials yet to be synthesised.[421] This allows discovery and testing of potentially useful materials more quickly. In our group, computational models were found to be capable of making quantitative predictions of attachment of single and multiple pathogens to a polymer library.[7, 8, 254, 388, 421] However, pathogens use sophisticated and diverse strategies to colonise a surface, and different chemistries might affect such strategies. Therefore, a greater focus on aggregation and materials properties could produce interesting findings that help to create more accurate predictive models to design a super-material which affects multiple bacterial strategies and species.

Lastly, all the experiments in this project have been run using *P. aeruginosa*, but there is abundant room for further research in determining whether the observed phenomena and mechanisms are conserved or not in other bacterial species although they presented different genomes and phenotypes (i.e. multiple flagella, absence of T4P or flagella). The assessment of multiple strategies used by different bacteria to infect a surface could help to reinforce models of surface colonisation. For this reason, it would be interesting to study other Gram-

negative pathogens such as *E. coli*, *Proteus*, *Enterobacter* and *Klebsiella* species as well as Gram-positives including *S. aureus*, which are commonly found in polymicrobial infections with *Pseudomonas*.

Chapter 8

Appendixes

8.1 Appendix 1

DriftCorrection

```
Function [ output_args ] =
DriftCorrection(OBJECTS,dimensions,ZStep,Process,FileName,PathName, varargin )

%% Script that for determine cell density and avoid flow and drift effect of objects in 3D
stacks

% written by Alessandro Carabelli 10/2018
% The script uses variable from MasterStack: OBJECTS, dimensions, ZStep,
% Process, FileName, Pathname.

%% Variable description
% celldensity; cell density per mm^3
 % png plot will be saved in PathName

%% Display acquired data

close all

f1 = figure;
hold on

data = squeeze(OBJECTS);
% show data
for i=1:size(data,1)
    scatter3(data(i,1), data(i,2), data(i,3), 10, 'r', 'filled');
end


%% Dialog box for the user to find flow direction
% two different points are selected as same objects on different slices to
% calculate trajectory of flow and identify same objects
% As soon as the trajectory is identified, bacteria that are found within
% angle of 35 degrees and at a distance of 1.6 times the distance defined
% by user (selecting the two points) are recognise as same object.
% Also, bacteria that are close to point less than 0.5 are unified as
% single object, to avoid overestimated number of objects

f = msgbox('Pick object 1 for trajectory analysis','Analysis setup');
waitfor(f);


object1 = 0;
object2 = 0;
lastGCO = 0;
while size(findobj(f1))>0 % loop while the figure 1 exists
    clickedPlot = gco; % set clickedPlot to the handle of the current object
    %disp(clickedPlot);
```

```
    if strcmp(get(clickedPlot,'type'),'scatter')>0 && lastGCO ~= clickedPlot % check if a
new line was selected
        if object1 == 0
            object1 = clickedPlot;
            set(clickedPlot, 'MarkerFaceColor', 'b');

            f = msgbox('Pick object 2 for trajectory analysis','Analysis setup');
            waitfor(f);
        else
            object2 = clickedPlot;
            set(clickedPlot, 'MarkerFaceColor', 'g');
            break;
        end
        lastGCO = clickedPlot;
    end
    pause(0.1); % slight delay so loop doesn't try to run faster than necessary
end
pause(1);
% trajectory objects chosen
point1 = [object1.XData object1.YData object1.ZData];
point2 = [object2.XData object2.YData object2.ZData];
close(f1)

% calculate the trajectory from object1 to object2
trajectoryDirection = (point2 - point1)/norm(point2 - point1);
%disp('traject direction')
%disp(trajectoryDirection);
% the magnitude orf seach can now be set by using the objects speed and the
acquisition time
trajectoryMagnitude =  sqrt((point2(1) - point1(1))^2+(point2(2) - point1(2))^2+(point2(3)
- point1(3))^2);
%disp('traject magnitude')
%disp(trajectoryMagnitude);

tracks = [58]; % stores the track information
trackCount = 0; % keeps count of the number of tracks

OBJECT_COUNT = size(data,1);

for i=1:OBJECT_COUNT
    data(i,5) = 0;
end

% now loop through all the objects and find matches

%currentObject = data(1,:);

for i=1:OBJECT_COUNT
    trackIterator = 1;
    if data(i,5) == 0
        data(i,5) = 1;
        currentObject = data(i,:);


        trackCount = trackCount + 1;
        tracks{trackCount}(trackIterator, 1:5) = currentObject;
        trackIterator = trackIterator + 1;
```

```
        while 1 % loop until no more objects can be added to the tracks
            potentialList = {};
            adjacentList = {};
            adjacentCount = 0;
            nextCount = 0;
            for a=1:OBJECT_COUNT
                if data(a,5) == 0
                    unitVector = (data(a,1:3) - currentObject(1:3)) / norm(data(a,1:3) -
currentObject(1:3));
                    angle = acosd(dot(unitVector, trajectoryDirection));
                    distance = sqrt((data(a,1)-currentObject(1))^2+(data(a,2)-
currentObject(2))^2+(data(a,3)-currentObject(3))^2);

                    if distance < (trajectoryMagnitude*0.7)
                        adjacentCount = adjacentCount + 1;
                        adjacentList{adjacentCount} = [a, distance, angle];
                    end

                    if angle < 35 && distance < (trajectoryMagnitude*1.6)
                        %disp([a angle distance])
                        nextCount = nextCount + 1;
                        potentialList{nextCount} = [a, distance, angle];
                    end
                end
            end% end for
            if adjacentCount > 0
                % find min in adjacentList
                minIndex = adjacentList{adjacentCount}(1,1);
                minDist = adjacentList{adjacentCount}(1,2);
                for a=2:adjacentCount
                    if adjacentList{a}(1,2) < minDist
                        minDist = adjacentList{a}(1,2);
                        minIndex = adjacentList{a}(1,1);
                    end
                end

                % the currentObject is now updated
                data(minIndex,5) = 1;
                currentObject = data(minIndex,:);
                tracks{trackCount}(trackIterator,1:5) = currentObject;
                trackIterator = trackIterator + 1;

                disp(['*adding ' num2str(minIndex) ' to track ' num2str(trackCount)]);

            elseif nextCount > 0
                % find min in potentialList
                minIndex = potentialList{nextCount}(1,1);
                minDist = potentialList{nextCount}(1,2);
                for a=2:nextCount
                    if potentialList{a}(1,2) < minDist
                        minDist = potentialList{a}(1,2);
                        minIndex = potentialList{a}(1,1);
                    end
                end

                % the currentObject is now updated

                data(minIndex,5) = 1;
                currentObject = data(minIndex,:);
```

```
            tracks{trackCount}(trackIterator,1:5) = currentObject;
            trackIterator = trackIterator + 1;

            disp(['adding ' num2str(minIndex) ' to track ' num2str(trackCount)]);
        else
            break
        end
            end % end while
    end
end

%% Display new 3D scatter with new objects. Objects that were find in multiple
% slices were defined as new objects with coordinates the mean of all the
% position of points in tracks

f1 = figure;
hold on
for i=1:size(tracks,2)
    plot3(tracks{1,i}(:,1),tracks{1,i}(:,2),tracks{1,i}(:,3));
end
scatter3(data(:,1),data(:,2),data(:,3));

waitfor(f1);

f1 = figure;
hold on
 MAX_Z = max(data(:,3));
 colormap('hot');
 for i=1:size(tracks,2)
    if size(tracks{i},1) == 1
h=scatter3(tracks{i}(1,1),tracks{i}(1,2),tracks{i}(1,3),40,tracks{i}(1,3),'filled','MarkerEdg
eColor','k'); % if you want them square just put 's' after filled

        tracks2{i}(1,1:3)=tracks{1}(1,1:3)
    else

        xMean = mean(tracks{i}(:,1));
        yMean = mean(tracks{i}(:,2));
        zMean = mean(tracks{i}(:,3));
        tracks2{i}(1,1)=mean(tracks{i}(:,1));
        tracks2{i}(1,2)=mean(tracks{i}(:,2));
        tracks2{i}(1,3)=mean(tracks{i}(:,3));
        h=scatter3(xMean,yMean,zMean, 40,zMean, 'filled','MarkerEdgeColor','k');

    end
end
view(-30,10)
colormap hot;
h = colorbar;

title(h,'Z (\mum)'); %Add colormap label

xlabel(strcat('\fontsize{10} X (\mum)')); %Add x axis label
ylabel(strcat('\fontsize{10} Y (\mum)'));
zlabel(strcat('\fontsize{10} Z (\mum)'));
grid on
name = char (FileName);
splitname = strsplit(name,'.');
```

```
split=fullfile(PathName,char(splitname(1,1)));
saveas(gcf,split,'m');
saveas(gcf,split,'png');

gif('gif output.gif','frame',f1);
for i=-30:30
    view(i,30);
    gif
end

%% Tracking analysis: consider bacterial density

% calculate volume in um^3
Volume= (dimensions^2*(ZStep*Process))/10^9; %conversion in mm^3
%cell density in mm^3
celldensity=size(tracks2,2)/Volume;

%create arry with number of cells per z depth
B = size(tracks2,2);
clear ytracks;
clear a;
for a=1:B %Build array containing all objects
    if a == 1

        ytracks = tracks2{a};

    else
        ytracks(end+1:end+size(tracks2{a},1),1:size(ytracks,2))=tracks2{a};

    end
end

clear z zz t ii i
z=round(sort(ytracks(:,3)),0);
zz=unique(z)

frequency = zeros(size(zz)); % vector for freqs
% frequency for each value
for i = 1:length(zz)
    frequency(i) = sum(z == zz(i));
end
figure
bar (zz,frequency)
xlabel('z distance')
ylabel('Frequency')

assignin('base','celldensity',celldensity);

end
```

8.2 Appendix 2

TrackingAnalysis

Function

```
[y,z]= TrackingAnalysis (Tracks, OBJECTS, PathName, TStep, FileName, Selectionvar,
z800, varargin) % Analyzes the input Tracks and saves the resulting data into a folder.
%
%   Inputs:
%         Tracks should be {Frame} (x,y,t...)
%         OBJECTS      = all the objects for each frame
%         PathName     = string of the path name used for saving
%         TStep        = time step between frames (sec)
%         FileName     = filename of input tif image
%         Selectionvar = structure containing.....
%         z800         = boolean variable
%         varargin:
%            MinSpeed        = minimum speed to determine motility
%            MinDistance     = minimum distance from mean to determine motility
%            plotdimension   = dimensions of the plot
%
%   Outputs:
%         y =
%         z =
%
% Column information for Tracks
%  column 1:  x position
%  column 2:  y position
%  column 3:  time
%  column 4:  lengthmean
%  column 5:  widthmean
%  column 6:  Distance tot
%  column 7:  Average Speed
%  column 8:  # tracks
%  column 9:  fluorescence
%  column 10: tilt angle
%  column 11: instantaneous speed
%  column 12: residence time
%  column 13: average speed
%  column 14: starting time
%  column 15: ending time
%  column 16: MSD slope
%  column 17: orbisum
%  column 18: circularity

CFields = fieldnames(Selectionvar);
if z800 == 0;
   Q5  =  bttnChoiseDialog(CFields,  'Selectionvar',  'Rainbow','Select  your  variable  to
plot');
   Q5 = CFields(Q5);Q5=Q5{1};
   C = getfield(Selectionvar,Q5);
   Choice = C(1,1);
else
   Choice=11;
end
clear C

%% Analyze data after 2D tracking
% all composed by Alessandro Carabelli, 03/2018
% outputs xls files with all data about tracks
% sum distance from mean, average speed, MSD, radius of curvature, circularity,
fluorescence intensity
% Final Array with all data about tracks is the output
% column 1: distancetot
% column 2: speedaverage
```

```
% column 3: espeedaverage
% column 4: lenghtmean
% column 5: widthmean
% column 6: elength
% column 7: ewidth
% column 8: circularity
% column 9: angleellipse
% column 10: eangleellipse
% column 11: orbtot2
% column 12: MSD slopet1
% column 13: fluorescence intensity

% SpeedBugs is exported as an excel file with data about bugs moving.
% Cutoff default : 0.001 (um/sec) and sum of distance from mean: 5


%% Process varagin
% Set defaults
Inputs(1) = 0.001; % (in um/s) MinSpeed - Minimum speed bug needs to be considered
as a motile bug
Inputs(2) = 5; % (in um) MinDistance - Minumum distance bug needs to be considered
as a motile bug

C2 = 0;
% Process varargin
if size(varargin,2)>0 %identifies varargin needs to be processed
   % First check varargin for manual input
   if sum(strcmp(varargin, 'MinSpeed')) > 0
      Inputs(1)=varargin{find(strcmp(varargin, 'MinSpeed')==1,1)+1};
   end
   if sum(strcmp(varargin, 'MinDistance')) > 0
      Inputs(2)=varargin{find(strcmp(varargin, 'MinDistance')==1,1)+1};
   end
   % ordered processing
   if isnumeric(varargin{1}) == 1 %if first entry is manual, no category selection
      Inputs(1)=varargin{1};
      C2 = C2 + 1;
      if size(varargin,2)>C2 && isnumeric(varargin{C2 + 1})==1
         Inputs(2)=varargin{C2 + 1};
         C2 = C2 + 1;
      end
   end
end
MinSpeed = Inputs(1);
MinDistance = Inputs(2);

%% Pre process data sequence
% convert Nan object in 0 tracks
for a = 1:size(Tracks,2)
   Tracks{1,a}(Tracks{1,a}==0) = nan;
   if isnan(Tracks{1,a}(1,3)) == 1
      Tracks{1,a}(1,3)=0;
   end;
end;

% identify number of objects detected (mean over 5 frames)
if size(OBJECTS,2)>5
   coun                                                                    =
round(mean([size(OBJECTS{1},1),size(OBJECTS{2},1),size(OBJECTS{3},1),size(OBJ
ECTS{4},1), (OBJECTS{5},1)]),0);
```

```
else
   coun = size(OBJECTS{1},1);
end

% identify number of frames
for i = 1:size(Tracks,2)
   frames2(i,1) = size(Tracks{i},1);
end
frames = max(frames2);

%% Measure diffent parameters: angular speed, tilt angle, average speed,
% resident time
for i = 1:size(Tracks,2)
   % measure angular speed and tilt angle for spinning motility
   for j = 1:size(Tracks{i},1)
      L = max(Tracks{i}(:,4));  % value of average length if the cell is completely alligned
to surface
      if Tracks{i}(j,4)~= 0
         width =  Tracks{i}(j,5);  % width of cell
         length = Tracks{i}(j,4);  % length of cell

         a1 = L^2 + width^2;
         b1 = -2*width*length;
         c1 = length^2-L^2;
         x1 = (-b1-sqrt(b1^2-4*a1*c1))/(2*a1);
         x2 = (-b1+sqrt(b1^2-4*a1*c1))/(2*a1);

         tiltAngle(j,i) = abs(asin(x1)*180/pi); %find tilt angle
         Tracks{i}(j,10) = tiltAngle(j,i);

         tiltAngle2(j,i) = abs(asin(x2)*180/pi); %depending on quadrant
         Tracks{i}(j,10) = tiltAngle2(j,i);
         ratio(j,i) = length/width;

         if ratio(j,i) <= 2 && ratio(j,i) > 1.7
            ratio1(j,i) = ratio(j,i);
            tilting(j,i) = 0;
         elseif ratio(j,1) < 1.7
            ratio1(j,i) = nan;
            tilting(j,i) = 1;
         else
            ratio1(j,i) = nan;
            tilting(j,i) = nan;
         end
      end
   end
   tiltingfraction(i,1) = nanmean(tilting(:,i));

   %% Measure average speed and resident time (plus appearence time and off bug
time)
   if size(Tracks{i},1)>1
      for j = 2:size(Tracks{i},1)
         SP1{i}(j,1)    =    ((Tracks{i}(j,1)-(Tracks{i}(j-1,1)))^2+(Tracks{i}(j,2)-(Tracks{i}(j-
1,2)))^2)^0.5/(abs(Tracks{i}(j,3)-(Tracks{i}(j-1,3))));
         endingtime(i,1) = Tracks{i}(end,3); % time off bug
      end
   else
      SP1{i}(1,1) = 0;
   end
   startingtime(i,1) = Tracks{i}(1,3);  %time of bug appereance
```

```
    Tracks{i}(1:end,11) = SP1{i}(1:end);

    speedaverage(i,1)   = nanmean(nonzeros(SP1{i}(:,1)));
    Tracks{i}(1:end,7)  = speedaverage(i,1);
    residenttime(i,1)   = (size(Tracks{i},1)-1)* TStep;
    Tracks{i}(1:end,12) = residenttime(i,1);
    espeedaverage(i,1)  = std(nonzeros(SP1{i}(:,1)));
    Tracks{i}(1:end,13) = speedaverage(i,1);
    Tracks{i}(1:end,14) = Tracks{i}(1,3);
    Tracks{i}(1:end,15) = Tracks{i}(end,3);
end

%% Measure distance from mean, MSD, and radius of curvature
lasttime = TStep*(frames);
time(:,1) = linspace(TStep,lasttime,frames);
logtime(:,1) = log10(time(:,1));

for i = 1:size(Tracks,2)
    medx  = mean(nonzeros(Tracks{i}(:,1)));
    medy = mean(nonzeros(Tracks{i}(:,2)));

    if size(Tracks{i},1)>1
        for s = 1:size(Tracks{i},1)
            % find distance from each point of trajectory to mean
            distance(s,i) = ((Tracks{i}(s,1)-medx)^2)+((Tracks{i}(s,2) - medy)^2)^0.5;
        end
    else
      distance(1,i) = 0;
    end
    % sum all the distances from point to mean
    distancetot(i,1) = nansum(distance(:,i));
    Tracks{i}(1:end,6) = distancetot(i,1);

    % calculate MSD for swimming trajectory
    if speedaverage(i,1) > MinSpeed && distancetot(i,1) > MinDistance
        for j = 1:(size(Tracks{i},1) - 1)
            r = 1;
            while r <= size(Tracks{i},1) - j
                if Tracks{i}(r+j,1) ~= 0 && Tracks{i}(r+j,2) ~= 0
                    EX1{1,i}(r,j)      =      (Tracks{i}(r,1)-Tracks{i}(r+j,1))^2      +(Tracks{i}(r,2)-
Tracks{i}(r+j,2))^2 ;
                end
                r = r + 1;
            end
            EX2{1,i}(j,1) = mean(nonzeros(EX1{1,i}(:,j)));
            LOGMSD{1,i}(j,1) = log10(EX2{1,i}(j,1));
        end

        j = 1;
        while j <= size(Tracks{i},1)-2
            if LOGMSD{1,i}(j+1,1) ~= LOGMSD{1,i}(j,1)
                LOGm{1,i}(j,1) = LOGMSD{1,i}(j,1);
                logt{1,i}(j,1) = logtime(j,1);
            end
            j = j + 1;
        end

        if exist('logt') == 1
```

```
            slopet = polyfit(logt{1,i},LOGm{1,i},1);
            slopet1(i,1) = slopet(1,1);
        end

        clear LOGm;
        clear logt;
        %calculate slope of linear regression line
        if isnan(LOGMSD{1,i}(1,1)) ~= 1
            rrr = size(LOGMSD{1,i},1);
            slope = polyfit(logtime(1:rrr),LOGMSD{1,i}(1:end,1),1);
        end
    else
        slopet1(i,1)= 0;
    end

    % Measure radius of curvature
    question(1,1) = 1;
    if question(1,1) == 1
        if speedaverage(i,1) > MinSpeed(1,1) && distancetot(i,1) > MinDistance(1,1)
            if size(Tracks{i},1)>2
                for t = 1:(size(Tracks{i},1)-2)
                    x1 = Tracks{i}(t,1);
                    x2 = Tracks{i}(t+1,1);
                    x3 = Tracks{i}(t+2,1);
                    y1 = Tracks{i}(t,2);
                    y2 = Tracks{i}(t+1,2);
                    y3 = Tracks{i}(t+2,2);
                    A  = (x1*x1)+ (y1*y1)-(x2*x2)-(y2*y2);
                    B  =(x1*x1)+ (y1*y1)-(x3*x3)-(y3*y3);
                    C(t,1) = A;
                    D(t,1) = B;
                    u = x1-x2;
                    theta = A/2;
                    gheta = B/2;
                    gamma = y1-y2;
                    b   =   ((u*gheta)-(x1*theta)+(x3*theta))/((x3*gamma)-(x1*gamma)+(u*y1)-
(u*y3));
                    a = (theta-(b*(y1-y2)))/(x1-x2);
                    %distance from each point to the center of circle
                    distancecm(t,i) = (( Tracks{i}(t,1) - a)^2+( Tracks{i}(t,2) - b)^2);
                end
            else
                distancecm(1,i) = 0;
            end
            distancetot2(i,1) = nansum(distancecm(1:end,i));
            gggg1 = sum(~isnan(distancecm),1);
            orbtot2(i,1) = (nansum(distancecm(:,i))/gggg1(1,i))^0.5;
        else
            orbtot2(i,1) = 0;
        end
    else
        orbtot2(i,1) = 0;
    end
    Tracks{i}(1:end,17) = orbtot2(i,1);

    %Measure circularity
    tiltmean(i,1) = mean(nonzeros(Tracks{i}(:,10)));
    lenghtmean(i,1) = mean(nonzeros(Tracks{i}(:,4)));
    widthmean(i,1) = mean(nonzeros(Tracks{i}(:,5)));
    a1 = lenghtmean(i,1)/2;
```

```
    b1 = widthmean(i,1)/2;
    p = pi*((3*(a1+b1))-sqrt((3*a1+b1)*(a1+3*b1)));
    Area = pi*a1*b1;

    elength(i,1) = std(Tracks{i}(:,4));
    ewidth(i,1) = std(Tracks{i}(:,5));
    circularity(i,1) = 4*pi*Area/(p^2);
    Tracks{i}(1:end,18) = circularity(i,1);
end


%% Measure average fluorescence for bacteria present on polymers most of the
% time
for i = 1:size(Tracks,2)
    if  size(Tracks{i},1) > (frames-9)
        averagefluorescence(i,1) = nanmean(nonzeros(Tracks{i}(:,9)));
    else
        averagefluorescence(i,1) = 0;
    end
end

%% Array of all data
FinalArray(:,1)  = distancetot(:,1);
FinalArray(:,2)  = speedaverage(:,1);
FinalArray(:,3)  = espeedaverage(:,1);
FinalArray(:,5)  = lenghtmean(:,1);
FinalArray(:,6)  = widthmean(:,1);
FinalArray(:,7)  = elength(:,1);
FinalArray(:,8)  = ewidth(:,1);
FinalArray(:,9)  = circularity(:,1);
FinalArray(:,10) = tiltmean(:,1);
FinalArray(:,12) = orbtot2(:,1);
FinalArray(:,13) = slopet1(:,1);
FinalArray(:,14) = averagefluorescence(:,1);
FinalArray(:,15) = tiltingfraction(:,1);

%% Organise data for moving and not moving cells
nrows3 = size(FinalArray,1);
rac3 = 1;
rac4 = 0;
barabba2 = FinalArray(:,2);
barabba3 = FinalArray (:,1);

spinningcount = 0;
nonspin = 0;
SpeedBugs = cell(nrows3,12);
y = 0;
SpeedBugs  = {'Sum of distance from mean','Average Speed','Circularity','Resident
time','Starting time','Ending time','Average radius from centre circle','Slope
MSD','Average fluorescence','Average tilt angle'};
for bar7 = 1:nrows3
    if barabba2(bar7,1) > MinSpeed(1,1) && barabba3(bar7,1) > MinDistance(1,1) &&
FinalArray(bar7,12) ~= Inf && FinalArray(bar7,2) ~= Inf
        rac3 = rac3+1;

        SpeedBugs{rac3,1} = FinalArray(bar7,1);
        SpeedBugs{rac3,2} = FinalArray(bar7,2);
        SpeedBugs{rac3,3} = FinalArray(bar7,9);
        SpeedBugs{rac3,4} = residenttime(bar7,1);
        SpeedBugs{rac3,5} = startingtime(bar7,1);
```

```
        SpeedBugs{rac3,6} = endingtime(bar7,1);
        SpeedBugs{rac3,7} = FinalArray(bar7,12);
        SpeedBugs{rac3,8} = FinalArray(bar7,13);

        SpeedBugs{rac3,9} = FinalArray(bar7,14);
        SpeedBugs{rac3,10} = tiltmean(bar7,1);
        SpeedBugs{rac3,11} = tiltingfraction(bar7,1);
        % count spinning cells
        if FinalArray(bar7,13) < 0.2 && FinalArray(bar7,12) < 5;
            y = y+1;
            spinningcount = spinningcount +1;
            SpeedBugs{rac3,11} = {'x'};
        else
            nonspin = nonspin+1;
        end
    else
        if barabba2(bar7,1) < MinSpeed (1,1)
            rac4 = rac4+1;

            NonSpeedBugs(rac4,1) = FinalArray(bar7,1); % organise data for non moving
cells
            NonSpeedBugs(rac4,2) = FinalArray(bar7,2);
            NonSpeedBugs(rac4,3) = FinalArray(bar7,3);
            NonSpeedBugs(rac4,4) = FinalArray(bar7,9);
            NonSpeedBugs(rac4,5) = FinalArray(bar7,10);
            NonSpeedBugs(rac4,6) = FinalArray(bar7,11);
            NonSpeedBugs(rac4,7) = FinalArray(bar7,12);
            NonSpeedBugs(rac4,8) = FinalArray(bar7,13);
            NonSpeedBugs(rac4,10) = tiltmean(bar7,1);
            if size(Tracks{1,1},2) == 9
                NonSpeedBugs(rac4,9) = FinalArray(bar7,14);
            end
        end
    end
end

SpeedBugs{1,12} = {'% motile cells'};
sizeTracks = size(Tracks);
ft = sizeTracks(2);
sizeSpeedBugs = size(SpeedBugs);
rt = sizeSpeedBugs(1)-1;

motilecells = 100*(rt)/ft;
SpeedBugs{2,12} = motilecells;
SpeedBugs{1,13} = {'% spinning cells'};
spinningcells = 100*spinningcount/coun;
SpeedBugs{2,13} = spinningcells;

%% Save objects, Tracks...
%create a folder with specific name
name = char(FileName);
splitname = strsplit(name,'.');
split = fullfile(PathName,char(splitname(1,1)));
File = strcat(split,'\');
mkdir(File)
File2 = strcat(File,'\Objects','.mat');
save(File2,'OBJECTS')
File3 = strcat(File,'\Tracks','.mat');
save(File3,'Tracks')
File4 = strcat(File,'\data');
```

```
% Save all variables from workspace
save Workspace
input = fullfile(pwd,'Workspace.mat');
output = fullfile(File);
copyfile(input,output)
delete([pwd '\Workspace.mat'])

%save and name xls file
xlswrite(File4,FinalArray);
xlswrite(File4,SpeedBugs);

hExcel = actxserver('Excel.Application');
File2 = strcat(File4,'.xls');
hExcel.visible = 1;
hWorkbook = hExcel.Workbooks.Open(File2);

hExcel.Range('A1:I1').Select;
set(hExcel.Range('A1:I1').Font,'bold',true);
set(hExcel.Range('A1:I1').Font,'Size',13);
set(hExcel.Range('A1:I1').Interior,'ColorIndex',19);
hExcel.Range('A1:I1').Borders.Item('xlEdgeLeft').Weight          = -4138;
hExcel.Range('A1:I1').Borders.Item('xlEdgeLeft').LineStyle       = 1;
hExcel.Range('A1:I1').Borders.Item('xlEdgeRight').Weight         = -4138;
hExcel.Range('A1:I1').Borders.Item('xlEdgeRight').LineStyle      = 1;
hExcel.Range('A1:I1').Borders.Item('xlEdgeTop').Weight           = -4138;
hExcel.Range('A1:I1').Borders.Item('xlEdgeTop').LineStyle        = 1;
hExcel.Range('A1:I1').Borders.Item('xlEdgeBottom').Weight        = -4138;
hExcel.Range('A1:I1').Borders.Item('xlEdgeBottom').LineStyle     = 1;
hExcel.Range('A1:I1').Borders.Item('xlInsideVertical').Weight    = -4138;
hExcel.Range('A1:I1').Borders.Item('xlInsideVertical').LineStyle = 1;

hExcel.Cells.EntireColumn.AutoFit;

hWorkbook.Save
hWorkbook.Close
hExcel.Quit

%% Post-processed data
B = size(Tracks,2);
for a = 1:B %Build array containing all objects
   if a == 1
      yTracks = Tracks{a};
      yTracks(:,1+size(Tracks{a},2)) = a; %Output number of tracj
      yTracks(:,2+size(Tracks{a},2)) = Tracks{a}(1,3); %Output initial timepoint for track
into each point of track (column 10 of y1)
   else
      yTracks(end+1:end+size(Tracks{a},1),1:(size(yTracks,2)-2)) = Tracks{a};
      yTracks(end+1-size(Tracks{a},1):end,1+size(Tracks{a},2)) = a;
      yTracks(end+1-size(Tracks{a},1):end,2+size(Tracks{a},2)) = Tracks{a}(1,3);
   end
end

%% graph of bacterial parameters
%Create scatter plot with colour map and marker sike depending on speed
if z800 == 0
   SeeAll = questdlg('Do you want to change marker size with speed');
   if strcmp(SeeAll,'Yes') == 1
      SeeAll = 1;
   else
```

```
        SeeAll = 0;
    end
else
    SeeAll = 0;
end

for t = 1:size(Tracks,2)
    n = (t*6)-5;
    r = n+1;
    ru = n+5;

    %display only swimming bug
    ff = size(Tracks{1,t},1);
    xx(1:ff,t) = Tracks{1,t}(1:end,1);
    yy(1:ff,t) = Tracks{1,t}(1:end,2);
    z(1:ff,t)  = Tracks{1,t}(1:end,Choice);
    speed(1:ff,t) = Tracks{1,t}(1:end,7);
end

percentile = prctile(yTracks,[5 95],1);

for a = 1:size(yTracks,1)
    if yTracks(a,Choice) == 0
        yTracks(a,Choice) = nan;
    end
end

maxplot = percentile(2,Choice);
minplot = percentile(1,Choice);

k3 = size(z);
ncol4 = k3(2);
nrows4 = k3(1)-1;

for t = 1:size(yy,2)
    for a = 1:size(yy,1)
        if isnan(yy(a,t)) == 1
            yy(a,t) = 0;
        end
    end
end
for t = 1:size(xx,2)
    for a = 1:size(xx,1)
        if isnan(xx(a,t)) == 1
            xx(a,t) = 0;
        end;
    end;
end

% titles figure
Title{1,3}  = {'tine (s)'};
Title{1,4}  = {'length (\mum)'};
Title{1,5}  = {'width (\mum)'};
Title{1,9}  = {'F'};
Title{1,11} = {'Speed (\mum/s)'};
Title{1,12} = {'Resident time (s)'};
Title{1,13} = {'Speed (\mum/s)'};
Title{1,14} = {'On time (s)'};
Title{1,15} = {'Off time (s)'};
Title{1,16} = {'MSD slope'};
```

```
Title{1,17} = {'ROC (\mum)'};
Title{1,18} = {'Circularity'};

figure
XX = reshape(xx,k3(2)*size(yy,1),1);
YY = reshape(yy,k3(2)*size(yy,1),1);
ZZ = reshape(z,k3(2)*size(yy,1),1);
SPeed = reshape(speed,k3(2)*size(yy,1),1)*10000;
for i = 1:size(SPeed,1)
    if SPeed(i) == 0
        SPeed(i) = 1;
    end
end

if SeeAll == 1
    scatter(XX,YY,SPeed,ZZ,'filled');
else
    scatter(XX,YY,40,ZZ,'filled');
end
caxis([minplot,maxplot])
colormap hot;
h = colorbar;
set(gca, 'color', [0.5843 0.8157 0.9882])

title(h,Title{1,Choice})

set(gca,'XLim',[0 max(yTracks(:,1))],'YLim',[0 max(yTracks(:,2))])
set(gcf,'Position',[100,100,488,400]);
set(gca,'YDir','reverse');

xlabel(strcat('\fontsize{',num2str(20),'} X (\mum)')); % add x axis label
ylabel(strcat('\fontsize{',num2str(20),'} Y (\mum)')); % add y axis label
saveas(gcf,File4,'m');
set(gcf,'pos',[10 10 800 700]);
set(gca,'fontsize',15);
fullFileName = fullfile(File, 'fig');
saveas(gcf,fullFileName,'png');

File=strcat(split,'.mat');
save(File)
clear split;
```

8.3 Appendix 3

VideoMaker

```
function h = VideoMaker(y,TStep,FileName,varargin)
% Script to take y into video sequence
% Takes tracks (y) matrix (track, frame, {Variables})
% Output sequence of images in filename determined directory
% Requires filename of where to save as string defining directory
% varargin will determine font size (default = 10)

%% Setup
frame = [];
Tot=1; %Counter
clear Alldots
if size(varargin,1)==0
```

```
    i=10;
else
    i=varargin{1};
end
TimeStep = (y{1,1}(2,3)-y{1,1}(1,3));
F=char(FileName);
mkdir(F);

load('C://Users/pazalh/Documents/MATLAB/ColourScheme.mat'); %Directory of
where colourscheme saved
CFields=fieldnames(ColourScheme);
clear ColourScheme
Q1=bttnChoiseDialog(CFields, 'Colour Scheme Selection', 'Rainbow','Select Colour
Scheme');
Q1=CFields(Q1);Q1=Q1{1};

%% Pre process data sequence
B = size(y,2);

for a=1:B %Build array containing all objects
    if a == 1
        y1 = y{a};
        y1(:,9)=a;
        y1(:,10)=y{a}(1,3); %Output initial timepoint for track into each point of track
(column 10 of y1)
    else
        y1(end+1:end+size(y{a},1),1:8)=y{a};
        y1(end+1-size(y{a},1):end,9)=a;
        y1(end+1-size(y{a},1):end,10)=y{a}(1,3);
    end
end

B = ceil(y1(end,3)/TimeStep)+1;
%% Create colormap
B1=min(y1(:,3))/TimeStep+1;
for a=1:100
    C1(a,1:3)=colourcalc((B-B1)/100*(a-1),B-B1,Q1);
end
for a=1:6 %Create colormap labels
    C2{a}=num2str(min(y1(:,3))+(a-1)*max(y1(:,3))/5);
end
%% Produce image sequence
for a=B1:B
    close all
    clear f
    f=figure;hold on;
    b=a;
    b=num2str(b);
    if a < 10 % setup naming for filename
        b=strcat('000',b);
    elseif a < 100
        b=strcat('00',b);
    elseif a < 1000
        b=strcat('0',b);
    end
    FileName = strcat(F,'Frame',b,'.png');
    if a==min(y1(:,3))/TimeStep+2
        Alldots(1:size(frame,1),1:4)=frame(:,1:4); % Data set of trails
        clear frame
    elseif a>min(y1(:,3))/TimeStep+2 && exist('frame','var') == 1
```

```
        Alldots(end+1:end+size(frame,1),1:4)=frame(:,1:4); % Data set of trails
        clear frame
    end
    for k = 1 : size(y1,1)
        if round(a-1)==round(y1(k,3)/TimeStep)
            if exist('frame','var') == 0
                frame(1,1:4)=y1(k,1:4); % Current postion of bacteria
                frame(1,5)=y1(k,9);
            else
                frame(end+1,1:4)=y1(k,1:4);
                frame(end,5)=y1(k,9);
            end
        end
    end
    %frame( all(~frame,2), : ) = [];
    if exist('frame','var') == 1
        clear C
        for k = 1:size(frame,1)
            C(k,1:3)=colourcalc(frame(1,10),max(y1(:,3)),Q1); %Chose column to colour
points by in frame(1,?)
        end
        scatter(frame(:,1),frame(:,2),10,C,'filled'); %Conditions for track front
        whitebg(1,'w'); set(gcf,'Color','w');
        if a > min(y1(:,3))/TimeStep+1
            scatter(Alldots(:,1),Alldots(:,2),4,'filled','k'); %Conditions for track rear
        end
    elseif a > min(y1(:,3))/TimeStep+1
        scatter(Alldots(:,1),Alldots(:,2),4,'filled','k'); %Conditions for track rear
    end
    colormap(C1);
    c=colorbar('Ticks',[0,0.2,0.4,0.6,0.8,1],'TickLabels',C2);
    c.Label.String = strcat('\fontsize{',num2str(i),'} time (s)'); %Add colormap label
    set(gca,'XLim',[0 max(y1(:,1))],'YLim',[0 max(y1(:,2))])
    set(gcf,'Position',[100,100,488,400]);
    set(gca,'YDir','reverse');
    set(gca, 'FontSize', i)
    f.PaperPositionMode = 'auto';
    %text(180,180,0,'Glass'); text(180,180,90,'Glass'); %Labels
    time = (a-1)*TimeStep; time=num2str(time);
    if mod((a-1)*TimeStep,1) == 0
        time = strcat(time,'.00');
    elseif mod(a,2)>0
        time = strcat(time,'0');
    end

    time = strcat('\fontsize{',num2str(i),'} t = ',time,' s');
    text(-20,-10,time);% Counter
    xlabel(strcat('\fontsize{',num2str(i),'} X (microns)')); %Add x axis label
    ylabel(strcat('\fontsize{',num2str(i),'} Y (microns)')); %Add y axis label

    saveas(f,FileName);
    %Tot=Tot+size(frame,1);
end
h=y;
```

8.4 Appendix 4

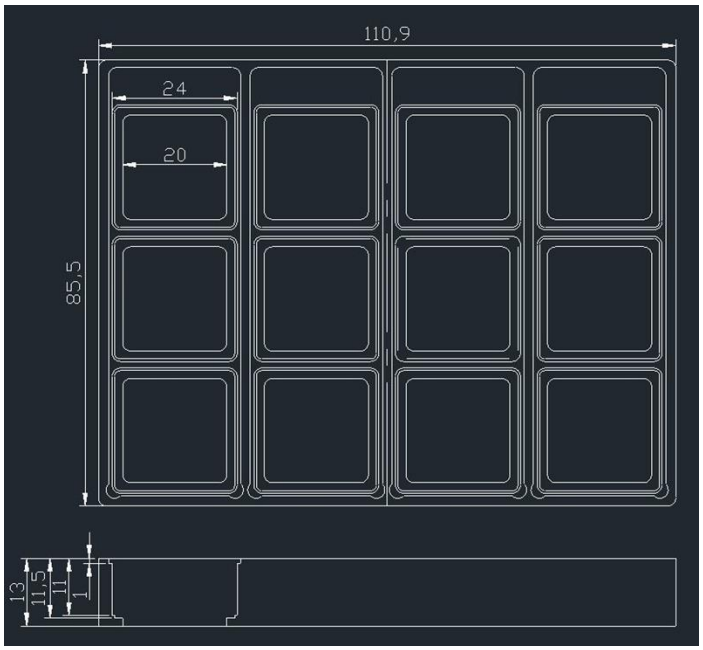

Figure 8.1 Technical drawing of a custom designed 12 wells holder to run multiple samples (measures are in mm).

8.5 Appendix 5

FluorescenceIntensity

```
%% script that identifies fluorescent intensity for pixels DIC objects
% composed by Alessandro Carabelli, 08/2018
% Outputs file Tracks updated with fluorescent intensity (9th row)
 %%import fluorescent files

exist PathNamefluor;
if ans == 0
   off = 1;
else
   off = questdlg('Import new dataset with fluorescent images?');
   if strcmp(off,'Cancel')==1
      STOP=1;
      return
   end
end

a=1;

exist PathNamefluor;
if ans == 0
   [FileNamefluor,PathNamefluor] = uigetfile({'*.tif;*.jpg','Image Files (*.tif,*.jpg)';'*.*','All
Files (*.*)'}, ...
      'Pick a File','MultiSelect','on');
else
   abcdef = strcat('Pick File',num2str(a),' of',num2str(Loops));
```

```
    %abcdef=cellstr(abcdef);
    [FileNamefluor,PathNamefluor] = uigetfile({'*.tif;*.jpg','Image Files (*.tif,*.jpg)';'*.*','All
Files (*.*)'},abcdef,PathNamefluor,'MultiSelect','on');
end

if size(FileNamefluor,1)==1
    FileNamefluor=cellstr(FileNamefluor);
end

FileNameList{a}=FileNamefluor;
PathNameList{a}=PathNamefluor;
clear a;
 %% Import images
FileTiffluor=strcat(PathNamefluor,FileNamefluor);
FileTiffluor=char(FileTiffluor);
InfoImagefluor=imfinfo(FileTiffluor);
mImagefluor=InfoImagefluor(1).Width;
nImagefluor=InfoImagefluor(1).Height;
NumberImagesfluor=length(InfoImagefluor);
FinalImagefluor=zeros(nImagefluor,mImagefluor,NumberImagesfluor,'uint16');

TifLinkfluor = Tiff(FileTiffluor, 'r');
for i=1:NumberImagesfluor
    TifLinkfluor.setDirectory(i);
    FinalImagefluor(:,:,i)=TifLinkfluor.read();
end

%%

height = size(FinalImagefluor,1);
pixels = size(FinalImagefluor,2);
%dimensions = 110;%user defined scale of image
pixelsize=dimensions/pixels;

 %% Subtract alternative background
clear Yfluor
Yfluor=FinalImagefluor(:,:); Y1=FinalImagefluor(:,:,end);
%   Yfluor=im2double(Yfluor);Y1=im2double(Y1);
for a=1:size(Yfluor,2); %converts image data to X,Y,Z coordinates
    x(1+size(Yfluor,1)*(a-1):size(Yfluor,1)+size(Yfluor,1)*(a-1),1)=a;
    for b = 1:size(Yfluor,1);
        y(b+size(Yfluor,1)*(a-1),1)=b;
    end
    z(1+size(Yfluor,1)*(a-1):size(Yfluor,1)+size(Yfluor,1)*(a-
1),1)=Yfluor(1:size(Yfluor,1),a);
end
%
%% Find background signal
% considerat fluorescence expressed at the corners of the image
BackF1=Yfluor(1,1);
BackF2=Yfluor(nImagefluor,1);
BackF3=Yfluor(1,pixels*NumberImagesfluor);
BackF4=Yfluor(nImagefluor,pixels*NumberImagesfluor);
Backaverage= (BackF1+BackF2+BackF3+BackF4)/4;

clear BackF1 BackF2 BackF3 BackF4

for a=1:size(Yfluor,2)
    for b=1:size(Yfluor,1)
```

```
        Yfluor2(b,a)=Yfluor(b,a)-Backaverage;
    end
end
sf = fit([x, y],z,'poly33'); %calculates polynomial plane fit
plot(sf)
a1=sf.p00;
a2=sf.p10;
a3=sf.p01;
a4=sf.p20;
a5=sf.p11;
a6=sf.p02;
a7=sf.p30;
a8=sf.p21;
a9=sf.p12;
a10=sf.p03;
for a=1:size(Yfluor,2);
    for b = 1:size(Yfluor,1);
        Yfluor(b,a)=Yfluor(b,a)-a1-a2*a-a3*b-a4*a^2-a5*a*b-a6*b^2-a7*a^3-a8*a^2*b-
a9*a*b^2-a10*b^3;
    end
end

%%
clear a;
clear b;
for a=1:size(Tracks,2);

    for b=1:size (Tracks{1,a},1);
        if isnan(Tracks{1,a}(b,1))==0 && Tracks{1,a}(b,1)~=0;

            OBJECTSfluor{1,a}(b,1)=floor(Tracks{1,a}(b,1)/pixelsize);
            x9=OBJECTSfluor{1,a}(b,1);
            OBJECTSfluor{1,a}(b,2)=floor(Tracks{1,a}(b,2)/pixelsize);
            y9=OBJECTSfluor{1,a}(b,2);
            if y9>size(Yfluor,1);
                y9=size(Yfluor,1);
            end
            frames= Tracks{1,a}(b,3)/TStep;
            Tracks{1,a}(b,9)=Yfluor(y9,(frames*pixels)+x9);
        else
        end
    end
end
```

8.6 Appendix 6

Table 8.1 Sidak's multiple comparison test with different mutants on pNGPDA and pEGdPEA considering the three branching divisions.

Sidak's multiple comparisons test	Significant?	Summary	P
WT:N vs. WT:E	Yes	****	<0.0001
WT:N vs. pilA:N	Yes	****	<0.0001
WT:N vs. pilA:E	Yes	****	<0.0001
WT:N vs. fliC:N	Yes	****	<0.0001

WT:N vs. fliC:E	Yes	****	<0.0001
WT:N vs. motAB:N	Yes	****	<0.0001
WT:N vs. motAB:E	Yes	****	<0.0001
WT:N vs. motCD:N	Yes	****	<0.0001
WT:N vs. motCD:E	Yes	****	<0.0001
WT:N vs. motAB sadB+:N	Yes	****	<0.0001
WT:N vs. motAB sadB+:E	Yes	****	<0.0001
WT:N vs. motCD sadB+:N	Yes	****	<0.0001
WT:N vs. motCD sadB+:E	Yes	****	<0.0001
WT:N vs. sadB+:N	Yes	****	<0.0001
WT:N vs. sadB+:E	Yes	****	<0.0001
WT:E vs. pilA:N	Yes	****	<0.0001
WT:E vs. pilA:E	Yes	****	<0.0001
WT:E vs. fliC:N	Yes	****	<0.0001
WT:E vs. fliC:E	Yes	****	<0.0001
WT:E vs. motAB:N	Yes	****	<0.0001
WT:E vs. motAB:E	Yes	****	<0.0001
WT:E vs. motCD:N	Yes	****	<0.0001
WT:E vs. motCD:E	Yes	****	<0.0001
WT:E vs. motAB sadB+:N	Yes	****	<0.0001
WT:E vs. motAB sadB+:E	Yes	****	<0.0001
WT:E vs. motCD sadB+:N	Yes	****	<0.0001
WT:E vs. motCD sadB+:E	Yes	****	<0.0001
WT:E vs. sadB+:N	Yes	****	<0.0001
WT:E vs. sadB+:E	Yes	****	<0.0001
pilA:N vs. pilA:E	No	ns	>0.9999
pilA:N vs. fliC:N	No	ns	>0.9999
pilA:N vs. fliC:E	No	ns	0.7505
pilA:N vs. motAB:N	Yes	****	<0.0001
pilA:N vs. motAB:E	Yes	****	<0.0001
pilA:N vs. motCD:N	Yes	****	<0.0001
pilA:N vs. motCD:E	Yes	****	<0.0001
pilA:N vs. motAB sadB+:N	Yes	****	<0.0001
pilA:N vs. motAB sadB+:E	Yes	****	<0.0001
pilA:N vs. motCD sadB+:N	Yes	****	<0.0001
pilA:N vs. motCD sadB+:E	Yes	****	<0.0001
pilA:N vs. sadB+:N	No	ns	0.9791
pilA:N vs. sadB+:E	No	ns	0.8374
pilA:E vs. fliC:N	No	ns	>0.9999
pilA:E vs. fliC:E	No	ns	0.2122

pilA:E vs. motAB:N	Yes	****	<0.0001
pilA:E vs. motAB:E	Yes	****	<0.0001
pilA:E vs. motCD:N	Yes	****	<0.0001
pilA:E vs. motCD:E	Yes	****	<0.0001
pilA:E vs. motAB sadB+:N	Yes	****	<0.0001
pilA:E vs. motAB sadB+:E	Yes	****	<0.0001
pilA:E vs. motCD sadB+:N	Yes	****	<0.0001
pilA:E vs. motCD sadB+:E	Yes	****	<0.0001
pilA:E vs. sadB+:N	No	ns	>0.9999
pilA:E vs. sadB+:E	No	ns	0.9984
fliC:N vs. fliC:E	No	ns	0.7882
fliC:N vs. motAB:N	Yes	****	<0.0001
fliC:N vs. motAB:E	Yes	****	<0.0001
fliC:N vs. motCD:N	Yes	****	<0.0001
fliC:N vs. motCD:E	Yes	****	<0.0001
fliC:N vs. motAB sadB+:N	Yes	****	<0.0001
motCD sadB+:N vs. motCD sadB+:E	Yes	****	<0.0001
motCD sadB+:N vs. sadB+:N	Yes	****	<0.0001
motCD sadB+:N vs. sadB+:E	Yes	****	<0.0001
motCD sadB+:E vs. sadB+:N	Yes	****	<0.0001
motCD sadB+:E vs. sadB+:E	Yes	****	<0.0001
sadB+:N vs. sadB+:E	No	ns	>0.9999
fliC:N vs. motAB sadB+:E	Yes	****	<0.0001
fliC:N vs. motCD sadB+:N	Yes	****	<0.0001
fliC:N vs. motCD sadB+:E	Yes	****	<0.0001
fliC:N vs. sadB+:N	No	ns	0.9704
fliC:N vs. sadB+:E	No	ns	0.8041
fliC:E vs. motAB:N	Yes	****	<0.0001
fliC:E vs. motAB:E	Yes	****	<0.0001
fliC:E vs. motCD:N	Yes	****	<0.0001
fliC:E vs. motCD:E	Yes	****	<0.0001
fliC:E vs. motAB sadB+:N	Yes	****	<0.0001
fliC:E vs. motAB sadB+:E	Yes	****	<0.0001
fliC:E vs. motCD sadB+:N	Yes	****	<0.0001
fliC:E vs. motCD sadB+:E	Yes	****	<0.0001
fliC:E vs. sadB+:N	Yes	*	0.0241
fliC:E vs. sadB+:E	Yes	**	0.0044
motAB:N vs. motAB:E	Yes	****	<0.0001
motAB:N vs. motCD:N	Yes	****	<0.0001
motAB:N vs. motCD:E	Yes	****	<0.0001

motAB:N vs. motAB sadB+:N	Yes	****	<0.0001
motAB:N vs. motAB sadB+:E	Yes	****	<0.0001
motAB:N vs. motCD sadB+:N	Yes	****	<0.0001
motAB:N vs. motCD sadB+:E	Yes	****	<0.0001
motAB:N vs. sadB+:N	Yes	****	<0.0001
motAB:N vs. sadB+:E	Yes	****	<0.0001
motAB:E vs. motCD:N	Yes	****	<0.0001
motAB:E vs. motCD:E	Yes	****	<0.0001
motAB:E vs. motAB sadB+:N	Yes	****	<0.0001
motAB:E vs. motAB sadB+:E	Yes	****	<0.0001
motAB:E vs. motCD sadB+:N	Yes	****	<0.0001
motAB:E vs. motCD sadB+:E	Yes	****	<0.0001
motAB:E vs. sadB+:N	Yes	****	<0.0001
motAB:E vs. sadB+:E	Yes	****	<0.0001
motCD:N vs. motCD:E	Yes	****	<0.0001
motCD:N vs. motAB sadB+:N	Yes	****	<0.0001
motCD:N vs. motAB sadB+:E	Yes	****	<0.0001
motCD:N vs. motCD sadB+:N	No	ns	0.5069
motCD:N vs. motCD sadB+:E	Yes	****	<0.0001
motCD:N vs. sadB+:N	Yes	****	<0.0001
motCD:N vs. sadB+:E	Yes	****	<0.0001
motCD:E vs. motAB sadB+:N	Yes	****	<0.0001
motCD:E vs. motAB sadB+:E	Yes	****	<0.0001
motCD:E vs. motCD sadB+:N	Yes	****	<0.0001
motCD:E vs. motCD sadB+:E	No	ns	0.3224
motCD:E vs. sadB+:N	Yes	****	<0.0001
motCD:E vs. sadB+:E	Yes	****	<0.0001
motAB sadB+:N vs. motAB sadB+:E	Yes	****	<0.0001
motAB sadB+:N vs. motCD sadB+:N	Yes	****	<0.0001
motAB sadB+:N vs. motCD sadB+:E	Yes	****	<0.0001
motAB sadB+:N vs. sadB+:N	Yes	****	<0.0001
motAB sadB+:N vs. sadB+:E	Yes	****	<0.0001
motAB sadB+:E vs. motCD sadB+:N	Yes	****	<0.0001
motAB sadB+:E vs. motCD sadB+:E	Yes	****	<0.0001
motAB sadB+:E vs. sadB+:N	Yes	****	<0.0001
motAB sadB+:E vs. sadB+:E	Yes	****	<0.0001

8.7 Appendix 7

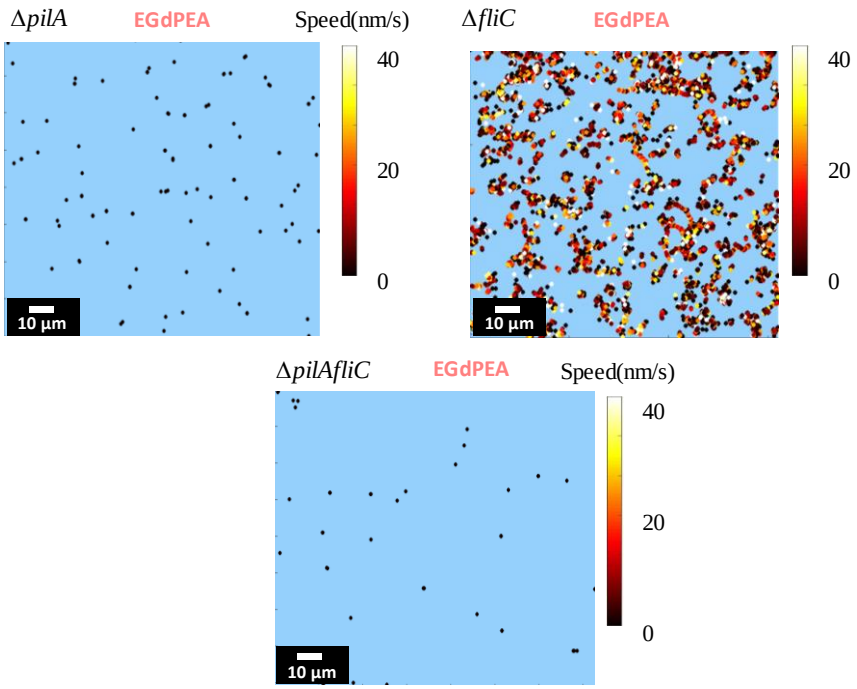

Figure 8.2 Representative colour maps of tracks of *P. aeruginosa* Δ*pilA* (top-left) Δ*fliC* (top-right) and *ΔpilAΔfliC* (bottom) on pEGdPEA measured in situ over 1 h of exposure to surfaces. No motility was observed using *P. aeruginosa* Δ*pilA*. On the contrary, motility was observed using *P. aeruginosa* Δ*fliC*. Thus, motility observed was T4P driven. Scale bar is 10 µm.

8.8 Appendix 8

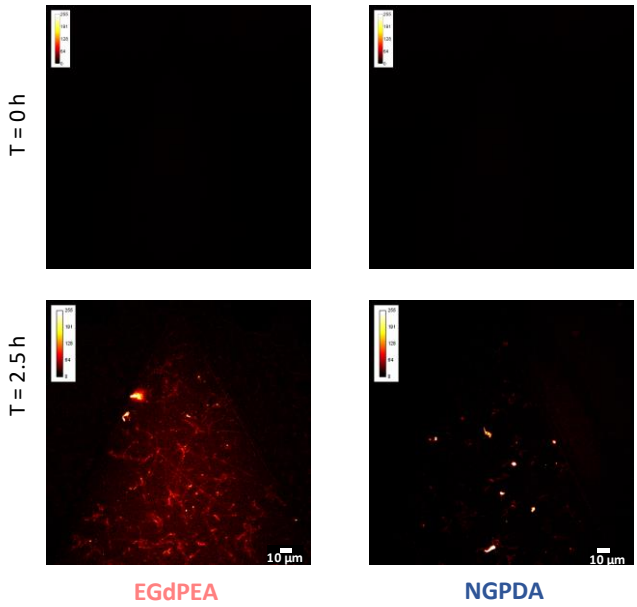

Figure 8.3 CLSM images captured a t = 0 h (top) and t = 2.5 h (bottom) on pEGdPEA (right) and pNGPDA (left). Scale bar is 10 µm.

8.9 **Appendix 9**

Table 8.2 Sidak's multiple comparison test with different mutants on pNGPDA and pEGdPEA considering the fraction of cells expressing c-di-GMP.

Sidak's multiple comparisons test	Significant?	Summary	Adjusted P Value
WT:N vs. WT:E	Yes	*	0.0106
WT:N vs. motAB:N	Yes	****	<0.0001
WT:N vs. motAB:E	Yes	****	<0.0001
WT:N vs. motCD:N	Yes	****	<0.0001
WT:N vs. motCD:E	Yes	****	<0.0001
WT:N vs. motABCD:N	Yes	****	<0.0001
WT:N vs. motABCD:E	Yes	****	<0.0001
WT:N vs. sadB+:N	No	ns	>0.9999
WT:N vs. sadB+:E	No	ns	>0.9999
WT:N vs. motAB sadb+:N	No	ns	0.2431
WT:N vs. motAB sadb+:E	Yes	*	0.0241
WT:N vs. motCD sadB+:N	Yes	****	<0.0001
WT:N vs. motCD sadB+:E	Yes	**	0.0031
WT:N vs. motABCD sadb+:N	Yes	****	<0.0001
WT:N vs. motABCD sadb+:E	Yes	****	<0.0001
WT:E vs. motAB:N	Yes	**	0.0014
WT:E vs. motAB:E	Yes	**	0.0025
WT:E vs. motCD:N	No	ns	>0.9999
WT:E vs. motCD:E	Yes	**	0.0039
WT:E vs. motABCD:N	Yes	****	<0.0001
WT:E vs. motABCD:E	Yes	****	<0.0001
WT:E vs. sadB+:N	Yes	**	0.0053
WT:E vs. sadB+:E	Yes	***	0.0006
WT:E vs. motAB sadb+:N	No	ns	>0.9999
WT:E vs. motAB sadb+:E	No	ns	>0.9999
WT:E vs. motCD sadB+:N	No	ns	0.9998
WT:E vs. motCD sadB+:E	No	ns	>0.9999
WT:E vs. motABCD sadb+:N	Yes	****	<0.0001
WT:E vs. motABCD sadb+:E	Yes	****	<0.0001
motAB:N vs. motAB:E	No	ns	>0.9999
motAB:N vs. motCD:N	No	ns	0.1616
motAB:N vs. motCD:E	No	ns	>0.9999
motAB:N vs. motABCD:N	No	ns	0.9946

motAB:N vs. motABCD:E	No	ns	>0.9999
motAB:N vs. sadB+:N	Yes	****	<0.0001
motAB:N vs. sadB+:E	Yes	****	<0.0001
motAB:N vs. motAB sadb+:N	Yes	ns	>0.9999
motAB:N vs. motAB sadb+:E	Yes	***	0.0006
motAB:N vs. motCD sadB+:N	No	ns	0.2463
motAB:N vs. motCD sadB+:E	Yes	**	0.0049
motAB:N vs. motABCD sadb+:N	No	ns	>0.9999
motAB:N vs. motABCD sadb+:E	No	ns	0.922
motAB:E vs. motCD:N	No	ns	0.2598
motAB:E vs. motCD:E	No	ns	>0.9999
motAB:E vs. motABCD:N	No	ns	0.9641
motAB:E vs. motABCD:E	No	ns	0.9995
motAB:E vs. sadB+:N	Yes	****	<0.0001
motAB:E vs. sadB+:E	Yes	****	<0.0001
motAB:E vs. motAB sadb+:N	Yes	****	<0.0001
motAB:E vs. motAB sadb+:E	Yes	ns	>0.9999
motAB:E vs. motCD sadB+:N	No	ns	0.3798
motAB:E vs. motCD sadB+:E	Yes	**	0.0088
motAB:E vs. motABCD sadb+:N	No	ns	0.9982
motAB:E vs. motABCD sadb+:E	No	ns	0.7951
motCD:N vs. motCD:E	No	ns	0.3581
motCD:N vs. motABCD:N	Yes	***	0.0004
motCD:N vs. motABCD:E	Yes	**	0.0013
motCD:N vs. sadB+:N	Yes	****	<0.0001
motCD:N vs. sadB+:E	Yes	****	<0.0001
motCD:N vs. motAB sadb+:N	No	ns	0.5833
motCD:N vs. motAB sadb+:E	No	ns	0.999
motCD:N vs. motCD sadB+:N	No	**	0.0017
motCD:N vs. motCD sadB+:E	No	ns	>0.9999
motCD:N vs. motABCD sadb+:N	Yes	***	0.001
motCD:N vs. motABCD sadb+:E	Yes	***	0.0002
motCD:E vs. motABCD:N	No	ns	0.9056
motCD:E vs. motABCD:E	No	ns	0.996
motCD:E vs. sadB+:N	Yes	****	<0.0001
motCD:E vs. sadB+:E	Yes	****	<0.0001
motCD:E vs. motAB sadb+:N	Yes	***	0.0001
motCD:E vs. motAB sadb+:E	Yes	**	0.0017
motCD:E vs. motCD sadB+:N	No	ns	0.5025
motCD:E vs. motCD sadB+:E	Yes	*	0.0134

motCD:E vs. motABCD sadb+:N	No	ns	0.9895
motCD:E vs. motABCD sadb+:E	No	ns	0.6684
motABCD:N vs. motABCD:E	No	ns	>0.9999
motABCD:N vs. sadB+:N	Yes	****	<0.0001
motABCD:N vs. sadB+:E	Yes	****	<0.0001
motABCD:N vs. motAB sadb+:N	Yes	****	<0.0001
motABCD:N vs. motAB sadb+:E	Yes	****	<0.0001
motABCD:N vs. motCD sadB+:N	Yes	***	0.0007
motABCD:N vs. motCD sadB+:E	Yes	****	<0.0001
motABCD:N vs. motABCD sadb+:N	No	ns	>0.9999
motABCD:N vs. motABCD sadb+:E	No	ns	>0.9999
motABCD:E vs. sadB+:N	Yes	****	<0.0001
motABCD:E vs. sadB+:E	Yes	****	<0.0001
motABCD:E vs. motAB sadb+:N	Yes	****	<0.0001
motABCD:E vs. motAB sadb+:E	Yes	****	<0.0001
motABCD:E vs. motCD sadB+:N	Yes	**	0.0021
motABCD:E vs. motCD sadB+:E	Yes	****	<0.0001
motABCD:E vs. motABCD sadb+:N	No	ns	>0.9999
motABCD:E vs. motABCD sadb+:E	No	ns	>0.9999
sadB+:N vs. sadB+:E	No	ns	>0.9999
sadB+:N vs. motAB sadb+:N	No	ns	0.1348
sadB+:N vs. motAB sadb+:E	Yes	*	0.0121
sadB+:N vs. motCD sadB+:N	Yes	****	<0.0001
sadB+:N vs. motCD sadB+:E	Yes	**	0.0015
sadB+:N vs. motABCD sadb+:N	Yes	****	<0.0001
sadB+:N vs. motABCD sadb+:E	Yes	****	<0.0001
sadB+:E vs. motAB sadb+:N	Yes	*	0.0169
sadB+:E vs. motAB sadb+:E	Yes	**	0.0013
sadB+:E vs. motCD sadB+:N	Yes	****	<0.0001
sadB+:E vs. motCD sadB+:E	Yes	***	0.0002
sadB+:E vs. motABCD sadb+:N	Yes	****	<0.0001
sadB+:E vs. motABCD sadb+:E	Yes	****	<0.0001
motAB sadb+:N vs. motAB sadb+:E	No	ns	>0.9999
motAB sadb+:N vs. motCD sadB+:N	No	ns	0.4281
motAB sadb+:N vs. motCD sadB+:E	No	ns	>0.9999
motAB sadb+:N vs. motABCD sadb+:N	Yes	****	<0.0001
motAB sadb+:N vs. motABCD sadb+:E	Yes	****	<0.0001
motAB sadb+:E vs. motCD sadB+:N	No	ns	0.9908
motAB sadb+:E vs. motCD sadB+:E	No	ns	>0.9999
motAB sadb+:E vs. motABCD sadb+:N	Yes	****	<0.0001

motAB sadb+:E vs. motABCD sadb+:E	Yes	****	<0.0001
motCD sadB+:N vs. motCD sadB+:E	No	ns	>0.9999
motCD sadB+:N vs. motABCD sadb+:N	Yes	**	0.0016
motCD sadB+:N vs. motABCD sadb+:E	Yes	***	0.0003
motCD sadB+:E vs. motABCD sadb+:N	Yes	****	<0.0001
motCD sadB+:E vs. motABCD sadb+:E	Yes	****	<0.0001
motABCD sadb+:N vs. motABCD sadb+:E	No	ns	>0.9999

Bibliography

1. O'Neill, J., *The review on antimicrobial resistance: tackling drug-resistant infections globally*. 2014.

2. Mann, E.E. and Wozniak, D.J., *Pseudomonas biofilm matrix composition and niche biology*. Fems Microbiology Reviews, 2012. **36**(4): p. 893-916.

3. Davies, D., *Understanding biofilm resistance to antibacterial agents.* Nature Reviews Drug Discovery, 2003. **2**(2): p. 114-122.

4. Fisher, L.E., Hook, A.L., Ashraf, W., Yousef, A., Barrett, D.A., Scurr, D.J., Chen, X.Y., Smith, E.F., Fay, M., Parmenter, C.D.J., Parkinson, R., and Bayston, R., *Biomaterial modification of urinary catheters with antimicrobials to give long-term broadspectrum antibiofilm activity.* Journal of Controlled Release, 2015. **202**: p. 57-64.

5. Hook, A.L., Chang, C.Y., Scurr, D.J., Langer, R., Anderson, D.G., Williams, P., Davies, M.C. and Alexander, M.R., *Thermally switchable polymers achieve controlled Escherichia coli detachment.* Advanced Healthcare Materials, 2014. **3**(7): p. 1020-1025.

6. Hook, A.L., Scurr, D.J., Anderson, D.G., Langer, R., Williams, P., Davies, M. and Alexander, M.R., *High throughput discovery of thermo-responsive materials using water contact angle measurements and time-of-flight secondary ion mass spectrometry.* Surface and Interface Analysis, 2013. **45**(1): p. 181-184.

7. Hook, A.L., Chang, C.Y., Yang, J., Luckett, J., Cockayne, A., Atkinson, S., Mei, Y., Bayston, R., Irvine, D.J., Langer, R., Anderson, D.G., Williams, P., Davies, M.C., and Alexander, M.R., *Combinatorial discovery of polymers resistant to bacterial attachment.* Nature Biotechnology, 2012. **30**(9): p. 868.

8. Sanni, O., Chang, C.Y., Anderson, D.G., Langer, R., Davies, M.C., Williams, P.M., Williams, P., Alexander, M.R. and Hook, A.L., *Bacterial Attachment to Polymeric Materials Correlates with Molecular Flexibility and Hydrophilicity.* Advanced Healthcare Materials, 2015. **4**(5): p. 695-701.

9. Liu, C., Xia, Z. and Czernuszka, J.T., *Design and development of three-dimensional scaffolds for tissue engineering.* Chemical Engineering Research & Design, 2007. **85**(7): p. 1051-1064.

10. *What is a medical device?* ; Available from: https://www.lifechanginginnovation.org/about-us/what-medical-device.

11. van Kleef, E., Robotham, J.V., Jit, M., Deeny, S.R. and Edmunds, W.J., *Modelling the transmission of healthcare associated infections: a systematic review.* Bmc Infectious Diseases, 2013. **13**(294).

12. Percival, S.L., Suleman, L., Vuotto, C. and Donelli, G., *Healthcare-associated infections, medical devices and biofilms: risk, tolerance and control.* Journal of Medical Microbiology, 2015. **64**(4): p. 323-34.

13. Rochford, E.T., Richards, R.G. and Moriarty, T.F., *Influence of material on the development of device-associated infections.* Clinical Microbiology Infectiions, 2012. **18**(12): p. 1162-1167.

14. Arciola, C.R., Campoccia, D. and Montanaro, L., *Implant infections: adhesion, biofilm formation and immune evasion.* Nature Review Microbiology, 2018. **16**(7): p. 397-409.

15. Bisht, R. and Saxena, P., *Antibiotic abuse: post-antibiotic apocalypse, superbugs and superfoods.* Current Science, 2019. **116**(7): p. 1055-1056.

16. *2016-2060 Deaths - World Health Organization*. 2018; Available from: http://www.who.int/healthinfo/global_burden_disease/GHE_DthWBInc_Proj_2016-2060.xlsx.

17. Douafer, H., Andrieu, V., Phanstiel, O.t. and Brunel, J.M., *Antibiotic Adjuvants: Make Antibiotics Great Again!* Journal of Medical Chemistry, 2019.

18. Guitor, A.K. and Wright, G.D., *Antimicrobial Resistance and Respiratory Infections.* Chest, 2018. **154**(5): p. 1202-1212.

19. Lloyd-Price, J., Abu-Ali, G. and Huttenhower, C., *The healthy human microbiome.* Genome Medicine, 2016. **8**(51).

20. Sleator, R.D. and Hill, C., *Patho-biotechnology: using bad bugs to do good-things.* Current Opinion in Biotechnology, 2006. **17**(2): p. 211-216.

21. Costerton, J.W., Cheng, K.J., Geesey, G.G., Ladd, T.I., Nickel, J.C., Dasgupta, M. and Marrie, T.J., *Bacterial biofilms in nature and disease.* Annual Review of Microbiology, 1987. **41**: p. 435-464.

22. Webb, J.S., Givskov, M. and Kjelleberg, S., *Bacterial biofilms: prokaryotic adventures in multicellularity.* Current Opinions in Microbiology, 2003. **6**(6): p. 578-585.

23. Costerton, J.W., Lewandowski, Z., Caldwell, D.E., Korber, D.R. and Lappin-Scott, H.M., *Microbial biofilms.* Annual Review of Microbiology, 1995. **49**: p. 711-745.

24. Davies, D.G., Parsek, M.R., Pearson, J.P., Iglewski, B.H., Costerton, J.W. and Greenberg, E.P., *The involvement of cell-to-cell signals in the development of a bacterial biofilm.* Science, 1998. **280**(5361): p. 295-298.

25. Bayles, K.W., *The biological role of death and lysis in biofilm development.* Nature Reviews Microbiology, 2007. **5**(9): p. 721-6.

26. *Bacteria Biofilm Under Microscope*. Available from: http://starawaterhygiene.co.uk/service-list/home-h20-water-disinfection-service/.

27. Vlamakis, H., Aguilar, C., Losick, R. and Kolter, R., *Control of cell fate by the formation of an architecturally complex bacterial community.* Genes Development, 2008. **22**(7): p. 945-953.

28. Haagensen, J.A., Klausen, M., Ernst, R.K., Miller, S.I., Folkesson, A., Tolker-Nielsen, T. and Molin, S., *Differentiation and distribution of colistin- and sodium dodecyl sulfate-tolerant cells in Pseudomonas aeruginosa biofilms.* Journal of Bacteriology, 2007. **189**(1): p. 28-37.

29. Feng, J.S., Ma, L.N., Nie, J.T., Konkel, M.E. and Lu, X.N., *Environmental Stress-Induced Bacterial Lysis and Extracellular DNA Release Contribute to Campylobacter jejuni Biofilm Formation.* Applied and Environmental Microbiology, 2018. **84**(5).

30. Ciofu, O. and Tolker-Nielsen, T., *Tolerance and Resistance of Pseudomonas aeruginosa Biofilms to Antimicrobial Agents-How P. aeruginosa Can Escape Antibiotics.* Frontiers in Microbiology, 2019. **10**(913).

31. Hall-Stoodley, L., Costerton, J.W. and Stoodley, P., *Bacterial biofilms: from the natural environment to infectious diseases.* Nature Reviews Microbiology, 2004. **2**(2): p. 95-108.

32. Mah, T.F.C. and O'Toole, G.A., *Mechanisms of biofilm resistance to antimicrobial agents.* Trends in Microbiology, 2001. **9**(1): p. 34-39.

33. Stewart, P.S., Zhang, T.Y., Xu, R.F., Pitts, B., Walters, M.C., Roe, F., Kikhney, J. and Moter, A., *Reaction-diffusion theory explains hypoxia and heterogeneous growth within microbial biofilms associated with chronic infections.* Npj Biofilms and Microbiomes, 2016. **2**.

34. Chandra, J., Patel, J.D., Li, J., Zhou, G., Mukherjee, P.K., McCormick, T.S., Anderson, J.M. and Ghannoum, M.A., *Modification of surface properties of biomaterials influences the ability of Candida albicans to form biofilms.* Applied and Environmental Microbiology, 2005. **71**(12): p. 8795-8801.

35. Stoodley, P., Sauer, K., Davies, D.G. and Costerton, J.W., *Biofilms as complex differentiated communities.* Annual Review of Microbiology, 2002. **56**: p. 187-209.

36. O'Toole, G.A. and Kolter, R., *Flagellar and twitching motility are necessary for Pseudomonas aeruginosa biofilm development.* Molecular Microbiology 1998. **30**(2): p. 295-304.

37. Ramsey, M.M. and Whiteley, M., *Pseudomonas aeruginosa attachment and biofilm development in dynamic environments.* Molecular Microbiology, 2004. **53**(4): p. 1075-87.

38. O'Toole, G., Kaplan, H.B. and Kolter, R., *Biofilm formation as microbial development.* Annual Review of Microbiology, 2000. **54**: p. 49-79.

39. Landry, R.M., An, D., Hupp, J.T., Singh, P.K. and Parsek, M.R., *Mucin-Pseudomonas aeruginosa interactions promote biofilm formation and antibiotic resistance.* Molecular Microbiology, 2006. **59**(1): p. 142-51.

40. Dewanti, R. and Wong, A.C., *Influence of culture conditions on biofilm formation by Escherichia coli O157:H7.* International Journal of Food Microbiology, 1995. **26**(2): p. 147-164.

41. Agladze, K., Wang, X. and Romeo, T., *Spatial periodicity of Escherichia coli K-12 biofilm microstructure initiates during a reversible, polar attachment phase of development and requires the polysaccharide adhesin PGA.* Journal of Bacteriology, 2005. **187**(24): p. 8237-8246.

42. Sauer, K., Camper, A.K., Ehrlich, G.D., Costerton, J.W. and Davies, D.G., *Pseudomonas aeruginosa displays multiple phenotypes during development as a biofilm.* Journal of Bacteriology, 2002. **184**(4): p. 1140-1154.

43. Vasseur, P., Vallet-Gely, I., Soscia, C., Genin, S. and Filloux, A., *The pel genes of the Pseudomonas aeruginosa PAK strain are involved at early and late stages of biofilm formation.* Microbiology, 2005. **151**(3): p. 985-997.

44. Jackson, K.D., Starkey, M., Kremer, S., Parsek, M.R. and Wozniak, D.J., *Identification of psl, a locus encoding a potential exopolysaccharide that is essential for Pseudomonas aeruginosa PAO1 biofilm formation.* Journal of Bacteriology, 2004. **186**(14): p. 4466-4475.

45. Pratt, L.A. and Kolter, R., *Genetic analysis of Escherichia coli biofilm formation: roles of flagella, motility, chemotaxis and type I pili.* Molecular Microbiology, 1998. **30**(2): p. 285-293.

46. Klausen, M., Aaes-Jorgensen, A., Molin, S. and Tolker-Nielsen, T., *Involvement of bacterial migration in the development of complex multicellular structures in Pseudomonas aeruginosa biofilms.* Molecular Microbiology, 2003. **50**(1): p. 61-68.

47. Jenal, U. and Malone, J., *Mechanisms of cyclic-di-GMP signaling in bacteria.* Annual Review of Genetics, 2006. **40**: p. 385-407.

48. Romling, U. and Amikam, D., *Cyclic di-GMP as a second messenger.* Current Opinion in Microbiology, 2006. **9**(2): p. 218-28.

49. Ryan, R.P., Fouhy, Y., Lucey, J.F. and Dow, J.M., *Cyclic di-GMP signaling in bacteria: recent advances and new puzzles.* Journal of Bacteriology, 2006. **188**(24): p. 8327-8334.

50. Sriramulu, D.D., Lunsdorf, H., Lam, J.S. and Romling, U., *Microcolony formation: a novel biofilm model of Pseudomonas aeruginosa for the cystic fibrosis lung.* Journal of Medical Microbiology, 2005. **54**(Pt 7): p. 667-676.

51. Hermanowicz, S.W., *A simple 2D biofilm model yields a variety of morphological features.* Mathematical Biosciences, 2001. **169**(1): p. 1-14.

52. Klausen, M., Gjermansen, M., Kreft, J.U. and Tolker-Nielsen, T., *Dynamics of development and dispersal in sessile microbial communities: examples from Pseudomonas aeruginosa and Pseudomonas putida model biofilms.* FEMS Microbiology Letters, 2006. **261**(1): p. 1-11.

53. Parsek, M.R. and Tolker-Nielsen, T., *Pattern formation in Pseudomonas aeruginosa biofilms.* Current Opinion in Microbiology, 2008. **11**(6): p. 560-566.

54. Sauer, K., Cullen, M.C., Rickard, A.H., Zeef, L.A., Davies, D.G. and Gilbert, P., *Characterization of nutrient-induced dispersion in Pseudomonas aeruginosa PAO1 biofilm.* Journal of Bacteriology, 2004. **186**(21): p. 7312-7326.

55. Barraud, N., Hassett, D.J., Hwang, S.H., Rice, S.A., Kjelleberg, S. and Webb, J.S., *Involvement of nitric oxide in biofilm dispersal of Pseudomonas aeruginosa.* Journal of Bacteriology, 2006. **188**(21): p. 7344-7353.

56. Donlan, R.M., *Biofilms and device-associated infections.* Emerging Infectious Diseases, 2001. **7**(2): p. 277-281.

57. Tamar, E., Koler, M. and Vaknin, A., *The role of motility and chemotaxis in the bacterial colonization of protected surfaces.* Scientific Reports, 2016. **6**.

58. Kazmierczak, B.I., Schniederberend, M. and Jain, R., *Cross-regulation of Pseudomonas motility systems: the intimate relationship between flagella, pili and virulence.* Current Opinion in Microbiology, 2015. **28**: p. 78-82.

59. Proft, T. and Baker, E.N., *Pili in Gram-negative and Gram-positive bacteria - structure, assembly and their role in disease.* Cellular and Molecular Life Sciences, 2009. **66**(4): p. 613-635.

60. Laventie, B.J., Sangermani, M., Estermann, F., Manfredi, P., Planes, R., Hug, I., Jaeger, T., Meunier, E., Broz, P., and Jenal, U., *A Surface-*

Induced Asymmetric Program Promotes Tissue Colonization by Pseudomonas aeruginosa. Cell Host & Microbe, 2019. **25**(1): p. 140.

61. Costa, T.R., Felisberto-Rodrigues, C., Meir, A., Prevost, M.S., Redzej, A., Trokter, M. and Waksman, G., *Secretion systems in Gram-negative bacteria: structural and mechanistic insights.* Nature Reviews Microbiology, 2015. **13**(6): p. 343-359.

62. Jones, C.H., Pinkner, J.S., Roth, R., Heuser, J., Nicholes, A.V., Abraham, S.N. and Hultgren, S.J., *FimH adhesin of type 1 pili is assembled into a fibrillar tip structure in the Enterobacteriaceae.* Proceedings of the National Academy of Sciences of the United States of America, 1995. **92**(6): p. 2081-2085.

63. Rocha, S.P., Pelayo, J.S. and Elias, W.P., *Fimbriae of uropathogenic Proteus mirabilis.* FEMS Immunology and Medical Microbiology, 2007. **51**(1): p. 1-7.

64. Kuehn, M.J., Heuser, J., Normark, S. and Hultgren, S.J., *P pili in uropathogenic E. coli are composite fibres with distinct fibrillar adhesive tips.* Nature, 1992. **356**(6366): p. 252-255.

65. Busch, A., Phan, G. and Waksman, G., *Molecular mechanism of bacterial type 1 and P pili assembly.* Philosophical Transactions of The Royal Society A Mathematical Physical and Engineering Sciences, 2015. **373**(2036).

66. Vallet, I., Diggle, S.P., Stacey, R.E., Camara, M., Ventre, I., Lory, S., Lazdunski, A., Williams, P. and Filloux, A., *Biofilm formation in Pseudomonas aeruginosa: Fimbrial cup gene clusters are controlled by the transcriptional regulator MvaT.* Journal of Bacteriology, 2004. **186**(9): p. 2880-2890.

67. Mikkelsen, H., Sivaneson, M. and Filloux, A., *Key two-component regulatory systems that control biofilm formation in Pseudomonas aeruginosa.* Environmental Microbiology, 2011. **13**(7): p. 1666-1681.

68. Salzer, R., Joos, F. and Averhoff, B., *Type IV pilus biogenesis, twitching motility, and DNA uptake in Thermus thermophilus: discrete roles of antagonistic ATPases PilF, PilT1, and PilT2.* Applied and Environmental Microbiology, 2014. **80**(2): p. 644-652.

69. Burrows, L.L., *Pseudomonas aeruginosa twitching motility: type IV pili in action.* Annual Review of Microbiology, 2012. **66**: p. 493-520.

70. Gold, V.A., Salzer, R., Averhoff, B. and Kuhlbrandt, W., *Structure of a type IV pilus machinery in the open and closed state.* Elife, 2015. **4**.

71. Mattick, J.S., *Type IV pili and twitching motility.* Annual Review of Microbiology, 2002. **56**: p. 289-314.

72. Karuppiah, V. and Derrick, J.P., *Structure of the PilM-PilN inner membrane type IV pilus biogenesis complex from Thermus thermophilus.* Journal of Biological Chemistry, 2011. **286**(27): p. 24434-24442.

73. Hahn, H.P., *The type-4 pilus is the major virulence-associated adhesin of Pseudomonas aeruginosa - A review.* Gene, 1997. **192**(1): p. 99-108.

74. Persat, A., Inclan, Y.F., Engel, J.N., Stone, H.A. and Gitai, Z., *Type IV pili mechanochemically regulate virulence factors in Pseudomonas aeruginosa.* Proceedings of the National Academy of Sciences of the United States of America, 2015. **112**(24): p. 7563-7568.

75. Arts, J., van Boxtel, R., Filloux, A., Tommassen, J. and Koster, M., *Export of the pseudopilin XcpT of the Pseudomonas aeruginosa type II secretion system via the signal recognition particle-Sec pathway.* Journal of Bacteriology, 2007. **189**(5): p. 2069-2076.

76. Nunn, D.N. and Lory, S., *Product of the Pseudomonas-Aeruginosa Gene Pild Is a Prepilin Leader Peptidase.* Proceedings of the National Academy of Sciences of the United States of America, 1991. **88**(8): p. 3281-3285.

77. Strom, M.S. and Lory, S., *Amino-Acid Substitutions in Pilin of Pseudomonas-Aeruginosa - Effect on Leader Peptide Cleavage, Amino-Terminal Methylation, and Pilus Assembly.* Journal of Biological Chemistry, 1991. **266**(3): p. 1656-1664.

78. Morand, P.C., Bille, E., Morelle, S., Eugene, E., Beretti, J.L., Wolfgang, M., Meyer, T.F., Koomey, M. and Nassif, X., *Type IV pilus retraction in pathogenic Neisseria is regulated by the PilC proteins.* Embo Journal, 2004. **23**(9): p. 2009-2017.

79. Goyal, P., Krasteva, P.V., Van Gerven, N., Gubellini, F., Van den Broeck, I., Troupiotis-Tsailaki, A., Jonckheere, W., Pehau-Arnaudet, G., Pinkner, J.S., Chapman, M.R., Hultgren, S.J., Howorka, S., Fronzes, R., and Remaut, H., *Structural and mechanistic insights into the bacterial amyloid secretion channel CsgG.* Nature, 2014. **516**(7530): p. 250-253.

80. Chang, C., Huang, I.H., Hendrickx, A.P. and Ton-That, H., *Visualization of Gram-positive bacterial pili.* Methods in Molecular Biology, 2013. **966**: p. 77-95.

81. Tsai, J.Y.C., Loh, J.M.S., Clow, F., Lorenz, N. and Proft, T., *The Group A Streptococcus serotype M2 pilus plays a role in host cell adhesion and immune evasion.* Molecular Microbiology, 2017. **103**(2): p. 282-298.

82. Morimoto, Y.V. and Minamino, T., *Structure and function of the bi-directional bacterial flagellar motor.* Biomolecules, 2014. **4**(1): p. 217-234.

83. Minamino, T., Imada, K., Kinoshita, M., Nakamura, S., Morimoto, Y.V. and Namba, K., *Structural insight into the rotational switching*

mechanism of the bacterial flagellar motor. PLoS Biology, 2011. **9**(5): p. e1000616.

84. Leake, M.C., Chandler, J.H., Wadhams, G.H., Bai, F., Berry, R.M. and Armitage, J.P., *Stoichiometry and turnover in single, functioning membrane protein complexes.* Nature, 2006. **443**(7109): p. 355-358.

85. Maiti, S. and Mitra, P., *Bacterial flagellar switching: a molecular mechanism directed by the logic of an electric motor.* Journal of Molecular Modeling, 2018. **24**(10).

86. Nord, A.L., Sowa, Y., Steel, B.C., Lo, C.J. and Berry, R.M., *Speed of the bacterial flagellar motor near zero load depends on the number of stator units.* Proceedings of the National Academy of Sciences of the United States of America, 2017. **114**(44): p. 11603-11608.

87. McCarter, L.L. and Gomelsky, M., *Fifty Ways To Inhibit Motility via Cyclic Di-GMP: the Emerging Pseudomonas aeruginosa Swarming Story.* Journal of Bacteriology, 2015. **197**(3): p. 406-409.

88. Guttenplan, S.B. and Kearns, D.B., *Regulation of flagellar motility during biofilm formation.* Fems Microbiology Reviews, 2013. **37**(6): p. 849-71.

89. Indrani Banerjee, R.C.P., and Ravi S. Kane, *Antifouling coatings: recent developments in the design of surfaces that prevent fouling by proteins, bacteria and marine organisms.* Advanced Materials, 2011. **23**: p. 690-718.

90. Son K. Guasto J. S., S.R., *Bacteria can exploit a flagellar buckling instability to change direction.* Nature Physics, 2013. **9**: p. 494-498.

91. Berg, H.C. and Brown, D.A., *Chemotaxis in Escherichia coli analysed by three-dimensional tracking.* Nature, 1972. **239**(5374): p. 500-504.

92. Ahmed, T. and Stocker, R., *Experimental verification of the behavioral foundation of bacterial transport parameters using microfluidics.* Biophysical Journal, 2008. **95**(9): p. 4481-4493.

93. Xie, L., Altindal, T., Chattopadhyay, S. and Wu, X.L., *From the Cover: Bacterial flagellum as a propeller and as a rudder for efficient chemotaxis.* Proceedings of the National Academy of Sciences of the United States of America, 2011. **108**(6): p. 2246-2251.

94. Rosenhahn, A. and Sendra, G.H., *Surface sensing and settlement strategies of marine biofouling organisms.* Biointerphases, 2012. **7**(1-4): p. 63.

95. Wood, T.K., Gonzalez Barrios, A.F., Herzberg, M. and Lee, J., *Motility influences biofilm architecture in Escherichia coli.* Applied Microbiology and Biotechnology, 2006. **72**(2): p. 361-267.

96. Schuhmacher, J.S., Thormann K.M., and Bange G., *How bacteria maintain location and number of flagella?* FEMS Microbiology Reviews, 2015. **39**: p. 812–822.

97. Vater, S.M., Weisse, S., Maleschlijski, S., Lotz, C., Koschitzki, F., Schwartz, T., Obst, U. and Rosenhahn, A., *Swimming Behavior of Pseudomonas aeruginosa Studied by Holographic 3D Tracking.* Plos One, 2014. **9**(1).

98. Karimi, A., Karig, D., Kumar, A. and Ardekani, A.M., *Interplay of physical mechanisms and biofilm processes: review of microfluidic methods.* Lab Chip, 2015. **15**(1): p. 23-42.

99. Lauga, E., DiLuzio, W.R., Whitesides, G.M. and Stone, H.A., *Swimming in circles: Motion of bacteria near solid boundaries.* Biophysical Journal, 2006. **90**(2): p. 400-412.

100. Nirody, J.A., Sun, Y.R. and Lo, C.J., *The biophysicist's guide to the bacterial flagellar motor.* Advances in Physics: X, 2017. **2**(2): p. 324-343.

101. Xue, R.D., Ma, Q., Baker, M.A.B. and Bai, F., *A Delicate Nanoscale Motor Made by Nature-The Bacterial Flagellar Motor.* Advanced Science, 2015. **2**(9): p. 1500129.

102. Son, K., Brumley, D.R. and Stocker, R., *Live from under the lens: exploring microbial motility with dynamic imaging and microfluidics.* Nature Reviews Microbiology, 2015. **13**(12): p. 761-775.

103. Conrad, J.C., Gibiansky, M.L., Jin, F., Gordon, V.D., Motto, D.A., Mathewson, M.A., Stopka, W.G., Zelasko, D.C., Shrout, J.D., and Wong, G.C., *Flagella and pili-mediated near-surface single-cell motility mechanisms in P. aeruginosa.* Biophysical Journal, 2011. **100**(7): p. 1608-1616.

104. Beatson, S.A., Whitchurch, C.B., Sargent, J.L., Levesque, R.C. and Mattick, J.S., *Differential regulation of twitching motility and elastase production by Vfr in Pseudomonas aeruginosa.* Journal of Bacteriology, 2002. **184**(13): p. 3605-3613.

105. Skerker, J.M. and Berg, H.C., *Direct observation of extension and retraction of type IV pili.* Proceedings of the National Academy of Sciences of the United States of America, 2001. **98**(12): p. 6901-6904.

106. Jin, F., Conrad, J.C., Gibiansky, M.L. and Wong, G.C., *Bacteria use type-IV pili to slingshot on surfaces.* Proceedings of the National Academy of Sciences of the United States of America, 2011. **108**(31): p. 12617-12622.

107. Rodesney, C.A., Roman, B., Dhamani, N., Cooley, B.J., Touhami, A. and Gordon, V.D., *Mechanosensing of shear by Pseudomonas aeruginosa leads to increased levels of the cyclic-di-GMP signal*

initiating biofilm development. Proceedings of the National Academy of Sciences of the United States of America, 2017. **114**(23): p. 5906-5911.

108. Houry, A., Gohar, M., Deschamps, J., Tischenko, E., Aymerich, S., Gruss, A. and Briandet, R., *Bacterial swimmers that infiltrate and take over the biofilm matrix.* Proceedings of the National Academy of Sciences of the United States of America, 2012. **109**(32): p. 13088-13093.

109. Harmsen, M., Yang, L., Pamp, S.J. and Tolker-Nielsen, T., *An update on Pseudomonas aeruginosa biofilm formation, tolerance, and dispersal.* FEMS Immunology and Medical Microbiology, 2010. **59**(3): p. 253-268.

110. Merritt, P.M., Danhorn, T. and Fuqua, C., *Motility and chemotaxis in Agrobacterium tumefaciens surface attachment and biofilm formation.* Journal of Bacteriology, 2007. **189**(22): p. 8005-8014.

111. Chiang, P. and Burrows, L.L., *Biofilm formation by hyperpiliated mutants of Pseudomonas aeruginosa.* Journal of Bacteriology, 2003. **185**(7): p. 2374-2378.

112. Sourjik, V., *Receptor clustering and signal processing in E. coli chemotaxis.* Trends in Microbiology, 2004. **12**(12): p. 569-576.

113. Thar, R. and Kuhl, M., *Bacteria are not too small for spatial sensing of chemical gradients: an experimental evidence.* Proceedings of the National Academy of Sciences of the United States of America, 2003. **100**(10): p. 5748-5753.

114. Armitage, J.P. and Schmitt, R., *Bacterial chemotaxis: Rhodobacter sphaeroides and Sinorhizobium meliloti--variations on a theme?* Microbiology, 1997. **143** (12): p. 3671-3682.

115. Wadhams, G.H. and Armitage, J.P., *Making sense of it all: Bacterial chemotaxis.* Nature Reviews Molecular Cell Biology, 2004. **5**(12): p. 1024-1037.

116. Heydt, M., Pettitt, M.E., Cao, X., Callow, M.E., Callow, J.A., Grunze, M. and Rosenhahn, A., *Settlement Behavior of Zoospores of Ulva linza During Surface Selection Studied by Digital Holographic Microscopy.* Biointerphases, 2012. **7**(33).

117. Ellison, C. and Brun, Y.V., *Mechanosensing: a regulation sensation.* Current Biology, 2015. **25**(3): p. 113-115.

118. Gode-Potratz, C.J., Kustusch, R.J., Breheny, P.J., Weiss, D.S. and McCarter, L.L., *Surface sensing in Vibrio parahaemolyticus triggers a programme of gene expression that promotes colonization and virulence.* Molecular Microbiology, 2011. **79**(1): p. 240-263.

119. Lee, Y.Y. and Belas, R., *Loss of FliL alters Proteus mirabilis surface sensing and temperature-dependent swarming.* Journal of Bacteriology, 2015. **197**(1): p. 159-173.

120. Van Dellen, K.L., Houot, L. and Watnick, P.I., *Genetic analysis of Vibrio cholerae monolayer formation reveals a key role for DeltaPsi in the transition to permanent attachment.* Journal of Bacteriology, 2008. **190**(24): p. 8185-8196.

121. Li, G., Brown, P.J., Tang, J.X., Xu, J., Quardokus, E.M., Fuqua, C. and Brun, Y.V., *Surface contact stimulates the just-in-time deployment of bacterial adhesins.* Molecular Microbiology, 2012. **83**(1): p. 41-51.

122. Belas, R., *Biofilms, flagella, and mechanosensing of surfaces by bacteria.* Trends in Microbiology, 2014. **22**(9): p. 517-527.

123. Harshey, R.M. and Partridge, J.D., *Shelter in a Swarm.* Journal of Molecular Biology, 2015. **427**(23): p. 3683-3694.

124. Hug, I., Deshpande, S., Sprecher, K.S., Pfohl, T. and Jenal, U., *Second messenger-mediated tactile response by a bacterial rotary motor.* Science, 2017. **358**(6362): p. 531-534.

125. Kuchma, S.L., Delalez, N.J., Filkins, L.M., Snavely, E.A., Armitage, J.P. and O'Toole, G.A., *Cyclic Di-GMP-Mediated Repression of Swarming Motility by Pseudomonas aeruginosa PA14 Requires the MotAB Stator.* Journal of Bacteriology, 2015. **197**(3): p. 420-430.

126. Baker, A.E., Webster, S.S., Diepold, A., Kuchma, S.L., Bordeleau, E., Armitage, J.P. and O'Toole, G.A., *Flagellar stators stimulate c-di-GMP production by Pseudomonas aeruginosa.* Journal of Bacteriology, 2019. **201**(18): p. e00741.

127. Baraquet, C., Murakami, K., Parsek, M.R. and Harwood, C.S., *The FleQ protein from Pseudomonas aeruginosa functions as both a repressor and an activator to control gene expression from the pel operon promoter in response to c-di-GMP.* Nucleic Acids Research, 2012. **40**(15): p. 7207-7218.

128. Harapanahalli, A.K., Chen, Y., Li, J., Busscher, H.J. and van der Mei, H.C., *Influence of Adhesion Force on icaA and cidA Gene Expression and Production of Matrix Components in Staphylococcus aureus Biofilms.* Applied and Environmental Microbiology, 2015. **81**(10): p. 3369-3378.

129. Chi, E., Mehl, T., Nunn, D. and Lory, S., *Interaction of Pseudomonas-Aeruginosa with A549 Pneumocyte Cells.* Infection and Immunity, 1991. **59**(3): p. 822-828.

130. Persat, A., Nadell, C.D., Kim, M.K., Ingremeau, F., Siryaporn, A., Drescher, K., Wingreen, N.S., Bassler, B.L., Gitai, Z., and Stone, H.A., *The Mechanical World of Bacteria.* Cell, 2015. **161**(5): p. 988-997.

131. Fuchs, E.L., Brutinel, E.D., Jones, A.K., Fulcher, N.B., Urbanowski, M.L., Yahr, T.L. and Wolfgang, M.C., *The Pseudomonas aeruginosa Vfr Regulator Controls Global Virulence Factor Expression through Cyclic AMP-Dependent and -Independent Mechanisms.* Journal of Bacteriology, 2010. **192**(14): p. 3553-3564.

132. Marko, V.A., Kilmury, S.L.N., MacNeil, L.T. and Burrows, L.L., *Pseudomonas aeruginosa type IV minor pilins and PilY1 regulate virulence by modulating FimS-AIgR activity.* Plos Pathogens, 2018. **14**(5).

133. Ha, D.G. and O'Toole, G.A., *c-di-GMP and its Effects on Biofilm Formation and Dispersion: a Pseudomonas Aeruginosa Review.* Microbiology Spectrum, 2015. **3**(2).

134. Jenal, U., Reinders, A. and Lori, C., *Cyclic di-GMP: second messenger extraordinaire.* Nature Reviews Microbiology, 2017. **15**(5): p. 271-284.

135. Mills, E., Petersen, E., Kulasekara, B.R. and Miller, S.I., *A direct screen for c-di-GMP modulators reveals a Salmonella Typhimurium periplasmic L-arginine-sensing pathway.* Science Signaling, 2015. **8**(380).

136. Romling, U., Galperin, M.Y. and Gomelsky, M., *Cyclic di-GMP: the First 25 Years of a Universal Bacterial Second Messenger.* Microbiology and Molecular Biology Reviews, 2013. **77**(1): p. 1-52.

137. Ma, L.M., Conover, M., Lu, H.P., Parsek, M.R., Bayles, K. and Wozniak, D.J., *Assembly and Development of the Pseudomonas aeruginosa Biofilm Matrix.* Plos Pathogens, 2009. **5**(3).

138. Huangyutitham, V., Guvener, Z.T. and Harwood, C.S., *Subcellular Clustering of the Phosphorylated WspR Response Regulator Protein Stimulates Its Diguanylate Cyclase Activity.* Mbio, 2013. **4**(3).

139. Gula, G., Dorotkiewicz-Jach, A., Korzekwa, K., Valvano, M.A. and Drulis-Kawa, Z., *Complex Signaling Networks Controlling Dynamic Molecular Changes in Pseudomonas aeruginosa Biofilm.* Current Medicinal Chemistry, 2019. **26**(11): p. 1979-1993.

140. Zobell, C.E. and Grant, C.W., *Bacterial Utilization of Low Concentrations of Organic Matter.* J Bacteriol, 1943. **45**(6): p. 555-564.

141. Tuson, H.H. and Weibel, D.B., *Bacteria-surface interactions.* Soft Matter, 2013. **9**(18): p. 4368-4380.

142. Kaya, T. and Koser, H., *Direct Upstream Motility in Escherichia coli.* Biophysical Journal, 2012. **102**(7): p. 1514-1523.

143. Hill, J., Kalkanci, O., McMurry, J.L. and Koser, H., *Hydrodynamic surface interactions enable Escherichia coli to seek efficient routes to swim upstream.* Physical Review Letters, 2007. **98**(6).

144. Qu, Y., Daley, A.J., Istivan, T.S., Rouch, D.A. and Deighton, M.A., *Densely adherent growth mode, rather than extracellular polymer substance matrix build-up ability, contributes to high resistance of Staphylococcus epidermidis biofilms to antibiotics.* Journal of Antimicrobial Chemotherapy, 2010. **65**(7): p. 1405-1411.

145. John, A.K., Schmaler, M., Khanna, N. and Landmann, R., *Reversible daptomycin tolerance of adherent staphylococci in an implant infection model.* Antimicrobial Agents and Chemotherapy, 2011. **55**(7): p. 3510-3516.

146. Hermansson, M., *The DLVO theory in microbial adhesion.* Colloids and Surfaces B: Biointerfaces, 1999. **14**(1-4): p. 105-119.

147. Malescio, G., *Intermolecular potentials - past, present, future.* Nature Materials, 2003. **2**(8): p. 501-503.

148. Otto, K., Elwing, H. and Hermansson, M., *Effect of ionic strength on initial interactions of Escherichia coli with surfaces, studied on-line by a novel quartz crystal microbalance technique.* Journal of Bacteriology, 1999. **181**(17): p. 5210-5218.

149. Hori, K. and Matsumoto, S., *Bacterial adhesion: From mechanism to control.* Biochemical Engineering Journal, 2010. **48**(3): p. 424-434.

150. An, Y.H. and Friedman, R.J., *Concise review of mechanisms of bacterial adhesion to biomaterial surfaces.* Journal of Biomedical Materials Research, 1998. **43**(3): p. 338-348.

151. Vigeant, M.A., Ford, R.M., Wagner, M. and Tamm, L.K., *Reversible and irreversible adhesion of motile Escherichia coli cells analyzed by total internal reflection aqueous fluorescence microscopy.* Applied and Environmental Microbiology, 2002. **68**(6): p. 2794-2801.

152. Boks, N.P., Busscher, H.J., van der Mei, H.C. and Norde, W., *Bond-strengthening in staphylococcal adhesion to hydrophilic and hydrophobic surfaces using atomic force microscopy.* Langmuir, 2008. **24**(22): p. 12990-12994.

153. Li, J., Busscher, H.J., Norde, W. and Sjollema, J., *Analysis of the contribution of sedimentation to bacterial mass transport in a parallel plate flow chamber.* Colloids and Surfaces B: Biointerfaces, 2011. **84**(1): p. 76-81.

154. Zhao, K., Tseng, B.S., Beckerman, B., Jin, F., Gibiansky, M.L., Harrison, J.J., Luijten, E., Parsek, M.R. and Wong, G.C.L., *Psl trails guide exploration and microcolony formation in Pseudomonas aeruginosa biofilms.* Nature, 2013. **497**(7449): p. 388.

155. Renner, L.D. and Weibel, D.B., *Physicochemical regulation of biofilm formation.* MRS Bull, 2011. **36**(5): p. 347-355.

156. Walker, S.L., Redman, J.A. and Elimelech, M., *Role of Cell Surface Lipopolysaccharides in Escherichia coli K12 adhesion and transport.* Langmuir, 2004. **20**(18): p. 7736-7746.

157. Chapman, R.G., Ostuni, E., Liang, M.N., Meluleni, G., Kim, E., Yan, L., Pier, G., Warren, H.S. and Whitesides, G.M., *Polymeric thin films that resist the adsorption of proteins and the adhesion of bacteria.* Langmuir, 2001. **17**(4): p. 1225-1233.

158. Alexander, M.R. and Williams, P., *Water contact angle is not a good predictor of biological responses to materials.* Biointerphases, 2017. **12**(2).

159. Song, F.C. and Ren, D.C., *Stiffness of Cross-Linked Poly(Dimethylsiloxane) Affects Bacterial Adhesion and Antibiotic Susceptibility of Attached Cells.* Langmuir, 2014. **30**(34): p. 10354-10362.

160. Siddiqui, S., Chandrasekaran, A., Lin, N., Tufenkji, N. and Moraes, C., *Microfluidic Shear Assay to Distinguish between Bacterial Adhesion and Attachment Strength on Stiffness-Tunable Silicone Substrates.* Langmuir, 2019. **35**(26): p. 8840-8849.

161. Rosenhahn, A., Schilp, S., Kreuzer, H.J. and Grunze, M., *The role of "inert" surface chemistry in marine biofouling prevention.* Physical Chemistry Chemical Physics, 2010. **12**(17): p. 4275-4286.

162. Silhavy, T.J., Kahne, D. and Walker, S., *The Bacterial Cell Envelope.* Cold Spring Harbor Perspectives in Biology, 2010. **2**(5).

163. Smyth, C.J., Marron, M.B., Twohig, J.M. and Smith, S.G., *Fimbrial adhesins: similarities and variations in structure and biogenesis.* FEMS Immunology and Medical Microbiology, 1996. **16**(2): p. 127-139.

164. Azghani, A.O., Idell, S., Bains, M. and Hancock, R.E., *Pseudomonas aeruginosa outer membrane protein F is an adhesin in bacterial binding to lung epithelial cells in culture.* Microbial Pathogenesis, 2002. **33**(3): p. 109-114.

165. Klemm, P. and Schembri, M.A., *Bacterial adhesins: function and structure.* International Journal of Medical Microbiology, 2000. **290**(1): p. 27-35.

166. Li, X., Johnson, D.E. and Mobley, H.L., *Requirement of MrpH for mannose-resistant Proteus-like fimbria-mediated hemagglutination by Proteus mirabilis.* Infection and Immunity, 1999. **67**(6): p. 2822-2833.

167. Riegman, N., Hoschutzky, H., van Die, I., Hoekstra, W., Jann, K. and Bergmans, H., *Immunocytochemical analysis of P-fimbrial structure: localization of minor subunits and the influence of the minor subunit FsoE on the biogenesis of the adhesin.* Molecular Microbiology, 1990. **4**(7): p. 1193-1198.

168. Arnal, L., Longo, G., Stupar, P., Castez, M.F., Cattelan, N., Salvarezza, R.C., Yantorno, O.M., Kasas, S. and Vela, M.E., *Localization of adhesins on the surface of a pathogenic bacterial envelope through atomic force microscopy.* Nanoscale, 2015. **7**(41): p. 17563-17572.

169. Foster, T.J. and Hook, M., *Surface protein adhesins of Staphylococcus aureus.* Trends in Microbiology, 1998. **6**(12): p. 484-488.

170. Heilmann, C., *Adhesion Mechanisms of Staphylococci.* Bacterial Adhesion: Chemistry, Biology and Physics, 2011. **715**: p. 105-123.

171. Marshall, K.C., Stout, R. and Mitchell, R., *Selective sorption of bacteria from seawater.* Canadian Journal of Microbiology, 1971. **17**(11): p. 1413-1416.

172. Franklin, M.J., Nivens, D.E., Weadge, J.T. and Howell, P.L., *Biosynthesis of the Pseudomonas aeruginosa extracellular polysaccharides, alginate, Pel, and Psl.* Frontiers in Microbiology, 2011. **2**.

173. Franklin, M.J. and Ohman, D.E., *Identification of Algf in the Alginate Biosynthetic Gene-Cluster of Pseudomonas-Aeruginosa Which Is Required for Alginate Acetylation.* Journal of Bacteriology, 1993. **175**(16): p. 5057-5065.

174. Jones, C.J. and Wozniak, D.J., *Psl Produced by Mucoid Pseudomonas aeruginosa Contributes to the Establishment of Biofilms and Immune Evasion.* Mbio, 2017. **8**(3).

175. El-Kirat-Chatel, S., Boyd, C.D., O'Toole, G.A. and Dufrene, Y.F., *Single-molecule analysis of Pseudomonas fluorescens footprints.* ACS Nano, 2014. **8**(2): p. 1690-1698.

176. Beloin, C., Houry, A., Froment, M., Ghigo, J.M. and Henry, N., *A short-time scale colloidal system reveals early bacterial adhesion dynamics.* PLoS Biology, 2008. **6**(7): p. e167.

177. Alhede, M., Kragh, K.N., Qvortrup, K., Allesen-Holm, M., van Gennip, M., Christensen, L.D., Jensen, P.O., Nielsen, A.K., Parsek, M., Wozniak, D., Molin, S., Tolker-Nielsen, T., Hoiby, N., Givskov, M., and Bjarnsholt, T., *Phenotypes of Non-Attached Pseudomonas aeruginosa Aggregates Resemble Surface Attached Biofilm.* Plos One, 2011. **6**(11).

178. Schleheck, D., Barraud, N., Klebensberger, J., Webb, J.S., McDougald, D., Rice, S.A. and Kjelleberg, S., *Pseudomonas aeruginosa PAO1 Preferentially Grows as Aggregates in Liquid Batch Cultures and Disperses upon Starvation.* Plos One, 2009. **4**(5).

179. Kragh, K.N., Hutchison, J.B., Melaugh, G., Rodesney, C., Roberts, A.E.L., Irie, Y., Jensen, P.O., Diggle, S.P., Allen, R.J., Gordon, V., and Bjarnsholt, T., *Role of Multicellular Aggregates in Biofilm Formation.* Mbio, 2016. **7**(2).

180. Haaber, J., Cohn, M.T., Frees, D., Andersen, T.J. and Ingmer, H., *Planktonic Aggregates of Staphylococcus aureus Protect against Common Antibiotics.* Plos One, 2012. **7**(7).

181. Mashburn, L.M. and Whiteley, M., *Membrane vesicles traffic signals and facilitate group activities in a prokaryote.* Nature, 2005. **437**(7057): p. 422-425.

182. El-Naggar, M.Y., Wanger, G., Leung, K.M., Yuzvinsky, T.D., Southam, G., Yang, J., Lau, W.M., Nealson, K.H. and Gorby, Y.A., *Electrical transport along bacterial nanowires from Shewanella oneidensis MR-1.* Proceedings of the National Academy of Sciences of the United States of America, 2010. **107**(42): p. 18127-18131.

183. Remis, J.P., Wei, D., Gorur, A., Zemla, M., Haraga, J., Allen, S., Witkowska, H.E., Costerton, J.W., Berleman, J.E., and Auer, M., *Bacterial social networks: structure and composition of Myxococcus xanthus outer membrane vesicle chains.* Environmental Microbiology, 2014. **16**(2): p. 598-610.

184. Williams, P., Winzer, K., Chan, W.C. and Camara, M., *Look who's talking: communication and quorum sensing in the bacterial world.* Philosophical Transactions of the Royal Society B, 2007. **362**(1483): p. 1119-1134.

185. Abisado, R.G., Benomar, S., Klaus, J.R., Dandekar, A.A. and Chandler, J.R., *Bacterial Quorum Sensing and Microbial Community Interactions.* Mbio, 2018. **9**(3).

186. Waters, C.M. and Bassler, B.L., *Quorum sensing: cell-to-cell communication in bacteria.* Annual Review of Cell and Developmental Biology, 2005. **21**: p. 319-346.

187. Nealson, K.H. and Hastings, J.W., *Bacterial bioluminescence: its control and ecological significance.* Microbiological Reviews, 1979. **43**(4): p. 496-518.

188. Engebrecht, J. and Silverman, M., *Identification of genes and gene products necessary for bacterial bioluminescence.* Proceedings of the National Academy of Sciences of the United States of America, 1984. **81**(13): p. 4154-4158.

189. Stevens, A.M., Dolan, K.M. and Greenberg, E.P., *Synergistic binding of the Vibrio fischeri LuxR transcriptional activator domain and RNA polymerase to the lux promoter region.* Proceedings of the National Academy of Sciences of the United States of America, 1994. **91**(26): p. 12619-12623.

190. Fuqua, W.C., Winans, S.C. and Greenberg, E.P., *Quorum Sensing in Bacteria - the Luxr-Luxi Family of Cell Density-Responsive Transcriptional Regulators.* Journal of Bacteriology, 1994. **176**(2): p. 269-275.

191. Parsek, M.R., Val, D.L., Hanzelka, B.L., Cronan, J.E., Jr. and Greenberg, E.P., *Acyl homoserine-lactone quorum-sensing signal generation.* Proceedings of the National Academy of Sciences of the United States of America, 1999. **96**(8): p. 4360-4365.

192. Ansaldi, M., Marolt, D., Stebe, T., Mandic-Mulec, I. and Dubnau, D., *Specific activation of the Bacillus quorum-sensing systems by isoprenylated pheromone variants.* Molecular Microbiology, 2002. **44**(6): p. 1561-1573.

193. Lyon, G.J. and Novick, R.P., *Peptide signaling in Staphylococcus aureus and other Gram-positive bacteria.* Peptides, 2004. **25**(9): p. 1389-1403.

194. Ochsner, U.A., Koch, A.K., Fiechter, A. and Reiser, J., *Isolation and characterization of a regulatory gene affecting rhamnolipid biosurfactant synthesis in Pseudomonas aeruginosa.* Journal of Bacteriology, 1994. **176**(7): p. 2044-2054.

195. Pearson, J.P., Gray, K.M., Passador, L., Tucker, K.D., Eberhard, A., Iglewski, B.H. and Greenberg, E.P., *Structure of the autoinducer required for expression of Pseudomonas aeruginosa virulence genes.* Proceedings of the National Academy of Sciences of the United States of America, 1994. **91**(1): p. 197-201.

196. Wagner, V.E., Gillis, R.J. and Iglewski, B.H., *Transcriptome analysis of quorum-sensing regulation and virulence factor expression in Pseudomonas aeruginosa.* Vaccine, 2004. **22** p. 15-20.

197. Lee, J. and Zhang, L.H., *The hierarchy quorum sensing network in Pseudomonas aeruginosa.* Protein & Cell, 2015. **6**(1): p. 26-41.

198. Schuster, M. and Greenberg, E.P., *A network of networks: Quorum-sensing gene regulation in Pseudomonas aeruginosa.* International Journal of Medical Microbiology, 2006. **296**(2-3): p. 73-81.

199. Schuster, M., Lostroh, C.P., Ogi, T. and Greenberg, E.P., *Identification, timing, and signal specificity of Pseudomonas aeruginosa quorum-controlled genes: a transcriptome analysis.* Journal of Bacteriology, 2003. **185**(7): p. 2066-2079.

200. Sutherland, D.W., Blanks, Z.D., Zhang, X. and Charest, J.L., *Relationship Between Central Venous Catheter Protein Adsorption and Water Infused Surface Protection Mechanisms.* Artificial Organs, 2018. **42**(11): p. 369-379.

201. Coli, L., Donati, G., Cappuccilli, M.L., Cianciolo, G., Comai, G., Cuna, V., Carretta, E., La Manna, G. and Stefoni, S., *Role of the hemodialysis vascular access type in inflammation status and monocyte activation.* International Journal of Artificial Organs, 2011. **34**(6): p. 481-488.

202. Muller, R., Eidt, A., Hiller, K.A., Katzur, V., Subat, M., Schweikl, H., Imazato, S., Ruhl, S. and Schmalz, G., *Influences of protein films on*

antibacterial or bacteria-repellent surface coatings in a model system using silicon wafers. Biomaterials, 2009. **30**(28): p. 4921-4929.

203. Bearinger, J.P., Terrettaz, S., Michel, R., Tirelli, N., Vogel, H., Textor, M. and Hubbell, J.A., *Chemisorbed poly(propylene sulphide)-based copolymers resist biomolecular interactions.* Nature Materials, 2003. **2**(4): p. 259-264.

204. Amiji, M. and Park, K., *Surface modification of polymeric biomaterials with poly(ethylene oxide), albumin, and heparin for reduced thrombogenicity.* Journal of Biomaterials Science, Polymer Edition, 1993. **4**(3): p. 217-234.

205. Bernhard, C., Roeters, S.J., Franz, J., Weidner, T., Bonn, M. and Gonella, G., *Repelling and ordering: the influence of poly(ethylene glycol) on protein adsorption.* Physical Chemistry Chemical Physics, 2017. **19**(41): p. 28182-28188.

206. Schellekens, H., Hennink, W.E. and Brinks, V., *The Immunogenicity of Polyethylene Glycol: Facts and Fiction.* Pharmaceutical Research, 2013. **30**(7): p. 1729-1734.

207. Kingshott, P., Wei, J., Bagge-Ravn, D., Gadegaard, N. and Gram, L., *Covalent attachment of poly(ethylene glycol) to surfaces, critical for reducing bacterial adhesion.* Langmuir, 2003. **19**(17): p. 6912-6921.

208. Razatos, A., Ong, Y.L., Boulay, F., Elbert, D.L., Hubbell, J.A., Sharma, M.M. and Georgiou, G., *Force measurements between bacteria and poly(ethylene glycol)-coated surfaces.* Langmuir, 2000. **16**(24): p. 9155-9158.

209. Harris, L.G., Tosatti, S., Wieland, M., Textor, M. and Richards, R.G., *Staphylococcus aureus adhesion to titanium oxide surfaces coated with non-functionalized and peptide-functionalized poly(L-lysine)-grafted-poly(ethylene glycol) copolymers.* Biomaterials, 2004. **25**(18): p. 4135-4148.

210. Hucknall, A., Rangarajan, S. and Chilkoti, A., *In Pursuit of Zero: Polymer Brushes that Resist the Adsorption of Proteins.* Advanced Materials, 2009. **21**(23): p. 2441-2446.

211. Roosjen, A., van der Mei, H.C., Busscher, H.J. and Norde, W., *Microbial adhesion to poly(ethylene oxide) brushes: influence of polymer chain length and temperature.* Langmuir, 2004. **20**(25): p. 10949-10955.

212. Michel, R., Pasche, S., Textor, M. and Castner, D.G., *Influence of PEG architecture on protein adsorption and conformation.* Langmuir, 2005. **21**(26): p. 12327-12332.

213. Hemenway, J.N., Carvalho, T.C., Rao, V.M., Wu, Y.M., Levons, J.K., Narang, A.S., Paruchuri, S.R., Stamato, H.J. and Varia, S.A., *Formation of reactive impurities in aqueous and neat polyethylene glycol 400 and*

effects of antioxidants and oxidation inducers. Journal of Pharmaceutical Sciences, 2012. **101**(9): p. 3305-3318.

214. Prime, K.L. and Whitesides, G.M., *Adsorption of Proteins onto Surfaces Containing End-Attached Oligo(Ethylene Oxide) - a Model System Using Self-Assembled Monolayers.* Journal of the American Chemical Society, 1993. **115**(23): p. 10714-10721.

215. Holmlin, R.E., Chen, X.X., Chapman, R.G., Takayama, S. and Whitesides, G.M., *Zwitterionic SAMs that resist nonspecific adsorption of protein from aqueous buffer.* Langmuir, 2001. **17**(9): p. 2841-2850.

216. Chapman, R.G., Ostuni, E., Takayama, S., Holmlin, R.E., Yan, L. and Whitesides, G.M., *Surveying for surfaces that resist the adsorption of proteins.* Journal of the American Chemical Society, 2000. **122**(34): p. 8303-8304.

217. Ma, H.W., Hyun, J.H., Stiller, P. and Chilkoti, A., *"Non-fouling" oligo(ethylene glycol)-functionalized polymer brushes synthesized by surface-initiated atom transfer radical polymerization.* Advanced Materials, 2004. **16**(4): p. 338.

218. Chen, S.F., Zheng, J., Li, L.Y. and Jiang, S.Y., *Strong resistance of phosphorylcholine self-assembled monolayers to protein adsorption: Insights into nonfouling properties of zwitterionic materials.* Journal of the American Chemical Society, 2005. **127**(41): p. 14473-14478.

219. Tegoulia, V.A., Rao, W.S., Kalambur, A.T., Rabolt, J.R. and Cooper, S.L., *Surface properties, fibrinogen adsorption, and cellular interactions of a novel phosphorylcholine-containing self-assembled monolayer on gold.* Langmuir, 2001. **17**(14): p. 4396-4404.

220. Zhang, L., Cao, Z.Q., Bai, T., Carr, L., Ella-Menye, J.R., Irvin, C., Ratner, B.D. and Jiang, S.Y., *Zwitterionic hydrogels implanted in mice resist the foreign-body reaction.* Nature Biotechnology, 2013. **31**(6): p. 553.

221. Garapaty, A. and Champion, J.A., *Non-covalent phosphorylcholine coating reduces protein adsorption and phagocytic uptake of microparticles.* Chemical Communications, 2015. **51**(72): p. 13814-13817.

222. Lu, J.R., Murphy, E.F., Su, T.J., Lewis, A.L., Stratford, P.W. and Satija, S.K., *Reduced protein adsorption on the surface of a chemically grafted phospholipid monolayer.* Langmuir, 2001. **17**(11): p. 3382-3389.

223. Smith, R.S., Zhang, Z., Bouchard, M., Li, J., Lapp, H.S., Brotske, G.R., Lucchino, D.L., Weaver, D., Roth, L.A., Coury, A., Biggerstaff, J., Sukavaneshvar, S., Langer, R., and Loose, C., *Vascular Catheters with a Nonleaching Poly-Sulfobetaine Surface Modification Reduce Thrombus Formation and Microbial Attachment.* Science Translational Medicine, 2012. **4**(153).

224. Kim, Y.D., Dordick, J.S. and Clark, D.S., *Siloxane-based biocatalytic films and paints for use as reactive coatings.* Biotechnology and Bioengineering, 2001. **72**(4): p. 475-482.

225. Perni, S., Piccirillo, C., Pratten, J., Prokopovich, P., Chrzanowski, W., Parkin, I.P. and Wilson, M., *The antimicrobial properties of light-activated polymers containing methylene blue and gold nanoparticles.* Biomaterials, 2009. **30**(1): p. 89-93.

226. Page, K., Wilson, M. and Parkin, I.P., *Antimicrobial surfaces and their potential in reducing the role of the inanimate environment in the incidence of hospital-acquired infections.* Journal of Materials Chemistry, 2009. **19**(23): p. 3819-3831.

227. Ohko, Y., Utsumi, Y., Niwa, C., Tatsuma, T., Kobayakawa, K., Satoh, Y., Kubota, Y. and Fujishima, A., *Self-sterilizing and self-cleaning of silicone catheters coated with TiO(2) photocatalyst thin films: a preclinical work.* Journal of Biomedical Materials Research, 2001. **58**(1): p. 97-101.

228. Joshi, A., Punyani, S., Bale, S.S., Yang, H., Borca-Tasciuc, T. and Kane, R.S., *Nanotube-assisted protein deactivation.* Nature Nanotechnology, 2008. **3**(1): p. 41-45.

229. Yao, Y., Li, G., Ciston, S., Lueptow, R.M. and Gray, K.A., *Photoreactive TiO2/carbon nanotube composites: synthesis and reactivity.* Environmental Science & Technology, 2008. **42**(13): p. 4952-4957.

230. Ista, L.K., Perez-Luna, V.H. and Lopez, G.P., *Surface-grafted, environmentally sensitive polymers for biofilm release.* Applied and Environmental Microbiology, 1999. **65**(4): p. 1603-1609.

231. Hook, A.L., Anderson, D.G., Langer, R., Williams, P., Davies, M.C. and Alexander, M.R., *High throughput methods applied in biomaterial development and discovery.* Biomaterials, 2010. **31**(2): p. 187-198.

232. Jeffery N., K.K., Dubern J., Lomiteng A., Dragova M., Frost A., Macrae B., Mundy A., Alexander M., Williams P., Andrich D. , *A new bacterial resistant polymer catheter coating to reduce catheter associated urinary tract infection (CAUTI): A first-in-man pilot study.* European Urology Supplements 2019. **18**(1): p. 377.

233. S. Pernagallo, M.W., M.P. Gallagher, M. Bradley, *Colonising new frontiers—microarrays reveal biofilm modulating polymers.* J. Mater. Chem., 2011. **21**(1): p. 96–101.

234. Venkateswaran, S., Wu, M., Gwynne, P.J., Hardman, A., Lilienkampf, A., Pernagallo, S., Blakely, G., Swann, D.G., Gallagher, M.P., and Bradley, M., *Bacteria repelling poly(methylmethacrylate--dimethylacrylamide) coatings for biomedical devices.* Journal of Materials Chemistry, 2014. **2**(39): p. 6723-6729.

235. Epstein, A.K., Wong, T.S., Belisle, R.A., Boggs, E.M. and Aizenberg, J., *Liquid-infused structured surfaces with exceptional anti-biofouling performance.* Proceedings of the National Academy of Sciences of the United States of America, 2012. **109**(33): p. 13182-13187.

236. Kratochvil, M.J., Welsh, M.A., Manna, U., Ortiz, B.J., Blackwell, H.E. and Lynn, D.M., *Slippery Liquid-Infused Porous Surfaces that Prevent Bacterial Surface Fouling and Inhibit Virulence Phenotypes in Surrounding Planktonic Cells.* Acs Infectious Diseases, 2016. **2**(7): p. 509-517.

237. Barras, F., Aussel, L. and Ezraty, B., *Silver and Antibiotic, New Facts to an Old Story.* Antibiotics-Basel, 2018. **7**(3).

238. Wright, J.B., Lam, K. and Burrell, R.E., *Wound management in an era of increasing bacterial antibiotic resistance: A role for topical silver treatment.* American Journal of Infection Control, 1998. **26**(6): p. 572-577.

239. Dotzauer, D.M., Dai, J., Sun, L. and Bruening, M.L., *Catalytic membranes prepared using layer-by-layer adsorption of polyelectrolyte/metal nanoparticle films in porous supports.* Nano Letters, 2006. **6**(10): p. 2268-2272.

240. Agarwal, A., Guthrie, K.M., Czuprynski, C.J., Schurr, M.J., McAnulty, J.F., Murphy, C.J. and Abbott, N.L., *Polymeric Multilayers that Contain Silver Nanoparticles can be Stamped onto Biological Tissues to Provide Antibacterial Activity.* Advanced Functional Materials, 2011. **21**(10): p. 1863-1873.

241. Lee, D., Cohen, R.E. and Rubner, M.F., *Antibacterial properties of Ag nanoparticle loaded multilayers and formation of magnetically directed antibacterial microparticles.* Langmuir, 2005. **21**(21): p. 9651-9659.

242. Larese, F.F., D'Agostin, F., Crosera, M., Adami, G., Renzi, N., Bovenzi, M. and Maina, G., *Human skin penetration of silver nanoparticles through intact and damaged skin.* Toxicology, 2009. **255**(1-2): p. 33-37.

243. Samberg, M.E., Oldenburg, S.J. and Monteiro-Riviere, N.A., *Evaluation of silver nanoparticle toxicity in skin in vivo and keratinocytes in vitro.* Environmental Health Perspectives, 2010. **118**(3): p. 407-413.

244. Greenfeld, J.I., Sampath, L., Popilskis, S.J., Brunnert, S.R., Stylianos, S. and Modak, S., *Decreased bacterial adherence and biofilm formation on chlorhexidine and silver sulfadiazine-impregnated central venous catheters implanted in swine.* Critical Care Medicine, 1995. **23**(5): p. 894-900.

245. Schierholz, J.M., Beuth, J. and Pulverer, G., *The quantity and duration of the antimicrobial efficacy of a chlorhexidine and silversulfadiazine impregnated catheter.* Journal of Hospital Infection, 1999. **42**(2): p. 163-165.

246. Smith, A.W., *Biofilms and antibiotic therapy: is there a role for combating bacterial resistance by the use of novel drug delivery systems?* Advanced Drug Delivery Reviews, 2005. **57**(10): p. 1539-1550.

247. Bayston, R., Fisher, L.E. and Weber, K., *An antimicrobial modified silicone peritoneal catheter with activity against both Gram-positive and Gram-negative bacteria.* Biomaterials, 2009. **30**(18): p. 3167-3173.

248. Woo, G.L.Y., Yang, M.L., Yin, H.Q., Jaffer, F., Mittleman, M.W. and Santerre, J.P., *Biological characterization of a novel biodegradable antimicrobial polymer synthesized with fluoroquinolones.* Journal of Biomedical Materials Research, 2002. **59**(1): p. 35-45.

249. Singha, P., Locklin, J. and Handa, H., *A review of the recent advances in antimicrobial coatings for urinary catheters.* Acta Biomaterialia, 2017. **50**: p. 20-40.

250. Zarie, E.S., Kaidas, V., Gedamu, D., Mishra, Y.K., Adelung, R., Furkert, F.H., Scherliess, R., Steckel, H. and Groessner-Schreiber, B., *Solvent free fabrication of micro and nanostructured drug coatings by thermal evaporation for controlled release and increased effects.* PLoS One, 2012. **7**(8): p. e40746.

251. Canaparo, R., Foglietta, F., Giuntini, F., Della Pepa, C., Dosio, F. and Serpe, L., *Recent Developments in Antibacterial Therapy: Focus on Stimuli-Responsive Drug-Delivery Systems and Therapeutic Nanoparticles.* Molecules, 2019. **24**(10).

252. Cloutier, M., Mantovani, D. and Rosei, F., *Antibacterial Coatings: Challenges, Perspectives, and Opportunities.* Trends in Biotechnology, 2015. **33**(11): p. 637-652.

253. Hook, A.L., Chang, C., Yang, J., Atkinson, S., Langer, R., Anderson, D.G., Davies, M.C., Williams, P. and Alexander, M.R., *Discovery of novel materials with broad resistance to bacterial attachment using combinatorial polymer microarrays.* Advanced Materials, 2013. **25**(18): p. 2542-2547.

254. Hook, A.L., Chang, C., Yang, J., Luckett, J., Cockrayne, A., Atkinson, S., Mei, Y., Bayston, R., Irvine, D.J., Langer, R., Anderson, D.G., Williams, P., Davies, M.C., and Alexander, M.R., *Combinatorial discovery of polymers resistant to bacterial attachment.* Nature Biotechnology, 2012. **30**(9): p. 868-875.

255. Gridnev, A.A. and Ittel, S.D., *Catalytic chain transfer in free-radical polymerizations.* Chemical Reviews, 2001. **101**(12): p. 3611-3659.

256. Szynkowska, M.I., Czerski, K., Rogowski, J., Paryjczak, T. and Parczewski, A., *Detection of exogenous contaminants of fingerprints using ToF-SIMS.* Surface and Interface Analysis, 2010. **42**(5): p. 393-397.

257. Van Nuffel, S., Parmenter, C., Scurr, D.J., Russell, N.A. and Zelzer, M., *Multivariate analysis of 3D ToF-SIMS images: method validation and application to cultured neuronal networks.* Analyst, 2016. **141**(1): p. 90-95.

258. Musat, N., Foster, R., Vagner, T., Adam, B. and Kuypers, M.M.M., *Detecting metabolic activities in single cells, with emphasis on nanoSIMS.* Fems Microbiology Reviews, 2012. **36**(2): p. 486-511.

259. Vickerman, J.C., *Molecular SIMS - A journey from single crystal to biological surface studies.* Surface Science, 2009. **603**(10-12): p. 1926-1936.

260. Graham, D.J. and Castner, D.G., *Image and Spectral Processing for ToF-SIMS Analysis of Biological Materials.* The Mass Spectrometry Society of Japan, 2013. **2**: p. S0014.

261. *Introduction to SIMS*. Available from: https://www.cameca.com/products/sims/technique.

262. Yuan, Y., Hays, M.P., Hardwidge, P.R. and Kim, J., *Surface characteristics influencing bacterial adhesion to polymeric substrates.* Rsc Advances, 2017. **7**(23): p. 14254-14261.

263. Taylor, M., Urquhart, A.J., Zelzer, M., Davies, M.C. and Alexander, M.R., *Picoliter water contact angle measurement on polymers.* Langmuir, 2007. **23**(13): p. 6875-6878.

264. Bruker. *Fundamentals of Contact Mode and Tapping Mode Atomic Force Microscopy*. Available from: https://www.azonano.com/article.aspx?ArticleID=3010.

265. Dokukin, M.E. and Sokolov, I., *Quantitative Mapping of the Elastic Modulus of Soft Materials with HarmoniX and Peak Force QNM AFM Modes.* Langmuir, 2012. **28**(46): p. 16060-16071.

266. Kearns, D.B., *A field guide to bacterial swarming motility.* Nature Reviews Microbiology, 2010. **8**(9): p. 634-644.

267. Botcherby, E.J., Juskaitis, R., Booth, M.J. and Wilson, T., *An optical technique for remote focusing in microscopy.* Optics Communications, 2008. **281**(4): p. 880-887.

268. Hook, A.L., Flewellen, J.F., Dubern, J.-F., Carabelli, A.M., Zaid, I.W., Berry, R.M., Wildman, R.D., Russell, N., Williams, P., and M.R., A., *Simultaneous Tracking of Pseudomonas aeruginosa Motility in Liquid and at the Solid-Liquid Interface Reveals Differential Roles for the Flagellar Stators.* American Society for Microbiology, 2019. **4**(5): p. e00390-19.

269. Murphy, B.D. *https://www.olympus-lifescience.com/en/microscope-resource/primer/techniques/dic/dicintro/*.

270. Warner, J.C., Rothwell, S.D. and Keevil, C.W., *Use of episcopic differential interference contrast microscopy to identify bacterial biofilms on salad leaves and track colonization by Salmonella Thompson.* Environmental Microbiology, 2008. **10**(4): p. 918-925.

271. Flewellen, J.L., Zaid, I.M. and Berry, R.M., *A multi-mode digital holographic microscope.* Review of Scientific Instruments, 2019. **90**.

272. *Matlab scripts for DHM processing*. Available from: https://github.com/fishhooky/DHMTrack.

273. Murphy, D.B. and Davidson, M.W., *Fundamentals of Light Microscopy and Electronic Imaging*, ed. Wiley-Blackwell. 2013: John Wilew & sons, inc.

274. El Abed, S., Ibnsouda, S.K., Latrache, H. and Hamadi, F., *Scanning Electron Microscopy (SEM) and Environmental SEM: Suitable Tools for Study of Adhesion Stage and Biofilm Formation.* Scanning Electron Microscopy, 2012: p. 717-730.

275. Fernandez-Delgado, M., Duque, Z., Rojas, H., Suarez, P., Contreras, M., Garcia-Amado, M.A. and Alciaturi, C., *Environmental scanning electron microscopy analysis of Proteus mirabilis biofilms grown on chitin and stainless steel.* Annals of Microbiology, 2015. **65**(3): p. 1401-1409.

276. Brehm-Stecher, B.F. and Johnson, E.A., *Single-cell microbiology: Tools, technologies, and applications.* Microbiology and Molecular Biology Reviews, 2004. **68**(3): p. 538.

277. Elowitz, M.B., Levine, A.J., Siggia, E.D. and Swain, P.S., *Stochastic gene expression in a single cell.* Science, 2002. **297**(5584): p. 1183-1186.

278. Turner, N.A., Harris, J., Russell, A.D. and Lloyd, D., *Microbial differentiation and changes in susceptibility to antimicrobial agents.* Journal of Applied Microbiology, 2000. **89**(5): p. 751-759.

279. Booth, I.R., *Stress and the single cell: Intrapopulation diversity is a mechanism to ensure survival upon exposure to stress.* International Journal of Food Microbiology, 2002. **78**(1-2): p. 19-30.

280. Papadopoulos, D., Schneider, D., Meier-Eiss, J., Arber, W., Lenski, R.E. and Blot, M., *Genomic evolution during a 10,000-generation experiment with bacteria.* Proceedings of the National Academy of Sciences of the United States of America, 1999. **96**(7): p. 3807-3812.

281. Kysela, D.T., Brown, P.J.B., Huang, K.C. and Brun, Y.V., *Biological Consequences and Advantages of Asymmetric Bacterial Growth.* Annual Review of Microbiology, 2013. **67**: p. 417-435.

282. Guarente, L. and Kenyon, C., *Genetic pathways that regulate ageing in model organisms.* Nature, 2000. **408**(6809): p. 255-262.

283. Cluzel, P., Surette, M. and Leibler, S., *An ultrasensitive bacterial motor revealed by monitoring signaling proteins in single cells.* Science, 2000. **287**(5458): p. 1652-1655.

284. Oliveira, N.M., Fostera, K.R. and Durham, W.M., *Single-cell twitching chemotaxis in developing biofilms.* Proceedings of the National Academy of Sciences of the United States of America, 2016. **113**(23): p. 6532-6537.

285. Merritt, J.H., Ha, D.G., Cowles, K.N., Lu, W.Y., Morales, D.K., Rabinowitz, J., Gitai, Z. and O'Toole, G.A., *Specific Control of Pseudomonas aeruginosa Surface-Associated Behaviors by Two c-di-GMP Diguanylate Cyclases.* Mbio, 2010. **1**(4).

286. Tyler, B.J., Hook, A., Pelster, A., Williams, P., Alexander, M. and Arlinghaus, H.F., *Development and characterization of a stable adhesive bond between a poly(dimethylsiloxane) catheter material and a bacterial biofilm resistant acrylate polymer coating.* Biointerphases, 2017. **12**(2): p. 02C412.

287. Heydorn, A., Nielsen, A.T., Hentzer, M., Sternberg, C., Givskov, M., Ersboll, B.K. and Molin, S., *Quantification of biofilm structures by the novel computer program COMSTAT.* Microbiology-Sgm, 2000. **146**: p. 2395-2407.

288. Utada, A.S., Bennett, R.R., Fong, J.C.N., Gibiansky, M.L., Yildiz, F.H., Golestanian, R. and Wong, G.C.L., *Vibrio cholerae use pili and flagella synergistically to effect motility switching and conditional surface attachment.* Nature Communications, 2014. **5**.

289. Qian, H., Sheetz, M.P. and Elson, E.L., *Single particle tracking. Analysis of diffusion and flow in two-dimensional systems.* Biophysical Journal, 1991. **60**(4): p. 910-921.

290. Ingram, G.A. and Molyneux, D.H., *Lectins (Hemagglutinins) in the Hemolymph of Glossina-Fuscipes-Fuscipes - Isolation, Partial Characterization, Selected Physicochemical Properties and Carbohydrate-Binding Specificities.* Insect Biochemistry, 1990. **20**(1): p. 13-27.

291. *https://www.thermofisher.com/uk/en/home/life-science/cell-analysis/fluorophores/propidium-iodide.html*.

292. Gibiansky, M.L., Conrad, J.C., Jin, F., Gordon, V.D., Motto, D.A., Mathewson, M.A., Stopka, W.G., Zelasko, D.C., Shrout, J.D., and Wong, G.C.L., *Bacteria Use Type IV Pili to Walk Upright and Detach from Surfaces.* Science, 2010. **330**(6001): p. 197.

293. O'Toole, G.A. and Wong, G.C.L., *Sensational biofilms: surface sensing in bacteria.* Current Opinion in Microbiology, 2016. **30**: p. 139-146.

294. Rodesney, C.A., Roman, B., Dhamani, N., Cooley, B.J., Katira, P., Touhami, A. and Gordon, V.D., *Mechanosensing of shear by Pseudomonas aeruginosa leads to increased levels of the cyclic-di-GMP signal initiating biofilm development.* Proceedings of the National Academy of Sciences of the United States of America, 2017. **114**(28): p. 5906-5911.

295. Luo, Y., Zhao, K., Baker, A.E., Kuchma, S.L., Coggan, K.A., Wolfgang, M.C., Wong, G.C.L. and O'Toole, G.A., *A Hierarchical Cascade of Second Messengers Regulates Pseudomonas aeruginosa Surface Behaviors.* Mbio, 2015. **6**(1).

296. Armbruster, C.R., Lee, C.K., Parker-Gilham, J., de Anda, J., Xia, A.G., Zhao, K., Murakami, K., Tseng, B.S., Hoffman, L.R., Jin, F., Harwood, C.S., Wong, G.C.L., and Parsek, M.R., *Heterogeneity in surface sensing suggests a division of labor in Pseudomonas aeruginosa populations.* Elife, 2019. **8**.

297. Purcell, E.B., McKee, R.W., Bordeleau, E., Burrus, V. and Tamayo, R., *Regulation of Type IV Pili Contributes to Surface Behaviors of Historical and Epidemic Strains of Clostridium difficile.* Journal of Bacteriology, 2016. **198**(3): p. 565-577.

298. Valentini, M. and Filloux, A., *Biofilms and Cyclic di-GMP (c-di-GMP) Signaling: Lessons from Pseudomonas aeruginosa and Other Bacteria.* Journal of Biological Chemistry, 2016. **291**(24): p. 12547-12555.

299. Wozniak, D.J., Wyckoff, T.J.O., Starkey, M., Keyser, R., Azadi, P., O'Toole, G.A. and Parsek, M.R., *Alginate is not a significant component of the extracellular polysaccharide matrix of PA14 and PAO1 Pseudomonas aeruginosa biofilms.* Proceedings of the National Academy of Sciences of the United States of America, 2003. **100**(13): p. 7907-7912.

300. Jennings, L.K., Storek, K.M., Ledvina, H.E., Coulon, C., Marmont, L.S., Sadovskaya, I., Secor, P.R., Tseng, B.S., Scian, M., Filloux, A., Wozniak, D.J., Howell, P.L., and Parsek, M.R., *Pel is a cationic exopolysaccharide that cross-links extracellular DNA in the Pseudomonas aeruginosa biofilm matrix.* Proceedings of the National Academy of Sciences of the United States of America, 2015. **112**(36): p. 11353-11358.

301. Ma, L.Y., Lu, H.P., Sprinkle, A., Parsek, M.R. and Wozniak, D.J., *Pseudomonas aeruginosa PSl is a galactose- and mannose-rich exopolysaccharide.* Journal of Bacteriology, 2007. **189**(22): p. 8353-8356.

302. Macara, I.G. and Mili, S., *Polarity and Differential Inheritance-Universal Attributes of Life?* Cell, 2008. **135**(5): p. 801-812.

303. Shapiro, L., McAdams, H.H. and Losick, R., *Generating and exploiting polarity in bacteria.* Science, 2002. **298**(5600): p. 1942-1946.

304. Bowman, G.R., Lyuksyutova, A.I. and Shapiro, L., *Bacterial polarity.* Current Opinion in Cell Biology, 2011. **23**(1): p. 71-77.

305. Lee, C.K., de Anda, J., Baker, A.E., Bennett, R.R., Luo, Y., Lee, E.Y., Keefe, J.A., Helali, J.S., Ma, J., Zhao, K., Golestanian, R., O'Toole, G.A., and Wong, G.C.L., *Multigenerational memory and adaptive adhesion in early bacterial biofilm communities.* Proceedings of the National Academy of Sciences of the United States of America, 2018. **115**(17): p. 4471-4476.

306. Barbier, M., Damron, F.H., Bielecki, P., Suarez-Diez, M., Puchalka, J., Alberti, S., dos Santos, V.M. and Goldberg, J.B., *From the Environment to the Host: Re-Wiring of the Transcriptome of Pseudomonas aeruginosa from 22 degrees C to 37 degrees C.* Plos One, 2014. **9**(2).

307. Ni, L., Yang, S., Zhang, R.R., Jin, Z.Y., Chen, H., Conrad, J.C. and Jin, F., *Bacteria differently deploy type-IV pili on surfaces to adapt to nutrient availability.* Npj Biofilms and Microbiomes, 2016. **2**.

308. Boyd, C.D. and O'Toole, G.A., *Second Messenger Regulation of Biofilm Formation: Breakthroughs in Understanding c-di-GMP Effector Systems.* Annual Review of Cell and Developmental Biology, 2012. **28**: p. 439-462.

309. Kulasekara, B.R., Kamischke, C., Kulasekara, H.D., Christen, M., Wiggins, P.A. and Miller, S.I., *c-di-GMP heterogeneity is generated by the chemotaxis machinery to regulate flagellar motility.* Elife, 2013. **2**.

310. Chang, A.L., Tuckerman, J.R., Gonzalez, G., Mayer, R., Weinhouse, H., Volman, G., Amikam, D., Benziman, M. and Gilles-Gonzalez, M.A., *Phosphodiesterase A1, a regulator of cellulose synthesis in Acetobacter xylinum, is a heme-based sensor.* Biochemistry, 2001. **40**(12): p. 3420-3426.

311. Rajagopal, S., Key, J.M., Purcell, E.B., Boerema, D.J. and Moffat, K., *Purification and initial characterization of a putative blue light-regulated phosphodiesterase from Escherichia coli.* Photochemistry and Photobiology, 2004. **80**(3): p. 542-547.

312. Gjermansen, M., Nilsson, M., Yang, L. and Tolker-Nielsen, T., *Characterization of starvation-induced dispersion in Pseudomonas putida biofilms: genetic elements and molecular mechanisms.* Molecular Microbiology, 2010. **75**(4): p. 815-826.

313. Hoffman, L.R., D'Argenio, D.A., MacCoss, M.J., Zhang, Z.Y., Jones, R.A. and Miller, S.I., *Aminoglycoside antibiotics induce bacterial biofilm formation.* Nature, 2005. **436**(7054): p. 1171-1175.

314. Whitesides, G.M., *The origins and the future of microfluidics.* Nature, 2006. **442**(7101): p. 368-373.

315. Kunz, R., Anders, C. and Gersonde, K., *Principles for the reduction of bacterial adhesion to surface-modified polymers.* New Biomedical Materials, 1998. **16**: p. 115-121.

316. Fang, H.H.P., Chan, K.Y. and Xu, L.C., *Quantification of bacterial adhesion forces using atomic force microscopy (AFM).* Journal of Microbiological Methods, 2000. **40**(1): p. 89-97.

317. Hoffman, M.D., Zucker, L.I., Brown, P.J.B., Kysela, D.T., Brun, Y.V. and Jacobson, S.C., *Timescales and Frequencies of Reversible and Irreversible Adhesion Events of Single Bacterial Cells.* Analytical Chemistry, 2015. **87**(24): p. 12032-12039.

318. Berne, C., Ma, X., Licata, N.A., Neves, B.R.A., Setayeshgar, S., Brun, Y.V. and Dragnea, B., *Physiochemical Properties of Caulobacter crescentus Holdfast: A Localized Bacterial Adhesive.* Journal of Physical Chemistry B, 2013. **117**(36): p. 10492-10503.

319. Li, G.L., Brun, Y.V. and Tang, J.X., *Holdfast spreading and thickening during Caulobacter crescentus attachment to surfaces.* Bmc Microbiology, 2013. **13**.

320. Berne, C., Ellison, C.K., Ducret, A. and Brun, Y.V., *Bacterial adhesion at the single-cell level.* Nature Reviews Microbiology, 2018. **16**(10): p. 616-627.

321. Heindl, J.E., Hibbing, M.E., Xu, J., Natarajan, R., Buechlein, A.M. and Fuqua, C., *Discrete Responses to Limitation for Iron and Manganese in Agrobacterium tumefaciens: Influence on Attachment and Biofilm Formation.* Journal of Bacteriology, 2016. **198**(5): p. 816-829.

322. Danhorn, T., Hentzer, M., Givskov, M., Parsek, M.R. and Fuqua, C., *Phosphorus limitation enhances biofilm formation of the plant pathogen Agrobacterium tumefaciens through the PhoR-PhoB regulatory system.* Journal of Bacteriology, 2004. **186**(14): p. 4492-4501.

323. Alam, F., Kumar, S. and Varadarajan, K.M., *Quantification of Adhesion Force of Bacteria on the Surface of Biomaterials: Techniques and Assays.* Acs Biomaterials Science & Engineering, 2019. **5**(5): p. 2093-2110.

324. Ista, L.K., Mendez, S. and Lopez, G.P., *Attachment and detachment of bacteria on surfaces with tunable and switchable wettability.* Biofouling, 2010. **26**(1): p. 111-118.

325. Weder, G., Blondiaux, N., Giazzon, M., Matthey, N., Klein, M., Pugin, R., Heinzelmann, H. and Liley, M., *Use of Force Spectroscopy to Investigate the Adhesion of Living Adherent Cells.* Langmuir, 2010. **26**(11): p. 8180-8186.

326. Nolte, K.A., Schwarze, J., Beyer, C.D., Ozcan, O. and Rosenhahn, A., *Parallelized microfluidic diatom accumulation assay to test fouling-release coatings.* Biointerphases, 2018. **13**(4).

327. Nolte, K.A., Schwarze, J. and Rosenhahn, A., *Microfluidic accumulation assay probes attachment of biofilm forming diatom cells.* Biofouling, 2017. **33**(7): p. 531-543.

328. Alles, M. and Rosenhahn, A., *Microfluidic detachment assay to probe the adhesion strength of diatoms.* Biofouling, 2015. **31**(5): p. 469-480.

329. Arpa-Sancet, M.P., Christophis, C. and Rosenhahn, A., *Microfluidic Assay to Quantify the Adhesion of Marine Bacteria.* Biointerphases, 2012. **7**(1-4).

330. Christophis, C., Grunze, M. and Rosenhahn, A., *Quantification of the adhesion strength of fibroblast cells on ethylene glycol terminated self-assembled monolayers by a microfluidic shear force assay.* Physical Chemistry Chemical Physics, 2010. **12**(17): p. 4498-4504.

331. Westerhof, N., Stergiopulos, N. and Noble, M.I.M., *Bernoulli's Equation.* Snapshots of Hemodynamics: An Aid for Clinical Research and Graduate Education, Second Edition, 2010: p. 15-20.

332. Moxey, D. and Barkley, D., *Distinct large-scale turbulent-laminar states in transitional pipe flow.* Proceedings of the National Academy of Sciences of the United States of America, 2010. **107**(18): p. 8091-8096.

333. Nie, J., Gao, Q., Wang, Y., Zeng, J., Zhao, H., Sun, Y., Shen, J., Ramezani, H., Fu, Z., Liu, Z., Xiang, M., Fu, J., Zhao, P., Chen, W., and He, Y., *Vessel-on-a-chip with Hydrogel-based Microfluidics.* Small, 2018. **14**(45): p. e1802368.

334. Unger, M.A., Chou, H.P., Thorsen, T., Scherer, A. and Quake, S.R., *Monolithic microfabricated valves and pumps by multilayer soft lithography.* Science, 2000. **288**(5463): p. 113-116.

335. McDonald, J.C. and Whitesides, G.M., *Poly(dimethylsiloxane) as a material for fabricating microfluidic devices.* Accounts of Chemical Research, 2002. **35**(7): p. 491-499.

336. *Sylgard 184*. Available from: http://drajput.com/research/sylgard184-pdms.php.

337. Bartholomeusz, D.A., Boutte, R.W. and Andrade, J.D., *Xurography: rapid prototyping of microstructures using a cutting plotter.* Journal of Microelectromechanical Systems, 2005. **14** p. 1364–1374.

338. Stone, H.A., Stroock, A.D. and Ajdari, A., *Engineering flows in small devices: Microfluidics toward a lab-on-a-chip.* Annual Review of Fluid Mechanics, 2004. **36**: p. 381-411.

339. Meyvantsson, I., Warrick, J.W., Hayes, S., Skoien, A. and Beebe, D.J., *Automated cell culture in high density tubeless microfluidic device arrays.* Lab on a Chip, 2008. **8**(5): p. 717-724.

340. Kim, D., Chesler, N.C. and Beebe, D.J., *A method for dynamic system characterization using hydraulic series resistance.* Lab on a Chip, 2006. **6**(5): p. 639-644.

341. Christophis, C., Sekeroglu, K., Demirel, G., Thome, I., Grunze, M., Demirel, M.C. and Rosenhahn, A., *Fibroblast adhesion on unidirectional polymeric nanofilms.* Biointerphases, 2011. **6**(4): p. 158-163.

342. Chen, X., Zeng, L.S., Wang, Z.Y., Zhang, X.L., Wang, Q., Yang, Z., Hu, N., Luo, H., Liao, Y.Y., and Yang, J.J., *Simultaneous assay of platelet adhesion at multiple shear rates within a single microfluidic channel.* Microfluidics and Nanofluidics, 2017. **21**(3).

343. Moran, G., Ramos-Chagas, G., Hugelier, S., Xie, X., Boudjemaa, R., Ruckebusch, C., Sliwa, M., Darmanin, T., Gaucher, A., Prim, D., Godeau, G., Amigoni, S., Guittard, F., and Meallet-Renault, R., *Superhydrophobic polypyrene films to prevent Staphylococcus aureus and Pseudomonas aeruginosa biofilm adhesion on surfaces: high efficiency deciphered by fluorescence microscopy.* Photochemical & Photobiological Sciences, 2018. **17**(8).

344. Graham, M.V. and Cady, N.C., *Nano and Microscale Topographies for the Prevention of Bacterial Surface Fouling.* Coatings, 2014. **4**(1): p. 37-59.

345. Armentano, I., Arciola, C.R., Fortunati, E., Ferrari, D., Mattioli, S., Amoroso, C.F., Rizzo, J., Kenny, J.M., Imbriani, M., and Visai, L., *The Interaction of Bacteria with Engineered Nanostructured Polymeric Materials: A Review.* Scientific World Journal, 2014.

346. Saha, N., Monge, C., Dulong, V., Picart, C. and Glinel, K., *Influence of Polyelectrolyte Film Stiffness on Bacterial Growth.* Biomacromolecules, 2013. **14**(2): p. 520-528.

347. Lichter, J.A., Thompson, M.T., Delga-Dillo, M., Nishikawa, T., Rubner, M.F. and Van Vliet, K.J., *Substrata Mechanical Stiffness Can Regulate Adhesion of Viable Bacteria* Biomacromolecules, 2008. **9**(10): p. 2967-2967.

348. Lichter, J.A., Thompson, M.T., Delgadillo, M., Nishikawa, T., Rubner, M.F. and Van Vliet, K.J., *Substrata mechanical stiffness can regulate adhesion of viable bacteria.* Biomacromolecules, 2008. **9**(6): p. 1571-1578.

349. Lecuyer, S., Rusconi, R., Shen, Y., Forsyth, A., Vlamakis, H., Kolter, R. and Stone, H.A., *Shear Stress Increases the Residence Time of Adhesion*

of Pseudomonas aeruginosa. Biophysical Journal, 2011. **100**(2): p. 341-350.

350. Park, K.D., Kim, Y.S., Han, D.K., Kim, Y.H., Lee, E.H., Suh, H. and Choi, K.S., *Bacterial adhesion on PEG modified polyurethane surfaces.* Biomaterials, 1998. **19**(7-9): p. 851-859.

351. Saldarriaga Fernandez, I.C., Mei, H.C., Metzger, S., Grainger, D.W., Engelsman, A.F., Nejadnik, M.R. and Busscher, H.J., *In vitro and in vivo comparisons of staphylococcal biofilm formation on a cross-linked poly(ethylene glycol)-based polymer coating.* Acta Biomaterialia, 2010. **6**(3): p. 1119-1124.

352. Aykent, F., Yondem, I., Ozyesil, A.G., Gunal, S.K., Avunduk, M.C. and Ozkan, S., *Effect of Different Finishing Techniques for Restorative Materials on Surface Roughness and Bacterial Adhesion.* Journal of Prosthetic Dentistry, 2010. **103**(4): p. 221-227.

353. Liu, J. and Ford, R.M., *Idling Time of Swimming Bacteria near Particulate Surfaces Contributes to Apparent Adsorption Coefficients at the Macroscopic Scale under Static Conditions.* Environmental Science & Technology, 2009. **43**(23): p. 8874-8880.

354. Pranzetti, A., Salaun, S., Mieszkin, S., Callow, M.E., Callow, J.A., Preece, J.A. and Mendes, P.M., *Model Organic Surfaces to Probe Marine Bacterial Adhesion Kinetics by Surface Plasmon Resonance.* Advanced Functional Materials, 2012. **22**(17): p. 3672-3681.

355. Preedy, E., Perni, S., Nipic, D., Bohinc, K. and Prokopovich, P., *Surface Roughness Mediated Adhesion Forces between Borosilicate Glass and Gram-Positive Bacteria.* Langmuir, 2014. **30**(31): p. 9466-9476.

356. Kargar, M., Chang, Y.R., Hoseinabad, H.K., Pruden, A. and Ducker, W.A., *Colloidal Crystals Delay Formation of Early Stage Bacterial Biofilms.* Acs Biomaterials Science & Engineering, 2016. **2**(6): p. 1039-1048.

357. Kelleher, S.M., Habimana, O., Lawler, J., O'Rilly, B., Daniels, S., Casey, E. and Cowley, A., *Cicada Wing Surface Topography: An Investigation into the Bactericidal Properties of Nanostructural Features.* Acs Applied Materials & Interfaces, 2016. **8**(24): p. 14966-14974.

358. Manabe, K., Nishizawa, S. and Shiratori, S., *Porous Surface Structure Fabricated by Breath Figures that Suppresses Pseudomonas aeruginosa Biofilm Formation.* Acs Applied Materials & Interfaces, 2013. **5**(22): p. 11900-11905.

359. Nadell, C.D., Drescher, K. and Foster, K.R., *Spatial structure, cooperation and competition in biofilms.* Nature Reviews Microbiology, 2016. **14**(9): p. 589-600.

360. Hengge, R., *Principles of c-di-GMP signalling in bacteria.* Nature Reviews Microbiology, 2009. **7**(4): p. 263-273.

361. Song, F.C., Wang, H., Sauer, K. and Ren, D.C., *Cyclic-di-GMP and oprF Are Involved in the Response of Pseudomonas aeruginosa to Substrate Material Stiffness during Attachment on Polydimethylsiloxane (PDMS).* Frontiers in Microbiology, 2018. **9**.

362. Song, F., Koo, H. and Ren, D., *Effects of Material Properties on Bacterial Adhesion and Biofilm Formation.* Journal of Dental Research, 2015. **94**(8): p. 1027-1034.

363. Kolewe, K.W., Peyton, S.R. and Schiffman, J.D., *Fewer Bacteria Adhere to Softer Hydrogels.* Acs Applied Materials & Interfaces, 2015. **7**(35): p. 19562-19569.

364. Wang, Y., Guan, A., Isayeva, I., Vorvolakos, K., Das, S., Li, Z.Y. and Phillips, K.S., *Interactions of Staphylococcus aureus with ultrasoft hydrogel biomaterials.* Biomaterials, 2016. **95**: p. 74-85.

365. Cheng, Y.F., Feng, G.P. and Moraru, C.I., *Micro- and Nanotopography Sensitive Bacterial Attachment Mechanisms: A Review.* Frontiers in Microbiology, 2019. **10**.

366. Ellison, C.K., Kan, J.B., Dillard, R.S., Kysela, D.T., Ducret, A., Berne, C., Hampton, C.M., Ke, Z.L., Wright, E.R., Biais, N., Dalia, A.B., and Brun, Y.V., *Obstruction of pilus retraction stimulates bacterial surface sensing.* Science, 2017. **358**(6362): p. 535-538.

367. Toutain, C.M., Caizza, N.C., Zegans, M.E. and O'Toole, G.A., *Roles for flagellar stators in biofilm formation by Pseudomonas aeruginosa.* Research in Microbiology, 2007. **158**(5): p. 471-477.

368. Pompilio, A., Piccolomini, R., Picciani, C., D'Antonio, D., Savini, V. and Di Bonaventura, G., *Factors associated with adherence to and biofilm formation on polystyrene by Stenotrophomonas maltophilia: the role of cell surface hydrophobicity and motility.* Fems Microbiology Letters, 2008. **287**(1): p. 41-47.

369. Siryaporn, A., Kuchma, S.L., O'Toole, G.A. and Gitai, Z., *Surface attachment induces Pseudomonas aeruginosa virulence.* Proceedings of the National Academy of Sciences of the United States of America, 2014. **111**(47): p. 16860-16865.

370. Palmer, J., Flint, S. and Brooks, J., *Bacterial cell attachment, the beginning of a biofilm.* Journal of Industrial Microbiology & Biotechnology, 2007. **34**(9): p. 577-588.

371. Friedlander, R.S., Vlamakis, H., Kim, P., Khan, M., Kolter, R. and Aizenberg, J., *Bacterial flagella explore microscale hummocks and hollows to increase adhesion.* Proceedings of the National Academy of Sciences of the United States of America, 2013. **110**(14): p. 5624-5629.

372. Baker, A.E., Diepold, A., Kuchma, S.L., Scott, J.E., Ha, D.G., Orazi, G., Armitage, J.P. and O'Toole, G.A., *PilZ Domain Protein FlgZ Mediates Cyclic Di-GMP-Dependent Swarming Motility Control in Pseudomonas aeruginosa.* Journal of Bacteriology, 2016. **198**(13): p. 1837-1846.

373. Lee, V.T., Matewish, J.M., Kessler, J.L., Hyodo, M., Hayakawa, Y. and Lory, S., *A cyclic-di-GMP receptor required for bacterial exopolysaccharide production.* Molecular Microbiology, 2007. **65**(6): p. 1474-1484.

374. Moradali, M.F., Donati, I., Sims, I.M., Ghods, S. and Rehm, B.H.A., *Alginate Polymerization and Modification Are Linked in Pseudomonas aeruginosa.* Mbio, 2015. **6**(3).

375. Hickman, J.W., Tifrea, D.F. and Harwood, C.S., *A chemosensory system that regulates biofilm formation through modulation of cyclic diguanylate levels.* Proceedings of the National Academy of Sciences of the United States of America, 2005. **102**(40): p. 14422-14427.

376. Su, T.T., Liu, S.H., Wang, K., Chi, K.K., Zhu, D.Y., Wei, T.D., Huang, Y., Guo, L.M., Hu, W., Xu, S.J., Lin, Z., and Gu, L.C., *The REC domain mediated dimerization is critical for FleQ, from Pseudomonas aeruginosa to function as a c-di-GMP receptor and flagella gene regulator.* Journal of Structural Biology, 2015. **192**(1): p. 1-13.

377. Muriel, C., Blanco-Romero, E., Trampari, E., Arrebola, E., Duran, D., Redondo-Nieto, M., Malone, J.G., Martin, M. and Rivilla, R., *The diguanylate cyclase AdrA regulates flagellar biosynthesis in Pseudomonas fluorescens F113 through SadB.* Scientific Reports, 2019. **9**.

378. Arora, S.K., Ritchings, B.W., Almira, E.C., Lory, S. and Ramphal, R., *Transcriptional activator, FleQ, regulates mucin adhesion and flagellar gene expression in Pseudomonas aeruginosa in a cascade manner.* Journal of Bacteriology, 1997. **179**(17): p. 5574-5581.

379. Dasgupta, N., Wolfgang, M.C., Goodman, A.L., Arora, S.K., Jyot, J., Lory, S. and Ramphal, R., *A four-tiered transcriptional regulatory circuit controls flagellar biogenesis in Pseudomonas aeruginosa.* Molecular Microbiology, 2003. **50**(3): p. 809-824.

380. Caiazza, N.C. and O'Toole, G.A., *SadB is required for the transition from reversible to irreversible attachment during biofilm formation by Pseudomonas aeruginosa PA14.* Journal of Bacteriology, 2004. **186**(14): p. 4476-4485.

381. Caiazza, N.C., Merritt, J.H., Brothers, K.M. and O'Toole, G.A., *Inverse regulation of biofilm formation and swarming motility by Pseudomonas aeruginosa PA14.* Journal of Bacteriology, 2007. **189**(9): p. 3603-3612.

382. Merritt, J.H., Brothers, K.M., Kuchma, S.L. and O'Toole, G.A., *SadC reciprocally influences biofilm formation and swarming motility via*

modulation of exopolysaccharide production and flagellar function. Journal of Bacteriology, 2007. **189**(22): p. 8154-8164.

383. Chang, C.Y., *Surface Sensing for Biofilm Formation in Pseudomonas aeruginosa.* Frontiers in Microbiology, 2018. **8**.

384. D'Argenio, D.A., Gallagher, L.A., Berg, C.A. and Manoil, C., *Drosophila as a model host for Pseudomonas aeruginosa infection.* Journal of Bacteriology, 2001. **183**(4): p. 1466-1471.

385. DeLange, P.A., Collins, T.L., Pierce, G.E. and Robinson, J.B., *PilJ localizes to cell poles and is required for type IV pilus extension in Pseudomonas aeruginosa.* Current Microbiology, 2007. **55**(5): p. 389-395.

386. Kuchma, S.L., Ballok, A.E., Merritt, J.H., Hammond, J.H., Lu, W., Rabinowitz, J.D. and O'Toole, G.A., *Cyclic-di-GMP-Mediated Repression of Swarming Motility by Pseudomonas aeruginosa: the pilY1 Gene and Its Impact on Surface-Associated Behaviors.* Journal of Bacteriology, 2010. **192**(12): p. 2950-2964.

387. Meinders, J.M., vanderMei, H.C. and Busscher, H.J., *Deposition efficiency and reversibility of bacterial adhesion under flow.* Journal of Colloid and Interface Science, 1995. **176**(2): p. 329-341.

388. Hook, A.L., Chang, C.Y., Yang, J., Atkinson, S., Langer, R., Anderson, D.G., Davies, M.C., Williams, P. and Alexander, M.R., *Discovery of Novel Materials with Broad Resistance to Bacterial Attachment Using Combinatorial Polymer Microarrays.* Advanced Materials, 2013. **25**(18): p. 2542-2547.

389. Rybtke, M.T., Borlee, B.R., Murakami, K., Irie, Y., Hentzer, M., Nielsen, T.E., Givskov, M., Parsek, M.R. and Tolker-Nielsen, T., *Fluorescence-Based Reporter for Gauging Cyclic Di-GMP Levels in Pseudomonas aeruginosa.* Applied and Environmental Microbiology, 2012. **78**(15): p. 5060-5069.

390. Kuchma, S.L., Brothers, K.M., Merritt, J.H., Liberati, N.T., Ausubel, F.M. and O'Toole, G.A., *BifA, a cyclic-di-GMP phosphodiesterase, inversely regulates biofilm formation and swarming motility by Pseudomonas aeruginosa PA14.* Journal of Bacteriology, 2007. **189**(22): p. 8165-8178.

391. Borlee, B.R., Goldman, A.D., Murakami, K., Samudrala, R., Wozniak, D.J. and Parsek, M.R., *Pseudomonas aeruginosa uses a cyclic-di-GMP-regulated adhesin to reinforce the biofilm extracellular matrix.* Molecular Microbiology, 2010. **75**(4): p. 827-842.

392. Serra, D.O. and Hengge, R., *A c-di-GMP-Based Switch Controls Local Heterogeneity of Extracellular Matrix Synthesis which Is Crucial for Integrity and Morphogenesis of Escherichia coli Macrocolony Biofilms.* Journal of Molecular Biology, 2019.

393. Galperin, M.Y., *Bacterial signal transduction network in a genomic perspective.* Environmental Microbiology, 2004. **6**(6): p. 552-567.

394. Lee, H.M., Liao, C.T., Chiang, Y.C., Chang, Y.Y., Yeh, Y.T., Du, S.C. and Hsiao, Y.M., *Characterization of genes encoding proteins containing HD-related output domain in Xanthomonas campestris pv. campestris.* Antonie Van Leeuwenhoek International Journal of General and Molecular Microbiology, 2016. **109**(4): p. 509-522.

395. Navazo, A., Barahona, E., Redondo-Nieto, M., Martinez-Granero, F., Rivilla, R. and Martin, M., *Three independent signalling pathways repress motility in Pseudomonas fluorescens F113.* Microbial Biotechnology, 2009. **2**(4): p. 489-498.

396. Davenport, P.W., Griffin, J.L. and Welch, M., *Quorum Sensing Is Accompanied by Global Metabolic Changes in the Opportunistic Human Pathogen Pseudomonas aeruginosa.* Journal of Bacteriology, 2015. **197**(12): p. 2072-2082.

397. Kang, D., Turner, K.E. and Kirienko, N.V., *PqsA Promotes Pyoverdine Production via Biofilm Formation.* Pathogens, 2018. **7**(1).

398. Rampioni, G., Falcone, M., Heeb, S., Frangipani, E., Fletcher, M.P., Dubern, J.F., Visca, P., Leoni, L., Camara, M., and Williams, P., *Unravelling the Genome-Wide Contributions of Specific 2-Alkyl-4-Quinolones and PqsE to Quorum Sensing in Pseudomonas aeruginosa.* Plos Pathogens, 2016. **12**(11).

399. Kang, D. and Kirienko, N.V., *High-Throughput Genetic Screen Reveals that Early Attachment and Biofilm Formation Are Necessary for Full Pyoverdine Production by Pseudomonas aeruginosa.* Frontiers in Microbiology, 2017. **8**.

400. Darch, S.E., Simoska, O., Fitzpatrick, M., Barraza, J.P., Stevenson, K.J., Bonnecaze, R.T., Shear, J.B. and Whiteley, M., *Spatial determinants of quorum signaling in a Pseudomonas aeruginosa infection model.* Proceedings of the National Academy of Sciences of the United States of America, 2018. **115**(18): p. 4779-4784.

401. Ortori, C.A., Halliday, N., Camara, M., Williams, P. and Barrett, D.A., *LC-MS/MS Quantitative Analysis of Quorum Sensing Signal Molecules.* Pseudomonas: Methods and Protocols, 2014. **1149**: p. 255-270.

402. Carniello, V., Peterson, B.W., van der Mei, H.C. and Busscher, H.J., *Physico-chemistry from initial bacterial adhesion to surface-programmed biofilm growth.* Advances in Colloid and Interface Science, 2018. **261**: p. 1-14.

403. Kavanaugh, J.S., Flack, C.E., Lister, J., Ricker, E.B., Ibberson, C.B., Jenul, C., Moormeier, D.E., Delmain, E.A., Bayles, K.W., and Horswill, A.R., *Identification of Extracellular DNA-Binding Proteins in the Biofilm Matrix.* Mbio, 2019. **10**(3).

404. Das, T., Sharma, P.K., Busscher, H.J., van der Mei, H.C. and Krom, B.P., *Role of Extracellular DNA in Initial Bacterial Adhesion and Surface Aggregation.* Applied and Environmental Microbiology, 2010. **76**(10): p. 3405-3408.

405. Jayathilake, P.G., Jana, S., Rushton, S., Swailes, D., Bridgens, B., Curtis, T. and Chen, J.J., *Extracellular Polymeric Substance Production and Aggregated Bacteria Colonization Influence the Competition of Microbes in Biofilms.* Frontiers in Microbiology, 2017. **8**.

406. Klockgether, J., Munder, A., Neugebauer, J., Davenport, C.F., Stanke, F., Larbig, K.D., Heeb, S., Schock, U., Pohl, T.M., Wiehlmann, L., and Tummler, B., *Genome Diversity of Pseudomonas aeruginosa PAO1 Laboratory Strains.* Journal of Bacteriology, 2010. **192**(4): p. 1113-1121.

407. Diggle, S.P., Cornelis, P., Williams, P. and Camara, M., *4-Quinolone signalling in Pseudomonas aeruginosa: Old molecules, new perspectives.* International Journal of Medical Microbiology, 2006. **296**(2-3): p. 83-91.

408. Antunes, L.C.M., Ferreira, R.B.R., Buckner, M.M.C. and Finlay, B.B., *Quorum sensing in bacterial virulence.* Microbiology-Sgm, 2010. **156**: p. 2271-2282.

409. Eickhoff, M.J. and Bassler, B.L., *SnapShot: Bacterial Quorum Sensing.* Cell, 2018. **174**(5): p. 1328.

410. Ortori, C.A., Dubern, J.F., Chhabra, S.R., Camara, M., Hardie, K., Williams, P. and Barrett, D.A., *Simultaneous quantitative profiling of N-acyl-l-homoserine lactone and 2-alkyl-4(1H)-quinolone families of quorum-sensing signaling molecules using LC-MS/MS.* Analytical and Bioanalytical Chemistry, 2011. **399**(2): p. 839-850.

411. Cooley, M.A., Whittall, C. and Rolph, M.S., *Pseudomonas signal molecule 3-oxo-C12-homoserine lactone interferes with binding of rosiglitazone to human PPAR gamma.* Microbes and Infection, 2010. **12**(3): p. 231-237.

412. Oinuma, K.I. and Greenberg, E.P., *Acyl-Homoserine Lactone Binding to and Stability of the Orphan Pseudomonas aeruginosa Quorum-Sensing Signal Receptor QscR.* Journal of Bacteriology, 2011. **193**(2): p. 421-428.

413. Strugala, P., Dudra, A., Kucharska, A.Z., Sokol-Letowska, A., Wojnicz, D., Cisowska, A., Walkowski, S., Sroka, Z., Gabrielska, J., and Hendrich, A.B., *Biological Activity of the Methanol and Water Extracts of the Fruits of Anthocyanin-Rich Plants Grown in South-West Poland.* Natural Product Communications, 2015. **10**(3): p. 467-474.

414. Otto, M., *Staphylococcal Infections: Mechanisms of Biofilm Maturation and Detachment as Critical Determinants of Pathogenicity.* Annual Review of Medicine, Vol 64, 2013. **64**: p. 175-188.

415. Rutherford, S.T. and Bassler, B.L., *Bacterial Quorum Sensing: Its Role in Virulence and Possibilities for Its Control.* Cold Spring Harbor Perspectives in Medicine, 2012. **2**(11).

416. Connell, J.L., Kim, J., Shear, J.B., Bard, A.J. and Whiteley, M., *Real-time monitoring of quorum sensing in 3D-printed bacterial aggregates using scanning electrochemical microscopy.* Proceedings of the National Academy of Sciences of the United States of America, 2014. **111**(51): p. 18255-18260.

417. Tala, L., Fineberg, A., Kukura, P. and Persat, A., *Pseudomonas aeruginosa orchestrates twitching motility by sequential control of type IV pili movements.* Nature Microbiology, 2019. **4**(5): p. 774-780.

418. Passarelli, M.K., Pirkl, A., Moellers, R., Grinfeld, D., Kollmer, F., Havelund, R., Newman, C.F., Marshall, P.S., Arlinghaus, H., Alexander, M.R., West, A., Horning, S., Niehuis, E., Makarov, A., Dollery, C.T., and Gilmore, I.S., *The 3D OrbiSIMS-label-free metabolic imaging with subcellular lateral resolution and high mass-resolving power.* Nature Methods, 2017. **14**(12): p. 1175.

419. Wurtzel, O., Yoder-Himes, D.R., Han, K., Dandekar, A.A., Edelheit, S., Greenberg, E.P., Sorek, R. and Lory, S., *The Single-Nucleotide Resolution Transcriptome of Pseudomonas aeruginosa Grown in Body Temperature.* Plos Pathogens, 2012. **8**(9).

420. Vogel, J. and Luisi, B.F., *Hfq and its constellation of RNA.* Nature Reviews Microbiology, 2011. **9**(8): p. 578-589.

421. Mikulskis, P., Hook, A., Dundas, A.A., Irvine, D., Sanni, O., Anderson, D., Langer, R., Alexander, M.R., Williams, P., and Winkler, D.A., *Prediction of Broad-Spectrum Pathogen Attachment to Coating Materials for Biomedical Devices.* Acs Applied Materials & Interfaces, 2018. **10**(1): p. 139-149.